UNIVERSIDADE D
COIMBRA

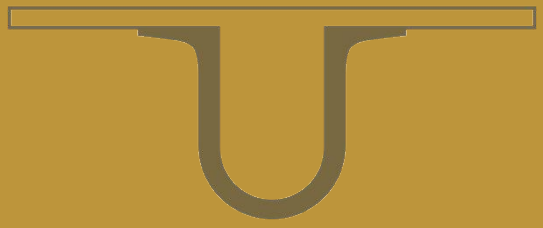

Nataliya Sakharova

Elastic Properties of Carbon Nanotubes and their Heterojunctions: Numerical Evaluation

Doctoral Thesis in Mechanical Engineering, branch of Nanomaterials and Micromanufacturing, supervised by Professor José Valdemar Bidarra Fernandes and submitted to the Department of Mechanical Engineering, Faculty of Sciences and Technology of the University of Coimbra.

July 2018

Department of Mechanical Engineering
Faculty of Sciences and Technology
University of Coimbra

Elastic Properties of Carbon Nanotubes and their Heterojunctions: Numerical Evaluation

Nataliya Sakharova

Doctoral Thesis in Mechanical Engineering, branch of Nanomaterials and Micromanufacturing, supervised by Professor José Valdemar Bidarra Fernandes and submitted to the Department of Mechanical Engineering, Faculty of Sciences and Technology of the University of Coimbra.

July 2018

UNIVERSIDADE D
COIMBRA

To my son

″La logique, qui peut seule donner la certitude, est l'instrument de la démonstration: l'intuition est l'instrument de l'invention.″

(“Logic, which can only give certainties, is the instrument of demonstration; intuition is that of invention.”)

Henri Poincaré

La Valeur de la Science (1905)

(Page intentionally left blank)

Acknowledgements

Foremost, I want to express my deepest gratitude to my supervisor, Professor José Valdemar Fernandes, for a wise guidance and wholehearted encouragement all through my research. I am eternally grateful to him for believing in me fourteen years ago and giving me an opportunity to live and work in Portugal, as well as an unforgettable experience of learning, engineering education, and personal development.

I am grateful for the excellent support given within the research unit in which this thesis was conducted, CEMMPRE - Centre for Mechanical Engineering, Materials and Processes. I also wish to thank all members of CEMMPRE, and to all current and former colleagues from Advanced Manufacturing Systems group, for friendly environment and scientifically encouraging atmosphere at the research centre.

Also, I want to express my truthful gratitude to my colleagues Professor Marta Oliveira and Professor Jorge Antunes for their moral support, readiness, valuable discussions, and, above all, their precious friendship.

To Professor Maria Teresa Vieira, my sincere thankfulness for teaching the disciplines "*Nanomaterials and Nanotechnologies"* and "*Micromanufacturing"*, and helping me to improve and organize my knowledge in these areas.

To publishers, copyright holders and scientific journals editors, my acknowledgement for providing the licences allowing the print and electronic reuse of the papers published under the scope of this research.

I wish to thank my son in whose eyes I am a great scientist forever.

Finally, I want to express my heartfelt gratefulness to my father for his unconditional support while he was with us. My father regrettably witnessed only part of this journey, and if he could have been present, this day would have been the happiest day for him.

This thesis is sponsored by national funds from the Portuguese Foundation for Science and Technology (FCT) via the projects PTDC/EME–TME/122472/2010, PEst-C/EME/UI0285/2013 and UID/EMS/00285/2013. It was also supported in the framework of the projects with the references CENTRO-07-0224-FEDER-002001 (MT4MOBI) and CENTRO-01-0145-FEDER-000014 (MATIS) co-financed by UE/FEDER funds, through "Programa Operacional da Região Centro". During 2016 and 2017 years N.A. Sakharova was also supported by scientific research grant from the FCT with reference SFRH/BPD/107888/2015. All supports are gratefully acknowledged.

Abstract

High-tech miniaturization is a strategic area to empower new scientific challenges for which carbon nanotubes have been proposed as ideal candidates, with outstanding electronic, optical and mechanical properties. Carbon nanotubes and their heterojunctions are efficient components for the reinforcement of composites, for constructing nanodevices and for designing new materials with required electronic and mechanical properties. Since the stability and efficiency of carbon nanotubes based devices and carbon nanotubes reinforced composites are strongly dependent on the mechanical properties of the building blocks, i.e. individual carbon nanotubes and their heterojunctions, it is crucial to understand their deformation behaviour. The research on the evaluation of the mechanical properties of carbon nanotubes and their heterojunctions has been mainly driven theoretically, due to technical difficulties to operate with nanoscale objects. The scattering commonly observed in the results of analytical and numerical studies calls into question their reliability and affects their interpretation.

This work focuses on the systematic study by numerical simulation of the elastic properties of the single-walled carbon nanotubes and their heterojunctions, grounded on a modelling approach in nanoscale continuum mechanics. A three-dimensional finite element model is used in order to evaluate the tensile, bending and torsional rigidities, and subsequently the Young's and shear moduli, and also the Poisson's ratio of single-walled carbon nanotubes, for a wide range of nanotube lengths, chiral indices and diameters. Correlations between the tensile, bending and torsional rigidities and the nanotube diameter, allowing the easy evaluation of each rigidity, are established. This allows developing methodologies for evaluating the Young's and shear moduli, and the Poisson's ratio. The proposed models are validated, using numerical and experimental results accessible in the literature.

The numerical simulation of the mechanical properties of carbon nanotubes with defects is an important task, providing data that can be compared with experimental results. In this context, a systematic study involving non-chiral and chiral single-walled carbon nanotubes, containing different percentage (up to 10%) and types of vacancy defects is carried out over a wide range of diameters. The Young's and shear moduli, and Poisson's ratio of the single-walled carbon

nanotubes with vacancy defects are assessed using the methodologies suggested in this work. The evolution of the Young's and shear moduli, and Poisson's ratio with the percentage of the vacancy defects is analysed.

Finally, a comprehensive numerical simulation study to evaluate the mechanical properties of carbon nanotubes heterojunctions is performed. The modelling of the mechanical response of armchair – armchair and zigzag – zigzag heterojunctions (of nanotubes with different diameters) allows clarifying the effect of the heterojunction geometry (diameters ratio and relative lengths of the constituent nanotubes) on their tensile, bending and torsional rigidities, and Young's and shear moduli. Expressions for the easy evaluation of the heterojunctions rigidities from the knowledge of the rigidities of single-walled carbon nanotubes, which are their constituent key units, are established. This enables the evaluation of the Young's and shear moduli of the heterojunction, assuming that its diameter is equal to the mean value of the single-walled carbon nanotubes that make up the heterojunction.

Keywords: Carbon Nanotubes, Heterojunctions, Elastic Properties, Mechanical Properties, Numerical Simulation.

Resumo

A miniaturização altamente tecnológica é uma área estratégica capaz de potencializar novos desafios científicos para os quais os nanotubos de carbono têm sido propostos como candidatos ideais, com excelentes propriedades electrónicas, ópticas e mecânicas. Os nanotubos de carbono e suas junções heterogéneas são componentes eficazes para o reforço de compósitos, para a elaboração de nano-dispositivos e para a conceição de novos materiais com propriedades mecânicas e electrónicas solicitadas. Uma vez que a estabilidade e a eficiência de dispositivos à base de nanotubos de carbono e compósitos reforçados com nanotubos de carbono são fortemente dependentes das propriedades mecânicas dos blocos de construção, ou seja, dos nanotubos de carbono individuais e junções heterogéneas, é crucial compreender seu comportamento de deformação. A investigação sobre a avaliação das propriedades mecânicas dos nanotubos de carbono e suas junções heterogéneas tem sido principalmente impulsionada teoricamente, devido a dificuldades técnicas para operar com objectos em nanoescala. A dispersão geralmente observada nos resultados de estudos analíticos e numéricos levanta a questão da sua confiabilidade e afecta a sua interpretação.

Este trabalho está focado no estudo sistemático por simulação numérica das propriedades elásticas dos nanotubos de carbono de parede única e das suas junções heterogéneas, e baseia-se numa abordagem de modelação de mecânica dos meios contínuos em nano-escala. Um modelo tridimensional de elementos finitos é utilizado para avaliar as rigidezes em tração, flexão e torção, e subsequentemente os módulos de Young e de corte, e também o coeficiente de Poisson de nanotubos de carbono de parede única, para uma ampla gama de comprimentos de nanotubos, índices quirais e diâmetros. Correlações entre as rigidezes em tração, flexão e torção e o diâmetro do nanotubo, as quais permitem a fácil avaliação de cada rigidez, são apresentadas. Isto possibilita o desenvolvimento de metodologias para avaliar os módulos de Young e de corte e o coeficiente de Poisson. Os modelos propostos são validados, utilizando resultados numéricos e experimentais acessíveis na literatura.

A simulação numérica das propriedades mecânicas de nanotubos de carbono com defeitos é uma tarefa importante, facultando dados que podem ser comparados

com resultados experimentais. Neste contexto, é realizado um estudo sistemático de nanotubos de carbono não quirais e quirais de parede única, os quais contêm diferentes percentagens (até 10%) e tipos de lacunas, numa ampla gama de diâmetros. Os módulos de Young e de corte, e o coeficiente de Poisson dos nanotubos de carbono de parede única com defeitos de lacuna são avaliados com as metodologias sugeridas neste trabalho. A evolução dos módulos de Young e de cisalhamento e do coeficiente de Poisson com a percentagem das lacunas são analisadas.

Finalmente, é realizado um estudo abrangente de simulação numérica para avaliar as propriedades mecânicas de junções heterogéneas de nanotubos de carbono. A modelação da resposta mecânica de junções heterogéneas de "*armchair* – *armchair*" e "*zigzag* – *zigzag*" (nanotubos com diferentes diâmetros) permite esclarecer o efeito da geometria da junção heterogénea (relação entre diâmetros e comprimentos relativos dos nanotubos constituintes) nas suas rigidezes em tração, flexão e torção e os módulos Young e de corte. Expressões para a avaliação fácil das rigidezes das junções heterogéneas a partir do conhecimento da rigidez dos nanotubos de carbono de parede única, que são suas unidades-chave constituintes, são apresentadas. Isto possibilita a avaliação dos módulos de Young e de corte da junção heterogénea, assumindo que seu diâmetro é igual ao valor médio dos nanotubos de carbono de parede única que compõem a junção heterogénea.

Palavras-Chave: Nanotubos de carbono, Junções heterogéneas, Propriedades elásticas, Propriedades mecânicas, Simulação numérica.

Résumé

La miniaturisation hautement technologique est un domaine stratégique capable de potentialiser de nouveaux défis scientifiques pour lesquels les nanotubes de carbone ont été proposés comme candidats idéaux ayant d'excellentes propriétés électroniques, optiques et mécaniques. Les nanotubes de carbone et leurs jonctions hétérogènes sont des composants efficaces pour le renforcement des composites, pour l'élaboration de nano-dispositifs et pour la conception de nouveaux matériaux avec les propriétés mécaniques et électroniques demandées. Puisque la stabilité et l'efficacité des dispositifs sur la base des nanotubes de carbone et des composites renforcés par des nanotubes de carbone dépendent fortement des propriétés mécaniques des blocs de construction, c'est-à-dire, ils dépendent des nanotubes de carbone individuels et des jonctions hétérogènes. De ce fait, il est crucial de comprendre leur comportement de déformation. Les études sur l'évaluation des propriétés mécaniques des nanotubes de carbone et de leurs jonctions hétérogènes ont été menées principalement sur le plan théorique, ceci se doit aux difficultés techniques à opérer avec des objets à l'échelle nanométrique. La dispersion généralement observée dans les résultats des études analytiques et numériques soulève la question de sa fiabilité et affecte son interprétation.

Ce travail est axé sur l'étude systématique par simulation numérique des propriétés élastiques des nanotubes de carbone à paroi unique et de leurs jonctions hétérogènes, et repose sur une approche de modélisation de la mécanique des milieux continus à l'échelle nanométrique. Un modèle tridimensionnel d'éléments finis est utilisé pour évaluer la rigidité à la traction, à la flexion et à la torsion, et ensuite les modules de Young et de cisaillement, ainsi que le coefficient de Poisson des nanotubes de carbone à paroi unique, pour une large gamme des longueurs de nanotubes, d'indices chiraux et de diamètres. Les corrélations entre les rigidités de traction, de flexion et de torsion et le diamètre du nanotube, qui permettent l'évaluation facile de chaque rigidité, sont présentées. Cela permet le développement de méthodologies pour évaluer les modules de Young et de cisaillement et le coefficient de Poisson. Les modèles proposés sont validés à l'aide de résultats numériques et expérimentaux disponibles dans la littérature.

La simulation numérique des propriétés mécaniques des nanotubes de carbone avec des défauts est une activité importante, fournissant des données qui peuvent être comparées aux résultats expérimentaux. Dans ce contexte, une étude systématique des nanotubes de carbone à simple paroi non chiraux et chiraux, qui contiennent des différents pourcentages (jusqu'à 10%) et types de défauts lacunaires, est effectuée sur une large gamme de diamètres. Le module de Young et de cisaillement et le coefficient de Poisson des nanotubes de carbone à paroi unique avec des défauts lacunaires sont évalués en utilisant les méthodologies suggérées dans ce travail. L'évolution des modules de Young et de cisaillement et le coefficient de Poisson avec le pourcentage des lacunes sont analysés.

Enfin, une étude de simulation numérique complète est réalisée pour évaluer les propriétés mécaniques des jonctions hétérogènes des nanotubes de carbone. La modélisation de la réponse mécanique des jonctions hétérogènes des "*armchair* – *armchair*" et "*zigzag* – *zigzag*" (les nanotubes de diamètres différents) permet de clarifier l'effet de la géométrie de la jonction hétérogène (la relation entre les diamètres et les longueurs relatives des nanotubes constitutifs) dans leurs rigidités à la traction, à la flexion et à la torsion, et aux modules de Young et de cisaillement. Des expressions pour l'évaluation facile des rigidités des jonctions hétérogènes basée sur la connaissance de la rigidité des nanotubes de carbone à paroi unique, qui sont ses unités constitutives clés, sont présentées. Cela permet d'évaluer le module de Young et de cisaillement de la jonction hétérogène, en supposant que son diamètre est égal à la valeur moyenne des nanotubes de carbone à paroi unique qui composent la jonction hétérogène.

Mots-clés: Nanotubes de carbone, Jonctions hétérogènes, Propriétés élastiques, Propriétés mécaniques, Simulation numérique.

Contents

Acknowledgements iii

Abstract v

Resumo vii

Résumé ix

Contents xi

List of Figures xiii

List of Tables xv

Acronyms and Symbology xvii

Acronyms xvii

Symbology xviii

Chapter 1

Introduction 1

1.1. Motivation 3

1.2. Objectives and achievements 4

1.3. Outline of the thesis 5

References 7

Chapter 2

Overview on carbon nanotubes and their heterojunctions 9

2.1. Carbon nanotubes and their heterojunctions: basic concepts, structure, properties and applications 11

References 15

2.2. Evaluation of elastic properties of CNTs and their heterojunctions 17

Chapter 3

Finite element modelling and analysis of CNTs' structures 51

3.1. Finite element modelling of carbon nanotube structures 53

3.2. Molecular interactions and equivalent properties of beam elements 55

3.3. FE analysis of CNTs' structures 57
References 63

Chapter 4

Mechanical behaviour of CNTs' structures 65

4.1. Elastic properties of the perfect SWCNTs' structures 67
4.2. Elastic properties of the SWCNTs' structures containing vacancy defects 95
4.3. Modelling and mechanical behaviour of SWCNT HJs 111

Chapter 5

Conclusions and future perspectives 141

5.1. Introduction 143
5.2. Elastic properties of perfect and with defects SWCNTs' structures 143
5.3. Elastic properties of the SWCNT heterojunctions 148
5.4. Future perspectives 150
References 152

Appendix A 153

List of Figures

Figure 2.1. Structural models of armchair and zigzag SWCNTs, obtained by using Nanotube Modeler© software……..12

Figure 2.2. Table describing the Carbon Nanotubes characteristics (free download from http://quantumwise.com/documents/CNT_PeriodicTable.pdf)……..13

Figure 2.3. Different types of intramolecular junctions of CNTs (Wei and Liu, 2008): (a) Y-shaped junction, (b) T-shaped junction, (c) X-shaped junction, (d) ring-like junction, (e) multi-branched junction and (f) 3D network junction……14

Figure 3.1. Finite element meshes for (a) (10,10) armchair, (b) (15,0) zigzag and (c) (15,3) chiral SWCNTs, obtained by using academic software CoNTub 1.0© (Melchor and Dobado, 2004)……54

Figure 3.2. Finite element meshes for (a) (10, 10) – (15, 15) armchair – armchair and (b) (15, 0) – (20, 0) zigzag – zigzag SWCNT HJ, obtained by using academic software CoNTub 1.0© (Melchor and Dobado, 2004)……54

Figure 3.3. Modelling of CNT structure, replacing the C-C bonds by beam elements……59

Figure 3.4. Equivalence between bond interactions in carbon nanotube and beam elements……59

Figure 3.5. Loading and boundary conditions for (20, 20) armchair SWCNT: (a) tension; (b) bending; (c) torsion. ……61

Figure 3.6. Loading and boundary conditions for armchair – armchair (10, 10) – (15, 15) HJ: (a) tension; (b) bending; (c) torsion……62

(Page intentionally left blank)

List of Tables

Table 1.1. Most representative papers published within the scope of the thesis……..6

Table 3.1. Input parameters for FE simulations of CNT structures: geometrical and material properties of beam element……..58

Table 5.1. Fitting parameters α, β, γ and D_0…….....144

Table 5.2. The stabilized values of Young's and shear moduli, and Poisson's ratio of defective SWCNTs for different percentage of the vacancies……..147

(Page intentionally left blank)

Acronyms and Symbology

Acronyms

2D	Two Dimensional
3D	Three Dimensional
AFM	Atomic Force Microscopy
CEMMPRE	Centre for Mechanical Engineering, Materials and Processes
CM	Continuum Mechanics
C-C	Carbon-Carbon
CNT	Carbon Nanotube
CNT HJ	Carbon Nanotubes Heterojunction
ECM	Equivalent Continuum Modelling
DFT	Density Functional Theory
FE	Finite Element
FEA	Finite Element Analysis
HJ	Heterojunction
MD	Molecular Dynamics
MSM	Molecular Structure Mechanics
MWCNT	Multi Walled Carbon Nanotube
NCM	Nanoscale Continuum Modelling
SWCNT	Single-Walled Carbon Nanotube
STM	Scanning Tunnelling Microscopy
SWCNT HJ	Single-Walled Carbon Nanotubes Heterojunction
TBMD	Tight-Binding Molecular Dynamics
TEM	Transmission Electron Microscopy

Symbology

Greek symbols

α^p, α	Fitting parameter (tensile rigidity)
β^p, β	Fitting parameter (bending rigidity)
γ^p, γ	Fitting parameter (torsional rigidity)
$\Delta\beta$	Relative rotation between the ends of the beam
$\Delta\theta$	Bond angle bending variation
$\Delta\phi$	Angle variation of twist bond
$\varepsilon_{\perp}$	Normal strain in tension
$\varepsilon_{\parallel}$	Axial strain in tension
η	Aspect ratio of heterojunction
k_r	Bond stretching force constants
k_θ	Bond bending force constant
k_τ	Torsional resistance force constant
θ	Chiral angle
ν	Poisson's coefficient
φ	Twist angle
τ, α	Rotational angle at the ends of the beam

Roman symbols

A	Cross -sectional area
A_b	Cross -sectional area of beam
$\boldsymbol{a}$	Unit vectors of the hexagonal lattice
a_{C-C}	C-C covalent bond length
$\boldsymbol{C_h}$	Chiral vector
D	Nanotube mean diameter
$\overline{D}_{HJ}$	Heterojunction diameter
D_n	Nanotube diameter
D_0^p, D_0	Fitting parameter (equations for rigidities)
d	Beam diameter
E	Young's modulus

E_b	Young's modulus of beam
E_{HJ}	Young's modulus of heterojunction
EA	Tensile rigidity
E_bA_b	Tensile rigidity of beam
$(EA)_{HJ}$	Tensile rigidity of heterojunction
EI	Bending rigidity of beam
E_bI_b	Bending rigidity
$(EI)_{HJ}$	Bending rigidity of heterojunction
F_a	Axial tensile force
F_t	Transverse force
G	Shear modulus
G_b	Shear modulus of beam
G_{HJ}	Shear modulus of heterojunction
GJ	Torsional rigidity
G_bJ_b	Torsional rigidity of beam
$(GJ)_{HJ}$	Torsional rigidity of heterojunction
I	Moment of inertia
I_b	Moment of inertia of beam
J	Polar moment of inertia
J_b	Polar moment of inertia of beam
L	Nanotube length
L_3	Length of the connecting region of heterojunction
L_c	Nanotube circumference
L_{HJ}	Overall length of heterojunction
l	Beam length
Δl	Axial stretching displacement of beam
M	Pure bending moment (beam)
N	Pure axial force (beam)
(n, m)	Chiral indices
p	Percentage of vacancy defects
Δr	Bond stretching increment
T	Torsion moment

t_n	Nanotube wall thickness
U_A	Strain energy of beam under pure axial force
u_a	Axial displacement
U_M	Strain energy of beam under pure bending moment
U_T	Strain energy of beam under pure torsion moment
u_t	Transverse displacement
U_{tot}	Total inter-atomic potential energy of a molecular system
U_r	Bond stretching energy
U_θ	Bond bending energy
U_ϕ	Dihedral angle energy
U_ω	Out–of-plane torsion energy
U_{vdw}	Van der Waals interaction energy

Chapter 1

Introduction

This chapter regards the motivation for investigating the topics covered in the thesis. The objectives and achievements in the context of the evaluation of the elastic properties of the carbon nanotubes and their heterojunctions by numerical simulation are emphasized. In order to facilitate the readability and comprehension of the thesis, the outline of the text is also presented.

(Page intentionally left blank)

1.1. Motivation

In the past decade, systematic research has been conducted for developing nano-materials, such as carbon nanotubes (CNTs), which are unique nanostructures with extraordinary mechanical, optical, thermal and electrical properties (Saito *et al.*, 1998; Wilson *et al*., 2002; Robertson, 2004). The recent success in growing of carbon nanotube inside boron nitride nanotube with a potential application as the smallest co-axial cable (Walker *et al*., 2017), opens the perspective to create a new generation of heterostructures, where CNTs are the most appropriate constituents. The high stiffness together with low density suggests that the CNTs are optimal structures to reinforce composites and building blocks for optical and electronic nanodevices (Neubauer *et al*., 2010; Lan *et al*., 2011; Zhang *et al*., 2014). From the point of view of construction of nanodevices, the CNT heterojunctions (heterostructures representing two connected nanotubes) are necessary constituents for circuits, amplifiers, switches and nanodiodes (Wei and Liu, 2008). In order to design composites reinforced with CNTs, nanosensors and CNT-based electronic and electromechanical devices, the understanding of the CNTs mechanical properties is indispensable, since the stability and efficiency of nanodevices are highly dependent on the mechanical properties of their components. The carbon nanotubes have been studied experimentally, but a great inconsistency in experimental results has been observed, owing to the experimental difficulties in the characterization of nanomaterials at the atomic scale. For this reason, modelling and computer simulation for predicting the mechanical properties of CNTs have received much attention. The theoretical approaches used can be grouped into three main categories: the atomistic approach (Jin and Yuan, 2003), the continuum modelling (CM) (Pantano *et al*., 2004) and the nanoscale continuum modelling (NCM) (Li and Chou, 2003). The NCM approach, which consists of replacing the carbon-carbon (C-C) bonds by continuum elements (as a beam) was found the most suitable for effective computational simulation (see, for example, Tserpes and Papanikos, 2005; Ghadyani and Öchsner, 2015).

If the experimental studies towards determining of the CNT mechanical properties are constrained by the insufficiency of appropriate direct measuring techniques at

the nanometer scale, the theoretical studies (analytical and numerical) have led to a variety of results due to different modelling approaches and formulations.

The lack of systematic study for predicting the mechanical properties of single-walled carbon nanotubes (SWCNTs) by numerical simulation motivates the current research work. In fact, parametric studies on the effect of the nanotube length, diameter, chirality and wall thickness on the SWCNT elastic properties are scarce. This kind of study can be particularly useful for understanding and modelling the mechanical behaviour of CNT reinforced materials and other complex CNT-based structures.

Moreover, the systematic study will enable to improve the information concerning the influence of the presence and density of the vacancy defects on the SWCNT mechanical properties, which is also a relevant aspect concerning nanotube applications.

Finally, the systematic characterization of the mechanical properties of SWCNTs, which are fundamental structural units for complex structures, such as carbon nanotubes heterojunctions (CNT HJs), leads to the development of additional analyses for the understanding of the mechanical behaviour of these structures, whose study is at an early stage.

1.2. Objectives and achievements

The thesis is focused on the characterisation of mechanical properties of single-walled CNTs, and carbon nanotube heterojunctions by modelling their structure and mechanical behaviour. In this context, the systematic study by numerical simulation of the elastic properties of the single-walled CNT and their heterojunctions for a wide range of nanotube lengths, chiral indices and diameters is highlighted. It is intended resorting to nanoscale continuum modelling approach for modelling the structure of SWCNTs and SWCNT HJs and evaluating their mechanical properties. For this purpose, three-dimensional finite element models of SWCNTs and CNT HJs are intended to be obtained. These models are validated, using cases where numerical and experimental results are accessible in the literature.

Comprehensive studies on the modelling and numerical simulation of the mechanical behaviour under tension, bending and torsion of single-walled carbon nanotubes, without and with vacancies, and their heterojunctions are performed,

and their elastic constants, particularly the Young's and shear moduli, are obtained. The relationships between the rigidities and the nanotube diameter allow the easy evaluation of the Young's modulus and shear modulus of SWCNTs, without resorting to numerical simulation. Also, the mechanical properties of the CNT HJs can be deduced from the knowledge of the mechanical properties of the SWCNTs, which are their constituent key units.

Systematic studies to highlight the influence of the geometry of perfect and with vacancy defects SWCNTs (nanotube length, diameter, chirality, type and geometry of vacancy defect), as well cone-heterojunctions, i.e. HJs of nanotubes with a given chiral angle but different radii (configuration, type, diameters ratio and relative lengths of the constituent nanotubes), on their mechanical properties are carried out. It is intended that this systematic approach allows contributing to the optimization and the interpretation of the experimental procedures for describing the mechanical behaviour of CNTs and their heterojunctions and guiding their manufacturing processes.

1.3. Outline of the thesis

Following this introduction, the thesis consists of four chapters.

Chapter 2 contains the literature review on the accomplishments in the evaluation of the elastic properties of perfect and imperfect (with defects) carbon nanotubes, and carbon nanotube heterojunctions by modelling their structure and mechanical behaviour, using analytical and numerical approaches. This Chapter contains one of the published papers mentioned in **Table 1.1**.

Chapter 3 provides the formulation for the implementation of the NCM approach for modelling of the CNTs' structures mechanical behaviour. The framework of finite element analysis is also presented in this chapter.

Chapter 4 contains the innovative research within the framework of the thesis, concerning numerical simulation studies on the mechanical response of chiral and non-chiral SWCNTs, with and without vacancies, and SWCNT HJs, using NCM approach. This Chapter is essentially a collection of 5 the published papers mentioned in **Table 1.1**.

Chapter 5 contains the conclusions and perspectives for the work to be undertaken in the future.

In the framework of the thesis, six papers have been published as shown in **Table 1.1**: five in international journals indexed in the *ISI – Web of Knowledge*, and one in proceedings of international meeting also indexed in the *ISI – Web of Knowledge*. In this table is also specified the Chapter where the paper is included.

Table 1.1. Most representative papers published within the scope of the thesis.

Reference		Chapter
Sakharova et al., 2017a	**Sakharova NA**, Antunes JM, Pereira AFG, Fernandes JV (2017) Developments in the evaluation of elastic properties of carbon nanotubes and their heterojunctions by numerical simulation. AIMS Materials Science, 4, 706 – 737	Chapter 2, subchapter 2.2
Sakharova et al., 2015	**Sakharova NA**, Pereira AFG, Antunes JM, Brett CMA, Fernandes JV (2015) Mechanical characterization of single-walled carbon nanotubes: Numerical simulation study. Composites B, 75, 73–85	Chapter 4, subchapter 4.1
Pereira et al., 2016	Pereira AFG, Antunes JM, Fernandes JV, **Sakharova NA** (2016) Shear modulus and Poisson's ratio of single-walled carbon nanotubes: numerical evaluation. Physica Status Solidi B, 253, 366 – 376	
Sakharova et al., 2016a	**Sakharova NA**, Pereira AFG, Antunes JM, Fernandes JV (2016) Numerical simulation study of the elastic properties of single-walled carbon nanotubes containing vacancy defects. Composites B, 89, 155 – 168	Chapter 4, subchapter 4.2
Sakharova et al., 2016b	**Sakharova NA**, Pereira AFG, Antunes JM, Fernandes JV (2016) Numerical simulation of the mechanical behaviour of single-walled carbon nanotubes heterojunctions. Journal of Nano Research, 38, 73 – 87	Chapter 4, subchapter 4.3
Sakharova et al., 2017b	**Sakharova NA**, Antunes JM, Pereira AFG, Chaparro BM, Fernandes JV (2017) Elastic properties of carbon nanotubes and their heterojunctions. Proceedings (e-book) of XIV International Conference on Computational Plasticity. Fundamentals and Applications (COMPLAS 2017), Barcelona, Spain, 05-07 September 2017, Ed. by E. Oñate, D.R.J. Owen, D. Peric and M. Chiumenti, p. 963-974	

References

Ghadyani G and Öchsner A (2015) Derivation of a universal estimate for the stiffness of carbon nanotubes. Physica E: Low-dimensional Systems and Nanostructures, 73, 116 – 125.

Jin Y and Yuan FG (2003) Simulation of elastic properties of single-walled carbon nanotubes. Composites Science and Technology, 63, 1507 – 1515.

Neubauer E, Kitzmantel M, Hulman M, Angerer P (2010) Potential and challenges of metal-matrix-composites reinforced with carbon nanofibers and carbon nanotubes. Composites Science and Technology, 70, 2228 – 2236.

Lan Y, Wang Y, Ren ZF (2011) Physics and applications of aligned carbon nanotubes. Advances in Physics, 60, 553 – 678.

Pantano A, Parks DM, Boyce MC (2004) Mechanics of deformation of single- and multi-wall carbon nanotubes. Journal of Mechanics and Physics of Solids, 52, 789 – 821.

Pereira AFG, Antunes JM, Fernandes JV, Sakharova NA (2016) Shear modulus and Poisson's ratio of single-walled carbon nanotubes: numerical evaluation. Physica Status Solidi B, 253, 366 – 376.

Robertson J (2004) Realistic applications of CNTs. Materials Today, 7, 46 – 52.

Saito R, Dresselhaus G, Dresselhaus MS (1998) Physical Properties of Carbon Nanotubes. Imperial College Press, London, UK.

Sakharova NA, Pereira AFG, Antunes JM, Brett CMA, Fernandes JV (2015) Mechanical characterization of single-walled carbon nanotubes: Numerical simulation study. Composites B: Engineering, 75, 73 – 85.

Sakharova NA, Pereira AFG, Antunes JM, Fernandes JV (2016a) Numerical simulation study of the elastic properties of single-walled carbon nanotubes containing vacancy defects. Composites B: Engineering, 89, 155 – 168.

Sakharova NA, Pereira AFG, Antunes JM, Fernandes JV (2016b) Numerical simulation of the mechanical behaviour of single-walled carbon nanotubes heterojunctions. Journal of Nano Research, 38, 73 – 87.

Sakharova NA, Antunes JM, Pereira AFG, Fernandes JV (2017a) Developments in the evaluation of elastic properties of carbon nanotubes and their

heterojunctions by numerical simulation. AIMS Materials Science, 4, 706 – 737.

Sakharova NA, Antunes JM, Pereira AFG, Chaparro BM, Fernandes JV (2017b) Elastic properties of carbon nanotubes and their heterojunctions. Proceedings (e-book) of XIV International Conference on Computational Plasticity. Fundamentals and Applications (COMPLAS 2017), Barcelona, Spain, 05-07 September 2017, Ed. by E. Oñate, D.R.J. Owen, D. Peric and M. Chiumenti, p. 963-974.

Tserpes KI and Papanikos P (2008) Finite element modeling of single-walled carbon nanotubes. Composites B: Engineering, 36, 468 – 477.

Walker KE, Rance GA, Pekker A, Tóháti HM, Fay MW, Lodge RW, Stoppiello CT, Kamarás K, Khlobystov AN (2017) Growth of carbon nanotubes inside boron nitride nanotubes by coalescence of fullerenes: toward the world's smallest coaxial cable. Small Methods, 1, 1700184.

Wei DC and Liu YQ (2008) The intramolecular junctions of carbon nanotubes. Advanced Materials, 20, 2815 – 2841.

Wilson M, Kannagara K, Simmons M, Raguse B (2002) Nanotechnology: Basic Science and Emerging Technologies. Chapman and Hall/CRC Press, Boca Raton, FL, USA.

Zhang Y, Zhuang X, Muthu J, Mabrouki T, Fontaine M, Gong Y, Rabczuka T (2014) Load transfer of graphene/carbon nanotube/polyethylene hybrid nanocomposite by molecular dynamics simulation. Composites: Part B, 63: 27 – 33.

Li C and Chou TW (2003) A structural mechanics approach for the analysis of carbon nanotubes. International Journal of Solids and Structures, 40, 2487 – 2499.

Chapter 2

Overview on carbon nanotubes and their heterojunctions

This chapter summarizes the knowledge regarding the basic concepts, structure, properties and applications of carbon nanotubes and their heterojunctions. It includes the paper by Sakharova *et al*. (2017a), in Subchapter 2.2, which is an overview of the literature on the achievements in the characterisation of mechanical properties of single-walled carbon nanotubes and their heterojunctions by analytical and computational approaches.

(Page intentionally left blank)

2.1. Carbon nanotubes and their heterojunctions: basic concepts, structure, properties and applications

The experimental observation of multi-walled carbon nanotubes (MWCNTs) grown at the cathode, using arc-discharge evaporation method, was initially reported by Iijima (1991). Two years later, Iijima and Ichihashi (Iijima and Ichihashi, 1993) and Bethune and coworkers (Bethune *et al.*, 1993) discovered experimentally single-walled carbon nanotubes (SWCNTs). This outcome was especially important, since the SWCNTs comprising a cylindrical shell with only one atom of thickness can be considered as fundamental structural units (Dresselhaus and Avouris, 2001). These structural units are the building blocks for MWCNTs (multiple coaxial SWCNTs), carbon nanotube heterojunctions (two connected SWCNTs), and other complex CNT-based structures (such as 2D and 3D networks).

Originally, the interest of the research community by CNTs emerged due to their exotic electronic properties (Saito *et al.*, 1998). Nowadays, this interest grows as other extraordinary properties are explored and perspectives are opened for the creation of new materials and structures with unique electronic, optical and mechanical properties for attractive practical applications.

The structure of carbon nanotubes were explored by high resolution Transmission Electron Microscopy (TEM) and Scanning Tunneling Microscopy (STM) techniques (Olk and Heremans, 1994). These experimental studies provided a direct confirmation that the SWCNTs are seamless cylinders obtained from the honeycomb lattice representing a single atomic layer of crystalline graphite. Hexagonal carbon rings compose this hollow cylinder, while the end caps are of pentagonal rings (see **Figure 2.1**). The hexagonal pattern is repeated periodically resulting in the binding of each carbon atom to three neighbouring atoms with covalent bonds (Lau and Hui, 2002). A detailed description of the SWCNTs structure is given in the next subchapter 2.2.

Figure 2.2 provides a summary of the geometric characteristics that describe the SWCNTs structure. The so-called Periodic Table of Carbon Nanotubes in this figure also indicates the electrical properties of each SWCNT that can be metallic, semi-metallic or semiconducting, which influences the potential applications of the CNTs.

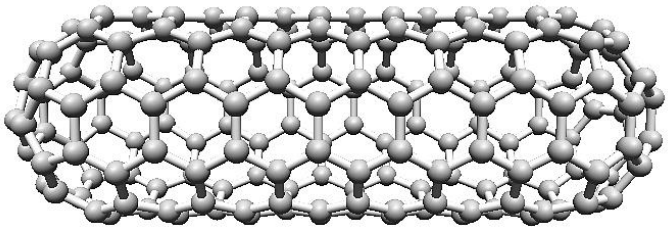

armchair

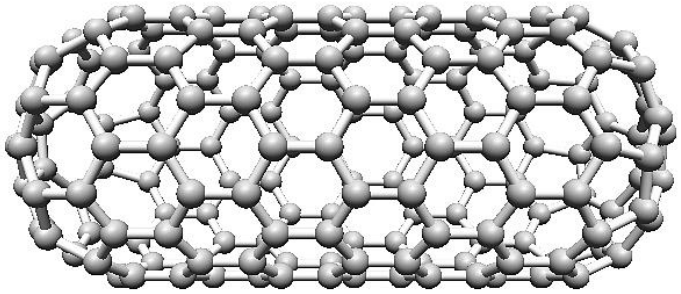

zigzag

Figure 2.1. Structural models of armchair and zigzag SWCNTs, obtained by using Nanotube Modeler© software.

The exceptional carbon – carbon (C-C) bond strength combined with the well-ordered structure of the SWCNTs provides the extraordinary properties of the carbon nanotubes, such as high thermal and electrical conductivity, high tensile strength and flexibility and low thermal expansion coefficient. There are numerous requests that take advantage of these unique properties of CNTs. Among their applications, the following can be highlighted: probe tips for high resolution STM; electron field emitters for low voltage cold cathode, lighting sources, electron microscope sources; energy and hydrogen storage; electronic circuits and interconnectors for nanoscale electronic devices; advanced reinforced composites; air and water filters (Saito, 1998; Wilson *et al*., 2002; Meyyappan, 2004; Reich *et al*., 2004).

An important branch of the investigation concerns the intramolecular junctions of CNTs, which have properties that the isolated CNTs do not fulfil and perspectives of applications in nanodevices. According to Wei and Liu (2008), there are many types of intramolecular junctions of CNTs, such as junctions between two SWCNTs, Y-shaped junctions, T-shaped junctions, X-shaped junctions, multibranched junctions, ring-like junctions, etc. (see, **Figure 2.3**).

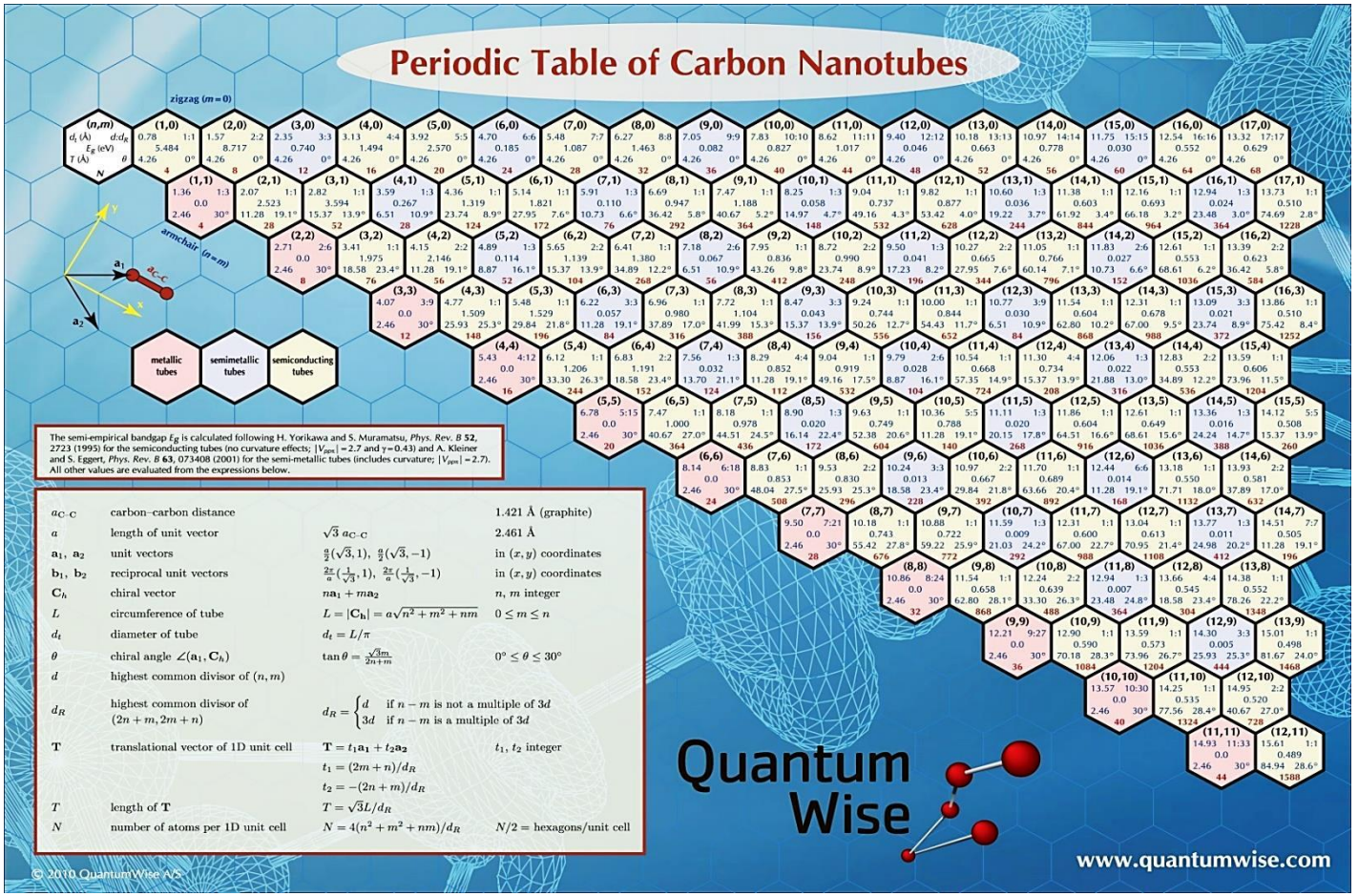

Figure 2.2. Table describing the Carbon Nanotubes characteristics (free download from http://quantumwise.com/documents/CNT_PeriodicTable.pdf)

These junctions can act as functional constituents of circuits, such as rectifiers, switches, amplifiers, and can provide reliable connections between the individual CNTs in order to build stable architectures of CNT-based complex structures. A typical example of CNT intramolecular junction, so-called CNT heterojunction (HJs), can be represented as two SWCNTs of different radii or with different chiral angles that are connected by introducing an intermediate region with Stone–Wales defects (Melchor and Dobado, 2004).

The CNT HJs are regarded as good candidates for nanodevices due their extraordinary properties, electrical (Frajian *et al.,* 1999), optical (Fa *et al.,* 2004), rectifying (Li *et al.,* 2006) and electromechanical (Tombler *et al.*, 2000). In fact, numerous devices have been fabricated based on CNT heterojunctions. The CNT heterojunctions are used in rectifiers (Lee *et al.,* 2004; Li *et al.,* 2007), diodes (Kong and Dai, 2001), quantum devices (Kong, *et al.,* 2002), and photovoltaic devices (Lee, 2005). It is worth to notice that the electromechanical devices are fabricated taking into account that the deformation of CNT HJs can significantly influence their electrical properties (see, for example, Tombler *et al.*, 2000; Sazonova *et al.*, 2004; Hall *et al.*, 2007).

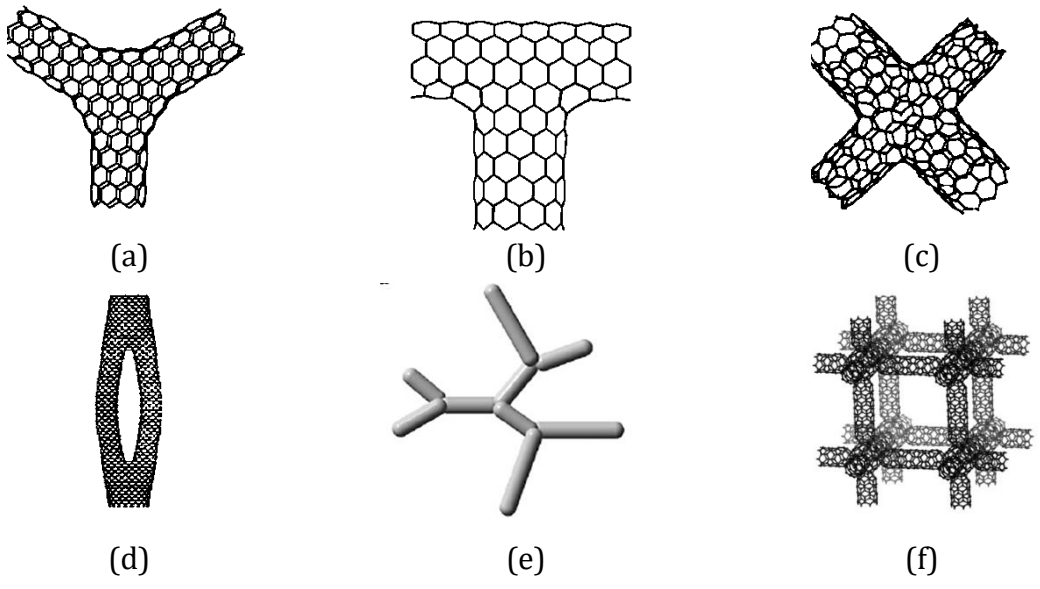

Figure 2.3. Different types of intramolecular junctions of CNTs (Wei and Liu, 2008): (a) Y-shaped junction, (b) T-shaped junction, (c) X-shaped junction, (d) ring-like junction, (e) multi-branched junction and (f) 3D network junction.

References

Bethune DS, Kiang CH, de Vries MS, Gorman G, Savoy R, Vazquez J, Beyers R (1993) Cobalt-catalysed growth of carbon nanotubes with single-atomic-layer walls. Nature, 363, 605 – 607.

Dresselhaus MS and Avouris Ph (2001) Introduction to carbon materials research, in Carbon Nanotubes: Synthesis, Structure, Properties, and Applications. Eds.: Dresselhaus, M. S., Dresselhaus, G., Avouris, Ph., Springer Book Series: Topics in Applied Physics, Springer-Verlag Berlin Heidelberg, Germany, 80, 1 – 9.

Iijima S (1991) Helical microtubules of graphitic carbon. Nature, 354, 56 – 58.

Iijima S and Ichihashi T (1993) Single-shell carbon nanotubes of 1-nm diameter. Nature, 363, 603 – 605.

Fa W, Yang XP, Chen JW, Dong JM (2004) Optical properties of the semiconductor carbon nanotube intramolecular junctions. Physics Letters A, 323, 122 – 131.

Frajian A, Esfarjani K, Kawazoe Y (1999) Nonlinear coherent transport through doped nanotube junctions. Physical Review Letters, 82, 5084 – 5087.

Hall AR, Falvo MR, Superfine R, Washburn S (2007) Electromechanical response of single-walled carbon nanotubes to torsional strain in a self-contained device. Nature Nanotechnology 2, 413 – 416.

Kong J, Cao J, Dai H, Anderson E (2002) Chemical profiling of single nanotubes: Intramolecular p–n–p junctions and on-tube single-electron transistors. Applied Physics Letters, 80, 73 – 75.

Kong J and Dai H (2001) Full and modulated chemical gating of individual carbon nanotubes by organic amine compounds. Journal of Physical Chemistry B, 105, 2890 – 2893.

Lau K-T and Hui D (2002) The revolutionary creation of new advanced materials – carbon nanotube composites. Composites B: Engineering, 33, 263 – 277.

Lee JU, Gipp PP, Heller CM (2004) Carbon nanotube *p-n* junction diodes. Applied Physics Letters, 85, 145 – 147.

Lee JU (2005) Photovoltaic effect in ideal carbon nanotube diodes. Applied Physics Letters, 87, 073101.

Li JQ, Zhang Q, Chan-Park MB (2006) Simulation of carbon nanotube based *p–n* junction diodes. Carbon, 44, 3087 – 3090.

Li YF, Hatakeyama R, Shishido J, Kato T, Kaneko T (2007) Air-stable p-n junction diodes based on single-walled carbon nanotubes encapsulating Fe nanoparticles. Applied Physics Letters, 90, 173127.

Melchor S and Dobado JA (2004) CoNTub: An algorithm for connecting two arbitrary carbon nanotubes. Journal of Chemical Information and Computer Sciences, 44, 1639 – 1646.

Meyyappan M (2004) Carbon Nanotubes: Science and Applications. CRC Press, Boca Raton, FL, USA.

Olk CH and Heremans JP (1994) Scanning tunneling spectroscopy of carbon nanotubes. Journal of Materials Research, 9, 259 – 262.

Reich S, Thomsen C, Maultzsch J (2004) Carbon Nanotubes : Basic Concepts and Physical Properties. Wiley – VCH.

Saito R, Dresselhaus G, Dresselhaus MS (1998) Physical Properties of Carbon Nanotubes. Imperial College Press, London, UK.

Sazonova V, Yaish Y, Ustunel H, Roundy D, Arias TA, McEuen PL (2004) A tunable carbon nanotube electromechanical oscillator. Nature 431, 284 – 287.

Tombler T W, Zhou CW, Alexseyev L, Kong J, Dai HJ, Liu L, Jayanthi CS, Tang M, Wu SY (2000) Reversible electromechanical characteristics of carbon nanotubes underlocal-probe manipulation. Nature, 405, 769 – 772.

Wei DC and Liu YQ (2008) The intramolecular junctions of carbon nanotubes. Advanced Materials, 20, 2815 – 2841.

Wilson M, Kannagara K, Simmons M, Raguse B (2002) Nanotechnology: Basic Science and Emerging Technologies. Chapman and Hall/CRC Press, Boca Raton, FL, USA.

2.2. Evaluation of elastic properties of CNTs and their heterojunctions

This subchapter contains the paper by Sakharova *et al.* (2017a), which gives a brief primer to the atomic structure and geometry of single-walled CNTs and their heterojunctions, and attempts to classify the accomplishments in predicting of the elastic properties of SWCNTs and CNT heterojunctions by analytical and computational approaches.

In the beginning, the work of Sakharova *et al*. (2017a) gives an introduction to the atomic structure and geometry of single-walled CNTs and their heterojunctions. The evaluation of the mechanical properties of CNTs and their structures is one of the most promising fields for mechanics and material science. As it is well-established, there are experimental and computational, approaches commonly used for the characterization of the elastic properties of CNTs. All experimental studies concerning CNTs show their unequalled mechanical properties, but a wide scattering of the results is still observed. The inconsistency in the experimental mechanical results reported in the literature owes to the complexity of the characterization of nanomaterials at the atomic scale, and to the presence of defects in the CNT's structure. Due to these reasons, modelling and computer simulation for predicting the mechanical properties of CNTs have been developed. The paper covers theoretical approaches for modelling and characterizing the CNTs' mechanical behaviour and discusses their applicability and efficacy for understanding the behaviour of CNTs. Also, the accomplishments in predicting of the elastic properties of SWCNTs, with and without vacancy defects, and CNT heterojunctions, using analytical and numerical approaches are systematized. The review of the results regarding elastic properties of the SWCNTs and their heterojunctions is specifically focused on the tensile, bending and torsional rigidities, Young's and shear moduli and Poisson's ratio. This paper already includes results of this thesis, which are shown later on.

It is worth to highlight that among the several approaches discussed in this chapter, the nanoscale continuum modelling proves to be efficient for simulating the mechanical behaviour of CNTs, not requiring extensive computation, which justifies its use in the present work.

(Page intentionally left blank)

AIMS Materials Science, 4(3): 706-737.
DOI: 10.3934/matersci.2017.3.706
Received: 06 March 2017
Accepted: 01 June 2017
Published: 13 June 2017

http://www.aimspress.com/journal/Materials

Review

Developments in the evaluation of elastic properties of carbon nanotubes and their heterojunctions by numerical simulation

Nataliya A. Sakharova [1,*], Jorge M. Antunes [1,2], Andre F. G. Pereira [1], and Jose V. Fernandes [1]

[1] CEMMPRE—Department of Mechanical Engineering, University of Coimbra, Rua Luís Reis Santos, Pinhal de Marrocos, 3030-788 Coimbra, Portugal
[2] Escola Superior de Tecnologia de Abrantes, Instituto Politécnico de Tomar, Rua 17 de Agosto de 1808-2200 Abrantes, Portugal

* **Correspondence:** Email: nataliya.sakharova@dem.uc.pt; Tel: +351-239-790-747.

Abstract: High-tech miniaturization is a strategic area to empower new scientific challenges for which carbon nanotubes are ideal candidates with outstanding electronic, optical and mechanical properties. Carbon nanotubes and their heterojunctions are efficient components for reinforcement of composites, for constructing micro- and nanodevices, and for designing new materials with required electronic and mechanical properties. The carbon nanotubes have been studied experimentally, but a big inconsistency in experimental results has been observed, because of the technical difficulties to operate with nanoscale objects. For this reason, modelling and computer simulation for predicting their mechanical properties have received much attention. This review attempts to classify the accomplishments in predicting of the elastic properties of carbon nanotubes and their heterojunctions by analytical and computational approaches. The literature results concerning Young's modulus, shear modulus and Poisson's ratio of perfect and with defects single-walled and multi-walled carbon nanotubes and their heterojunction are analysed and systematized.

Keywords: carbon nanotubes; heterojunctions; elastic properties; numerical simulation

1. Introduction

For more than two decades, systematic research has been conducted for developing nano-materials such as carbon nanotubes (CNTs) that are unique nanostructures with regard to their mechanical, optical, thermal and electrical properties [1], the latter of which can also be seen as a

prototypical quantum nanowire, where quantum effects influence the electrical transport properties [2]. Carbon nanotubes are optimal structures to reinforce composites, building blocks for optical and electronic nanodevices [3,4,5], and efficient components for designing new materials with required electronic and mechanical properties [6]. From the point of view of construction of nanodevices, the CNT heterojunctions are necessary constituents for the circuits, amplifiers, switches and nanodiodes [7]. In order to design composites reinforced with CNTs, nanosensors and CNT-based electronic devices, the understanding of the CNTs' mechanical properties is indispensable, since the stability and efficiency of nanodevices are highly dependent on the mechanical properties of their components.

There are two approaches commonly used to assess the elastic properties of CNTs: experimental and computational. Experimental methods for measuring the elastic modulus of CNTs, based on *in situ* techniques of atomic force microscopy (AFM) and transmission electron microscopy (TEM) have been established [8–11]. All experimental studies show the unparalleled mechanical properties of CNTs. However, there is inconsistency in the experimental mechanical results reported in the literature, owing to the complexity of the characterization of nanomaterials at the atomic scale. In fact, the experimental studies still show a wide scattering of their results. The reason of the scattering can also be associated with defects in the CNT's structure: it is almost impossible to produce carbon nanotubes with a perfect structure because of the manufacturing constraints. It should be noted, that the lack of perfection of the lattice of the CNTs, used in experimental studies, can influence the results [12,13]. Due to these reasons, modelling and computer simulation for predicting the mechanical properties of CNTs have been developed.

A considerable part of the theoretical investigations has been devoted to the modelling and the evaluation of the elastic properties, mainly Young's modulus, of perfect (without defects) single-walled carbon nanotubes (SWCNTs), as for example [14,15,16]. Less attention has been paid to understanding the mechanical behaviour of SWCNT with defects and nanotube heterojunctions. The building of adequate numerical models of the multi-walled carbon nanotubes (MWCNTs) has also received less analysis so far, in spite of their high level of commercialization.

Two recent review articles have been published under the scope of the work on carbon nanotubes. One, conducted by Rafiee and Moghadam [17], concerns the modelling techniques and simulation of mechanical and thermal properties, buckling and vibrational behaviour of perfect SWCNTs. Moreover, Yengejeh et al. [18] have reviewed the advances in the modelling and numerical characterization of the mechanical properties, buckling and vibrational behaviour of imperfect (with defects) and structurally modified carbon nanotubes, including CNT heterojunctions.

The present work is focused on the achievements in the characterisation of mechanical properties of perfect and imperfect (with defects) single-walled and multi-walled CNTs, as well as CNT heterojunctions (HJs) by modelling their structure and mechanical behaviour, using theoretical (analytical and numerical) approaches.

Following this introduction, the review gives a brief introduction to the atomic structure of CNTs and their heterojunctions. Afterwards, the modelling techniques for characterization of the CNTs' mechanical behaviour are described and the outcomes attained in the evaluation of the elastic properties (Young's and shear moduli, Poisson's ratio) of SWCNTs, MWCNTs and CNT heterojunctions, with and without vacancy defects, are presented and discussed.

2. Atomic Structure of CNTs and Their Heterojunctions

A simple way to describe an ideal single-walled nanotube is as a rolled-up graphene sheet giving rise to a hollow cylinder, whose surface is composed of hexagonal carbon rings (see, for example [19,20]). The hexagonal pattern is repeated periodically, leading to binding of each carbon atom to three neighbouring atoms by covalent bonds. A schematic illustration of an unrolled hexagonal graphene sheet is shown in Figure 1. The symmetry of the atomic structure of a nanotube is characterized by the chirality, which is defined by the chiral vector $\boldsymbol{C_h}$:

$$\boldsymbol{C_h} = n\boldsymbol{a_1} + m\boldsymbol{a_2} \tag{1}$$

where n and m are integers, and $\boldsymbol{a_1}$ and $\boldsymbol{a_2}$ are the unit vectors of the hexagonal lattice.

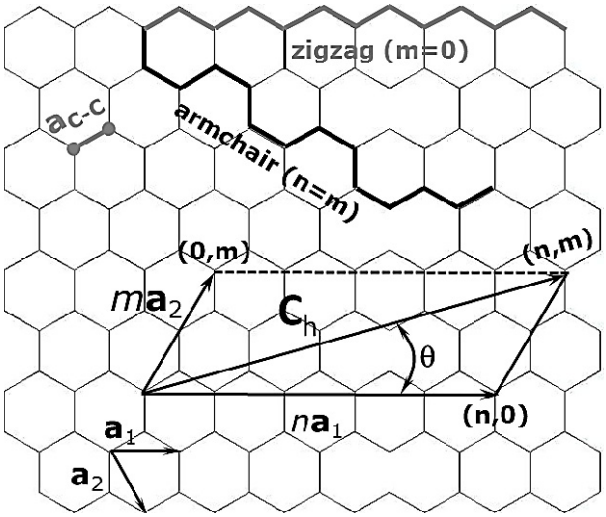

Figure 1. Illustration of an unrolled graphene sheet with definition of the chiral vector.

The length of the unit vector $\boldsymbol{a}$ is defined as $a = \sqrt{3}a_{C-C}$ with the equilibrium carbon–carbon (C–C) covalent bond length a_{C-C} usually taken to be 0.1421 nm [2]. The nanotube circumference, L_c, and diameter, D_n are:

$$L_c = |\boldsymbol{C_h}| = a\sqrt{n^2 + nm + m^2} \tag{2}$$

$$D_n = \frac{L_c}{\pi} \tag{3}$$

The chiral angle, θ, is defined by the angle between the chiral vector $\boldsymbol{C_h}$ and the direction (*n*, *0*). The chiral angle, θ, is given by Dresselhaus et al. [19]:

$$\theta = \sin^{-1}\frac{\sqrt{3}m}{2\sqrt{n^2 + nm + m^2}} \tag{4}$$

Three main symmetry groups of single-walled carbon nanotubes (SWCNTs) exist. When $n = m$, the structure *(n, n)* is called armchair configuration; when $m = 0$, the structure *(n, 0)* is named zigzag; when $n \neq m$, the structure *(n, m)* is chiral. These three major categories of carbon

nanotubes can also be defined based on the chiral angle θ, as can be deduced from Eq. (4). For the two limiting chiral angles of 0° and 30°, the nanotubes are referred to as non-chiral, zigzag and armchair, respectively. For θ different from 0° and 30°, the nanotubes are designated as chiral. Schematic representations of three types of SWCNTs are shown on the Figure 2.

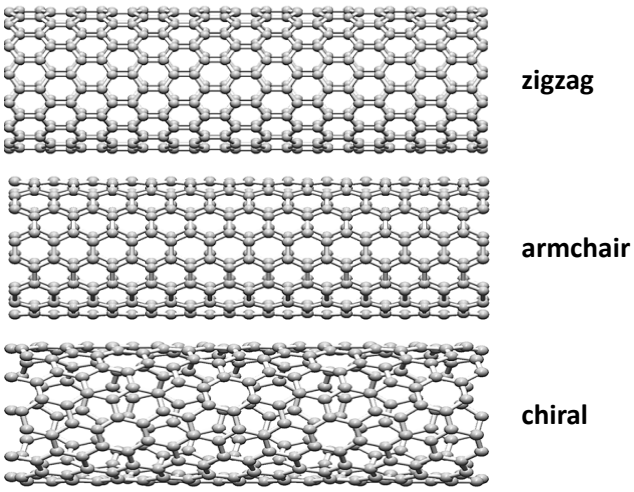

Figure 2. Three structural models of SWCNTs. Obtained by using Nanotube Modeler © software.

The multi-walled carbon nanotubes are composed of multiple coaxial SWCNTs, which interact with each other by non-covalent interactions, the weak van der Waals forces which can be adequately modelled by using the Lennard–Jones potential.

The CNT heterojunction can be represented as two CNTs that are connected by introducing an intermediate region with Stone–Wales defects [21], as illustrated in Figure 3 (Figure 3(a): heptagon defect; Figure 3(b): pentagon defect). Similarly to SWCNT structures, the geometrical parameters of heterojunctions (HJs) are the chirality, and diameter. There are two main heterojunction configurations [21]: (i) cone-heterojunctions (HJs of nanotubes with a given chiral angle but different radii) as armchair–armchair and zigzag–zigzag HJs, and (ii) radius-preserving heterojunctions (HJs preserving the radii, but with different chiral angles of the constituent nanotubes) as armchair–zigzag or chiral–armchair (or zigzag) HJs. Ghavamian et al. [22] also define heterojunctions of armchair–zigzag or chiral–armchair (or zigzag), with different radii, that designate as HJ with bent connection, in contrast to the cone-heterojunctions that they name as HJ with straight connection. According to the study of Yao et al. [23] most HJs (>95%) are cone-heterojunctions type. The geometry of different type of heterojunctions is shown in Figure 4(a–c).

The overall length of the heterojunction is defined as follows:

$$L_{HJ} = L_1 + L_2 + L_3 \tag{5}$$

where L_1, L_2 are the lengths of the narrower and wider SWCNTs regions, respectively, and L_3 is the length of the connecting region (see, Figure 4(a)).

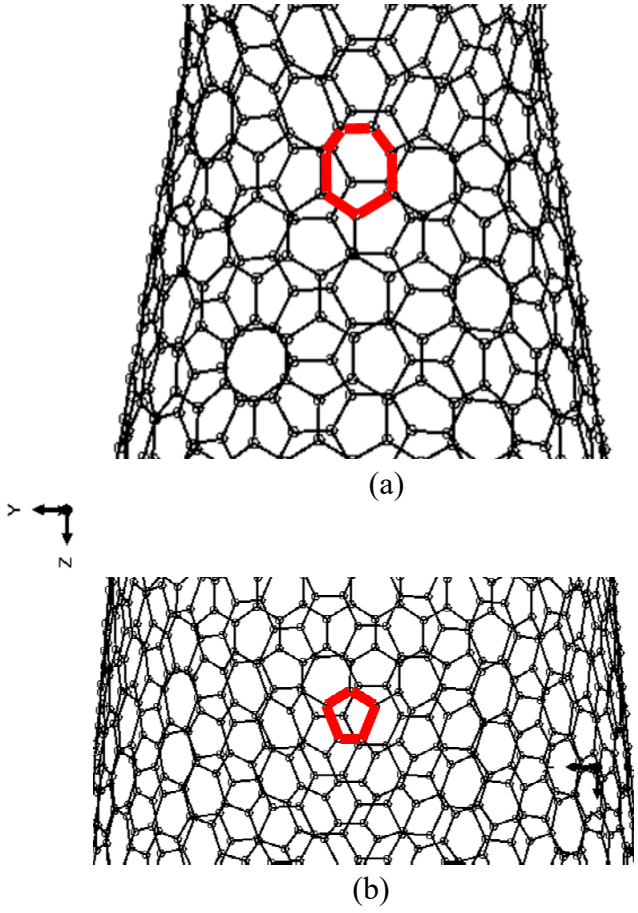

Figure 3. Defects (in bold red) in the connecting region of the armchair–armchair (10, 10)–(20, 20) heterojunction: (a) Heptagon defect; (b) Pentagon defect. HJ is obtained by using academic software CoNTub 1.0 © [21].

When the heterojunction consists of two SWCNTs with different diameters (i.e., cone-heterojunction), the diameter of HJ can be characterised by the average of the narrower and wider diameters (see, for example [21]):

$$\overline{D}_{HJ} = \frac{1}{2}(D_{n1} + D_{n2}) \tag{6}$$

And the aspect ratio of the cone-heterojunction is defined as [24]:

$$\eta = \frac{L_3}{\overline{D}_{HJ}} \tag{7}$$

According to Sakharova et al. [25], the length of the connecting region, L_3, follows a quasi linear function with $(D_{n2} - D_{n1})$, for armchair–armchair and zigzag–zigzag cone-heterojunctions. The fitted straight line equation allows determining L_3 as follows:

$$L_3 = 2.9157(D_{n2} - D_{n1}) \tag{8}$$

where D_{n1} and D_{n2} are diameters of the narrow and wider nanotubes, respectively. Similar relationship for the connecting region of cone-heterojunctions was proposed by Qin et al. [26],

basing on geometrical analysis:

$$L_3 = \frac{\sqrt{3}}{2}\pi(D_{n2} - D_{n1}) = 2.7207(D_{n2} - D_{n1}) \quad (9)$$

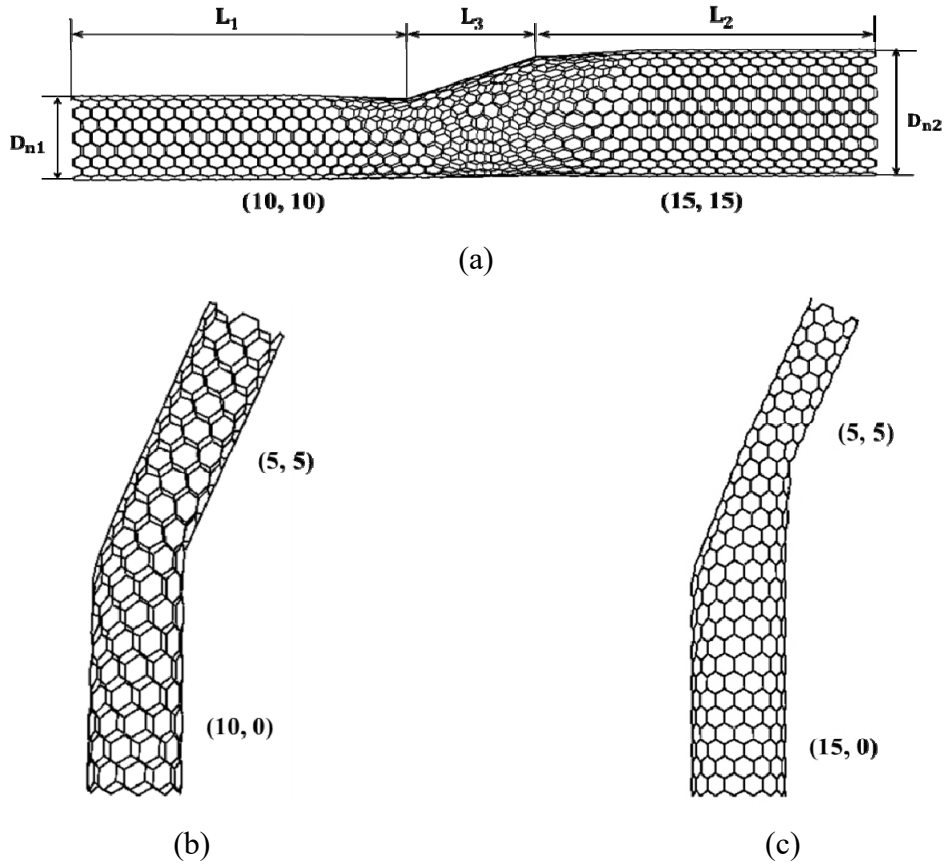

Figure 4. Geometry of (a) cone armchair–armchair (10, 10)–(15, 15) HJ; (b) radius-preserving armchair–zigzag (5, 5)–(10, 0) HJ and (c) armchair–zigzag (5, 5)–(15, 0) HJ with bent connection. HJs structures obtained by using academic software CoNTub 1.0 © [21].

3. Modelling Techniques

The theoretical approaches for the modelling and characterization of the CNTs' mechanical behaviour can be grouped into three main categories: the atomistic approach, the continuum mechanics (CM) approach and the nanoscale continuum modelling (NCM) approach, also called molecular structural mechanics (MSM), as it was firstly introduced by Rafie and Moghadam [17], who discussed the applicability and efficiency of these three approaches toward understanding behaviour of carbon nanotubes.

During the first years of theoretical studies on CNTs, solely atomistic modelling, which calculates the positions of atoms based on their interactive forces and boundary conditions (see, for example, [27]), has been used. Atomistic modelling, used solely during the first years of theoretical studies on CNTs. Atomistic modelling comprises the molecular dynamics (MD) [28–34] and *ab initio* approach [35]. MD is a numerical technique simulating the motions of a system of particles

based on Newton's second law. The key to the MD simulation is to choose an appropriate potential energy model to describe the bonding and nonbonding interactions between carbon atoms in nanotube. These interactions are described by means of analytical or empirical potential functions. Lu [29] employed an empirical force-constant model, where the atomic interactions near the equilibrium structure were approximated by the sum of pairwise harmonic potentials between atoms. Jin and Yuan [30] in their MD simulation adopted force-constant approach, using force potentials to describe the interatomic atomic interactions. In the MD simulation studies of Liew et al. [31] and WenXing et al. [32], the interaction force between atoms was modelled using a second generation reactive empirical bond order (REBO) potential coupled with the Lennard–Jones potential. Yakobson et al. [28] used a many-body interatomic potential (Tersoff–Brenner potential) with a continuum shell model. Zhang et al., [33] compared two MD modelling approaches, using for this purpose the Tersoff–Brenner and modified Morse potentials. The approach of Cheng et al. [34] integrated classical MD simulation with Tersoff–Brenner potential and nanoscale continuum modelling. Wilmes and Pinho [36] proposed a new molecular dynamics finite element method (MDFEM), where the equilibrium equations of MD are embedded within computationally more favourable FE method. Also, tight-binding molecular dynamics (TBMD), another atomistic modelling method, which offers a compromise between *ab initio* methods and MD simulations with empirical potentials, was developed [37,38]. Molecular dynamics can be used in large systems and provide good predictions of CNTs' mechanical properties under different loading conditions, but it is still restricted owing to its being very time consuming, especially when long or multi-walled CNTs are simulated. Generally, *ab initio* methods give more accurate results than MD, but they are highly expensive in terms of computational resources and are limited to be used for a small number of molecules or atoms. In recent years, the atomistic approaches, due to their big computation cost, have been gradually replaced by continuum approaches, which are at the moment the most indicated for effective computational simulation of large systems.

The basic assumption of the continuum mechanics (CM) approach consists of the modelling of CNTs as a continuum structure, concerning the distribution of mass, stiffness, etc., i.e., the real discrete structure of the nanotubes is neglected and replaced by a continuum medium. Some authors have explored continuum shell modelling for studying the mechanical behaviour of CNTs [39–42]. However, the chirality of CNTs is not taken into account in the continuous shell approach, and so its effect on the mechanical behaviour of CNTs cannot be captured. To overcome this obstacle, Chang proposed an anisotropic shell model for SWCNTs [43] that can predict some anisotropic effects, related to chirality. Besides shell structures, other continuum structures, such as tubes and plates, are employed in CM approaches. In the models of Sears and Batra [44], and Gupta and Batra [45] the whole single-walled CNT's structure was simulated as an equivalent continuum tube. Wang [46] employed the equivalent elastic plate model. Arash and Wang [47] show the advantages of the continuum theory applied to the modelling of shells and plates. However, whatever the type of the CM approach, the replacement of the whole CNT's structure by a continuum element is not a completely satisfactory method to evaluate CNT's mechanical properties, because it depends on additionally introduced material properties and it is restricted to certain mechanical behaviours of CNTs [17].

The nanoscale continuum modelling (or molecular structure mechanics: NCM/MSM) approach consists of replacing the carbon–carbon (C–C) bond with a continuum element. As a result, continuum mechanics theories can be used at the nanoscale, i.e., the connection between molecular

configuration and solid mechanics is considered. The NCM/MSM approach consists of considering different elements, such as rod, truss, spring and beam, well described in elasticity theory, to simulate C–C bonds (see, for example, [14,16,48–52]). The first nanoscale continuum model of CNTs was developed by Odegard et al. [48] and consisted of a continuum truss model. The disadvantage of the truss model is the impossibility of describing the CNTs' mechanical behaviour under torsional load, because the out-of-plane torsion of the C–C bond cannot be taken into account. Various FE models where the C–C bonds are simulated using diverse kinds of elastic spring elements, such as linear, non-linear, rotational, torsional, have been recently reported [15,53–59]. Although the use of spring elements is an effective way for simulating the bond angle variations, the accuracy of the determination of the elastic properties depends on the choice of the potential function for the calculation of the force constants.

Since Li and Chou [49] established a direct relationship between the structural mechanics parameters of the beam element and the molecular mechanics parameters, the NCM approach, employing the beam element for replacing the C–C bond, has been successfully used to simulate the mechanical behaviour of CNT, although with different formulations of the inter-atomic molecular potential energies and boundary conditions [14,16,51,52,60–67]. The FE models, which employed beam elements, developed by Tserpes and Papanikos [14], To [60], Papanikos et al. [61], Ávila and Lacerda [62], Sakharova et al. [16], and Ghadyani and Öchsner [67] differ from each other mainly due to the boundary conditions and the method for the Young's modulus calculation. The recent three-dimensional (3D) FE model of Lu and Hu [65] used the same formulation for the potential energy of the covalent system, but considering an elliptical cross-section area of the equivalent beam. In the works of Chen et al. [51] and Eberhardt and Wallmersperger [52] the original Li and Chou [46] model was modified, mainly with respect to the bending rigidity of the beam element. For this purpose, rectangular beam elements with minor and major axes of bending rigidities were considered by Chen et al. [51], for representation of the covalent bonds. Eberhardt and Wallmersperger [52] proposed that the geometrical and material parameters defining the beams can be obtained with the help of a specific modified molecular structural mechanics approach which is consistent in terms of the involved energies. In another analytical approach developed by Shokrieh and Rafiee [63], the deformations of the beam elements were obtained using the Castiglinao's theorem. In the works of Her and Liu [64], and Mohammadpour and Awang [61] the modified Morse potential function for the potential energy of the covalent system was applied for describing the non-linear behaviour of C–C bonds. In their recent work, Giannopoulos et al. [68], who employed linear bar elements to simulate interatomic interactions between carbon atoms, showed the efficiency of this model for the investigation of the stability of CNTs under compressive and radial loads. In contrast to abovementioned works, which used classical truss, spring, bar and beam elements to simulate C–C bond, Nasdala and Ernst [69] developed a special 4-node element for computing internal forces of the molecular system without necessity of the determination of material parameters. In a recent review, Rafiee and Moghadam [17] concluded that NCM is an efficient modelling approach for simulation of the CNT's behaviour, which does not require intensive computation and can be applied to complex systems without limitation of length scales, when comparing with atomistic modelling.

The knowledge of the bond length of CNTs is of fundamental importance for the modelling of their mechanical properties. Its value is generally considered to be equal to that of the graphene sheet, a_{C-C} = 0.1421 nm. Nevertheless other values have been considered: for example, Budyka [70] reported that rolling up the graphene sheet into armchair SWCNT leads to a slight elongation of the

C–C bond. The value of the wall thickness of CNTs is varied in the literature sources. Although a few theoretical reports have provided values for nanotube wall thickness, t_n, that range from 0.064 [40] to 0.69 nm [48], the most widely used value is 0.34 nm (equal to the interlayer spacing of graphite). Most of the elastic properties results, obtained in the theoretical and numerical simulation studies, depend on the assumption of the value of CNT's wall thickness. In recent times, an attempt to acquire a thickness free expression for the CNT's stiffness has been undertaken by Ghadyani and Öchsner [71].

4. Elastic Properties of the Single-walled Carbon Nanotubes

4.1. Rigidities of SWCNTs

Numerical simulation studies related to nanotube rigidities are infrequent in the literature [16,61,72]. The linear relationships between the nanotube elastic rigidities and chiral indices, n, were firstly obtained by Papanikos et al. [61] for non-chiral SWCNTs. Later, in the works of Sakharova et al. [16] and Pereira et al. [72], single equations valid for armchair, zigzag and chiral SWCNTs, which allows correlating the tensile, EA, bending, EI, and torsional, GJ, rigidities of the SWCNT with the nanotube diameter, D_n, were proposed:

$$EA = \alpha(D_n - D_0) \tag{10}$$

$$EI = \beta(D_n - D_0)^3 \tag{11}$$

$$GJ = \gamma(D_n - D_0)^3 \tag{12}$$

The values of the fitting parameters α, β, γ and D_0 obtained in the works [16,72], and those calculated based on the results of the work [61] are summarized in Table 1.

Table 1. Fitting parameters α, β, γ and D_0.

Parameter	Value* [16,72]	Value** [61]
$\alpha, nN \cdot nm^{-1}$	1131.66	1128.15
$\beta, nN \cdot nm^{-1}$	143.48	142.54
$\gamma,\ nN \cdot nm^{-1}$	130.39	135.38
$D_0, nm/n_0$	3.5×10^{-3}	0

* Includes armchair, zigzag and three families, $\theta = 8.9°, 13.9°, 19.1°$, of chiral SWCNTs.

** Includes armchair and zigzag SWCNTs (these values were obtained by equations similar to (10–12), in which n and n_0 replace D_n and D_0, respectively).

The relationships (10–12) and the values of the parameters α, β, γ and D_0, in Table 1, allow easy evaluation of the Young's modulus and the shear modulus as a function of the nanotube diameter [16,72]:

$$E = \frac{\alpha(D_n - D_0)}{\pi t_n \sqrt{8\frac{\beta(D_n - D_0)^2}{\alpha} - t_n^2}} \tag{13}$$

$$G = \frac{\gamma(D_n - D_0)}{2\pi t_n \left(\frac{\beta}{\alpha}\right)\sqrt{8\frac{\beta(D_n - D_0)^2}{\alpha} - t_n^2}} \tag{14}$$

4.2. Young's Modulus of SWCNTs

The results available in the literature, concerning the evaluation of SWCNTs' Young's modulus by different modelling methods, are summarized in Table 2. This table also includes experimental results reported by Krishnan et al. [73], who used thermal vibrations to estimate the Young's modulus, and the results of Yu et al. [74], who used the tensile test. The discrepancies observed between the Young's modulus results are due to different assumptions for the value of the CNT's wall thickness, t_n, (indicated in the Table 2), modelling approaches (MD, CM, NCM/MSM), potential functions, force fields constants, formulations for Young's modulus determinations, etc.

Reviewing the data available in the literature, concerning the prediction of the SWCNTs' elastic moduli, it can be seen that there are some discrepancies not only in the Young's modulus values, but also in the trend of their evolution with the nanotube diameter. This evolution can be separated into two tendencies, as shown in Figure 5: (i) the Young's modulus decreases with increase of the nanotube diameter, and with further increase of the nanotube diameter, the Young's modulus tends towards approximately a constant value [16,33,58,61,75] as shown in Figure 5(a); (ii) the Young's modulus is almost constant over the whole range of nanotube diameters [15,30,32,51,52,62,65,67,68] as shown in Figure 5(b). In some cases the Young's modulus slightly changes for small nanotube diameters [15,51,52,62,65,68]—see Figure 5(b). Concerning the effect of SWCNT's chirality on the Young's modulus, some authors reported similar values for non-chiral and chiral SWCNTs [16,61,75]. A small difference between the Young's modulus for armchair and zigzag SWCNTs is reported by Zhang et al. [31], Chen et al. [51] and Eberhardt and Wallmersperger [52], and for the three SWCNTs' chirality configurations by WengXing et al. [32], Avila and Lacerda [62], Lu and Hu [65], Ghadyani and Öchsner [67] and Giannopoulos et al. [68].

The evolution of the Young's modulus with the wall thickness follows a quasi-linear trend with the inverse of the wall thickness, $1/t_n$ as it was reported by Tserpes and Papanikos [14] and Avila and Lacerda [62], for the case of (8, 8) armchair SWCNT with diameter $D_n = 1.085\,nm$, by Ghadyani and Öchsner [71] for the (10, 10) armchair SWCNT with diameter $D_n = 1.356\,nm$, and by Sakharova et al. [16] for nanotubes with diameter $D_n \gtrsim 1.085\,nm$. In the latter case, for small nanotube diameters, $D_n \lesssim 1.085\,nm$, the deviation from the quasi-linear trend is pronounced for smaller values of $1/t_n$, particularly when the nanotube wall thickness approximates to half of its diameter, $t_n \gtrsim 1/2\,D_n$.

Table 2. Young's modulus results of SWCNTs, available in the literature.

	Reference		t_n, nm	Method	Young's modulus, E, TPa	
Atomistic modelling	[28]	Yakobson et al., 1996	0.066	MD: Tersoff–Brenner potential	5.5	average value
	[29]	Lu, 1997	0.34	MD: empirical force potential	0.97	average value
	[30]	Jin and Yuan, 2003	0.34	MD: force-constant approach	1.236	average value
	[31]	Liew et al., 2004	0.335	MD: REBO empirical potential	1.043	(10, 10) armchair
	[32]	WenXing et al., 2004	0.34	MD: REBO empirical potential	0.929	average value
	[33]	Zhang et al., 2005	0.335	MD: Tersoff–Brenner potential	1.08	converged value; zigzag
	[38]	Cheng et al., 2009	0.34	MD: Tersoff–Brenner potential	1.2	converged value; armchair
	[37]	Hernandez et al., 1998	0.34	TBMD	1.24	(10, 10) armchair
	[35]	Zhou et al., 2000	0.074	TBMD	5.1	average value
	[35]	Kudin et al., 2001	0.089	*ab initio*	3.859	average value
CM	[40]	Pantano et al., 2004	0.075	FE continuum shell model	4.84	average value
	[41]	Sears and Batra, 2004	0.134	Equivalent continuum tube	2.52	(16, 0) zigzag
	[44]	Kalamkarov et al., 2006	0.129	Analytical shell model	1.44	–
	[45]	Gupta and Batra, 2008	0.34	Equivalent continuum tube	0.964	av. value; non-chiral, chiral
NCM/MSM	[48]	Odegard et al., 2002	0.69	FE model: truss elements	0.49	–
	[53]	Natsuki et al., 2004	0.34	Analytical 2D model: springs	0.61	average value
	[54]	Meo and Rossi, 2006	0.34	FE model: non-linear springs and linear torsional springs	0.926	(10, 10) armchair
	[55]	Giannopoulos et al., 2008	0.34	3D FE model: linear springs	1.247	average value
	[58]	Parvaneh and Shariati, 2011	0.34	FE model: linear and non-linear springs	1.170	(22, 0) zigzag
	[15]	Rafiee and Heidarhaei, 2012	0.34	FE model: non-linear springs	1.325	converged value; non-chiral
	[59]	Mahmoudinezhad et al., 2012	0.34	3D FE model: rotational springs	0.85	converged value; armchair
	[49]	Li and Chou, 2003	0.34	3D FE model: linear beams	1.015	average value; non-chiral

NCM/MSM	[14]	Tserpes and Papanikos, 2005	0.147	3D FE model: linear beams	2.377	(8, 8) armchair
	[60]	To, 2006	0.34	3D FE model: linear beams	1.03	(17, 0) zigzag
	[61]	Papanikos et al., 2008	0.34	3D FE model: linear beams	1.072	converged value; non-chiral
	[62]	Ávila and Lacerda, 2008	0.34	3D FE model: linear beams	1.005	av. value; non-chiral, chiral
	[63]	Shokrieh and Rafiee, 2010	0.33	Analytical model: beams	1.042	converged value; armchair
	[51]	Cheng et al., 2010	–	Analytical model: rectangular beams	1.083	(24, 24) armchair
	[66]	Mohammadpour and Awang, 2011	0.147	FE model: nonlinear beams; Morse potential	2.037	(10, 10) armchair
	[64]	Her and Liu, 2012	0.34	FE model: nonlinear beams; Morse potential	0.927	(10, 10) armchair
	[65]	Lu and Hu, 2012	0.34	3D FE model: elliptical cross section beams	1.058	converged value; zigzag
	[68]	Giannopoulos et al., 2013	0.34	3D FE model: linear bar elements	1.347	converged value
	[67]	Ghadyani and Öchsner, 2015	0.34	3D FE model: linear beams	1.053	converged value; zigzag
	[52]	Eberhardt and Wallmersperger, 2015	0.34	3D FE model: tetrahedrons formed by beams	0.803	converged value; non-chiral
	[16]	Sakharova et al., 2015	0.34	3D FE model: linear beams	1.078	converged average value; non-chiral and chiral
Experimental	[73]	Krishnan et al., 1998	–	TEM, thermal vibrations	1.3 (−0.4/ +0.6)	average value; D_n in the range of $1.0 - 1.5\ nm$
	[74]	Yu et al., 2000	–	AFM, tensile test	1.0	average value

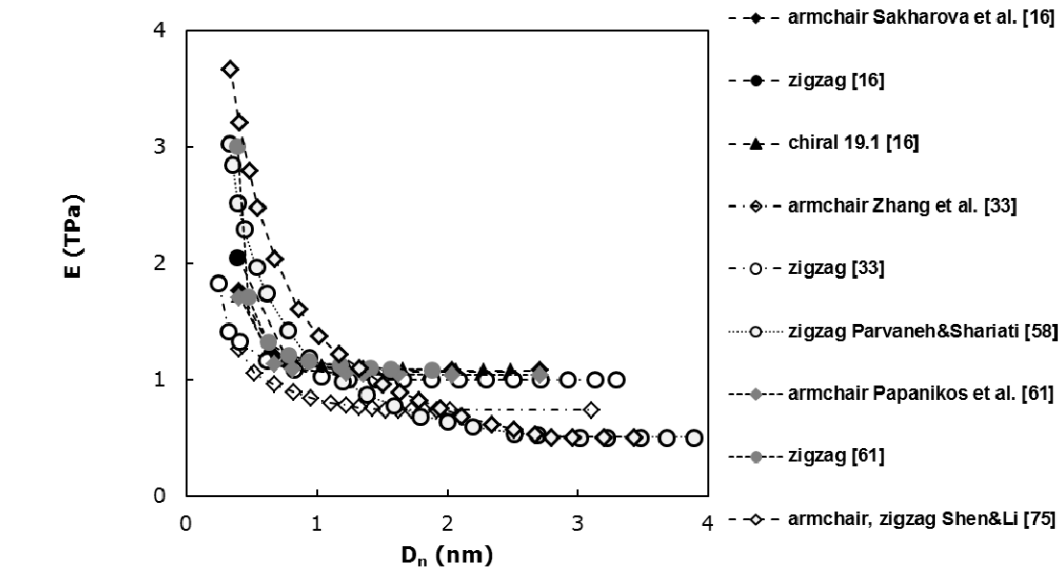

(a)

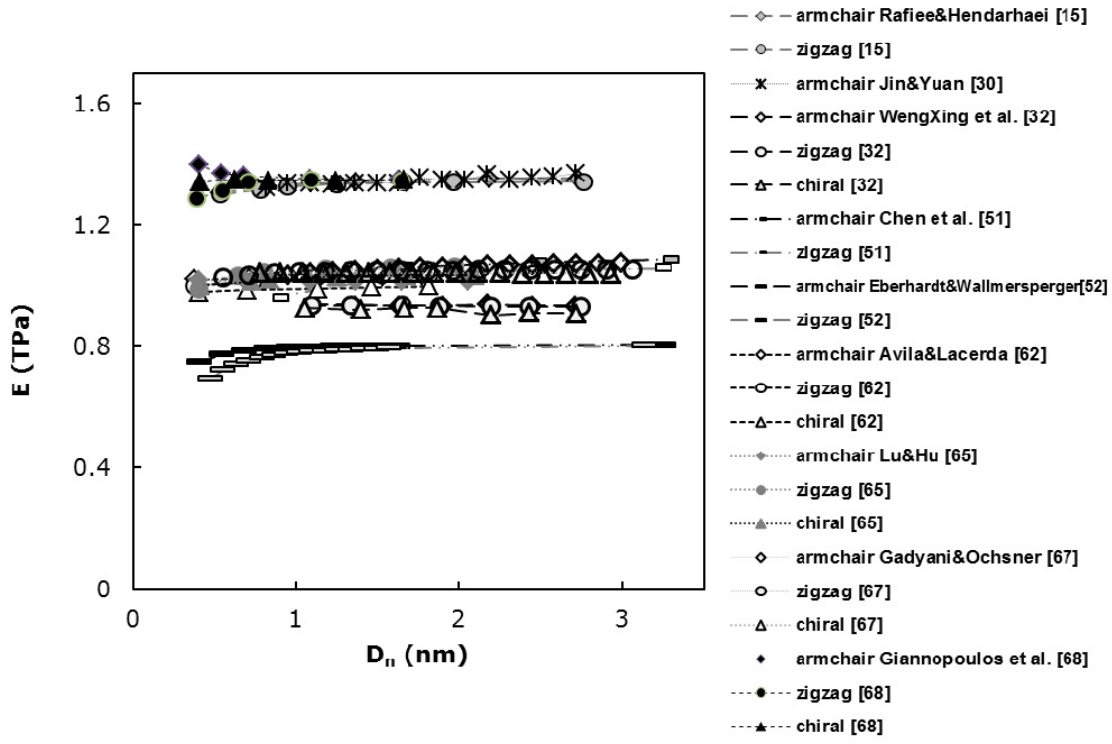

(b)

Figure 5. Literature results for the Young's modulus of SWCNTs. (a) and (b) show two different trends for the evolution of the Young's modulus E, with respect to the nanotube diameter, D_n.

4.3. Shear Modulus and Poisson's Ratio of SWCNTs

The works dealing with the evaluation of the shear modulus are scarcer than the ones determining the Young's modulus. It can be concluded from the available studies that there are two methods commonly used to evaluate the CNTs' shear modulus. One of them consists of the direct

determination of the shear modulus, from numerical simulation results of the torsion tests [30,45,50,55,60,61,65,68,76] or using analytical models that describe the torsional response [53,77,78]. The other method to assess the CNTs' shear modulus uses the results of the tensile test and resorts to the relationship between the Young's modulus and the Poisson's ratio, under isotropic conditions [30,50,75,79]. Only a few works compare results of the shear modulus, obtained by torsion and tensile tests [30,50,72]. A robust methodology for evaluating the shear modulus from results of tensile, bending and torsion tests was proposed by Pereira et al. [72].

Table 3 summarizes the numerical and analytical shear modulus results available in the literature. The only experimental result reported in the literature [8], to the best of our knowledge, was obtained by electrostatic torsion and is also shown in the Table 3. The discrepancies observed between the shear modulus values available in the literature are due to the same type of reasons above specified for the Young's modulus results: different assumptions for the value of the CNT's wall thickness, t_n, (indicated in the Table 3), modelling approaches (MD, CM, NCM), potential functions, force fields constants and formulations for shear modulus determinations. Figure 6 shows the evolutions of the shear modulus value with the nanotube diameter, D_n. In cases of Figure 6(a), the shear modulus decreases with increasing the nanotube diameter, and with further increase of the nanotube diameter, the shear modulus tends towards approximately a constant value [33,53,61,72]; in Figure 6(b) the shear modulus mainly increases with increasing the nanotube diameter [14,29,30,45,51,60,68,76,77].

Although several studies regarding the Poisson's ratio of SWCNTs have been carried out [29,30,45,52,62,72,75,77,78,80], there is still no commonly accepted value. The most common values reported in the literature are in range 0.1–0.3 (see, for example, [30,52,53,72,75,77]), but values of 0.64 [81], 0.66 [62] and close to zero [63,80] are also reported. Most authors [29,30,53,62,75,77,78,80] used the definition of Poisson's ratio for its evaluation. This requires the knowledge of the axial, $\varepsilon_{\parallel}$, and normal $\varepsilon_{\perp}$ strains in tension, as follows:

$$\nu = -\frac{\varepsilon_{\perp}}{\varepsilon_{\parallel}} \tag{15}$$

Recently, a robust methodology to assess Poisson's ratio from the results of the bending and torsion rigidities was recommended recently by Pereira et al. [65].

Figure 7 and Table 4 allow comparing the Poisson's ratio results currently available in the literature. Table 4 contains the comprehensive information on the methodology and formulation used for assessing the Poisson's ratio. Whenever possible, Table 4 also refers to whether or not it agree with the relationship $G = E\,/\,[2(1+\nu)]$, for isotropic conditions. Figure 7 and Table 4 show that the Poisson's ratio is very sensitive to different modelling approaches, analytical or numerical simulation methods, force fields constants used and formulation for Poisson's ratio assessment. For example, Dominguez-Rodriguez et al. [80] attributed the difference between the values of the Poisson's ratio obtained by the equivalent beam approach and density functional theory (DFT), to the input values of the force field constants (k_r, k_θ) in the numerical simulations. Nevertheless, the evaluation of the Poisson's ratio from the results of the tensile and torsion elastic moduli (E and G), by using the relationship $G = E\,/\,[2(1+\nu)]$, allows obtaining values similar to those determined by Eq. (15). Figure 7 also allows comparing the evolution of the Poisson's ratio value with the nanotube diameter, D_n, reported in the literature.

Table 3. Shear modulus results of SWCNTs, available in the literature.

	Reference		t_n, nm	Method	Test	Shear modulus, G, TPa	
MD	[29]	Lu, 1997	0.34	empirical force potential	tensile	0.455	av. value; non-chiral, chiral
	[30]	Jin and Yuan, 2003	0.34	force-constant approach	torsion	0.492	average value; armchair
					tensile	0.491	
				energy approach	torsion	0.547	
					tensile	0.536	
CM	[45]	Gupta and Batra, 2008	0.34	Equivalent continuum tube	torsional vibrations	0.403	av. value; non-chiral, chiral
NCM/MSM	[53]	Natsuki et al., 2004	0.34	Analytical 2D model: springs	torsion	0.300	average value; non-chiral
	[49]	Li and Chou, 2003	0.34	3D FE model: linear beams	torsion	0.480	average value; non-chiral
	[75]	Shen and Li, 2004	–	Analytical model	torsion	0.439	converged value; non-chiral
	[77]	Xiao et al., 2005	0.34	Analytical model	torsion	0.470	converged value; non-chiral
	[14]	Tserpes and Papanikos, 2005	0.147	3D FE model: linear beams	torsion	2.377	(8, 8) armchair
	[78]	Wu et al., 2006	0.268	Analytical model	torsion	0.418	converged value; non-chiral
	[60]	To, 2006	0.34	3D FE model: linear beams	torsion	0.475	(17, 0) zigzag
	[55]	Giannopoulos et al., 2008	0.34	3D FE model: linear springs	torsion	0.325	average value
	[61]	Papanikos et al., 2008	0.34	3D FE model: linear beams	torsion	0.509	converged value; non-chiral
	[51]	Cheng et al., 2010	–	Analytical model: rectangular beams	torsion	0.427	(24, 24) armchair
	[65]	Lu and Hu, 2012	0.34	3D FE model: elliptical cross section beams	torsion	0.469	(18, 18) armchair
	[68]	Giannopoulos et al., 2013	0.34	3D FE model: linear bars	torsion	0.327	converged value
	[50]	Ghavamian et al., 2013	0.34	3D FE model: linear beams	tensile	0.378	(10, 10) armchair
					torsion	0.500	
	[72]	Pereira et al., 2016	0.34	3D FE model: linear beams	tensile + bending + torsion	0.484	converged value; non-chiral, chiral
Exp	[9]	Hall et al., 2006	–	SEM	electrostatic torsion	0.410	unidentified type

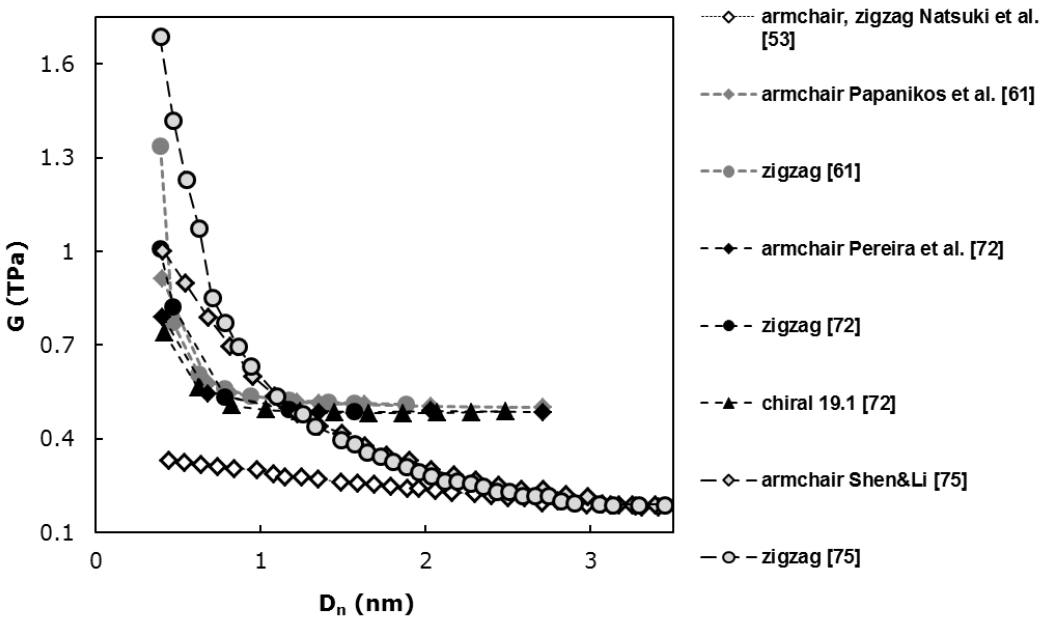

(a)

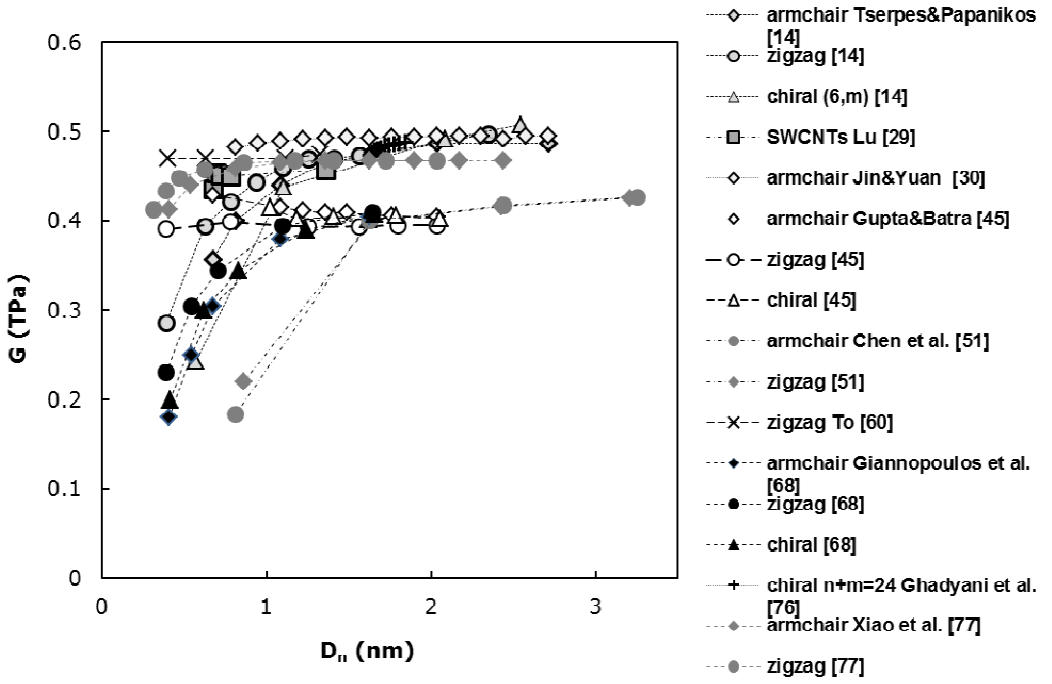

(b)

Figure 6. Literature results for the shear modulus of SWCNTs; (a) and (b) show two different trends for the evolution of the shear modulus G, with respect to the nanotube diameter, D_n.

Table 4. Poisson's ratio of SWCNTs, available in the literature.

	Reference		Method	Test	Formulation	Poisson's ratio, ν	
Atomistic approach	[27]	Lu, 1997	MD: empirical force potential	tensile	$\nu = -\varepsilon_{\perp}/\varepsilon_{\parallel}$	0.278**	average value; non-chiral, chiral
	[28]	Jin and Yuan, 2003	MD	tensile	$\nu = -\varepsilon_{\perp}/\varepsilon_{\parallel}$	0.259*	average value; armchair
	[73]	Domínguez-Rodríguez et al., 2014	*ab initio* (DFT)	tensile	$\nu = -\varepsilon_{\perp}/\varepsilon_{\parallel}$	0.185	average value; armchair
CM	[42]	Gupta and Batra, 2008	Equivalent continuum tube	axial + torsional vibrations	normal mode vibration	0.140–0.249*	non-chiral, chiral
NCM/MSM	[48]	Natsuki et al., 2004	Analytical 2D model: springs	tensile	$\nu = -\varepsilon_{\perp}/\varepsilon_{\parallel}$	0.27**	non-chiral
	[68]	Shen and Li, 2004	Analytical model	tensile	$\nu = -\varepsilon_{\perp}/\varepsilon_{\parallel}$	0.16**	converged value; non-chiral
	[70]	Xiao et al., 2005	Analytical model	tensile	$\nu = -\varepsilon_{\perp}/\varepsilon_{\parallel}$	0.2*	converged value; non-chiral
	[71]	Wu et al., 2006	Analytical model	tensile	$\nu = -\varepsilon_{\perp}/\varepsilon_{\parallel}$	0.273*	converged value; non-chiral
	[56]	Papanikos et al., 2008	3D FE model: linear beams	bending + torsion	$\nu = (\beta^*/\gamma^*) - 1$	0.056** 0.049**	armchair zigzag
	[57]	Ávila and Lacerda, 2008	3D FE model: linear beams	tensile	$\nu = -\varepsilon_{\perp}/\varepsilon_{\parallel}$	0.15–0.29	average value; non-chiral, chiral
	[73]	Domínguez-Rodríguez et al., 2014	3D FE model: linear beams	tensile	$\nu = -\varepsilon_{\perp}/\varepsilon_{\parallel}$	0.061	average value; armchair
	[52]	Eberhardt and Wallmersperger, 2015	3D FE model: tetrahedrons formed by beams	tensile	$\nu = -\varepsilon_{\perp}/\varepsilon_{\parallel}$	0.274	average value; non-chiral
	[72]	Pereira et al., 2016	3D FE model: linear beams	bending + torsion	$\nu = (EI/GJ) - 1$ $\nu = (\beta/\gamma) - 1$ (see Eqs. 10–12)	0.10*	converged value; non-chiral, chiral

β^* and γ^* relate the bending and torsion rigidities, respectively, with the chiral index, n by cubic equations: $EI = \beta^*(n - n_0)^3$ and $GJ = \gamma^*(n - n_0)^3$.

* ν value satisfies the relationship $G = E/[2(1 + \nu)]$.

** ν value does not satisfy the relationship $G = E/[2(1 + \nu)]$.

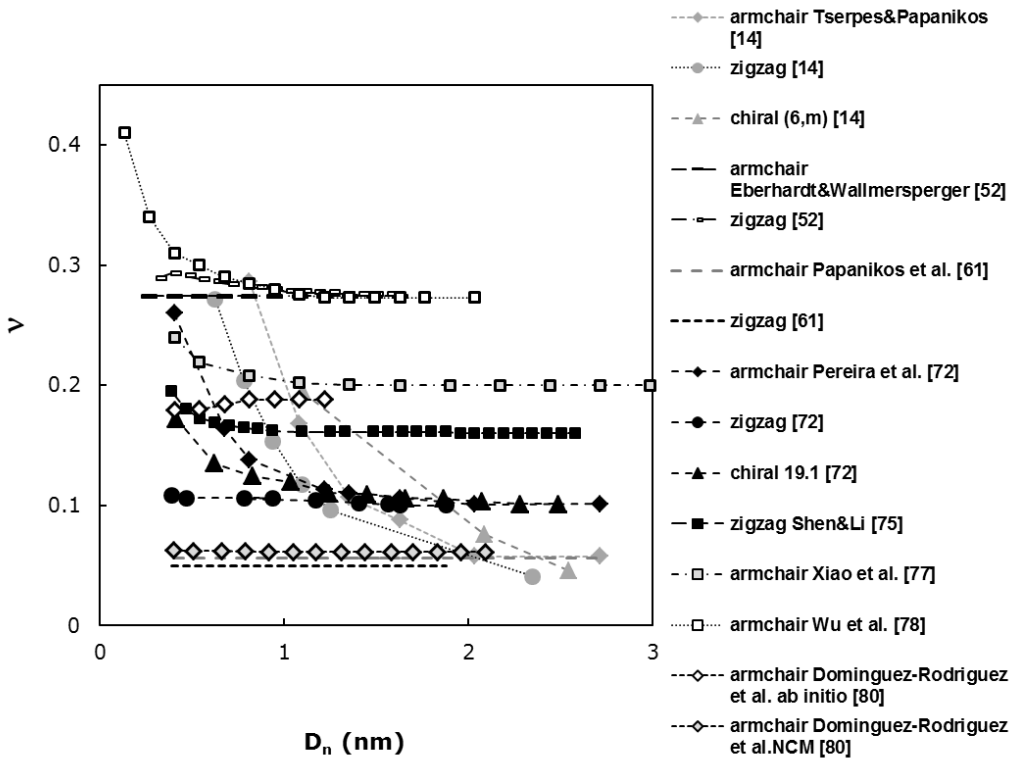

Figure 7. Literature results for the evolution of the Poisson's ratio, ν, with respect to the nanotube diameter, D_n.

4.4. Elastic Properties of SWCNTs with Vacancy Defects

The defects of the CNT's structure, such as single and multiple vacancies, show suitable effects for numerous applications of nanotubes. CNT's vacancy defects act as interfacial bonding places in reinforced nanocomposites, as storage of hydrogen and help the transition from one diameter to another in nanotube heterojunctions. The defects in CNTs are mainly due to their chemical synthesis [82] and to their chemical treatment in the purification process [83], or when the CNTs are subjected to irradiation [84].

In recent years, numerical studies regarding the effect of the defects on the CNT's mechanical properties have been carried out. For example, Scarpa et al. [85], Parvaneh and Shariati [58], Parvaneh et al. [86], Rahmandoust and Öchsner [87], Ghavamian et al. [88], Ghavamian and Öchsner [89,90], Poelma et al. [91], Sakharova et al. [92,93], Wong [94], Rafiee and Pourazizi [95], Zhang et al. [96] and Rafiee and Mahdavi [97] performed the simulations of the elastic behaviour of SWCNTs with vacancy defects; these defects consist in the absence of carbon atoms and their bonds. Other authors have reconstructed the C–C bonds near the atoms removed to form new bonds, as for example, Sharma et al. [98], Saxena and Lal [99] and Yuan and Liew [100].

The influence of vacancy defects on the Young's modulus has been extensively studied. The studies of Scarpa et al. [85], Parvaneh and Shariati [58], Parvaneh et al. [86], Rafiee and Pourazizi [95], Zhang et al. [96], Rafiee and Mahdavi [97], Sharma et al. [98], and Saxena and Lal [99] relate to a few specific types of nanotubes and vacancies, and also to relatively small

percentages of defects (less than 2.5% or in terms of the number of vacancies, up to 6).

Wong [94] considered a high number of the vacancies with several configurations, reaching a defect composed of twelve single vacancies together. Yuan and Liew [100] studied two types of vacancies (single and double ones) with percentages up to 8.0%. The studies of Sakharova et al. [92,93] have contributed to the understanding of the influence of the large amount (up to 10%) of different types of vacancies (single, double, triple and four single vacancies together) on the elastic properties of non-chiral and chiral SWCNTs, over a wide range of diameters.

The reduction of the Young's modulus observed in nanotubes with defects is a common result of the conducted studies. Several authors reported an approximately linear trend of the decreasing of Young's modulus with increasing of the number of vacancies (see, for example [87,88,92,96,97]. The literature results regarding the Young's modulus of defective SWCNTs are shown in the Table 5.

Also other SWCNTs' mechanical properties are deteriorated in presence of the vacancy defects. The studies of Ghavamian and Öchsner [89,90] showed that the presence of 0.5 and 1.0% of vacancy defects in the armchair and zigzag single-walled and multi-walled CNTs leads to a significant decrease of the CNT's critical buckling load [89] and natural frequencies [90]. Poelma et al. [91] found that the position of the single vacancy defect significantly influences the critical buckling load of the SWCNTs at low temperatures. The study of Wong [94] showed a drop of the ultimate tensile strength and the tensile failure strain when the number of vacancies increases in the armchair and zigzag SWCNTs, especially when the vacancies are situated along the cross-section of the nanotube. Saxena and Lal [99], and Sharma et al. [98] found, that the presence of vacancy defects reduces the tensile and compressive strengths, and failure strain of the nanotube. Zhang et al. [96] showed that the presence of double vacancy defect can deteriorate the radial mechanical properties of SWCNTs, reducing the collapse pressure.

For studying the fracture behaviour, some authors [12,13,101] have chosen to rebuild the C–C bonds around the atoms removed. Among their findings, a substantial reduction of the nanotube strength [13,101] and failure stresses and strains [12] should be pointed out.

5. Modelling and Elastic Properties of Multi-walled Carbon Nanotubes

In recent years, the research interest has also been focused on multi-walled carbon nanotubes (MWCNTs), i.e., structures formed by two or more concentric SWCNTs, because of their outstanding mechanical properties which can be advantageous for the improvement of structural composites and due to their high level of commercialization [102]. MWCNTs are comprised of 2 to 50 coaxial SWCNTs with an interlayer spacing generally considered similar to the interlayer spacing of graphene, 0.34 nm. The most common values experimentally determined for the interlayer distance are close to this value. For example, Kharissova and Kharisov [103] and Kiang et al. [104] reported values in the ranges of 0.32–0.35 nm and 0.342–0.375 nm, respectively. The diameter of MWCNTs can attain 30 nm in contrast to 0.7–2.0 nm for typical SWCNTs.

In spite of numerous numerical simulation studies performed towards the evaluation of the mechanical properties of carbon nanotubes, the modelling and numerical characterization of MWCNTs have received less research attention compared to SWCNTs. The essential difference between the simulation of SWCNTs and MWCNTs is to consider, in the simulation of the latter, the non-covalent weak van der Waals force. This requires significant modelling and computing efforts. The first simulations taking into account the van der Waals force were performed by Li and Chou [105],

introducing a nonlinear truss rod model in their study on the elastic behaviour of multi-walled carbon nanotubes with up to 4 layers under tension and torsion. This model comprises the complex mesh of the truss rods in addition to the beam element mesh for the simulation of each SWCNT composing the MWCNT. The studies that followed this work seek to simplify the MWCNT modelling technique. To this end, Kalmakarov et al. [41] recommended a massless non-linear spring element for the van der Waals force simulation. Also, several MWCNT's models with up to 5 layers using spring elements to describe the van der Waals interactions were successfully developed by Rahmandoust and Öchsner [79] and Ghavamian et al. [50,88]. Rahmandoust and Öchsner [79] concluded that the modelling of the van der Waals interactions between atoms of neighbour layers (SWCNTs) of the MWCNTs is not necessary in the case of uniaxial tensile test, because the MWCNT's models, whether or not taking into account the van der Waals force, showed similar Young's modulus results. In case of torsion test, a difference in the shear modulus values of about 9.0% is observed between results obtained with and without the van der Waals interactions. In their finite element model of double-walled carbon nanotubes, Fan et al. [106] proposed an interlayer pressure to model the van der Waals interaction. The mentioned models help to save the computing effort and show reasonable agreement with the results in the literature. Besides springs, other elements were tested to model the van der Waals force; for example, beam elements were used by Nahas and Abd-Rabou [107] to simulate not only the covalent C–C bonds but also the van der Waals force between layers, in double- and triple-walled CNTs. Recently, Sakharova et al. [108] have employed a simplified finite element model of MWCNTs without taking into account the van der Waals forces, but with boundary conditions allowing the simultaneous deformation of all the SWCNTs that constitute the respective MWCNT. With the help of this model, a systematic evaluation of the Young's modulus of non-chiral MWCNTs with up to 10 layers was carried out [108], from tensile and bending tests. The Young's modulus values obtained in their work [108] were in good agreement with the results available in the literature, where the van der Waals interactions were taken into account. The elastic moduli results for MWCNTs available in the literature are presented in the Table 6. In most cases, the Young's modulus and the shear modulus were calculated from the numerical results of the conventional tensile [41,50,88,105,106,107] and torsion [41,50,105,106] tests, using the respective definitions from the classical theory of elasticity. Sakharova et al. [107] evaluated the MWCNTs' Young's modulus from the values of the tensile and bending rigidities. With regard to the boundary conditions, the simulation of the MWCNT's tensile test, in the works [41,50,105,106], was achieved by subjecting all nodes at one end to the same axial force, while all nodes at the other end were fixed. In the simulation of torsion tests, Kalmakarov et al. [41] and Fan et al. [106] applied a torsional moment to all end nodes of multi-walled nanotube, when in the study of Li and Chou [105] only the outer layer of MWCNT was subjected to torsion. Ghavamian et al. [50,88], in tensile and torsion tests, Nahas and Abd-Rabou [107], in tensile tests, and Sakharova et al. [108], in tensile and bending tests, applied displacements, instead of forces or moments, to all nodes at one end of the MWCNT, leaving the other end fixed. Figure 8 compares the evolutions of the Young's modulus and shear modulus with the number of layers, N, constituting the MWCNTs.

Table 5. Results available in the literature on the reduction of the elastic moduli of SWCNTs due to vacancy defects.

Reference		Method	Numb./ percentage vac.	C–C bond reconstruction	Vac. configuration	SWCNT	E_{red} (%)	G_{red} (%)	Comments
[100]	Yuan and Liew, 2009	*ab initio* (DFT)	2.5% 8.0% 2.2% 8.5%	yes	single double	armchair (5, 5) armchair (10, 10)	≈18.0 ≈31.0 ≈21.0 ≈36.0	–	Young's modulus decreases with different rates with respect to the number of vacancy defects
[94]	Wong, 2010	MD: Tersoff–Brenner (TB) potential	8 16	no	single double 12 vac. cluster	zigzag (8, 0) armchair (10, 10)	≈12.0 ≈8.0	–	Approximately linear reduction of Young's modulus; vacancy location along the axial direction.
[58]	Parvaneh and Shariati, 2011	NCM: linear and non-linear springs	1.0% 1.25%	yes	single double triple	armchair (7, 7) zigzag (12, 0)	≈6.6 ≈8.2	–	The vacancy configuration does not influence the results.
[99]	Saxena and Lal, 2012	MD: COMPASS potential	1 4	no	single	armchair (6, 6), (10, 10)	0.9 5.09	–	Non-linear reduction of Young's modulus
[88]	Ghavamian et al., 2012	NCM: linear beams	0.5% 1.0%	no	single	armchair (10, 10) zigzag (14, 0)	≈3.8 ≈7.7	–	Linear reduction of Young's modulus: E_{red} = 7.69 Vac%.
[98]	Sharma et al., 2014	MD: COMPASS potential	1 4	yes	single	armchair (4, 4)	≈6.0 ≈17.0	≈8.0 ≈40.0	Non-linear reduction of elastic moduli.
[95]	Rafiee and Pourazizi, 2014	NCM: linear beams	1.0% 2.0%	no	single	armchair (5, 5), (7, 7) zigzag (0, 9), (0,12)	≈6.0 ≈12.0	–	Reduction of Young's modulus does not depend on the SWCNTs.
[97]	Rafiee and Mahdavi, 2016	MD: TB potential MD: REBO potential	6 6	no	single	armchair zigzag armchair zigzag	3.44 10.05 3.75 10.21	–	Approximately linear reduction of Young's modulus.
[92]	Sakharova et al., 2016	NCM: linear beams	5% 10%	no	single double triple 4 vac. cluster	non-chiral and chiral $D_n = 0.414 \div 2.713\ nm$	≈36.0 ≈43.0	≈44.0 ≈33.0	Linear reduction of both moduli up to 5% of vacancy defects: E_{red} = 7.12 Vac%; G_{red} = 8.85 Vac%.

Table 6. Results available in literature for the elastic moduli of MWCNTs, determined using NCM approaches.

	Reference	t_n, nm	Interlayer spacing, d_{int}, nm	Approach for the van der Waals interactions between layers	MWCNT	Max. number of layers	Young's modulus, TPa	Shear modulus, TPa
[105]	Li and Chou, 2003	0.34	0.339	truss rods	armchair (3, 3) (8, 8) (13, 13) (18, 18)	4	1.05–1.10	0.33–0.48
			0.352		zigzag (5, 0) (14, 0) (23, 0) (32, 0)		1.05–1.12	0.33–0.36
[41]	Kalamkarov et al., 2006	0.68	0.339	springs	armchair (5, 5) (10, 10) (15, 15) (20, 20)	4	1.00–1.45	0.44–0.47
			0.352		zigzag (5, 0) (14, 0) (23, 0) (32, 0)		0.96–1.50	0.44–0.47
[106]	Fan et al., 2009	0.34	0.352	springs: interlayer pressure	zigzag (5, 0) (14, 0) (23, 0)	3	1.006–1.011	0.43–0.34
					zigzag (18, 0) (27, 0) (36, 0)		1.040–1.019	0.36–0.33
[107]	Nahas and Abd-Rabou, 2010	0.346	–	beams	armchair	3	0.98–1.02	–
					zigzag		0.876–0.937	
[88]	Ghavamian et al., 2012	0.34	0.339	springs	armchair (10, 10) (15, 15) (20, 20) (25, 25) (30, 30)	5	1.040–1.044	–
			0.352		zigzag (14, 0) (23, 0) (32, 0) (41, 0) (50, 0)		1.030–1.035	
[50]	Ghavamian et al., 2013	0.34	0.339	springs	armchair (10, 10) (15, 15) (20, 20) (25, 25) (30, 30)	5	–	0.50
			0.352		zigzag (14, 0) (23, 0) (32, 0) (41, 0) (50, 0)			
[108]	Sakharova et al., 2017	0.34	0.339	–	armchair (10, 10) (15, 15) (20, 20) (25, 25) (30, 30) (35, 35) (40, 40) (45, 45) (50, 50) (55, 55)	10	1.061–1.054	–
			0.352		zigzag (14, 0) (23, 0) (32, 0) (41, 0) (50, 0) (59, 0) (68, 0) (77, 0) (86, 0) (95, 0)		1.069–1.012	

Some authors [105,106,107] pointed out that Young's modulus of MWCNTs is slightly higher than that of SWCNTs. The Young's modulus values for MWCNTs, which are very close to the values obtained for SWCNTs constituting the MWCNT, were also reported [88,108]. A substantial increase of the Young's modulus with the number of layers was reported by Kalmakarov et al. [41]. Shear modulus trends similar to the trend for the Young's modulus of MWCNTs were described in the works of Kalmakarov et al. [41] and Ghavamian et al. [50]. Li and Chou [105] and Fan et al. [106] reported values of the MWCNTs' shear modulus slightly lower than those of SWCNTs.

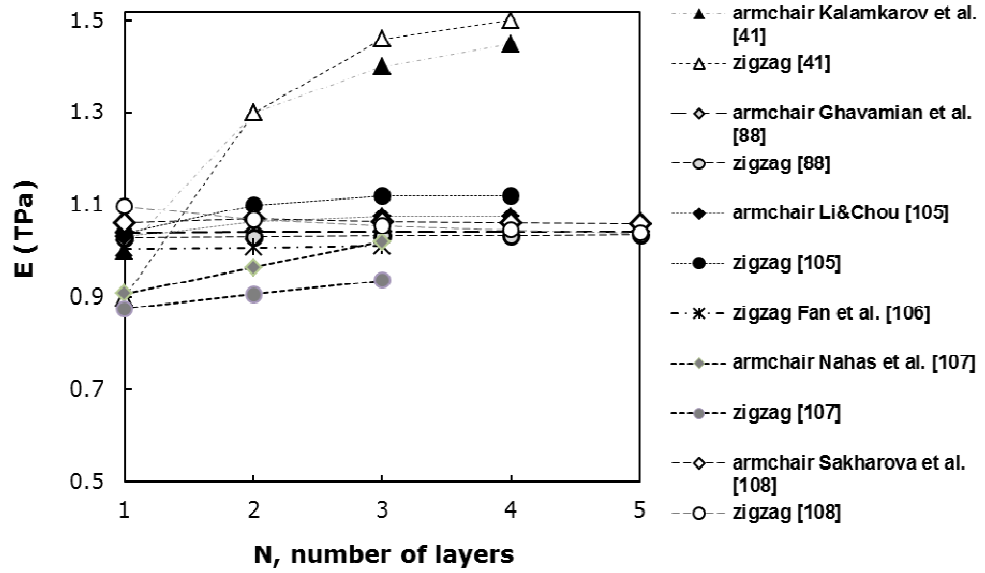

(a)

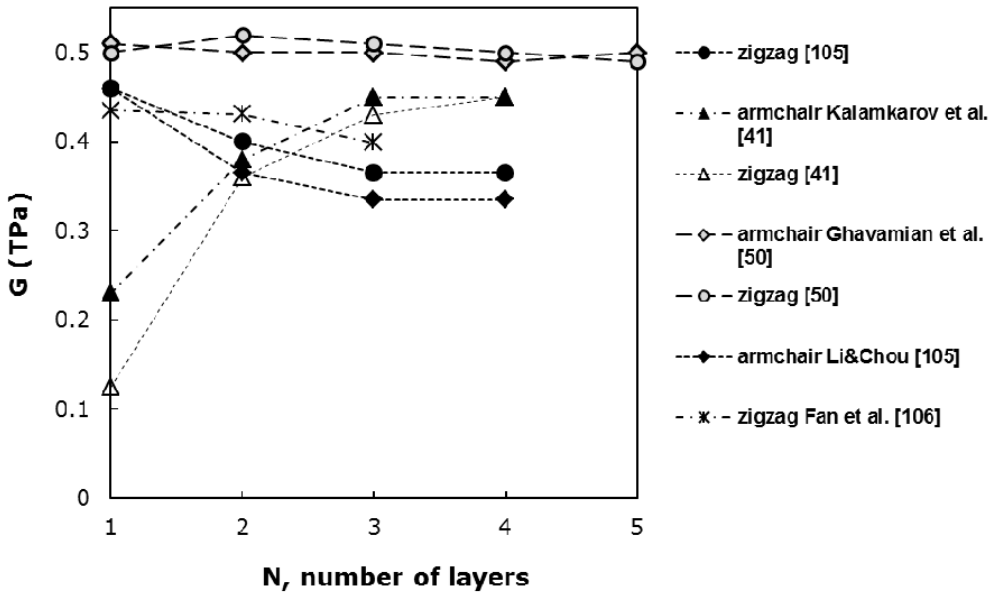

(b)

Figure 8. Literature results for elastic moduli of MWCNTs: (a) Young's modulus and (b) shear modulus with respect to the number of layers, N, constituting the MWCNT.

6. Modelling and Mechanical Behaviour of CNT HJs

From the point of view of the construction of nanodevices, the CNT junctions are necessary constituents for circuits, amplifiers, switches, rectifiers, molecular storages, field-effect transistors and nanodiodes. A comprehensive review on synthesis, properties and realistic applications of CNT junctions was published by Wei and Liu [6]. CNT HJs have attracted special research interest, because of their singular electrical and optical properties, and potentially attractive applications as nanodiodes and filters [109,110]. Despite the progress achieved in recent years in this research field, many challenges still remain. One of them is to understand the deformation behaviour of CNT heterojunctions, since the stability and efficiency of the nanodevices is highly dependent on the mechanical properties of their components.

Molecular dynamics and nanoscale continuum approaches combined with finite element modelling have become the most prevalent methods to simulate the mechanical behaviour of CNT heterojunctions. A few studies were performed using the MD approach [24,26,111]. Lee and Su [111] investigated the temperature effect on the mechanical properties, yield stress and Young's modulus, of (6, 0)–(8, 0) SWCNT HJs under tension and compression, by using an MD simulation approach, employing a REBO potential to describe the carbon–carbon (C–C) interaction. Also employing a REBO potential, Li et al. [24] investigated the tensile strength and failure modes of single-walled and double-walled CNT HJs at different temperatures and strain rates.

Qin et al. [26] performed an MD simulation study, using second-generation Tersoff–Brenner potential, in order to evaluate Young's modulus and failure stress of single-walled and double-walled CNT HJs. Kang et al. [112], also using MD simulation with Tersoff–Brenner potential coupled with NCM approach, studied the buckling behaviour of (7, 7)–(9, 9) HJs under compression. Kinoshita et al. [113] used *ab initio* density functional theory calculations in order to assess the Young's modulus and stress–strain relationship for (8, 0)–(6, 0)–(8, 0) SWCNT HJs structures. An MD simulation, employing second-generation Tersoff–Brenner potential, was used by Xi et al. [114] in order to study the mechanical behaviour of complex HJs structures consisting of four (n, n) armchair and five $(2n, 0)$ zigzag SWCNTs.

The studies using the NCM approach were devoted to the characterization of the buckling [115,116], tensile [22,25,116,117,118,119] and shear [22,25,116,120] behaviour of HJs, and the evaluation of their Poisson's ratio [110]. Sakharova et al. [22], analysing the mechanical behaviour of the armchair–armchair and zigzag–zigzag HJs, pointed out the occurrence of redundant bending deformation during the tensile test, making it difficult to analyse this test. Scarpa et al. [110] also reported this aspect when calculating the Poisson's ratio from the tensile test of (5, 5)–(10, 10) HJs.

Regarding the evaluation of the HJs elastic properties such as rigidities, Young's and shear moduli, some of the authors reported their decrease when compared with the elastic properties of the constituent SWCNTs [22,25,116,117,119]. The literature results on the studies of the heterojunction elastic properties are resumed in Table 7. The aforementioned investigations must be understood as the beginning of broader necessary studies on the mechanical properties of the carbon nanotube heterojunctions.

Table 7. Results for the elastic moduli of CNT HJs available in literature.

	Reference	Method	Type of HJs	*Young's modulus, E, TPa	*Shear modulus, G, TPa	Comments
[26]	Qin et al., 2008	MD: Tersoff-Brenner potential	armchair–armchair (5, 5)–(7, 7), (5, 5)–(8, 8), …(5, 5)–(10, 10)	0.775	–	Young's modulus of HJ about 20% higher than for the narrower (5, 5) or (9, 0) SWCNT;
			zigzag–zigzag (9, 0)–(10, 0), (9, 0)–(11, 0), …(9, 0)–(14, 0)	0.795	–	E value increases with increasing the HJ average diameter.
			double-walled, triple-walled and four-walled armchair composed by (5, 5), (10, 10), (15, 15), ...(25, 25)	0.773	–	Young's modulus decreases with the number of SWCNTs constituting an N-walled CNT heterojunction.
[110]	Scarpa et al., 2011	NCM: linear beams	armchair–armchair (5, 5)–(10, 10)	1.010	–	Bending deformation of HJ in tension were taken into account.
			zigzag–zigzag (9, 0)–(14, 0)	0.945		
[113]	Kinoshita et al., 2013	*ab initio* (DFT) with AIREBO potential	zigzag–zigzag–zigzag (8, 0)–(6, 0)–(8, 0)	0.995	–	The Young's modulus for a HJ structure is lower at about 10.23% than for the narrower (6, 0) SWCNT and at about 4.25% than for the wider (8, 0) SWCNT.
[117]	Hemmatian et al., 2014	NCM: linear beams	armchair–armchair (5, 5)–(10, 10), (10, 10)–(15, 15), …(25, 25)–(30, 30)	1.109	0.344	Elastic moduli are lower than those for constituent SWCNTs; E and G increase with increasing the HJ average diameter, $\overline{D}_{HJ}$, and decrease with increasing of overall length L_{HJ}.
[116]	Ghavamian and Ochsner, 2015;	NCM: linear beams	armchair–armchair composed by a variety of SWCNTs in a range of (3, 3) to (18, 18)	0.927	0.180	Elastic moduli are lower than those for constituent SWCNTs.
[119]	Yengejeh et al., 2015		zigzag–zigzag composed by a variety of SWCNTs in a range of (6, 0) to (19, 0)	0.939	0.270	
[22]	Ghavamian et al., 2015;	NCM: linear beams	armchair–zigzag with bent connection	0.177	0.179	The Young's modulus of HJs decreases drastically; the shear modulus is close to that of the constituent SWCNTs.
[116]	Ghavamian and Ochsner, 2015		chiral–armchair (zigzag) with bent connection	0.160	0.220	
[25]	Sakharova et al., 2016	NCM: linear beams	armchair–armchair (5, 5)–(10, 10), (10, 10)–(15, 15), (15, 15)–(20, 20)	Bending (EI) and torsional (GJ) rigidities increase with increasing the HJ average diameter. EI rigidities are comparable with those for narrower SWCNTs. GJ rigidities are higher than for narrower SWCNTs, and lower than for wider SWCNTs.		
			zigzag–zigzag (5, 0)–(10, 0), (10, 0)–(15, 0), (15, 0)–(20, 0)			

* Average values.

7. Conclusions

This review shows that a great investment has been made lately in the development of the modelling of mechanical properties of carbon nanotubes. These include the elastic moduli and the Poisson ratio of single and multi-walled carbon nanotubes and their heterojunctions, without and with vacancy defects. In spite of great developments has been made in predicting the mechanical properties of CNTs by numerical simulation, the theoretical studies (analytical and numerical) have led to some variety of results due to different modelling approaches and formulations. The resulting scattering in the values of the elastic constants raises questions on the reliability of the data obtained and can affect its interpretation. Among the several approaches, the nanoscale continuum modelling (NCM/MSM) proves to be efficient for simulating the nanotubes behaviour without requiring extensive computation.

Acknowledgments

The authors gratefully acknowledge the financial support of the Portuguese Foundation for Science and Technology (FCT), Portugal, via Projects PTDC/EMS-TEC/0702/2014 (POCI-01-0145-FEDER-016779), PTDC/EMS-TEC/6400/2014 (POCI-01-0145-FEDER-016876), and UID/EMS/00285/2013, by UE/FEDER through Program COMPETE2020. N. A. Sakharova and A. F. G. Pereira were supported by a grant for scientific research from the Portuguese Foundation for Science and Technology (refs. SFRH/BPD/107888/2015, and SFRH/BD/102519/2014, resp.). All supports are gratefully acknowledged.

Conflict of Interest

The authors declare that there is no conflict of interest regarding the publication of this manuscript.

References

1. Robertson J (2004) Realistic applications of CNTs. *Mater Today* 7: 46–52.
2. Dresselhaus MS, Avouris P (2001) Introduction to carbon materials research, In: Dresselhaus, MS, Dresselhaus G, Avouris P, *Carbon Nanotubes: Synthesis, Structure, Properties, and Applications*, Springer Book Series: Topics in Applied Physics, Germany: Springer-Verlag Berlin Heidelberg, 80: 1–9.
3. Neubauer E, Kitzmantel M, Hulman M, et al. (2010) Potential and challenges of metal-matrix-composites reinforced with carbon nanofibers and carbon nanotubes. *Compos Sci Technol* 70: 2228–2236.
4. Lan Y, Wang Y, Ren ZF (2011) Physics and applications of aligned carbon nanotubes. *Adv Phys* 60: 553–678.
5. Zhang Y, Zhuang X, Muthu J, et al. (2014) Load transfer of graphene/carbon nanotube/polyethylene hybrid nanocomposite by molecular dynamics simulation. *Compos Part B-Eng* 63: 27–33.

6. Schulz MJ, Shanov VN, Yin Z (2014) *Nanotube superfiber Materials*, Oxford (UK): Elsevier, 848.
7. Wei DC, Liu YQ (2008) The intramolecular junctions of carbon nanotubes. *Adv Mater* 20: 2815–2841.
8. Salvetat JP, Briggs GAD, Bonard JM, et al. (1999) Elastic and shear moduli of single-walled carbon nanotube ropes. *Phys Rev Lett* 82: 944–947.
9. Hall AR, An L, Liu J, et al. (2006) Experimental measurement of single-wall carbon nanotube torsional properties. *Phys Rev Lett* 96: 256102.
10. Kallesøe C, Larsen MB, Bøggild P, et al. (2012) 3D mechanical measurements with an atomic force microscope on 1D structures. *Rev Sci Instrum* 83: 023704.
11. Wang L, Zhang Z, Han X (2013) In situ experimental mechanics of nanomaterials at the atomic scale. *NPG Asia Mater* 5: e40.
12. Mielke SL, Troya D, Zhan S, et al. (2004) The role of vacancy defects and holes in the fracture of carbon nanotubes. *Chem Phys Lett* 390: 413–420.
13. Hou W, Xiao S (2007) Mechanical behaviors of carbon nanotubes with randomly located vacancy defects. *J Nanosci Nanotechnol* 7: 4478–4485.
14. Tserpes KI, Papanikos P (2005) Finite element modeling of single-walled carbon nanotubes. *Compos Part B-Eng* 36: 468–477.
15. Rafiee R, Heidarhaei M (2012) Investigation of chirality and diameter effects on the Young's modulus of carbon nanotubes using non-linear potentials. *Compos Struct* 94: 2460–2464.
16. Sakharova NA, Pereira AFG, Antunes JM, et al. (2015) Mechanical characterization of single-walled carbon nanotubes: Numerical simulation study. *Compos Part B-Eng* 75: 73–85.
17. Rafiee R, Moghadam RM (2014) On the modelling of carbon nanotubes: A critical review. *Compos Part B-Eng* 56: 435–449.
18. Yengejeh SI, Kazemi SA, Öchsner A (2016) Advances in mechanical analysis of structurally and atomically modified carbon nanotubes and degenerated nanostructures: A review. *Compos Part B-Eng* 86: 95–107.
19. Dresselhaus MS, Dresselhaus G, Saito R (1995) Physics of carbon nanotubes. *Carbon* 33: 883–891.
20. Barros EB, Jorio A, Samsonidze GG, et al. (2006) Review on the symmetry-related properties of carbon nanotubes. *Phys Rep* 431: 261–302.
21. Melchor S, Dobado JA (2004) CoNTub: An algorithm for connecting two arbitrary carbon nanotubes. *J Chem Inf Comp Sci* 44: 1639–1646.
22. Ghavamian A, Andriyana A, Chin AB, et al. (2015) Numerical investigation on the influence of atomic defects on the tensile and torsional behavior of hetero-junction carbon nanotubes. *Mater Chem Phys* 164: 122–137.
23. Yao YG, Li QW, Zhang J, et al. (2007) Temperature-mediated growth of single-walled carbon-nanotube intramolecular junctions. *Nat Mater* 6: 283–286.
24. Li M, Kang Z, Li R, et al. (2013) A molecular dynamics study on tensile strength and failure modes of carbon nanotube junctions. *J Phys D Appl Phys* 46: 495301.
25. Sakharova NA, Pereira AFG, Antunes JM, et al. (2016) Numerical simulation of the mechanical behaviour of single-walled carbon nanotubes heterojunctions. *J Nano Res* 38: 73–87.
26. Qin Z, Qin QH, Feng XQ (2008) Mechanical property of carbon nanotubes with intramolecular junctions: Molecular dynamics simulations. *Phys Lett A* 372: 6661–6666.

27. Lu Q, Bhattacharya B (2005) The role of atomistic simulations in probing the small scale aspects of fracture—a case study on a single-walled carbon nanotube. *Eng Fract Mech* 72: 2037–2071.
28. Yakobson BI, Brabec CJ, Bernholc J (1996) Nanomechanics of carbon tubes: instabilities beyond linear response. *Phys Rev Lett* 76: 2511–2514.
29. Lu JP (1997) Elastic properties of carbon nanotubes and nanoropes. *Phys Rev Lett* 79: 1298–1300.
30. Jin Y, Yuan FG (2003) Simulation of elastic properties of single-walled carbon nanotubes. *Compos Sci Technol* 63: 1507–1515.
31. Liew KM, He XQ, Wong CH (2004) On the study of elastic and plastic properties of multi-walled carbon nanotubes under axial tension using molecular dynamics simulation. *Acta Mater* 52: 2521–2527.
32. Bao WX, Zhu CC, Cui WZ (2004) Simulation of Young's modulus of single-walled carbon nanotubes by molecular dynamics. *Physica B* 352: 156–163.
33. Zhang HW, Wang JB, Guo X (2005) Predicting the elastic properties of single-walled carbon nanotubes. *J Mech Phys Solids* 53: 1929–1950.
34. Cheng HC, Liu YL, Hsu YC, et al. (2009) Atomistic continuum modelling for mechanical properties of single-walled carbon nanotubes. *Int J Solids Struct* 46: 1695–1704.
35. Kudin KN, Scuseria GE, Yakobson BI (2001) C_2F, BN and C nanoshell elasticity from ab initio computations. *Phys Rev B* 64: 235406.
36. Wilmes AA, Pinho ST (2014) A coupled mechanical-charge/dipole molecular dynamics finite element method, with multi-scale applications to the design of graphene nano-devices. *Int J Numer Meth Eng* 100: 243–276.
37. Hernandez E, Goze C, Bernier P, et al. (1998) Elastic properties of C and $B_xC_yN_z$ composite nanotubes. *Phys Rev Lett* 80: 4502–4505.
38. Zhou X, Zhou J, Ou-Yang ZC (2000) Strain energy and Young's modulus of single-wall carbon nanotubes calculated from electronic energy-band theory. *Phys Rev B* 62: 13692–13696.
39. Ru CQ (2000) Effective bending stiffness of carbon nanotubes. *Phys Rev B* 62: 9973–9976.
40. Pantano A, Parks DM, Boyce MC (2004) Mechanics of deformation of single- and multi-wall carbon nanotubes. *J Mech Phys Solids* 52: 789–821.
41. Kalamkarov AL, Georgiades AV, Rokkam SK, et al. (2006) Analytical and numerical techniques to predict carbon nanotubes properties. *Int J Solids Struct* 43: 6832–6854.
42. Muc A (2010) Design and identification methods of effective mechanical properties for carbon nanotubes. *Mater Design* 31: 1671–1675.
43. Chang TC (2010) A molecular based anisotropic shell model for single-walled carbon nanotubes. *J Mech Phys Solids* 58: 1422–1433.
44. Sears A, Batra RC (2004) Macroscopic properties of carbon nanotubes from molecular-mechanics simulations. *Phys Rev B* 69: 235406.
45. Gupta SS, Batra RC (2008) Continuum structures equivalent in normal mode vibrations to single-walled carbon nanotubes. *Comp Mater Sci* 43: 715–723.
46. Wang Q (2004) Effective in-plane stiffness and bending rigidity of armchair and zigzag carbon nanotubes. *Int J Solids Struct* 41: 5451–5461.
47. Arash B, Wang Q (2012) A review on the application of nonlocal elastic models in modelling of carbon nanotubes and graphenes. *Comp Mater Sci* 51: 303–313.

48. Odegard GM, Gates TS, Nicholson LM, et al. (2002) Equivalent continuum modelling of nano-structured materials. *Compos Sci Technol* 62: 1869–1880.
49. Li C, Chou TW (2003) A structural mechanics approach for the analysis of carbon nanotubes. *Int J Solids Struct* 40: 2487–2499.
50. Ghavamian A, Rahmandoust M, Öchsner A (2013) On the determination of the shear modulus of carbon nanotubes. *Compos Part B-Eng* 44: 52–59.
51. Chen WH, Cheng HC, Liu YL (2010) Radial mechanical properties of single-walled carbon nanotubes using modified molecular structure mechanics. *Comp Mater Sci* 47: 985–993.
52. Eberhardt O, Wallmersperger T (2015) Energy consistent modified molecular structural mechanics model for the determination of the elastic properties of single wall carbon nanotubes. *Carbon* 95: 166–180.
53. Natsuki T, Tantrakarn K, Endo M (2004) Prediction of elastic properties for single-walled carbon nanotubes. *Carbon* 42: 39–45.
54. Meo M, Rossi M (2006) Prediction of Young's modulus of single wall carbon nanotubes by molecular-mechanics based finite element modeling. *Compos Sci Technol* 66: 1597–1605.
55. Giannopoulos GI, Kakavas PA, Anifantis NK (2008) Evaluation of the effective mechanical properties of single-walled carbon nanotubes using a spring based finite element approach. *Comp Mater Sci* 41: 561–569.
56. Wernik JM, Meguid SA (2010) Atomistic-based continuum modelling of the nonlinear behavior of carbon nanotubes. *Acta Mech* 212: 167–179.
57. Ranjbartoreh AZ, Wang G (2010) Consideration of mechanical properties of single-walled carbon nanotubes under various loading conditions. *J Nanopart Res* 12: 537–543.
58. Parvaneh V, Shariati M (2011) Effect of defects and loading on prediction of Young's modulus of SWCNTs. *Acta Mech* 216: 281–289.
59. Mahmoudinezhad E, Ansari R, Basti A, et al. (2012) An accurate spring-mass model for predicting mechanical properties of single-walled carbon nanotubes. *Comp Mater Sci* 62: 6–11.
60. To CWS (2006) Bending and shear moduli of single-walled carbon nanotubes. *Finite Elem Anal Design* 42: 404–413.
61. Papanikos P, Nikolopoulos DD, Tserpes KI (2008) Equivalent beams for carbon nanotubes. *Comp Mater Sci* 43: 345–352.
62. Ávila AF, Lacerda GSR (2008) Molecular mechanics applied to single-walled carbon nanotubes. *Mater Res* 11: 325–333.
63. Shokrieh MM, Rafiee R (2010) Prediction of Young's modulus of graphene sheets and carbon nanotubes using nanoscale continuum mechanics approach. *Mater Design* 31: 790–795.
64. Her SC, Liu SJ (2012) Theoretical prediction of tensile behavior of single-walled carbon nanotubes. *Curr Nanosci* 8: 42–46.
65. Lu X, Hu Z (2012) Mechanical property evaluation of single-walled carbon nanotubes by finite element modeling. *Compos Part B-Eng* 43: 1902–1913.
66. Mohammadpour E, Awang M (2011) Predicting the nonlinear tensile behavior of carbon nanotubes using finite element simulation. *Appl Phys A-Mater* 104: 609–614.
67. Ghadyani G, Öchsner A (2015) Derivation of a universal estimate for the stiffness of carbon nanotubes. *Physica E* 73: 116–125.

68. Giannopoulos GI, Tsiros AP, Georgantzinos SK (2013) Prediction of Elastic Mechanical Behavior and Stability of Single-Walled Carbon Nanotubes Using Bar Elements. *Mech Adv Mater Struct* 20: 730–741.
69. Nasdala L, Ernst G (2005) Development of a 4-node finite element for the computation of nano-structured materials. *Comp Mater Sci* 33: 443–458.
70. Budyka MF, Zyubina TS, Ryabenko AG, et al. (2005) Bond lengths and diameters of armchair single wall carbon nanotubes. *Chem Phys Lett* 407: 266–271.
71. Ghadyani G, Öchsner A (2015) On a thickness free expression for the stiffness of carbon nanotubes. *Solid State Commun* 209: 38–44.
72. Pereira AFG, Antunes JM, Fernandes JV, et al. (2016) Shear modulus and Poisson's ratio of single-walled carbon nanotubes: numerical evaluation. *Phys Status Solidi B* 253: 366–376.
73. Krishnan A, Dujardin E, Ebbesen TW, et al. (1998) Young's modulus of single-walled nanotubes. *Phys Rev B* 58: 14013–14018.
74. Yu MF, Files BS, Arepalli S, et al. (2000) Tensile loading of ropes of single wall carbon nanotubes and their mechanical properties. *Phys Rev Lett* 84: 5552–5554.
75. Shen L, Li J (2004) Transversely isotropic elastic properties of single-walled carbon nanotubes. *Phys Rev B* 69: 045414.
76. Ghadyani G, Soufeiani L, Öchsner A (2017) Angle dependence of the shear behaviour of asymmetric carbon nanotubes. *Mater Design* 116:136–143.
77. Xiao JR, Gama BA, Gillespie Jr JW (2005) An analytical molecular structural mechanics model for the mechanical properties of carbon nanotubes. *Int J Solids Struct* 42: 3075–3092.
78. Wu Y, Zhang X, Leung AYT, et al. (2006) An energy-equivalent model on studying the mechanical properties of single-walled carbon nanotubes. *Thin Wall Struct* 44: 667–676.
79. Rahmandoust M, Öchsner A (2012) On finite element modeling of single- and multi-walled carbon nanotubes. *J Nanosci Nanotechnol* 12: 8129–8136.
80. Domínguez-Rodríguez G, Tapia A, Avilés F (2014) An assessment of finite element analysis to predict the elastic modulus and Poisson's ratio of singlewall carbon nanotubes. *Comp Mater Sci* 82: 257–263.
81. Popov VN, Van Doren VE, Balkanski M (2000) Elastic Properties of single-walled carbon nanotubes. *Phys Rev B* 61: 3078–3084.
82. Gao RP, Wang ZL, Bai ZG, et al. (2000) Nanomechanics of individual carbon nanotubes from pyrolytically grown arrays. *Phys Rev Lett* 85: 622–625.
83. Andrews R, Jacques D, Qian D, et al. (2001) Purification and structural annealing of multiwalled carbon nanotubes at graphitization temperatures. *Carbon* 39: 1681–1687.
84. Terrones M, Banhart F, Grobert N, et al. (2002) Molecular junctions by joining single-walled carbon nanotubes. *Phys Rev Lett* 89: 075505.
85. Scarpa F, Adhikari S, Wang CY (2009) Mechanical properties of non-reconstructed defective single-wall carbon nanotubes. *J Phys D Appl Phys* 42: 142002.
86. Parvaneh V, Shariati M, Torabi H (2012) Bending buckling behavior of perfect and defective single-walled carbon nanotubes via a structural mechanics model. *Acta Mech* 223: 2369–2378.
87. Rahmandoust M, Öchsner A (2009) Influence of structural imperfections and doping on the mechanical properties of single-walled carbon nanotubes. *J Nano Res* 6: 185–196.

88. Ghavamian A, Rahmandoust M, Öchsner A (2012) A numerical evaluation of the influence of defects on the elastic modulus of single and multi-walled carbon nanotubes. *Comp Mater Sci* 62: 110–116.
89. Ghavamian A, Öchsner A (2012) Numerical investigation on the influence of defects on the buckling behavior of single-and multi-walled carbon nanotubes. *Physica E* 46: 241–249.
90. Ghavamian A, Öchsner A (2013) Numerical modeling of eigenmodes and eigenfrequencies of single- and multi-walled carbon nanotubes under the influence of atomic defects. *Comp Mater Sci* 72: 42–48.
91. Poelma RH, Sadeghian H, Koh S, et al. (2012) Effects of single vacancy defect position on the stability of carbon nanotubes. *Microelectron Reliab* 52: 1279–1284.
92. Sakharova NA, Pereira AFG, Antunes JM, et al. (2016) Numerical simulation study of the elastic properties of single-walled carbon nanotubes containing vacancy defects. *Compos Part B-Eng* 89: 155–168.
93. Sakharova NA, Antunes JM, Pereira AFG, et al. (2015) The effect of vacancy defects on the evaluation of the mechanical properties of single-wall carbon nanotubes: Numerical simulation study, In: Öchsner A, Altenbach H, *Springer Book Series On Advanced Structured Materials: Mechanical and Materials Engineering of Modern Structure and Component Design*, Germany: Springer, 70: 323–339.
94. Wong CH (2010) Elastic properties of imperfect single-walled carbon nanotubes under axial tension. *Comp Mater Sci* 49: 143–147.
95. Rafiee R, Pourazizi R (2014) Evaluating the Influence of Defects on the Young's Modulus of Carbon Nanotubes Using Stochastic Modeling. *Mater Res* 17: 758–766.
96. Zhang YP, Ling CC, Li GX, et al. (2015) Radial collapse and physical mechanism of carbon nanotube with divacancy and 5-8-5 defects. *Chinese Phys B* 24: 046401.
97. Rafiee R, Mahdavi M (2016) Molecular dynamics simulation of defected carbon nanotubes. *P I Mech Eng L-J Mat* 230: 654–662.
98. Sharma S, Chandra R, Kumar P, et al. (2014) Effect of Stone-Wales and vacancy defects on elastic moduli of carbon nanotubes and their composites using molecular dynamics simulation. *Comp Mater Sci* 86: 1–8.
99. Saxena KK, Lal A (2012) Comparative molecular dynamics simulation study of mechanical properties of carbon nanotubes with number of Stone-Wales and vacancy defects. *Procedia Eng* 38: 2347–2355.
100. Yuan J, Liew KM (2009) Effects of vacancy defect reconstruction on the elastic properties of carbon nanotubes. *Carbon* 47: 1526–1533.
101. Xiao S, Hou W (2006) Fracture of vacancy-defected carbon nanotubes and their embedded nanocomposites. *Phys Rev B* 73: 115406.
102. Kurita H, Estili M, Kwon H, et al. (2015) Load-bearing contribution of multi-walled carbon nanotubes on tensile response of aluminium. *Compos Part A-Appl S* 68: 133–139.
103. Kharissova OV, Kharisov BI (2014) Variations of interlayer spacing in carbon nanotubes. *RSC Adv* 58: 30807–30815.
104. Kiang CH, Endo M, Ajayan PM, et al. (1998) Size effects in carbon nanotubes. *Phys Rev Lett* 81: 1869–1872.
105. Li C, Chou TW (2003) Elastic moduli of multi-walled carbon nanotubes and the effect of van der Waals forces. *Comp Sci Tech* 63: 1517–1524.

106. Fan CW, Liu YY, Hwu C (2009) Finite element simulation for estimating the mechanical properties of multi-walled carbon nanotubes. *Appl Phys A-Mater* 5: 819–831.
107. Nahas MN, Abd-Rabou M (2010) Finite element modeling of multi-walled carbon nanotubes. *Int J Eng Technol* 10: 63–71.
108. Sakharova NA, Pereira AFG, Antunes JM, et al. (2017) Numerical simulation on the mechanical behaviour of the multi-walled carbon nanotubes. *J Nano Res* 47: 106–119.
109. Liu Q, Liu W, Cui ZM, et al. (2007) Synthesis and characterization of 3D double branched K junction carbon nanotubes and nanorods. *Carbon* 45: 268–273.
110. Scarpa F, Narojczyk JW, Wojciechowski KW (2011) Unusual deformation mechanisms in carbon nanotube heterojunctions (5, 5)–(10, 10) under tensile loading. *Phys Status Solidi B* 248: 82–87.
111. Lee WJ, Su WS (2013) Investigation into the mechanical properties of single-walled carbon nanotube heterojunctions. *Phys Chem Chem Phys* 15: 11579–11585.
112. Kang Z, Li M, Tang Q (2010) Buckling behavior of carbon nanotube-based intramolecular junctions under compression: Molecular dynamics simulation and finite element analysis. *Comp Mater Sci* 50: 253–259.
113. Kinoshita Y, Murashima M, Kawachi M, et al. (2013) First-principles study of mechanical properties of one-dimensional carbon nanotube intramolecular junctions. *Comp Mater Sci* 70: 1–7.
114. Xi H, Song HY, Zou R (2015) Simulation of mechanical properties of carbon nanotubes with superlattice structure. *Curr Appl Phys* 15: 1216–1221.
115. Yengejeh SI, Zadeh MA, Öchsner A (2014) On the buckling behavior of connected carbon nanotubes with parallel longitudinal axes. *Appl Phys A-Mater* 115: 1335–1344.
116. Ghavamian A, Öchsner A (2015) A comprehensive numerical investigation on the mechanical properties of hetero-junction carbon nanotubes. *Commun Theor Phys* 64: 215–230.
117. Hemmatian H, Fereidoon A, Rajabpour M (2014) Mechanical properties investigation of defected, twisted, elliptic, bended and hetero-junction carbon nanotubes based on FEM. *Fuller Nanotub Car N* 22: 528–544.
118. Rajabpour M, Hemmatian H, Fereidoon A (2011) Investigation of Length and Chirality Effects on Young's Modulus of Heterojunction Nanotube with FEM. Proceedings of the 2nd International Conference on Nanotechnology: Fundamentals and Applications, Ottawa, Ontario, Canada.
119. Yengejeh SI, Zadeh MA, Öchsner A (2015) On the tensile behavior of hetero-junction carbon nanotubes. *Compos Part B-Eng* 75: 274–280.
120. Yengejeh SI, Zadeh MA, Öchsner A (2014) Numerical characterization of the shear behavior of hetero-junction carbon nanotubes. *J Nano Res* 26: 143–151.

AIMS Press

Chapter 3

Finite element modelling and analysis of CNTs' structures

This chapter provides an outline of the methodology of finite element (FE) modelling of the SWCNTs and SWCNT HJs, under the nanoscale continuum modelling (NCM) approach, as used in this work and in the papers by Sakharova *et al*. (2015, 2016a, 2016b) and Pereira *et al*. (2016), published within the scope of the thesis. In order to dispense the reading of the respective sections in the aforementioned papers (collected in Chapter 4), the description of the material and geometric properties of the SWCNTs and SWCNTs HJs, as well the details of the modelling method for the characterization of their mechanical behaviour are gathered together in the current chapter.

(Page intentionally left blank)

3.1. Finite element modelling of carbon nanotube structures

The NCM approach that replaces the carbon-carbon bonds of carbon nanotube by equivalent beam elements allows modelling the SWCNTs and SWCNT HJs structures. The FE method uses the coordinates of the carbon atoms for generating the nodes and their suitable connection creates the beam elements. The relationships between the inter-atomic potential energies of the molecular CNT structure and strain energies of the equivalent continuum structure, consisting of beam elements undergoing axial, bending and torsional deformations, are the basis for the application of continuum mechanics to the analysis of the mechanical behaviour of SWCNTs and SWCNT HJs (Li and Chou, 2003). The meshes of the SWCNTs and SWCNT HJs structures used in the FE analyses were built using the CoNTub 1.0 software (Melchor and Dobado, 2004). This software generates ASCII files, describing atom positions and their connectivity that will be used as input data in available commercial and in-house FE codes. The in-house application, called *InterfaceNanotubes*, was developed to convert the ASCII files, acquired from the CoNTub 1.0© software, into the format compatible with the ABAQUS® commercial FE code. Examples of finite element meshes constructed in this way, for SWCNT and SWCNT HJ, are shown in **Figure 3.1** and **Figure 3.2**, respectively.

Various SWCNT structures, as non-chiral (zigzag, $\theta = 0°$, and armchair, $\theta = 30°$) and families of chiral ($\theta = 8.9°$; $13.9°$; $19.1°$ among others) SWCNTs in a wide range of nanotube lengths, chiral indices and diameters, were chosen for the present systematic study. The range selected for chiral and non-chiral structures represents the SWCNTs typically found in literature, either for FE analysis and experimental characterization. The SWCNT length of 20 nm was chosen as modelling length for numerical simulation, so that the mechanical behaviour could be independent of the length. The armchair – armchair and zigzag – zigzag heterojunction were constructed in such a way that the lengths of the constituent nanotubes are almost equal to each other and their value is about two orders of magnitude of the length of the junction region.

The geometrical characteristics of SWCNTs and SWCNT HJs used in the FE analyses are summarized in the works of Sakharova *et al*. (2015, 2016a, 2016b, 2017b) and Pereira *et al*. (2016).

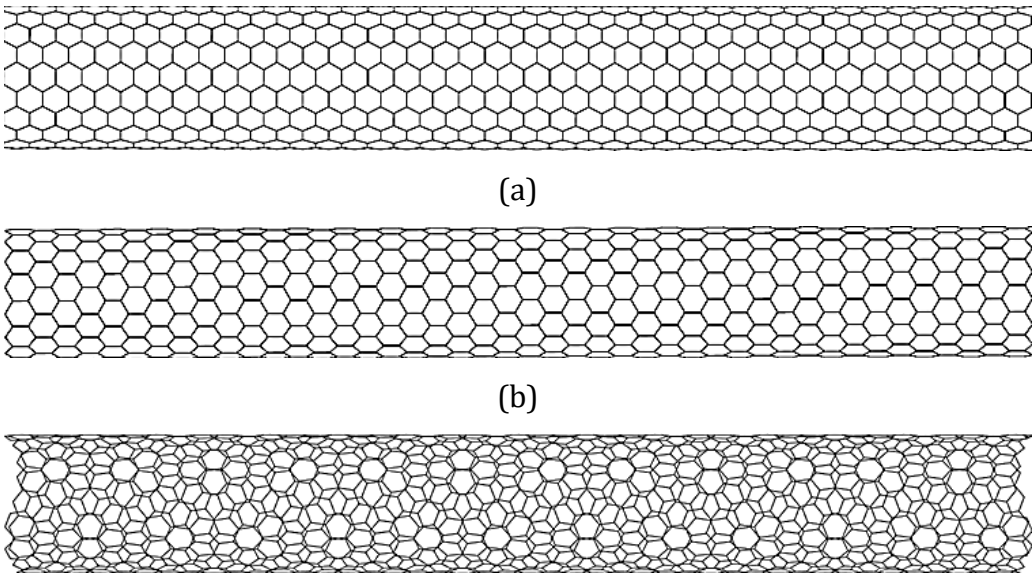

(a)

(b)

(c)

Figure 3.1. Finite element meshes for (a) (10,10) armchair, (b) (15,0) zigzag and (c) (15,3) chiral SWCNTs, obtained by using academic software CoNTub 1.0© (Melchor and Dobado, 2004).

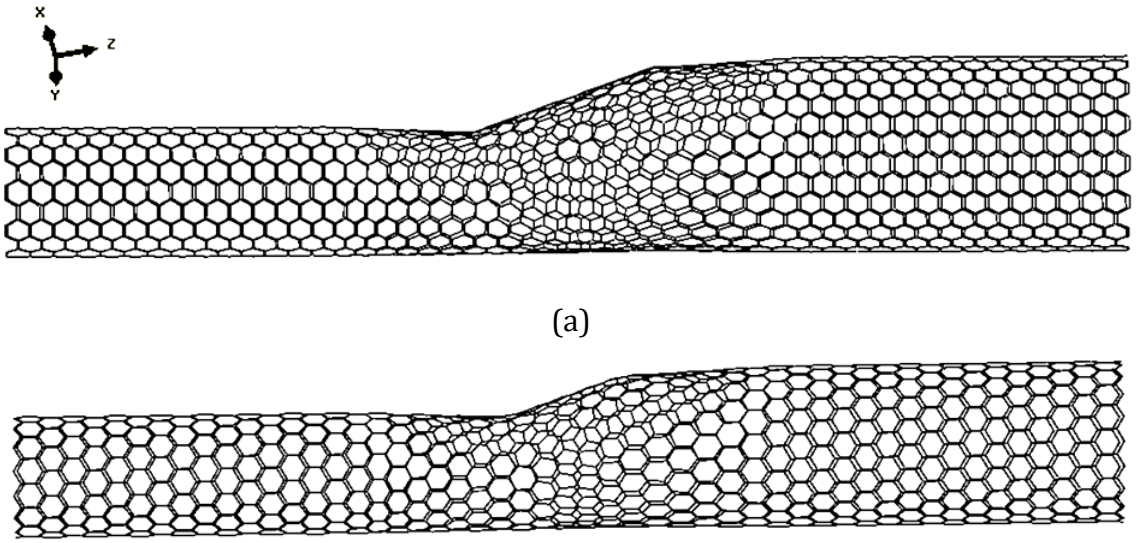

(a)

(b)

Figure 3.2. Finite element meshes for (a) (10, 10) – (15, 15) armchair – armchair and (b) (15, 0) – (20, 0) zigzag – zigzag SWCNT HJ, obtained by using academic software CoNTub 1.0© (Melchor and Dobado, 2004).

The knowledge of the bond length of CNTs is of fundamental importance for the modelling of their mechanical properties. Its value is generally considered to be equal to that of the graphene sheet, a_{C-C} = 0.1421 nm. The value of the wall thickness of CNTs is varied in the literature sources. Although theoretical reports have provided values for nanotube wall thickness, t_n, ranging from 0.064 (Pantano *et al*., 2004) to 0.69 nm (Odegard *et al.*, 2002), the most widely used value is 0.34 nm (equal to the interlayer spacing of graphite). Most of the elastic properties results, obtained in the theoretical and numerical simulation studies, depend on the assumed value for the CNT's wall thickness. The value of the wall thickness $t_n = 0.34\ nm$ was considered in the current study.

3.2. Molecular interactions and equivalent properties of beam elements

As was originally proposed by Odegard et al. (2002), and then developed by Li and Chou (2003), the elastic moduli of the beam elements are determined by establishing the link between inter-atomic potential energies of the molecular structure and strain energies of the equivalent continuum structure, comprising of frame members (beams) undergoing axial, bending and torsional deformations. Thus, the FE simulation under the NCM approach uses the analogy between the bond length, a_{C-C}, and the element length, l, assuming this element with a circular cross-section area (see, **Figure 3.3**).

According to molecular dynamics, the total inter-atomic potential energy of a molecular system is expressed as the sum of energy terms due to bonded and non-bonded interactions (Rappe et al., 1992):

$$U_{tot} = \sum U_r + \sum U_\theta + \sum U_\phi + \sum U_\omega + \sum U_{vdw} \qquad (3.1)$$

where U_r, U_θ, U_ϕ, U_ω are energies associated with bond stretching, bond bending, dihedral angle torsion, out-of plane torsion, respectively, and U_{vdw} is the energy associated with non-bonded van der Waals interaction. In covalent systems such as carbon nanotubes, non-bonded interactions are negligible in comparison with bonded ones (Tserpes and Papanikos, 2005) and the main contribution to the total potential energy comes from the first four terms of Eq. (3.1), as outlined in **Figure 3.4**.

Consequently, under the assumption of small deformation, the energies associated with bond stretching, bending and torsion (by merging dihedral angle torsion and out-of-plane torsion into a single equivalent term) can be estimated by the functions (Gelin, 1994):

$$U_r = \frac{1}{2}k_r(\Delta r)^2$$

$$U_\theta = \frac{1}{2}k_\theta(\Delta\theta)^2 \tag{3.2}$$

$$U_\tau = U_\phi + U_\omega = \frac{1}{2}k_\tau(\Delta\phi)^2$$

where k_r, k_θ and k_τ are the bond stretching, bond bending and torsional resistance force constants, respectively, and Δr, $\Delta\theta$ and $\Delta\phi$ are the bond stretching increment, bond angle bending variation and angle variation of twist bond, respectively.

The elastic properties of the beam elements can be determined by establishing the equivalence of the energies associated with the bond interactions, through Eq. (3.2), and the energies associated with elastic deformation of the beams.

Classical mechanics gives the following expression for the strain energy, U_A, of a beam with length, l, and cross-section area,A_b, under a pure axial force, N:

$$U_A = \frac{1}{2}\int_0^L \frac{N^2}{E_b A_b}dl = \frac{1}{2}\frac{N^2 l}{E_b A_b} = \frac{1}{2}\frac{E_b A_b}{l}(\Delta l)^2 \tag{3.3}$$

where Δl is the axial stretching displacement and E_b is the Young's modulus of the beam.

The strain energy, U_M, of a beam under a pure bending moment, M, according to classical mechanics, is expressed as:

$$U_M = \frac{1}{2}\int_0^L \frac{M^2}{E_b I_b}dl = \frac{1}{2}\frac{E_b I_b}{l}(2\tau)^2 \tag{3.4}$$

where τ is the rotational angle at the ends of the beam and I_b is the moment of inertia of the beam.

The strain energy, U_T, of a beam under a pure torsion moment, T, is expressed:

$$U_T = \frac{1}{2}\int_0^L \frac{T^2}{G_b J_b} dl = \frac{1}{2}\frac{G_b J_b}{l}(\Delta\beta)^2 \tag{3.5}$$

where $\Delta\beta$ is the relative rotation between the ends of the beam and J_b the polar moment of inertia.

The parameters U_r and U_A are stretching energies in molecular and structural systems, respectively, U_θ and U_M represent the bending energies, while U_τ and U_T are the torsional energies. Comparing Eqs. (3.2) with Eqs. (3.3) – (3.5), and assuming the equivalence of Δl to Δr, as well the equivalence of the rotational angle, 2τ, to the total variation of the bond angle, $\Delta\theta$, and $\Delta\beta$ to $\Delta\phi$, direct relationships can be established between the structural mechanics parameters, $E_b A_b$, $E_b I_b$, $G_b J_b$ and the force field constants, k_r, k_θ, k_τ (Li and Chou, 2003):

$$\begin{aligned} \frac{E_b A_b}{l} &= k_r \\ \frac{E_b I_b}{l} &= k_\theta \\ \frac{G_b J_b}{l} &= k_\tau \end{aligned} \tag{3.6}$$

Equations (3.6) are the basis for the application of continuum mechanics to the analysis of the mechanical behaviour of CNT structures. The input geometrical and material parameters of the beam element, for the numerical simulations, are summarized in **Table 3.1**.

3.3. FE analysis of CNTs' structures

The FE simulation is performed using the commercial FE code ABAQUS®. The tensile, bending and torsional rigidities of SWCNTs and SWCNT HJs are evaluated from conventional mechanical numerical tests. The boundary and loading conditions are shown in **Figure 3.5** for SWCNTs and in **Figure 3.6** for SWCNT HJs. The values of the tensile, EA, bending, EI, and torsional, GJ, rigidities were obtained from the respective numerical simulation tests results as described in the following for the case of SWCNTs.

Table 3.1. Input parameters for FE simulations of CNT structures: geometrical and material properties of beam element.

Parameter	Value	Formulation
Force constant, k_r (Cornell *et al*., 1995)	6.52×10^{-7} [N nm^{-1}]	–
Force constant, k_θ (Cornell *et al*., 1995)	8.76×10^{-10} [N·nm·rad^{-2}]	–
Force constant, k_τ (Cornell *et al*., 1995; Jorgensen and Severance, 1990)	2.78×10^{-10} [N·nm·rad^{-2}]	–
C-C bond/beam length ($l = a_{C-C}$)	0.1421 [nm]	–
Beam diameter (d)	0.147 [nm]	$d = 4\sqrt{k_\theta/k_r}$
Cross-sectional area, A_b	0.01688 [nm^2]	$A_b = \pi d^2/4$
Moment of inertia, I_b	2.269×10^{-5} [nm^4]	$I_b = \pi d^4/64$
Polar moment of inertia, J_b	4.537×10^{-5}·[nm^4]	$J_b = \pi d^4/32$
Young's modulus, E_b	5488 [GPa]	$E_b = k_r^2 l/4\pi k_\theta$
Shear modulus, G_b	870.7 [GPa]	$G_b = k_r^2 k_\tau l/8\pi k_\theta^2$
Tensile rigidity, E_bA_b	92.65 [nN]	$E_bA_b = k_r l$
Bending rigidity, E_bI_b	0.1245 [nN·nm^2]	$E_bI_b = k_\theta l$
Torsional rigidity, G_bJ_b	0.0395 [nN·nm^2]	$G_bJ_b = k_\tau l$

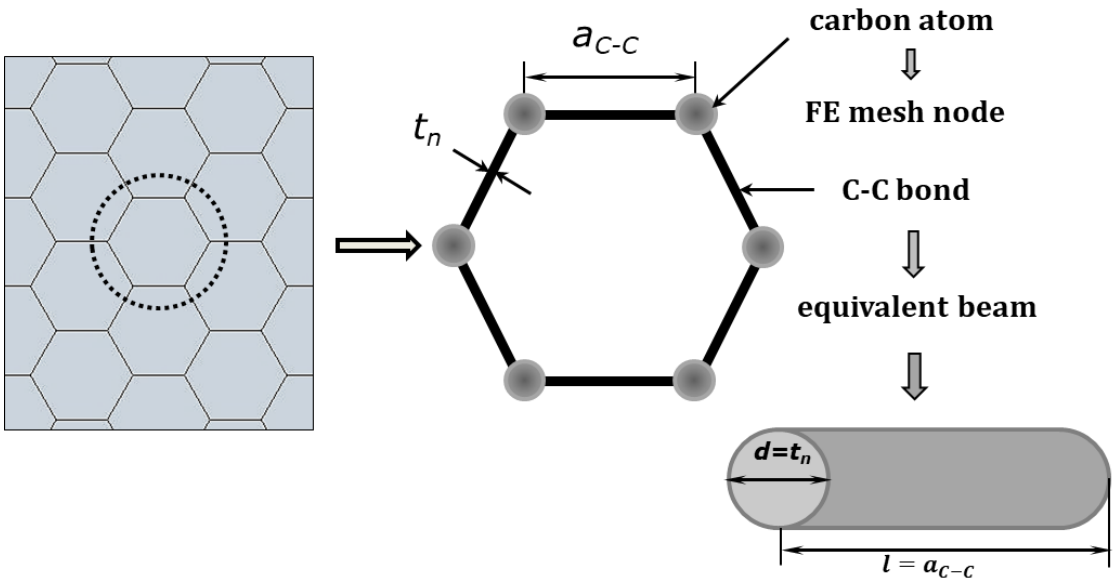

Figure 3.3. Modelling of CNT structure, replacing the C-C bonds by beam elements.

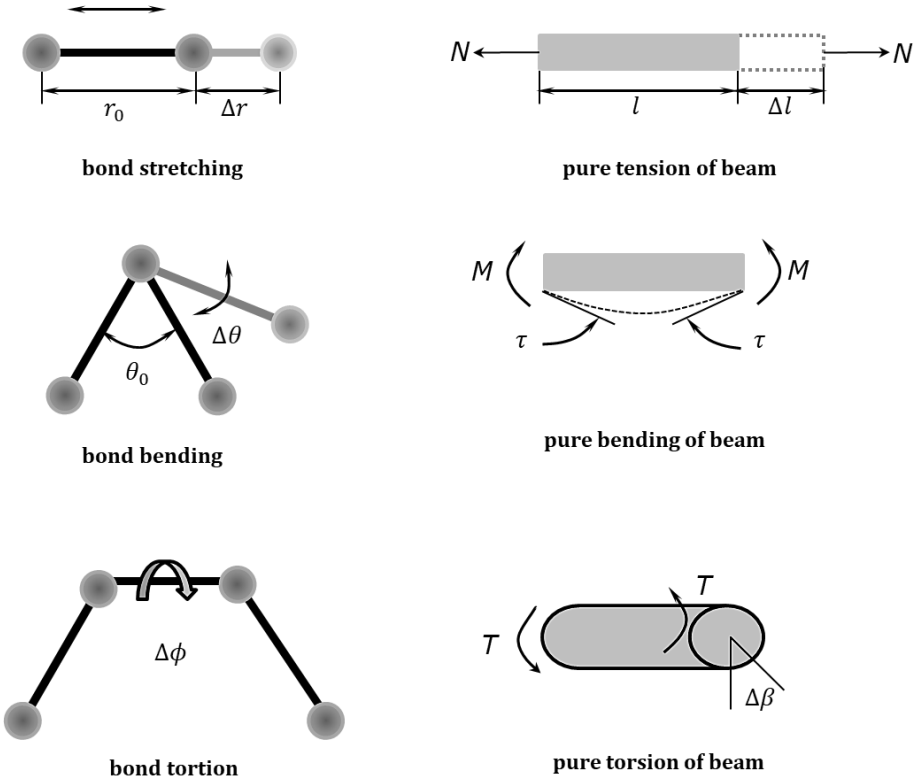

Figure 3.4. Equivalence between bond interactions in carbon nanotube and beam elements.

The tensile rigidity, EA, of SWCNT structures is determined as:

$$EA = \frac{F_a L}{u_a} \tag{3.7}$$

where F_a is the axial tensile force applied at one end of nanotube or heterojunction, leaving the other end fixed, L (L_{HJ} in case of SWCNT HJ) is the nanotube length and u_a is the axial displacement taken from the FE analysis.

Similarly, the bending rigidity of the SWCNT structures, EI, is represented as:

$$EI = \frac{F_t L^3}{3u_t} \tag{3.8}$$

where F_t is the transverse force applied at one end of the nanotube or heterojunction, leaving the other fixed, u_t is the transverse displacement, taken from the FE analysis.

Finally, the torsional rigidity of the SWCNT structures, GJ, is determined as:

$$GJ = \frac{TL}{\varphi} \tag{3.9}$$

where T is torsional moment applied at one end of the nanotube or heterojunction, leaving the other fixed and φ is the twist angle, taken from the FE analysis.

In case of torsion, the nodes under loading, at the end of the nanotube (or heterojunction), are prevented from moving in the radial direction.

In the case of SWCNT HJs, two loading conditions, which consist of fixing the narrower and the wider side of the HJ structure, were considered.

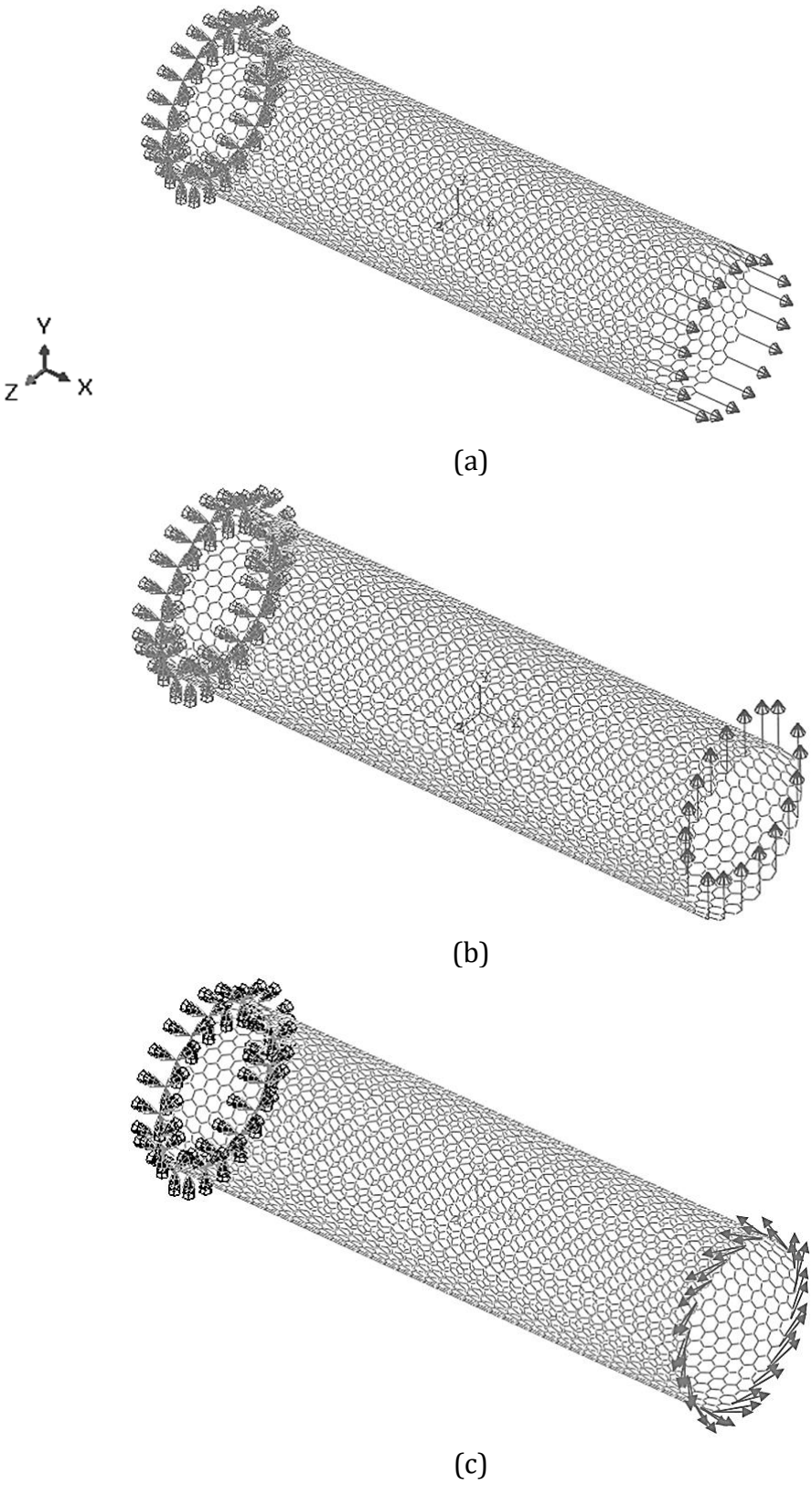

(a)

(b)

(c)

Figure 3.5. Loading and boundary conditions for (20, 20) armchair SWCNT: (a) tension; (b) bending; (c) torsion.

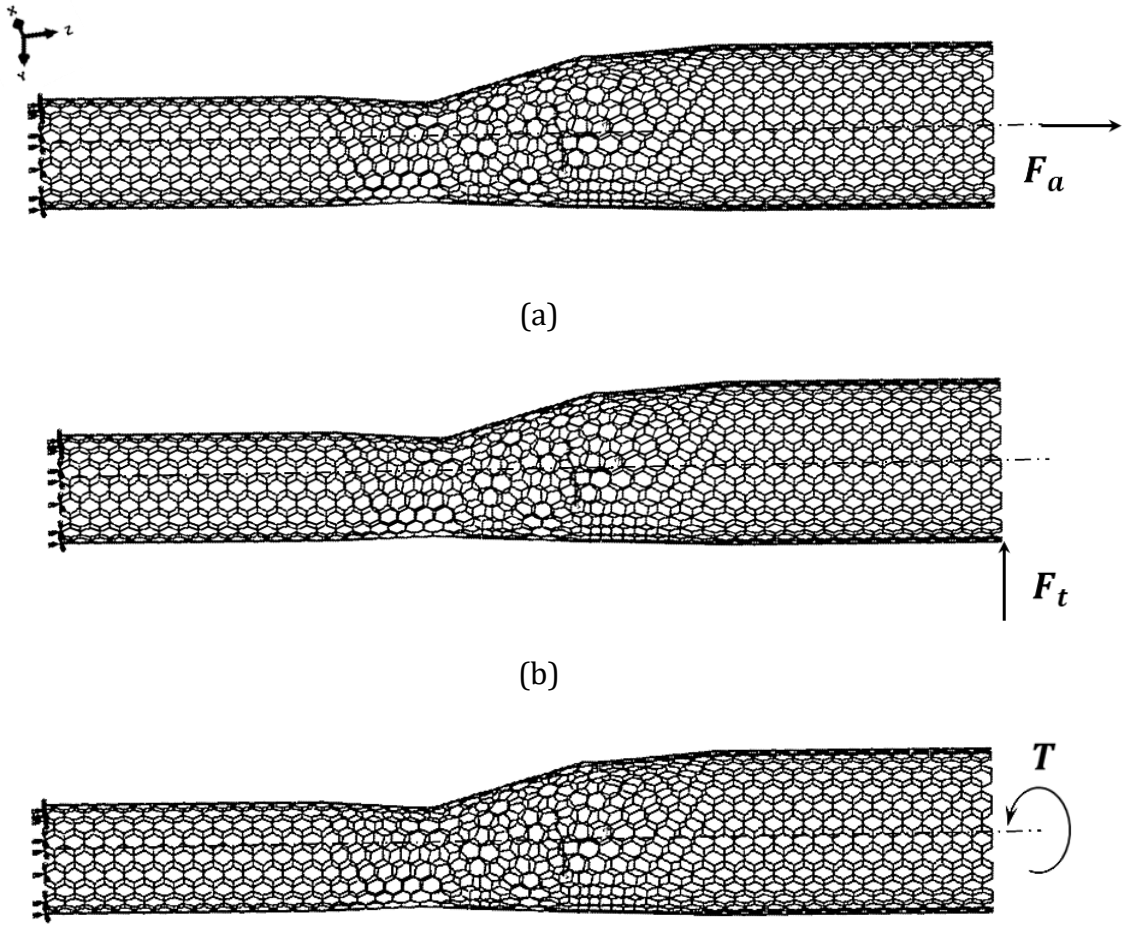

Figure 3.6. Loading and boundary conditions for armchair – armchair (10, 10) – (15, 15) HJ: (a) tension; (b) bending; (c) torsion.

References

Cornell WD, Cieplak P, Bayly CI, Gould IR, Merz KM, Ferguson DM, Spellmeyer DC, Fox T, Caldwell JW, Kollman PA (1995) A second generation force-field for the simulation of proteins, nucleic acids and organic molecules. Journal of the American Chemical Society, 117, 5179 – 5197.

Gelin BR (1994) Molecular modelling of polymer structures and properties. Cincinnati (OH): Hanser/Gardner Publishers.

Jorgensen WL and Severance DL (1990) Aromatic aromatic interactions – free energy profiles for the benzene dimer in water chloroform and liquid benzene. Journal of the American Chemical Society, 112, 4768 – 4774.

Li C and Chou TW (2003) A structural mechanics approach for the analysis of carbon nanotubes. International Journal of Solids and Structures, 40, 2487 – 2499.

Melchor S and Dobado JA (2004) CoNTub: An algorithm for connecting two arbitrary carbon nanotubes. Journal of Chemical Information and Computer Sciences, 44, 1639 – 1646.

Odegard GM, Gates TS, Nicholson LM, Wise KE (2002) Equivalent continuum modelling of nano-structured materials. Composites Science and Technology, 62, 1869 – 1880.

Pantano A, Parks DM, Boyce MC (2004) Mechanics of deformation of single- and multi-wall carbon nanotubes. Journal of Mechanics and Physics of Solids, 52, 789 – 821.

Pereira AFG, Antunes JM, Fernandes JV, Sakharova NA (2016) Shear modulus and Poisson's ratio of single-walled carbon nanotubes: numerical evaluation. Physica Status Solidi B, 253, 366 – 376.

Rappe AK, Casemit CJ, Colwell KS, Goddard WA, Skiff WM (1992) UFF, a full periodic-table force-field for molecular mechanics and molecular dynamics simulations. Journal of the American Chemical Society, 114, 10024 – 10035.

Sakharova NA, Pereira AFG, Antunes JM, Brett CMA, Fernandes JV (2015) Mechanical characterization of single-walled carbon nanotubes: Numerical simulation study. Composites B: Engineering, 75, 73 – 85.

Sakharova NA, Pereira AFG, Antunes JM, Fernandes JV (2016a) Numerical simulation study of the elastic properties of single-walled carbon nanotubes containing vacancy defects. Composites B: Engineering, 89, 155 – 168.

Sakharova NA, Pereira AFG, Antunes JM, Fernandes JV (2016b) Numerical simulation of the mechanical behaviour of single-walled carbon nanotubes heterojunctions. Journal of Nano Research, 38, 73 – 87.

Sakharova NA, Antunes JM, Pereira AFG, Chaparro BM, Fernandes JV (2017b) Elastic properties of carbon nanotubes and their heterojunctions. Proceedings (e-book) of XIV International Conference on Computational Plasticity. Fundamentals and Applications (COMPLAS 2017), Barcelona, Spain, 05-07 September 2017, Ed. by E. Oñate, D.R.J. Owen, D. Peric and M. Chiumenti, p. 963-974.

Tserpes KI and Papanikos P (2008) Finite element modeling of single-walled carbon nanotubes. Composites B: Engineering, 36, 468 – 477.

Chapter 4

Mechanical behaviour of CNTs' structures

This chapter is a collection of five papers (Sakharova *et al*., 2015, 2016a, 2016b, 2017b; Pereira *et al*., 2016), concerning numerical simulation studies on the mechanical response of SWCNTs, with and without vacancies, and SWCNT HJs, using NCM approach.

In the subchapter **4.1. Elastic properties of the perfect SWCNTs' structures,** the results related to the systematic evaluation of the elastic constants of the SWCNTs without defects are discussed. Afterwards, the evaluation of the elastic properties of SWCNTs containing vacancy defects is carried out in the subchapter **4.2. Elastic properties of the SWCNTs' structures containing vacancy defects**. Finally, the subchapter **4.3. Modelling and mechanical behaviour of SWCNT HJs**, is focused on a comprehensive numerical simulation study to evaluate the mechanical properties of SWCNT HJs.

(Page intentionally left blank)

4.1. Elastic properties of the perfect SWCNTs' structures

This subchapter consists of two complementary papers by Sakharova *et al*. (2015) and Pereira *et al*. (2016). The first paper, by Sakharova *et al*. (2015), deals with the evaluation of the tensile and bending rigidities, and subsequently, the Young's modulus of SWCNTs in a wide range of nanotube lengths, diameters, chiral angles and chiral indices. The second paper, by Pereira *et al*. (2016), is focused on the evaluation of the torsional properties, torsional rigidity and shear modulus of the same families of the SWCNTs studied in the first paper. A study on the Poisson's ratio evaluation is also carried out in this paper, using the results of the elastic tensile and shear moduli.

In summary, this subchapter analyses and discusses the results of systematic studies, regarding the influence of geometrical parameters of nanotubes on their elastic properties.

(Page intentionally left blank)

Composites Part B 75 (2015) 73–85

Contents lists available at ScienceDirect

Composites Part B

journal homepage: www.elsevier.com/locate/compositesb

Mechanical characterization of single-walled carbon nanotubes: Numerical simulation study

N.A. Sakharova [a, *], A.F.G. Pereira [a], J.M. Antunes [a, b], C.M.A. Brett [c], J.V. Fernandes [a]

[a] CEMUC – Department of Mechanical Engineering, University of Coimbra, Rua Luís Reis Santos, Pinhal de Marrocos, 3030-788 Coimbra, Portugal
[b] Escola Superior de Tecnologia de Abrantes, Instituto Politécnico de Tomar, Rua 17 de Agosto de 1808, 2200 Abrantes, Portugal
[c] CEMUC – Department of Chemistry, University of Coimbra, Rua Larga, 3004-535 Coimbra, Portugal

ARTICLE INFO

Article history:
Received 18 September 2014
Received in revised form
30 November 2014
Accepted 13 January 2015
Available online 29 January 2015

Keywords:
A. Nano-structures
B. Elasticity
B. Mechanical properties
C. Finite element analysis (FEA)
Young's modulus

ABSTRACT

The mechanical behaviour of non-chiral and chiral single-walled carbon nanotubes under tensile and bending loading conditions is investigated. For this purpose, three-dimensional finite element modelling is used in order to evaluate the tensile and bending rigidities and, subsequently, the Young's moduli. It is shown that the evolution of rigidity, tensile and bending, as a function of diameter can be described by a unique function for non-chiral and chiral single-walled nanotubes, i.e. regardless of the index or angles of chirality. A comprehensive study of the influence of the nanotube wall thickness and diameter on the Young's modulus values is also carried out. It is established that the evolution of the Young's modulus as a function of the inverse of the wall thickness follows a quasi-linear trend for nanotubes with diameters larger than 1.085 nm. The current numerical simulation results are compared with data reported in the literature. This work provides a benchmark in relation to ascertaining the mechanical properties of chiral and non-chiral single-walled carbon nanotubes by nanoscale continuum models.

1. Introduction

Carbon nanotubes (CNTs) are nanostructures attracting research interest due to their extraordinary mechanical, optical, thermal and electrical properties [1]. The CNTs outstanding physical properties such as strength and lightness enable applications in numerous different fields: chemistry, physics, engineering, materials science. From the point of view of structural application, the high stiffness together with low density indicates use of the CNTs as nanoscale fibres for reinforcement of nanocomposite structures (see, for example, [2–4]). This type of application of carbon nanotubes has required the investigation of their mechanical properties, including their deformation behaviour under different loading conditions.

There are two approaches commonly used to study the mechanical properties and deformation behaviour of CNTs: experimental and computational. For single-walled and multi-walled CNTs, methods for measuring Young's modulus based on *in situ* atomic force microscopy (AFM) and transmission electron microscopy (TEM) techniques have been established [5,6]. Although various experimental studies have been carried out to evaluate the mechanical properties of CNTs, there is inconsistency in the experimental results reported in the literature, owing to the complexity of the characterization of nanomaterials at the atomic scale. The common point in the experimental studies is the evidence of the unparallelled mechanical properties of CNTs. Concerning the accuracy of the values of the CNT mechanical properties that are determined, experimental studies still show a wide scatter of their values. From this point of view, computer simulation for predicting the mechanical properties of CNTs has been considered as a powerful tool, due to the experimental difficulties.

The theoretical approaches for the modelling and characterization of the CNTs behaviour can be divided into three main categories: the atomistic approach, the continuum approach and the nanoscale continuum approach. A comprehensive critical review concerning the modelling of the mechanical behaviour of carbon nanotubes has been undertaken by Rafiee and Moghadam [7]. Hereinafter, a brief assessment of main modelling methodologies is carried out.

Atomistic modelling, used solely during the first years of theoretical studies on CNTs, calculates the positions of atoms based on their interactive forces and boundary conditions (see, for example [8]). Atomistic modelling comprises an *ab initio* approach [9] and

* Corresponding author. Tel.: +351 239790747.
E-mail address: nataliya.sakharova@dem.uc.pt (N.A. Sakharova).

http://dx.doi.org/10.1016/j.compositesb.2015.01.014
1359-8368/

molecular dynamics (MD) [10–14]. After this, other atomistic modelling methods, such as tight-binding molecular dynamics (TBMD) [15,16] were developed.

Generally, *ab initio* methods give more accurate results than MD, but they are computationally expensive and only possible to use for a small number of molecules or atoms. Molecular dynamics can be used in large systems and provide good predictions of CNT mechanical properties under different loading conditions, but it is still limited owing to its being very time consuming, especially when long or multi-walled CNTs are simulated. In recent years, the atomistic approaches, due to their big computation cost, have been gradually replaced by continuum approaches, which are at the moment the most indicated for effective computational simulation of large systems.

The basic assumption of the continuum mechanics-based approach consists of the modelling of CNTs as a continuum structure, concerning the distribution of mass, stiffness, etc., i.e. the real discrete structure of the nanotubes is neglected and replaced by a continuum medium. Some authors have explored continuum shell modelling for studying the mechanical behaviour of CNTs [17–20]. However, the atomic characteristics of carbon nanotubes, such as chirality, are not taken into account in the continuous shell approach, and so their effects on the mechanical behaviour of CNTs cannot be captured. To overcome this obstacle, Chang proposed an anisotropic shell model for SWCNTs [21] that can predict some anisotropic effects related to chirality. Besides shell structures, other continuum structures, such as tubes and plates, are employed in continuum approaches. In the models of Sears and Batra [22], and Gupta and Batra [23] the whole single-walled CNT structure was simulated as an equivalent continuum tube. Wang [24] employed the equivalent elastic plate model. Arash and Wang [25] show the advantages of the continuum theory applied to the modelling of shells and plates. However, whatever the type of the continuum modelling approach, the replacement of the whole CNT structure by a continuum element is not a completely satisfactory method to evaluate CNT properties.

The nanoscale continuum modelling (NCM) consists of replacing the carbon–carbon (C–C) bond by a continuum element. As a result, continuum mechanics theories can be used at the nanoscale, i.e. a linkage between molecular configuration and solid mechanics is recognized. NCM is frequently accomplished by finite element modelling. The main approach in NCM consists of considering different elements, such as rod, truss, spring and beam, well described in elasticity theory, to simulate C–C bonds (see, for example, [26–29]). The first NCM model of CNTs was developed by Odegard et al. [26] and consisted of a continuum truss model. The disadvantage of the truss model is the impossibility of describing the CNT mechanical behaviour under torsional load, because the out-of-plane torsion of the C–C bond cannot be taken into account.

Various FEM models where the C–C bonds are simulated using diverse kinds of elastic spring element, such as linear, non-linear, rotational, torsional, have been recently reported [30–37]. Although the use of spring elements is an effective way for simulation of the bond angle variations, the accuracy of the Young's modulus results depends on the choice of the potential function for the calculation of the force constants.

Since Li and Chou [27] linked the interatomic potential energies to the strain energies of an equivalent beam element and established a direct relationship between sectional stiffness parameters and the force field constants, equivalent beam approaches have been successfully used to simulate the mechanical behaviour of CNT, although with different formulations of the inter-atomic molecular potential energies and boundary conditions [28,38–43]. The FE models, which employed beam elements in a three-dimensional (3D) space, developed by Tserpes and Papanikos [26], Papanikos et al. [38] and Avila and Lacerda [39] differ from each other mainly due to the boundary conditions and the method for the Young's modulus calculation. The recent 3D FE model of Lu and Hu [42] used the same formulation for potential energy of covalent system, but considering an elliptical cross-section area of equivalent beam. In another analytical approach developed by Shokrieh and Rafiee [40], the deformations of beam elements were obtained using Castigliano's theorem. In the works of Her [41] and Mohammadpour [43] the modified Morse potential function for the potential energy of the covalent system used to describe non-linear behaviour of C–C bonds was applied. It can be concluded from these studies that nanoscale continuum modelling (NCM) is an adequate modelling technique for predicting CNT mechanical properties and shows results in close agreement with those obtained from MD modelling.

In the present study, the equivalent beam approach is used in order to evaluate the tensile and bending rigidities and, subsequently, Young's modulus of various single-walled carbon nanotubes (SWCNT) structures, as non-chiral (zigzag, $\theta = 0°$, and armchair, $\theta = 30°$) and families of chiral ($\theta = 8.9°; 13.9°; 19.1°$ among others) SWCNTs for a wide range of chiral indices, nanotube length and diameter. A comprehensive study of the influence of the nanotube wall thickness and diameter on the Young's modulus results was carried out. Moreover, the present work provides a benchmark in relation to ascertaining the mechanical properties of chiral and non-chiral SWCNTs by nanoscale continuum models.

2. Materials and methods

2.1. Atomic structure of SWCNTs

A simple way to describe an SWCNT is as a rolled-up graphene sheet giving rise to a hollow cylinder, the surface of which is composed of hexagonal carbon rings (see, for example [44,45]). The hexagonal pattern is repeated periodically, leading to binding of each carbon atom to three neighbouring atoms by covalent bonds. A schematic illustration of an unrolled hexagonal graphene sheet is shown in Fig. 1. The symmetry of the atomic structure of SWCNTs is characterized by the chirality, which is defined by the chiral vector $\boldsymbol{C_h}$:

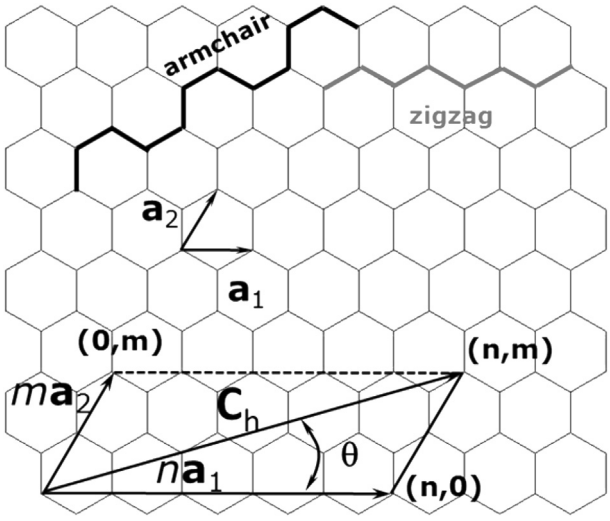

Fig. 1. Schematic illustration of an unrolled hexagonal graphene sheet with definition of chiral vector.

$$\boldsymbol{C_h} = n\boldsymbol{a}_1 + m\boldsymbol{a}_2 \quad (1)$$

where *(n,m)* is a pair of the lattice translation indices $\boldsymbol{a}_1$ and $\boldsymbol{a}_2$, the unit vectors of the hexagonal lattice, n and m are integers.

The length of the unit vector $\boldsymbol{a}$ is defined as $a = \sqrt{3}a_{C-C}$ with the equilibrium carbon–carbon (C–C) covalent bond length a_{C-C} usually taken to be 0.1421 nm. The nanotube circumference, L_c, and diameter, D_n are defined as:

$$L_c = |\boldsymbol{C_h}| = a\sqrt{n^2 + nm + m^2} \quad (2)$$

$$D_n = \frac{L_c}{\pi} \quad (3)$$

The chiral angle, θ, is the angle between the chiral vector $\boldsymbol{C_h}$ and the direction $(n, 0)$. The chiral angle, θ, is given by Ref. [44]:

$$\theta = \sin^{-1}\frac{\sqrt{3}m}{2\sqrt{n^2 + nm + m^2}} \quad (4)$$

Three main symmetry groups of SWCNTs exist. When $n = m$, the structure *(n, n)* is called the armchair configuration; when $m = 0$, the structure *(n, 0)* is called zigzag; when $n \neq m$, the structure *(n, m)* is called chiral. These three major categories of SWCNTs can also be defined based on the chiral angle, θ. For the two limiting chiral angles of 0° and 30°, the nanotubes are referred to as armchair and zigzag, respectively. For θ different from 0° and 30°, the nanotubes are designated as chiral [46].

2.2. FE modelling of SWCNTs

The displacement of individual carbon atoms in CNT under external forces is constrained by the covalent bonds. Therefore, the overall deformation of the CNT is the result of the interactions between bonds. Since the C–C bonds can be considered as load-carrying elements, and the carbon atoms as joints of connecting elements, it is possible to simulate CNTs as space-frame structures [27,28] and analyze their mechanical behaviour using classical structural mechanics methods.

In the present work, the 3D FE model, which is able to assess the mechanical properties of SWCNTs, proposed in Ref. [28], was adopted. Thus, characterization of the rigidities of SWCNTs is performed based on the equivalent continuum modelling (ECM) approach, where the equivalent beam elements replace the C–C bonds. This approach is based on the premise that the mechanical behaviour of CNTs and elastic beams is identical.

The FE meshes of the carbon nanotube structures used in the finite element analyses were constructed using the academic software CoNTub 1.0 [47], which permits building the CNT structures. This code generates ASCII files, describing atom positions, which can be entered as input in available commercial and in-house FEA codes, in order to perform the simulation of mechanical tests. To convert the ASCII files, obtained using the CoNTub 1.0 program, into the format usable by the commercial FEA code ABAQUS®, the in-house application designated *InterfaceNanotubes* was developed. The FE model uses the coordinates of the carbon atoms for generating the nodes and then the suitable connection of the nodes creates the beam elements. The FE simulation uses the analogy between the bond length, a_{C-C}, and the element length L and between the nanotube wall thickness and the element thickness. Assuming the beam element has a circular cross-section area, the wall thickness corresponds to the element diameter.

In the present work, chiral and non-chiral SWCNTs were simulated over a wide range of chiral indices, nanotube lengths and diameters. The FE model takes into account the chirality of the SWCNTs, and so is able to consider their anisotropic behaviour due to chirality. The geometrical characteristics of SWCNTs used for the FE analyses are summarized in Table 1, where the number of nodes and elements of the finite element meshes of the SWCNTs is also indicated for a nanotube with a length of 20 nm. The choice of SWCNT geometrical characteristics was made taking into account real nanotube sizes: for example, the (4, 2) chiral nanotube is the smallest diameter nanotube ever synthesized [48].

Knowledge of the exact dimensions of CNTs at the equilibrium state is still a challenge for research. Unlike the C–C bond length a_{C-C}, for which the experimentally observed value of 0.1421 nm is accepted as the exact value, the wall thickness of CNT, t, is not clearly specified in the literature. Since in the present study the SWCNTs are modelled as space-frame structures, the wall thickness, t, should be identified in a continuum sense. Although a few theoretical reports have provided values for nanotube wall thickness that range from 0.064 [18] to 0.69 nm [26], the most widely used value of 0.34 nm (equal to the interlayer spacing of graphite) is adopted for the SWCNT wall thickness, t, in order to enable comparison of the current results with those available in the literature. Nevertheless, taking in account the ambiguity of the value of CNT wall thickness in the literature, a parametric study of the effect of the wall thickness value on the calculation of SWCNT Young's modulus was performed.

2.3. FE analysis of SWCNTs

2.3.1. Structural mechanics of SWCNTs

As was originally proposed by Odegard et al. [26], and then developed by Li and Chou [27], the elastic moduli of the beam elements are determined by establishing the link between interatomic potential energies of the molecular structure and strain energies of the equivalent continuum structure comprising of frame members (beams) undergoing axial and bending deformations. From a molecular point of view, the CNTs can be envisaged as large molecules composed of carbon atoms. The force-field is expressed in the form of the total potential energy, which is uniquely defined by the relative positions of the nuclei composing the molecule. According to molecular dynamics, the total empirical inter-atomic potential energy of a molecular system is expressed as a sum of the individual energy terms due to bonded and non-bonded interactions [49]:

$$U_{tot} = \sum U_r + \sum U_\theta + \sum U_\phi + \sum U_\omega + \sum U_{vdw} \quad (5)$$

where U_r, U_θ, U_ϕ, U_ω are energies associated with bond stretching, bending (bond angle variation), dihedral angle torsion, out-of plane torsion, respectively, and U_{vdw} is the energy associated with non-bonded van der Waals interaction.

Generally, in covalent system, non-bonded interactions are negligible in comparison with bonded ones, and the main contribution to the total potential energy is from the first four terms of Eq. (5). The contributions of dihedral angle torsion and out-of plane torsion to total inter-atomic potential energy are insignificant, compared with contributions of other bonded interactions, and the main contribution to the inter-atomic potential energy is due to bond stretching. Consequently, under the assumption of small deformation, the total inter-atomic potential energy can be approximated by Ref. [50]:

$$U_r = \frac{1}{2}k_r(\Delta r)^2 \quad (6)$$

$$U_\theta = \frac{1}{2}k_\theta(\Delta\theta)^2 \quad (7)$$

Table 1
Geometrical characteristics of SWCNTs studied and number of nodes and elements of the finite element meshes used (nanotube length 20 nm).

SWCNT type			(n, m)	D_n, nm	θ°	Number of nodes	Number of elements
Non-chiral	Armchiar		(3, 3)	0.407	30	972	1448
			(5, 5)	0.678		1620	2414
			(6, 6)	0.814		1944	2897
			(8, 8)	1.085		2592	3863
			(9, 9)	1.221		2916	4346
			(10, 10)	1.356		3240	4829
			(12, 12)	1.628		3888	5795
			(15, 15)	2.034		4860	7244
			(20, 20)	2.713		6840	9659
	Zigzag		(3, 0)	0.235	0	558	830
			(5, 0)	0.392		930	1384
			(10, 0)	0.783		1860	2769
			(12, 0)	0.940		2232	3323
			(15, 0)	1.175		2790	4154
			(18, 0)	1.409		3348	4985
			(20, 0)	1.566		3720	5539
			(24, 0)	1.879		4464	6647
Chiral	Family θ 8.9		(5, 1)	0.436	8.9	1044	1554
			(10, 2)	0.872		2088	3109
			(15, 3)	1.308		3132	4664
			(20, 4)	1.744		4176	6219
			(25, 5)	2.180		5220	7774
			(30, 6)	2.616		6264	9329
	Family θ 13.9		(6, 2)	0.565	13.9	1352	2013
			(9, 3)	0.847		2028	3020
			(12, 4)	1.129		2740	4027
			(15, 5)	1.412		3380	5034
			(18, 6)	1.694		4056	6041
			(21, 7)	1.976		4732	7048
			(24, 8)	2.259		5408	8055
			(27, 9)	2.541		6084	9062
	Family θ 19.1		(4, 2)	0.414	19.1	992	1477
			(6, 3)	0.622		1488	2216
			(8, 4)	0.829		1984	2955
			(10, 5)	1.036		2840	3694
			(12, 6)	1.243		2976	4433
			(14, 7)	1.450		3472	5172
			(16, 8)	1.657		3968	5911
			(18, 9)	1.865		4464	6650
			(20, 10)	2.072		4960	7389
			(22, 11)	2.279		5456	8128
			(24, 12)	2.486		5952	8867
	$n + m$	12	(7, 5)	0.818	24.5	1960	2920
			(11, 1)	0.903	4.3	2167	3222
		18	(16, 2)	1.338	5.8	3208	4777
			(14, 4)	1.282	12.2	3072	4575
			(13, 5)	1.260	15.6	3020	4498
			(11, 7)	1.231	22.7	2950	4395
			(10, 8)	1.223	26.3	2932	4369
		24	(22, 2)	1.806	4.3	4328	6445
			(19, 5)	1.717	11.4	4116	6130
			(17, 7)	1.674	16.5	4012	5976
			(15, 9)	1.644	21.8	3942	5873
			(14, 10)	1.635	24.5	3920	5841
			(13, 11)	1.629	27.2	3906	5821

where k_r, k_θ, are the bond stretching and bond bending force constants, respectively, and Δr and $\Delta\theta$ are the respective bond stretching and bond angle variation increments.

The interatomic potential energy of the molecular structure comprises bond stretching and angle variation. Thus, the structural member for substituting the C–C bond has to be able to capture both axial and bending deformations. The beam is identified by the cross sectional area, elastic modulus, moment of inertia and length.

Relationships between the sectional stiffness parameters in structural mechanics and force field constants in molecular dynamics are required for the determination of the elastic modulus of beam elements. Thus, the elastic moduli can be determined by establishing the equivalence between the energies associated with the interatomic interactions (through Eqs. (6) and (7)) and with the deformation of the structural elements (i.e. beams) of the space-frame structure.

Classical mechanics gives the following expression for the strain energy of a uniform beam of length, l, and cross-section area, A_b, under a pure axial force, N:

$$U_A = \frac{1}{2}\int_0^L \frac{N^2}{E_b A_b} dl = \frac{1}{2}\frac{N^2\, l}{E_b A_b} = \frac{1}{2}\frac{E_b A_b}{l}(\Delta l)^2 \tag{8}$$

where Δl is the axial stretching deformation, and E_b is the Young's modulus of the beam.

The strain energy of a uniform beam, with moment of inertia, I_b, under a pure bending moment, M, according to classical mechanics, is expressed as:

$$U_M = \frac{1}{2}\int_0^L \frac{M^2}{E_b I_b} dl = \frac{1}{2}\frac{E_b I_b}{l}(2\alpha)^2 \tag{9}$$

where α is the rotational angle at the ends of the beam.

The parameters U_r and U_A are stretching energies in molecular and structural systems, respectively, and U_θ and U_M represent the corresponding bending energies. Comparing Eqs. (6) and (7) with Eqs. (8) and (9), and assuming the equivalences of the rotational angle, 2α, with the total variation of the bond angle, $\Delta\theta$, and of Δl with Δr, direct relationships can be established between the structural mechanics parameters, E_bA_b, E_bI_b, and the force field constants, k_r, k_θ, [27]:

$$\frac{E_b A_b}{l} = k_r, \tag{10}$$

$$\frac{E_b I_b}{l} = k_\theta, \tag{11}$$

where l is the bond length generally considered equal to 0.1421 nm. Consequently, Eqs. (10) and (11) establish the basis for application of continuum mechanics to the analysis of the mechanical behaviour of CNTs. In order to determine the rigidities of beam elements, the relationships between the sectional stiffness parameters and force-field constants need to be clarified. In the approach of Li and Chou [27], a solid circular cross-sectional area of the beams with diameter d is assumed and so the geometrical parameters A_b and I_b are as follows:

$$A_b = \frac{\pi d^2}{4} \tag{12}$$

$$I_b = \frac{\pi d^4}{64} \tag{13}$$

Assuming these settings, Eqs. (10) and (11) become, respectively:

$$d = 4\sqrt{\frac{k_\theta}{k_r}} \tag{14}$$

$$E_b = \frac{k_r^2 l}{4\pi k_\theta} \tag{15}$$

Eqs. (14) and (15) allow determining the necessary input parameters for the beam elements. In this study, the bond stretching and bond bending force constants used [51] are:

$$k_r = 6.52 \times 10^{-7}\ \text{N/nm}$$

$$k_\theta = 8.76 \times 10^{-10}\ \text{N nm rad}^{-2}$$

Then, substituting these values in Eqs. (14) and (15) and setting $l = a_{C-C} = 0.1421$ nm, the input parameters for the FE model are obtained. The geometrical and material parameters and values necessary for the finite element simulation of SWCNTs are summarized in Table 2.

Table 2
Input parameters for FE simulations of SWCNTs.

Parameter	Value	Formulation
C–C bond/beam length ($l = a_{C-C}$)	0.1421 nm	–
Diameter (d)	0.147 nm	$d = 4\sqrt{k_\theta/k_r}$
Cross section area, A_b	0.01688 nm^2	$A_b = \pi d^2/4$
Moment of inertia, I_b	2.269×10^{-5} nm^4	$I_b = \pi d^4/64$
Young's modulus, E_b	5488 GPa	$E_b = k_r^2 l/4\pi k_\theta$
Rigidity, E_bA_b	92.65 nN	$E_bA_b = k_r l$
Rigidity, E_bI_b	0.1245 nN nm^2	$E_bI_b = k_\theta l$

2.3.2. Loading conditions

Numerical simulation of conventional mechanical tension and bending tests was carried out in order to study the effect of nanotube length and diameter on their mechanical properties, focussing on the tensile and bending rigidities. The FE analysis was performed using the commercial FE code ABAQUS®.

In order to simulate the mechanical behaviour of SWCNT in tension, an axial force, F_x, is applied at one nanotube end, leaving the other end fixed. The tensile rigidity of the nanotube, EA, is determined as:

$$EA = \frac{F_x L}{u_x} \tag{16}$$

where L is the nanotube length and u_x is an axial displacement taken from the FE analysis.

Likewise, for simulating bending, a transverse force, F_y, is applied at one extremity of the nanotube, leaving the other fixed. The bending rigidity of the nanotube, EI, is determined as:

$$EI = \frac{F_y L^3}{3u_y} \tag{17}$$

where u_y is a transverse displacement taken from the FE analysis.

2.3.3. Evaluation of the Young's modulus of SWCNTs

The nanotube rigidities, EA and EI, are required for the evaluation of the SWCNT Young's modulus, E. Considering a hollow cylindrical profile for the equivalent beam, i.e. a geometry similar to the CNT, the cross-sectional area of the equivalent hollow cylinder and moment of inertia can be written as:

$$A = \frac{\pi}{4}\left[(D+t)^2 - (D-t)^2\right] = \pi D t \tag{18}$$

$$I = \frac{\pi}{64}\left[(D+t)^4 - (D-t)^4\right] \tag{19}$$

where D and t are the mean diameter and the thickness of the equivalent hollow cylinder, respectively.

Assuming $t = t_n$ (where t_n is the nanotube wall thickness), the expression for D can be derived from Eqs. (18) and (19):

$$\frac{EI}{EA} = \frac{1}{8}\left(D^2 + t_n^2\right) \Rightarrow$$

$$D = \sqrt{8\left(\frac{EI}{EA}\right) - t_n^2} \tag{20}$$

Thus, the Young's modulus of the SWCNT can be calculated using the following expression, taking into account the rigidities in tension and bending:

$$E = \frac{EA}{A} = \frac{EA}{\pi t_n \sqrt{8\left(\frac{EI}{EA}\right) - t_n^2}} \quad (21)$$

3. Results and discussion

3.1. Rigidities of SWCNTs

3.1.1. Effect of the SWCNT's length on the tensile and bending rigidities

The common length of carbon nanotubes currently produced is in the order of 1 μm, their diameter being in the range 0.5–3 nm. Consequently, the modelling of CNT with their real length leads to high computing costs. As is known from previous studies [38], the modelling of real nanotube length is not crucial because of its length-independent mechanical behaviour, with the exception of very small lengths. A study for estimating the minimum length above which the values of the tensile and bending rigidities become stable was performed in order to make a selection of the minimum modelling length of the CNTs.

Examples of the evolution of tensile, *EA*, and bending, *EI*, rigidities with nanotube length are shown in Fig. 2, for the cases of armchair (10, 10), zigzag (10, 0) and chiral of the family $\theta = 8.9°$ SWCNTs. The tensile, *EA*, and bending, *EI*, rigidities stabilize from a certain value of the nanotube length, which is always less than 20 nm, whatever the SWCNT type, chiral or non-chiral, the chiral angle and nanotube diameter. The tensile and bending rigidities are almost constant, with increasing *EA* and decreasing *EI* for small nanotube lengths. A similar evolution of the tensile and bending rigidities was observed for non-chiral SWCNTs by Papanikos et al. [38], who justify the evolution of the rigidities observed for small nanotube lengths by the small ratio between the nanotube length and its diameter.

Taking into account the fact that the CNTs currently synthesized have relatively high length to diameter ratio, numerical simulation of the mechanical behaviour of nanotubes with a small length to diameter ratio is not needed. For this reason, in the following, 20 nm was chosen as modelling length for numerical simulation.

3.1.2. Effect of the chiral indices and chiral angles on the rigidities of SWCNTs

The stabilized values of both the tensile and bending rigidities (i.e. determined for L = 20 nm) were used for evaluation of the effect of the SWCNT chiral indices, *n* and *m*, and chiral angle, θ, on their mechanical properties. The evolutions of the tensile, *EA*, and bending, *EI*, rigidities as a function of the chiral indices, *n*, for armchair and zigzag nanotubes, and as a function of the sum of chiral indices, $(n + m)$, for chiral nanotubes, are shown in Fig 3. The evolutions of the tensile and bending rigidities, for armchair, zigzag and chiral SWCNTs, are related to the chiral indices as follows: the tensile rigidity, *EA*, increases quasi-linearly with the chiral indices and the bending rigidity, *EI*, increases with the chiral indices according to a cubic power expression. The *EA* evolutions can be separated for armchair, zigzag and chiral SWCNTs. The same is true for *EI* evolutions. In order to analyze the evolution of tensile and bending rigidities with chiral angle, θ, SWCNTs with the same sum of chiral indices $(n + m)$ were considered. Fig. 4 shows that the values of both rigidities, *EA* and *EI*, for the three families $(n + m)$ studied, decrease from the rigidity values obtained for zigzag SWCNTs ($\theta = 0°$), with a rate that becomes smaller as θ increases.

In order to clarify the trends shown in Fig. 3, the values of the rigidities as a function of the SWCNT diameter, D_n, are plotted in Fig. 5. It can be seen that the evolution of the tensile rigidity, *EA*, can be unified for all SWCNTs studied, and the same is true for the bending rigidity, *EI*. The quasi-linear trend for the case of tensile rigidity, *EA*, and close to a cubic power trend for the case of bending rigidity, *EI*, can be expressed as follows:

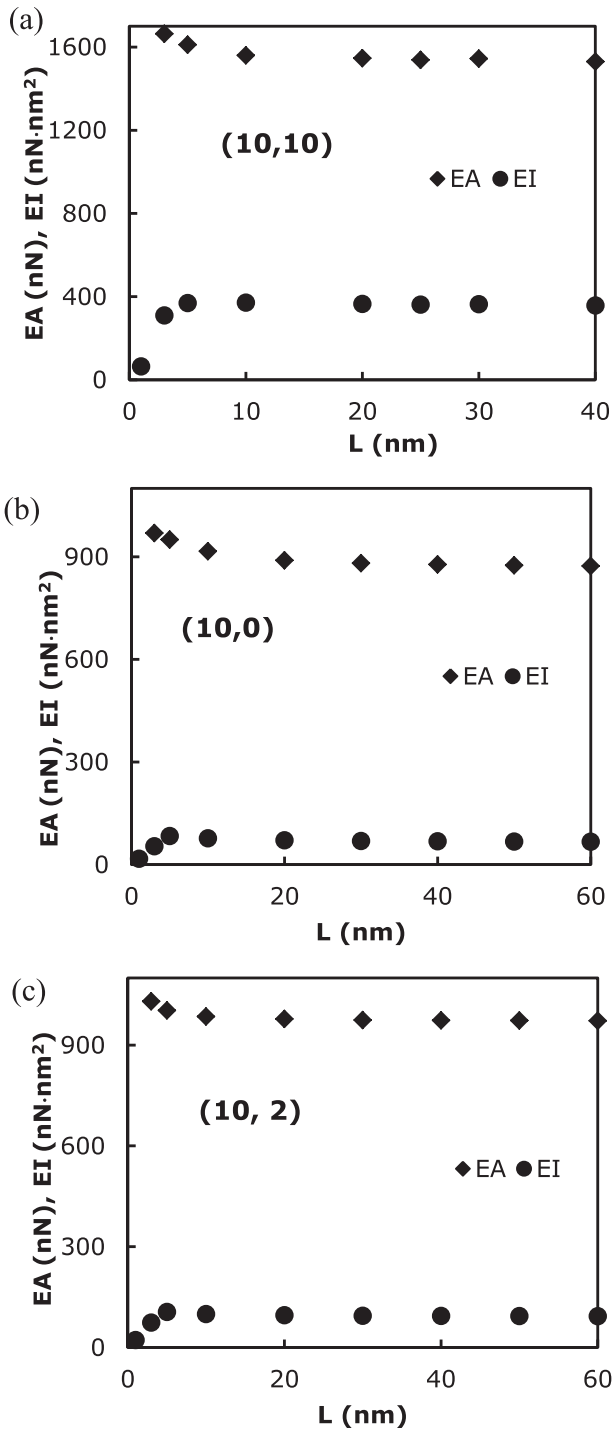

Fig. 2. Evolution of the tensile, *EA*, and bending, *EI*, rigidities with nanotube length, *L*, for (a) armchair (10, 10), (b) zigzag (10, 0) and (c) chiral (10, 2) SWCNTs.

$$EA = \alpha(D_n - D_0) \quad (22)$$

$$EI = \beta(D_n - D_0)^3 \quad (23)$$

These equations are of the same type as those previously proposed for non-chiral SWCNTs [38], but replacing the chiral index, *n*

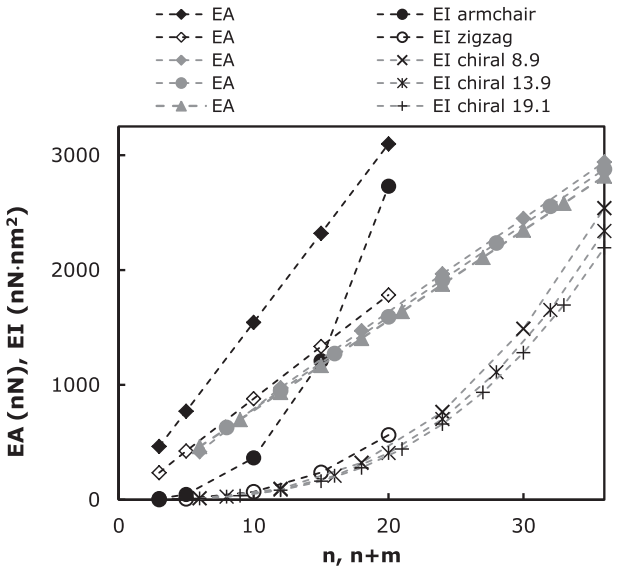

Fig. 3. Evolution of the tensile, *EA*, and bending, *EI*, rigidities of SWCNTs for armchair and zigzag, as a function of the chiral indices, n; and as a function of the sum of chiral indices, $(n+m)$, for three families $\theta = 8.9, 13.9, 19.1°$.

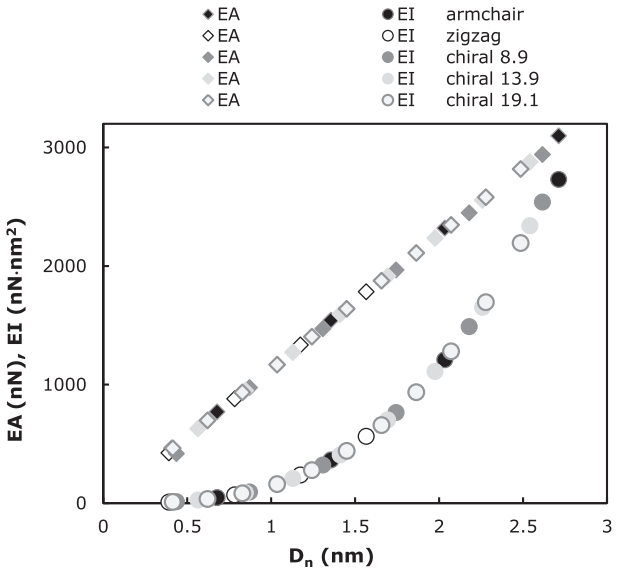

Fig. 5. Evolution of the tensile, *EA*, and bending, *EI*, rigidities as a function of the nanotube diameter, D_n for armchair, zigzag and three families $\theta = 8.9, 13.9, 19.1°$.

by the SWCNT diameter, D_n. In this study [38], the evolutions of *EA* as a function of *n* can be separated for armchair and zigzag nanotubes; the same is valid for *EI* evolutions. The fitting parameters α, β and D_0 obtained in the current work, and those calculated based on the results of previous works ([38] and [52]) are given in Table 3. Fig. 6 (a) and (b) shows the values of *EA* and *EI* as a function of $(D_n - D_0)$ and $(D_n - D_0)^3$, respectively; the fitting lines from Eqs (22) and (23) are also shown.

Eqs. (22) and (23) allow unifying the behaviour of the SWCNTs regarding the evolution of rigidity with nanotube diameter and permit accurate determination of the rigidity values for chiral and non-chiral SWCNTs. The mean difference between the values of *EA*, obtained from Eq. (22), and the values obtained directly from FE analysis, is 0.65% for armchair, 0.56% for zigzag and 0.25% for chiral SWCNTs. The mean differences between the values of *EI* estimated by Eq. (23) and those obtained from FE analysis are 1.29% for armchair, 2.54% for zigzag and 0.66% for chiral SWCNTs. It is therefore possible to conclude that Eqs. (22) and (23) allow calculation, with sufficient accuracy, of the values of the tensile rigidity, *EA*, and bending rigidity, *EI*, whatever the type of SWCNT configuration in the range of nanotube diameters studied in the current work. Also, Eqs (22) and (23) permit fast assessment of the Young's modulus of any type of SWCNT, as shown in the next section.

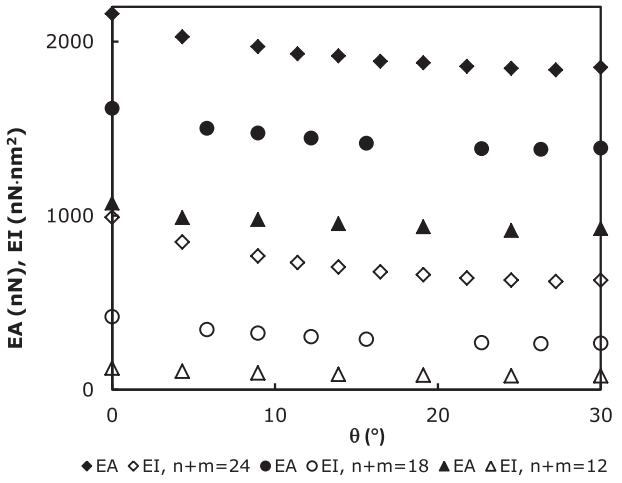

Fig. 4. Evolution of the tensile, *EA*, and bending, *EI*, rigidities as a function of the chiral angle, θ for three families of SWCNTs with $(n+m) = 12, 18, 24$.

3.2. Young's modulus of single-walled nanotubes

Eqs. (22) and (23) for the tensile and bending rigidities enable writing Eq. (21) as follows:

$$E = \frac{EA}{A} = \frac{\alpha(D_n - D_0)}{\pi t_n \sqrt{8\frac{\beta(D_n-D_0)^2}{\alpha} - t_n^2}} \tag{24}$$

This equation allows determination of the Young's modulus of any type of SWCNT, knowing the parameters of Table 3 and the wall thickness, t_n.

3.2.1. Effect of the wall thickness on the calculation of the Young's modulus

Eqs. (21) and (24) show that the choice of the value of the wall thickness of the nanotubes has a direct impact on the calculation of the SWCNT Young's modulus. The scatter of the wall thickness value from 0.066 to 0.69 nm reported in the literature demonstrates the need to study the effect of the value considered on the Young's modulus, in order to discuss the FE results of the Young's modulus and enable comparison with the results reported in the literature.

Table 3
Fitting parameters α, β and D_0.

Parameter	Current study[a]	Papanikos et al. [38] [b]	Chang&Gao [52] [b]
α (nN nm^{-1})	1131.66	1128.15	1141.3
β (nN nm^{-1})	143.48	142.54	–
D_0 (nm)	$2.8\cdot10^{-7}$	0	–

[a] Includes armchair, zigzag and all types of chiral SWCNT studied.
[b] Includes armchair and zigzag SWCNT.

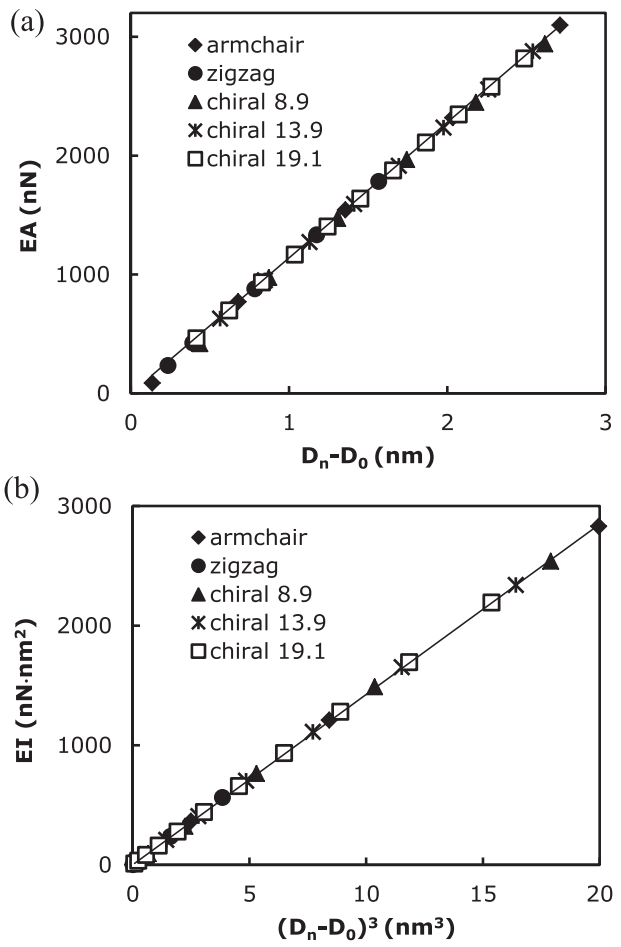

Fig. 6. Evolution of: (a) the tensile, *EA*, rigidity as a function of $(D_n - D_0)$ and (b) bending, *EI*, rigidity as a function of $(D_n - D_0)^3$. The results are represented by symbols and fitting trends by lines.

First, SWCNTs with different diameters were studied. Fig. 7 shows the Young's modulus determined by Eq. (24) as a function of the inverse of the nanotube wall thickness (for the range of t_n values 0.06–0.69 nm), for the cases of the diameters of armchair SWCNTs shown in Table 1. The evolution of the Young's modulus as a function of the inverse of the wall thickness follows a quasi-linear trend over the whole range of thicknesses, for nanotubes with diameter $D_n \gtrsim 1.085$ nm. Such a linear trend was also reported by Tserpes and Papanikos [28] and Avila and Lacerda [39], although

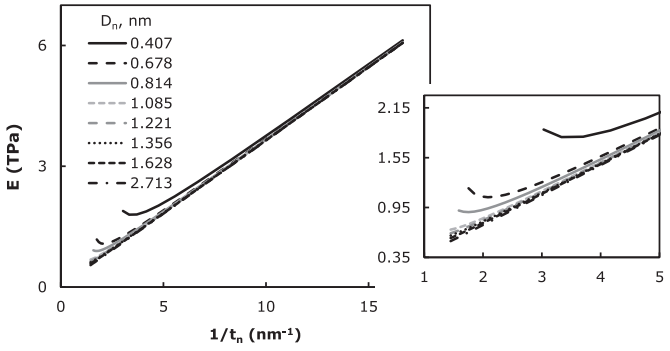

Fig. 7. Evolution of armchair SWCNTs Young's modulus with the inverse of the wall thickness for different nanotube diameters, according to Eq. (24).

only in one case of SWCNTs (8, 8) (diameter $D_n = 1.085$ nm). It is worth to notice that quasi-linear trends obtained here for different SWCNT diameters are nearly independent of D_n. This means that the SWCNTs Young's modulus behaviour as a function of nanotube diameter can be described by a single quasi-linear trend, for $D_n \gtrsim 1.085$ nm.

For the case of small nanotube diameters, $D_n \lesssim 1.085$ nm, the deviation from the quasi-linear trend is pronounced for smaller values of $1/t_n$, particularly when the nanotube wall thickness approximates to half of its diameter. The smaller the SWCNT diameter, the bigger is the deviation from the quasi-linear trend. For these cases, the SWCNT behaves as a solid cylinder, instead of a hollow tube, which influences the Young's modulus results. As long as the SWCNT wall thickness is equal to a half or less than its diameter, the Young's modulus becomes a quasi-linear function of the nanotube wall thickness. This is an interesting result, so far not reported in the literature to our knowledge, which allows unifying the elastic behaviour of CNTs, whatever their diameter or chirality.

Data from three main distinct modelling approaches –atomistic modelling, continuum modelling (CM) and nanoscale continuum mechanics modelling (NCM) – were chosen for comparison purposes. Seven studies, representing the atomistic approach, were considered: the *ab initio* approach of Kudin [9], the MD approaches of Yakobson [10], Zhang et al. [12], Cheng et al. [13] and Liew et al. [14], the TBMD models of Hernandez et al. [15] and Zhou [16]. Four cases of studies concerning the continuum mechanics approach reported in Refs. [18,20,22,23] were also considered. The remaining results were selected from the models developed employing the NCM approach: the equivalent truss model of Odegard et al. [26], six models, employing diverse kinds of spring elements: Meo and Rossi [30], Giannopoulos et al. [31], Mahmoudinezhad et al. [34], Natsuki et al. [35], Rafiee and Hendarhaei [36] and Parvaneh and Shariati [37], and seven models using beam elements: Papanikos et al. [38], Avila and Lacerda [39], Shokrieh and Rafiee [40], Her and Liu [41], Lu and Hu [42], Mohhamadpour and Awang [43].

Table 4 summarizes the results of the Young's modulus from the literature and the current results obtained from Eq. (24). The Young's modulus values were obtained for nanotube wall thicknesses, t_n, between 0.066 and 0.69 nm and are in the range 0.613–5.516 TPa. In order to facilitate comparison, the results given in Table 4 are plotted in Fig. 8. Fig. 8 shows that, for different wall thicknesses, the Young's modulus values obtained from Eq. (24) follow the trend of the Young's modulus reported in the literature, for a considerable number of approaches.

The current Young's modulus results are in particularly good agreement with those obtained in the studies basing on molecular dynamic modelling methods. The largest difference of 12.22%, observed with the TBMD model reported by Hernandez et al. [15], can be due to the fact that, in their work, the strain energy was calculated without taking the chiral angle into account. The difference of 6.90% in relation to the MD model of Liew et al. [14] can be due to the fact that empirical potentials were used by them. Empirical potentials are frequently not transferable to configurations different from those for which they were obtained. The smallest difference of 0.29% is found for the Young's modulus calculation performed with the MD model by Yakobson et al. [10], where non-linear behaviour of CNTs was considered, allowing correct identification of the strain energies.

Less good agreement is found when the Young's modulus results from the current study are compared with results from the CM models. The biggest difference (49.14%) is found with the Young's modulus results predicted by the analytical shell model of Kalamkarov et al. [20]. Comparison with the model reported by Gupta and Batra [23] shows a difference of 13.44%; this difference can be due to the fact that, in their work, the Young's modulus was evaluated

Table 4
Effect of the nanotube wall thickness on the Young's modulus results: comparison between the current results (Eq. (24)) and those reported in the literature.

Reference	t_n, nm	Method		E, TPa		E, TPa (10, 10); $D_n = 1.356$ nm
Yakobson et al. [10]	0.066	Atomistic modelling	MD	5.5	Average value	5.425
Zhou et al. [16]	0.074		TB model	5.1	Average value	4.840
Kudin et al. [9]	0.089		*ab initio*	3.859	Average value	4.027
Zhang et al. [12]	0.335		MD; Tersoff-Brenner potential	1.08	Converged value for zigzag SWCNTs	1.101
Liew et al. [14]	0.335		MD: empirical potentials	1.043	(10, 10) SWCNT	1.101
Hernandez et al. [15]	0.34		TBMD	1.24	(10, 10) SWCNT	1.086
Cheng et al. [13]	0.34		MD coupled with NCM	1.2	Converged value for armchair SWCNTs	1.086
Pantano et al. [18]	0.075	CM	FE continuum shell model	4.84	Average value	4.776
Kalamkarov et al. [20]	0.129		Analytical model: cylindrical network shell	1.44	–	2.785
Sears and Batra [22]	0.134		Equivalent continuum tube	2.52	(16, 0) SWCNT	2.682
Gupta and Batra [23]	0.34		Equivalent continuum tube	0.964	Average value for non-chiral and chiral SWCNTs	1.086
Odegard et al. [26]	0.69	NCM	Equivalent continuum modelling: truss elements	0.49	–	0.601
Meo and Rossi [30]	0.34		FE model: non-linear springs and linear torsional spring elements	0.926	(10, 10) SWCNT	1.086
Giannopoulos et al. [31]	0.34		3D FE model: linear spring elements	1.247	Average value	1.086
Mahmoudinezhad et al. [34]	0.34		3D FE model: rotational spring elements	0.85	Converged value for armchair SWCNTs	1.086
Natsuki et al. [35]	0.34		Analytical 2D model: spring elements	0.61	Average value	1.086
Rafiee and Heidarhaei [36]	0.34		FE model: non-linear spring elements	1.325	Converged value for non-chiral SWCNTs	1.086
Parvaneh and Shariati [37]	0.34		Structural mechanics model: springs and non-linear connectors	1.170	(22, 0) SWCNT	1.086
Tserpes and Papanikos [28]	0.147		3D FE model: linear elastic beam elements	2.377	(8, 8) SWCNT	2.447
Papanikos et al. [38]	0.34		3D FE model: linear elastic beam elements	1.072	Converged average value	1.086
Avila and Lacerda [39]	0.34		3D FE model: elastic beam elements; RVE concept	1.005	Average value	1.086
Shokrieh and Rafiee [40]	0.33		Analytical model: beam elements	1.042	Converged value for armchair SWCNTS	1.117
Her and Liu [41]	0.34		FE model: nonlinear beam elements; Morse potential	0.927	(10, 10) SWCNT	1.086
Lu and Hu [42]	0.34		3D FE model: beam elements of elliptical-like cross section area; non-linear potential	1.058	Converged value for zigzag SWCNTs	1.086
Mohammadpour and Awang [43]	0.147		FE model: nonlinear beam elements; Morse potential	2.037	(10, 10) SWCNT	2.447
Current work	0.34		3D FE model: linear elastic beam elements	1.078	Converged average value	1.086

by using free vibration simulations. Only the shell continuum model implemented in the work of Pantano et al. [18], shows a small difference (0.33%).

The nanoscale continuum models, employing string elements for C–C bond simulation, show a considerable scatter of the Young's modulus results, due to the values of the spring constants and the spring type selection. Differences with the current Young's modulus calculations are 12.92% (for the Giannopoulos et al. model [31] with linear spring elements) and 44.79% (for the analytical 2D model of Natsuki et al. [35]). The use of the 2D model by Natsuki et al. can explain the highest difference obtained. The model of Parvaneh and Shariati [37] provides the smallest difference of 6.24%.

The Young's modulus values evaluated in the current study show a 19.02% difference with the results of the truss model of Odegard et al. [26]. The models using the equivalent beam approach provided the smallest differences in relation to the current results. The difference of 9.04% observed with respect to the model of Avila and Lacerda [39] can be due to the representative volume element (RVE) concept applied in their work. The use of the RVE implies the numerical simulation of small length SWCNTs, which can affect the Young's modulus calculations. The highest difference observed with the ECM approach is of about 17%, reported in Refs. [41,43], where a modified Morse potential function was applied to the potential energy representation.

In order to simplify comparison with the literature, Table 5 shows the same cases as Table 4, but in the form of the product Et_n, which is called the averaging Young's modulus. The product Et_n evaluated with the present model is in a good agreement with most of the averaging Young's moduli found in the references chosen. A few discrepancies between the Young's modulus results available in the literature and the results of the current evaluation are due to different modelling approaches (MD, CM, NCM), potential functions, force fields constants, formulations for Young's modulus determinations, etc.

Finally, a comparison between the experimental results reported in the literature and those of the present study is shown in Table 6. The Young's modulus evaluated is in satisfactory agreement with the experimental results reported by Krishnan et al. [53], who used thermal vibrations of SWCNT to estimate the Young's modulus, and the results of Yu et al. [54] who used a direct tensile loading test of SWCNT.

3.2.2. *Effect of chiral indices and diameter on the Young's modulus of SWCNTs*

Finally, a study concerning the influence of the chiral indices on the SWCNT Young's modulus was carried out. The Young's modulus was calculated with Eq. (21). The evolution of the Young's modulus, E, with chiral indices, for non-chiral and three families of chiral SWCNTs studied, is shown in Fig. 9 (a). The Young's modulus of the

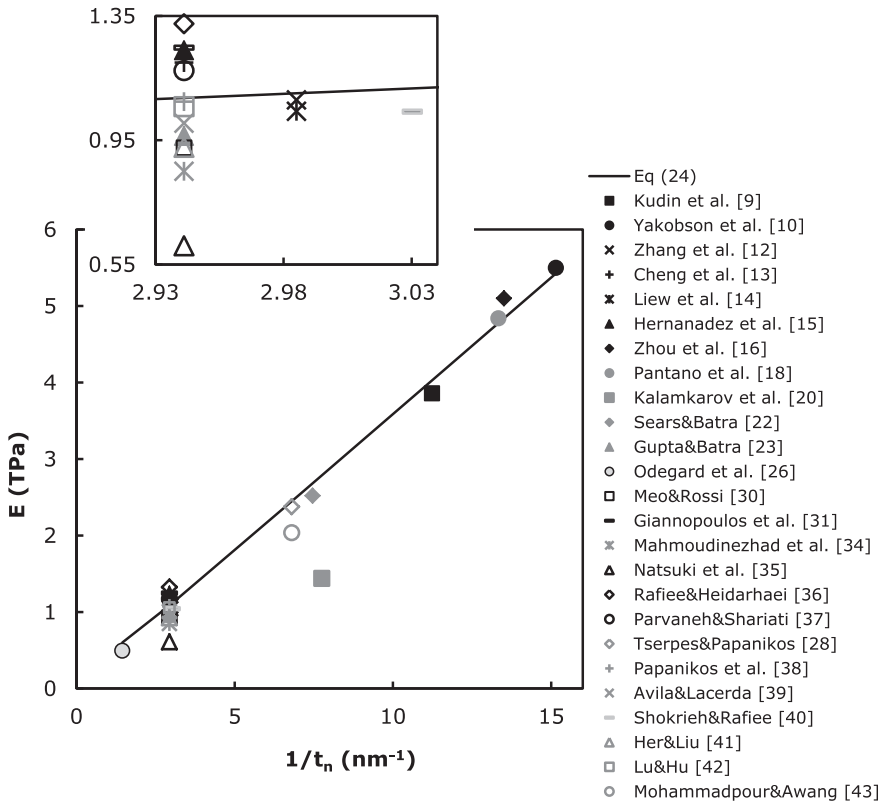

Fig. 8. Comparative study of the evolution of the Young's modulus of SWCNTs with the inverse of the wall thickness.

SWCNTs with small chiral indices $n,n + m \leq 10$ decreases with increasing n, for non-chiral, and $n+m$, for chiral nanotubes; afterwards the Young's modulus tends to stabilize at the value of about 1.1 TPa. In Fig. 9 (b), the results obtained for armchair and zigzag SWCNTs are compared with results available in the literature. For this purpose, literature Young's modulus results obtained for wall thickness $t_n = 0.34$ nm [38,41] and $t_n = 0.66$ nm [33] were chosen; also the work of Shen and Li [55] was considered, where the Young's modulus was deduced independently of the wall thickness. Fig. 9 (b) shows that the evolution of the Young's modulus reported by Papanikos et al. [38] is similar to that in the current work. The work of Her and Liu [41], where the equivalent beam approach was used, gives values of the Young's modulus for non-chiral SWCNTs, which are independent of the chiral indices in the range of $10 \leq n \leq 34$. The decrease of the Young's modulus with increase of n, for small chiral indices, $n = 3,4,5,6$, was observed by Ranjbartoreh and Wang [33]. Shen and Li [55] observed a decrease of the Young's modulus of armchair SWCNTs, even for $n > 10$, in a MD simulation study.

In order to clarify the trends shown in Fig. 9 (a), the Young's modulus results were represented as a function of the nanotube diameter in Fig. 10 (a). For all SWCNT configurations studied, the evolution of the Young's modulus can be described by the same trend: the Young's modulus decreases with increase of the nanotube diameter up to about $D_n = 1$ nm, then, with further increase in

Table 5
Comparative study of the averaging Young's modulus multiplied by the thickness, Et_n.

Reference	Et_n, TPa nm
Current work	0.369
Kudin et al. [9]	0.343
Yakobson et al. [10]	0.363
Zhang et al. [12]	0.362
Cheng et al. [13]	0.408
Liew et al. [14]	0.349
Hernandez et al. [15]	0.422
Zhou et al. [16]	0.377
Pantano et al. [18]	0.363
Kalamkarov et al. [20]	0.186
Sears and Batra [22]	0.338
Gupta and Batra [23]	0.328
Odegard et al. [26]	0.342
Meo and Rossi [30]	0.315
Giannopoulos et al. [31]	0.424
Mahmoudinezhad et al. [34]	0.289
Natsuki et al. [35]	0.207
Rafiee and Heidarhaei [36]	0.451
Parvaneh and Shariati [37]	0.399
Tserpes and Papanikos [28]	0.349
Papanikos et al. [38]	0.365
Avila and Lacerda [39]	0.342
Shokrieh and Rafiee [40]	0.344
Her and Liu [41]	0.315
Lu and Hu [42]	0.360
Mohammadpour and Awang [43]	0.299
Literature average	0.345

Table 6
Comparison between Young's modulus of SWCNTs estimated by the present method and experimental results in the available literature.

Reference	E, TPa	
Krishnan et al. [53]	1.3(−0.4/+0.6)	Average value of SWCNTs with diameter in the range of 1.0–1.5 nm
Yu et al. [54]	1.0	Average value for SWCNTs
Current work	1.078	Stabilized value for SWCNTs (see Figs. 9 (a) and 10 (a))

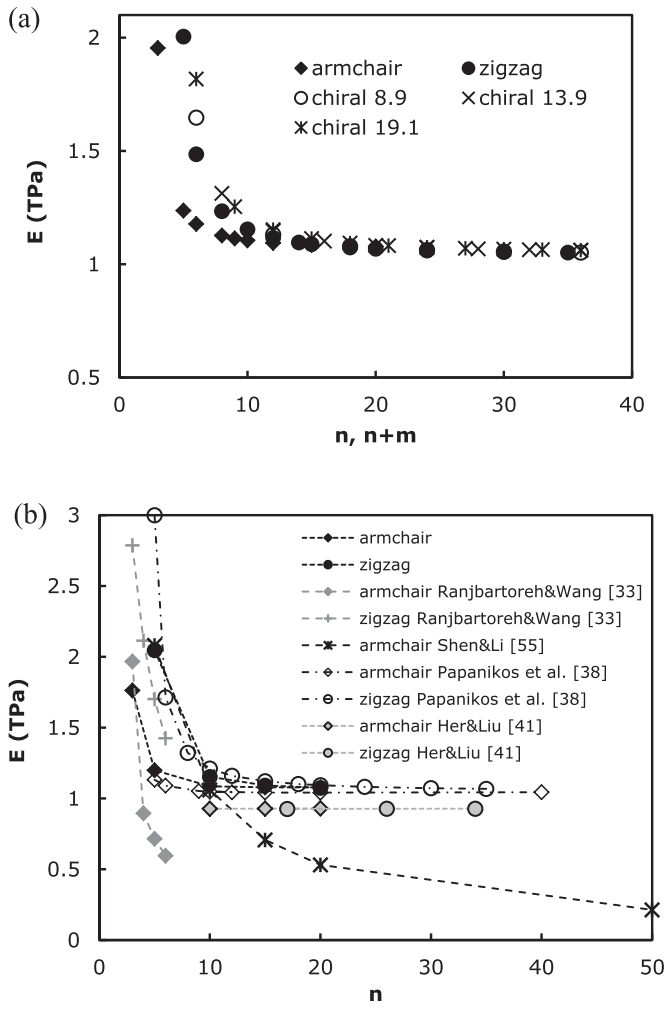

Fig. 9. (a) Evolution of the calculated Young's modulus of non-chiral and three families of chiral SWCNTs as a function of n (for armchair and zigzag nanotubes) and $n+m$ (for chiral nanotubes); (b) comparison of the calculated Young's modulus results for armchair and zigzag nanotubes with those reported in the literature.

the nanotube diameter, the Young's modulus tends towards approximately the same value whatever the type of nanotube.

The results available in the literature, for a nanotube wall thickness of $t_n = 0.34$ nm were selected for comparison. Fig. 10 (b) plots the current Young's modulus results together with those from the literature, showing comparable trends of the Young's modulus evolution, i.e. the Young's modulus decreases for small SWCNT diameters and then becomes almost constant with increasing SWCNT diameter. Good agreement is observed with the results of the work of Papanikos et al. [38], where the modelling approach is similar to that of the current study. The same trend was reported by Zhang et al. [12] for armchair and zigzag nanotubes using MD simulation, in which the Young's modulus value tends to 1.0 TPa for armchair and 0.7 TPa for zigzag SWCNTs for diameters $D_n > 1.500$ nm. The results obtained in the molecular dynamic study of Shen and Li [55], and in the non-linear spring element model of Parvaneh and Shariati [37] show that the Young's modulus tends to 0.5 TPa for large nanotube diameters $D_n \geq 3.000$ nm.

Fig. 10 (c) also presents the current Young's modulus results plotted together with literature results. The literature results show a Young's modulus evolution that is almost constant over the whole range of nanotube diameters [56], although in same cases the Young's modulus increases slightly for small nanotube diameters [36,39,42].

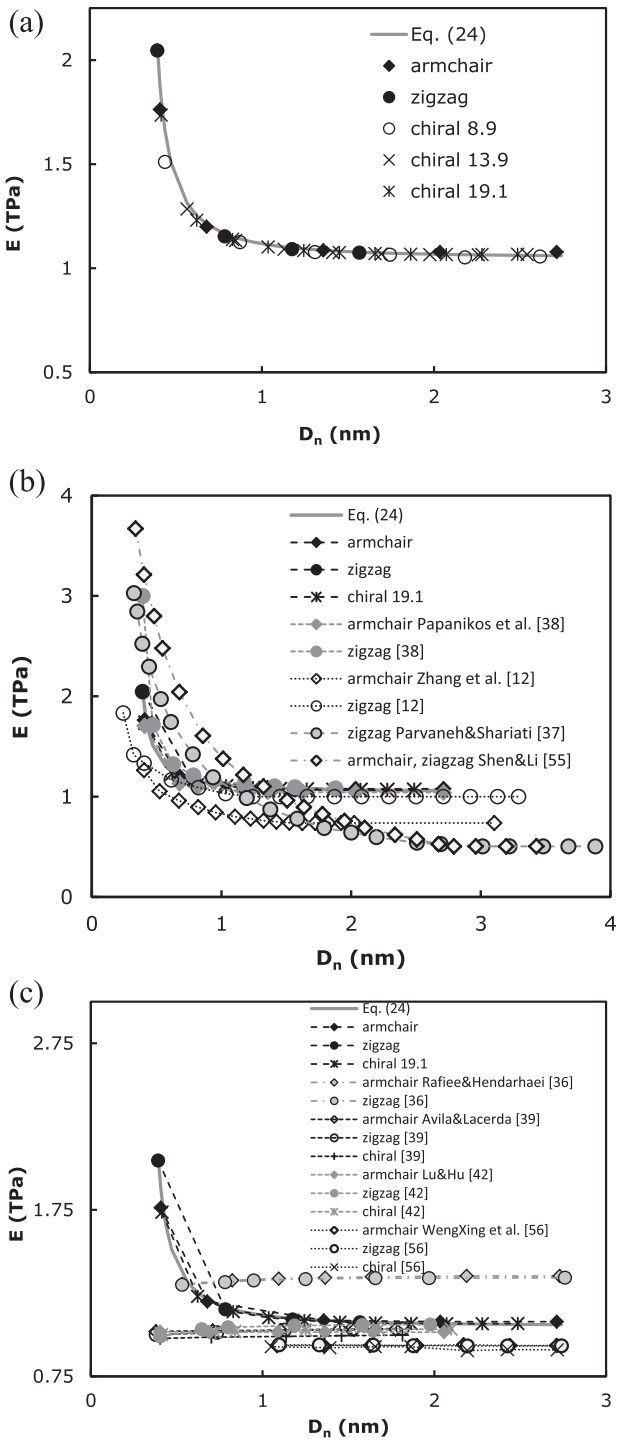

Fig. 10. (a) Evolution of the calculated Young's modulus of the SWCNTs with the nanotube diameter; (b) and (c) comparison of the calculated Young's modulus results with those reported in the literature.

Concerning the effect of SWCNT chirality on the Young's modulus, some authors reported similar values for armchair and zigzag SWCNTs [36,42,55]. In our study, and in agreement with results from the literature [38,56], the difference between the Young's modulus of armchair, zigzag and chiral SWCNTs, is also insignificant (see Figs. 9 and 10). A small difference between the Young's modulus for armchair and zigzag SWCNTs is reported by Zhang et al. [12], and for the three SWCNTs configurations by Avila and Lacerda [39] and Lu and Hu [42].

4. Conclusions

An equivalent beam approach has been used in order to carry out a systematic evaluation of the tensile and bending rigidities, and subsequently, Young's modulus of various SWCNT structures, namely non-chiral and families of chiral single-walled nanotubes over a wide range of chiral indices, nanotube lengths and diameters. The main conclusions of this comprehensive study are as follows:

- The evolution of the tensile rigidity, *EA*, as a function of the diameter, D_n, can be unified, for the SWCNTs studied; the same can be done for the bending rigidity, *EI*. Also, taking into consideration a given value of the wall thickness, the Young's modulus is about the same, whatever the chirality of the nanotube.
- An equation to correlate the tensile and bending rigidities of non-chiral and chiral SWCNTs with the nanotube diameter has been proposed. The accuracy of this relationship was tested using results available in the literature. A single equation is valid for armchair, zigzag and chiral SWCNTs, which allows easy evaluation of the Young's modulus.
- The Young's modulus values are proportional to the inverse of the wall thickness, for SWCNT diameters $D_n \gtrsim 1.085$ nm. For the case of small SWCNT diameters, deviation from this quasi-linear trend is observed, when the nanotube wall thickness is greater than a half of the nanotube diameter, $t_n \gtrsim 1/2D_n$. The quasi-linear trend of the Young's modulus as a function of the inverse of the wall thickness is in good agreement with the results of Young's modulus published by other authors.

Acknowledgements

This research work is sponsored by national funds from the Portuguese Foundation for Science and Technology (FCT) via the projects PTDC/EME–TME/122472/2010 and PEst-C/EME/UI0285/2013 and by FEDER funds via “Programa Operacional Factores de Competitividade” – COMPETE, under the project CENTRO-07-0224_FEDER-002001 (MT4MOBI). All supports are gratefully acknowledged.

References

[1] Robertson J. Realistic applications of CNTs. Mater Today 2004;7(10):46–52.
[2] Neubauer E, Kitzmantel M, Hulman M, Angerer P. Potential and challenges of metal-matrix-composites reinforced with carbon nanofibers and carbon nanotubes. Compos Sci Technol 2010;70(16):2228–36.
[3] Costa P, Silva J, Ansón-Casaos A, Martinez MT, Abad MJ, Viana J, et al. Effect of carbon nanotube type and functionalization on the electrical, thermal, mechanical and electromechanical properties of carbon nanotube/styrene–butadiene–styrene composites for large strain sensor applications. Compos Part B 2014;61:136–46.
[4] Zhang Y, Zhuang X, Muthu J, Mabrouki T, Fontaine M, Gong Y, et al. Load transfer of graphene/carbon nanotube/polyethylene hybrid nanocomposite by molecular dynamics simulation. Compos Part B 2014;63:27–33.
[5] Wang L, Zhang Z, Han X. In situ experimental mechanics of nanomaterials at the atomic scale. NPG Asia Mater 2013;5:e40.
[6] Kallesøe C, Larsen MB, Bøggild P, Mølhave K. 3D mechanical measurements with an atomic force microscope on 1D structures. Rev Sci Instrum 2012;83(2):023704.
[7] Rafiee R, Moghadam RM. On the modelling of carbon nanotubes: a critical review. Compos Part B 2014;56:435–49.
[8] Lu Q, Bhattacharya B. The role of atomistic simulations in probing the small scale aspects of fracture – a case study on a single-walled carbon nanotube. Eng Fract Mech 2005;72(13):2037–71.
[9] Kudin KN, Scuseria GE, Yakobson BI. C2F, BN and C nanoshell elasticity from ab initio computations. Phys Rev B 2001;64(23):235406.
[10] Yakobson BI, Brabec CJ, Bernholc J. Nanomechanics of carbon tubes: instabilities beyond linear response. Phys Rev Lett 1996;76(14):2511–4.
[11] Lu JP. Elastic properties of carbon nanotubes and nanoropes. Phys Rev Lett 1997;79(7):1298–300.
[12] Zhang HW, Wang JB, Guo X. Predicting the elastic properties of single-walled carbon nanotubes. J Mech Phys Solids 2005;53(9):1929–50.
[13] Cheng HC, Liu YL, Hsu YC, Chen WH. Atomistic continuum modelling for mechanical properties of single-walled carbon nanotubes. Int J Solids Struct 2009;46(7–8):1695–704.
[14] Liew KM, He XQ, Wong CH. On the study of elastic and plastic properties of multi-walled carbon nanotubes under axial tension using molecular dynamics simulation. Acta Mat 2004;52(9):2521–7.
[15] Hernandez E, Goze C, Bernier P, Rubio A. Elastic properties of C and BxCyNz composite nanotubes. Phys Rev Lett 1998;80(20):4502–5.
[16] Zhou X, Zhou J, Ou-Yang Z-C. Strain energy and Young's modulus of single-wall carbon nanotubes calculated from electronic energy-band theory. Phys Rev B 2000;62(20):13692.
[17] Ru CQ. Effective bending stiffness of carbon nanotubes. Phys Rev B 2000;62(15):9973.
[18] Pantano A, Parks DM, Boyce MC. Mechanics of deformation of single- and multi-wall carbon nanotubes. J Mech Phys Solids 2004;52(4):789–821.
[19] Muc A. Design and identification methods of effective mechanical properties for carbon nanotubes. Mater Des 2010;31(4):1671–5.
[20] Kalamkarov AL, Georgiades AV, Rokkam SK, Veedu VP, Ghasemi-Nejhad NM. Analytical and numerical techniques to predict carbon nanotubes properties. Int J Solids Struct 2006;43(22–23):6832–54.
[21] Chang TC. A molecular based anisotropic shell model for single-walled carbon nanotubes. J Mech Phys Solids 2010;58(9):1422–33.
[22] Sears A, Batra RC. Macroscopic properties of carbon nanotubes from molecular-mechanics simulations. Phys Rev B 2004;69(23):235406.
[23] Gupta SS, Batra RC. Continuum structures equivalent in normal mode vibrations to single-walled carbon nanotubes. Comput Mater Sci 2008;43(4):715–23.
[24] Wang Q. Effective in-plane stiffness and bending rigidity of armchair and zigzag carbon nanotubes. Int J Solids Struct 2004;41(20):5451–61.
[25] Arash B, Wang Q. A review on the application of nonlocal elastic models in modelling of carbon nanotubes and graphenes. Comput Mater Sci 2012;51(1):303–13.
[26] Odegard GM, Gates TS, Nicholson LM, Wise KE. Equivalent continuum modelling of nano-structured materials. Compos Sci Technol 2002;62(14):1869–80.
[27] Li C, Chou TW. Elastic moduli of multi-walled carbon nanotubes and the effect of van der Waals forces. Compos Sci Technol 2003;63(11):1517–24.
[28] Tserpes KI, Papanikos P. Finite element modeling of single-walled carbon nanotubes. Compos Part B 2005;36(5):468–77.
[29] Ghavamian A, Rahmandoust M, Öchsner A. On the determination of the shear modulus of carbon nanotubes. Compos Part B 2013;44(1):52–9.
[30] Meo M, Rossi M. Prediction of Young's modulus of single wall carbon nanotubes by molecular-mechanics based finite element modeling. Compos Sci Technol 2006;66(11–12):1597–605.
[31] Giannopoulos GI, Kakavas PA, Anifantis NK. Evaluation of the effective mechanical properties of single-walled carbon nanotubes using a spring based finite element approach. Comput Mater Sci 2008;41(4):561–9.
[32] Wernik JM, Meguid SA. Atomistic-based continuum modelling of the nonlinear behavior of carbon nanotubes. Acta Mech 2010;212(1–2):167–79.
[33] Ranjbartoreh AZ, Wang G. Consideration of mechanical properties of single-walled carbon nanotubes under various loading conditions. J Nanopart Res 2010;12(2):537–43.
[34] Mahmoudinezhad E, Ansari R, Basti A, Hemmatnezhad M. An accurate spring-mass model for predicting mechanical properties of single-walled carbon nanotubes. Comput Mater Sci 2012;62:6–11.
[35] Natsuki T, Tantrakarn K, Endo M. Prediction of elastic properties for single-walled carbon nanotubes. Carbon 2004;42(1):39–45.
[36] Rafiee R, Heidarhaei M. Investigation of chirality and diameter effects on the Young's modulus of carbon nanotubes using non-linear potentials. Compos Struct 2012;94(8):2460–4.
[37] Parvaneh V, Shariati M. Effect of defects and loading on prediction of Young's modulus of SWCNTs. Acta Mech 2011;216(1–4):281–9.
[38] Papanikos P, Nikolopoulos DD, Tserpes KI. Equivalent beams for carbon nanotubes. Comput Mater Sci 2008;43(2):345–52.
[39] Ávila AF, Lacerda GSR. Molecular mechanics applied to single-walled carbon nanotubes. Mater Res 2008;11(3):325–33.
[40] Shokrieh MM, Rafiee R. Prediction of Young's modulus of graphene sheets and carbon nanotubes using nanoscale continuum mechanics approach. Mater Des 2010;31(2):790–5.
[41] Her S-C, Liu S-J. Theoretical prediction of tensile behavior of single-walled carbon nanotubes. Curr Nanosci 2012;8(1):42–6.
[42] Lu X, Hu Z. Mechanical property evaluation of single-walled carbon nanotubes by finite element modeling. Compos Part B 2012;43(4):1902–13.
[43] Mohammadpour E, Awang M. Predicting the nonlinear tensile behavior of carbon nanotubes using finite element simulation. Appl Phys A 2011;104(2):609–14.
[44] Dresselhaus MS, Dresselhaus G, Saito R. Physics of carbon nanotubes. Carbon 1995;33(7):883–91.
[45] Barros EB, Jorio A, Samsonidz GG, Capaz RB, Souza Filho AG, Mendes Filho J, et al. Review on the symmetry-related properties of carbon nanotubes. Phys Rep 2006;431(6):261–302.
[46] Lau KT, Hui D. The revolutionary creation of new advanced materials – carbon nanotube composites. Compos Part B 2002;33(4):263–77.

[47] Melchor S, Dobado JA. CoNTub: an algorithm for connecting two arbitrary carbon nanotubes. J Chem Inf Comput Sci 2004;44(5):1639–46.
[48] Tang ZK, Sun HD, Wang J, Chen J, Li G. Mono-sized single-wall carbon nanotubes formed in channels of $AlPO_4$-5 single crystal. Appl Phys Lett 1998;73(16):2287.
[49] Rappe AK, Casemit CJ, Colwell KS, Goddard WA, Skiff WM. UFF, a full periodic-table force-field for molecular mechanics and molecular dynamics simulations. J Am Chem Soc 1992;114(25):10024–35.
[50] Gelin BR. Molecular modelling of polymer structures and properties. Cincinnati (OH): Hanser/Gardner Publishers; 1994.
[51] Cornell WD, Cieplak P, Bayly CI, Gould IR, Merz KM, Ferguson DM, et al. A second generation force-field for the simulation of proteins, nucleic acids and organic molecules. J Am Chem Soc 1995;117(19):5179–97.
[52] Chang T, Gao H. Size-dependent elastic properties of a single-walled carbon nanotube via a molecular mechanics model. J Mech Phys Solids 2003;51(6):1059–74.
[53] Krishnan A, Dujardin E, Ebbesen TW, Yianilos PN, Treacy MMJ. Young's modulus of single-walled nanotubes. Phys Rev B 1998;58(20):14013.
[54] Yu MF, Files BS, Arepalli S, Ruoff RS. Tensile loading of ropes of single wall carbon nanotubes and their mechanical properties. Phys Rev Lett 2000;84(24):5552–4.
[55] Shen L, Li J. Transversely isotropic elastic properties of single-walled carbon nanotubes. Phys Rev B 2004;69(4):045414.
[56] WenXing B, ChangChun Z, WanZhao C. Simulation of Young's modulus of single-walled carbon nanotubes by molecular dynamics. Phys B 2004;352(1–4):156–63.

(Page intentionally left blank)

Phys. Status Solidi B **253,** No. 2, 366–376 (2016) / **DOI** 10.1002/pssb.201552320

physica status solidi b
www.pss-b.com
basic solid state physics

Shear modulus and Poisson's ratio of single-walled carbon nanotubes: Numerical evaluation

A. F. G. Pereira[1], J. V. Fernandes[1], J. M. Antunes[1,2], and N. A. Sakharova[*,1]

[1] CEMUC – Department of Mechanical Engineering, University of Coimbra, Rua Luís Reis Santos, Pinhal de Marrocos, 3030-788 Coimbra, Portugal
[2] Escola Superior de Tecnologia de Abrantes, Instituto Politécnico de Tomar, Rua 17 de Agosto de 1808, 2200 Abrantes, Portugal

Received 15 May 2015, revised 8 September 2015, accepted 21 September 2015
Published online 14 October 2015

Keywords carbon nanotubes, numerical simulation, Poisson's ratio, shear modulus

[*] Corresponding author: e-mail nataliya.sakharova@dem.uc.pt, Phone: +351 239 790 700, Fax: +351 239 790 701

The mechanical behaviour of non-chiral and chiral single-walled carbon nanotubes under torsional loading is studied. For this purpose, three-dimensional finite element modelling is used in order to evaluate the torsional rigidity and shear modulus. It is shown that the evolution of torsional rigidity as a function of nanotube diameter can be described by a unique function for non-chiral and chiral single-walled nanotubes. A comprehensive study to evaluate the Poisson's ratio of single-walled carbon nanotubes is also carried out. Two robust methodologies, one for evaluating the shear modulus from results of tensile, bending and torsion tests, and the other to assess Poisson's ratio from results of bending and torsion tests, are recommended.

1 Introduction Carbon nanotubes (CNTs) are nanostructures with great potential to be used in the production of a new generation of materials and structures with extraordinary mechanical, optical, thermal and electrical properties [1]. The high stiffness together with low density suggests that the carbon nanotubes are optimal structures to reinforce composites and building blocks for optical and electronic nanodevices [2, 3]. In order to model and design composites reinforced with CNTs, nanosensors and CNT-based electronic devices, the understanding of the carbon nanotubes mechanical properties is indispensable.

There are two approaches commonly used to assess the elastic properties of CNTs: experimental and computational. Experimental methods for measuring the elastic modulus of CNTs, based on *in situ* techniques of atomic force microscopy (AFM) and transmission electron microscopy (TEM) have been established [4–7]. The common point in the experimental studies is the evidence of unequalled mechanical properties of the individual CNTs. In the remaining, the experimental results reported in the literature, especially concerning their shear modulus, are limited and inconsistent owing the complexity of characterization of nanomaterials at the atomic scale. Due to the experimental difficulties, modelling and computer simulation for predicting the mechanical properties of CNTs have been intensively developed.

There are three main groups of methodologies for the modelling of the CNTs mechanical behaviour: the atomistic approach, the continuum mechanics approach and the nanoscale continuum mechanics approach [8]. Atomistic modelling comprises an *ab initio* approach, molecular dynamics (MD) and tight-binding molecular dynamics (TBMD) (see, for example, [9–11]). In recent years, the atomistic modelling, due to its big computation cost, has been gradually replaced by the continuum mechanics modelling (CM). In this case, the most elementary assumption consists of the replacing of the real discrete CNT structure by a continuum medium (see, for example [12]). The representation of the entire CNT structure as a continuum element is not adequate enough to model carbon nanotube mechanical behaviour. In the nanoscale continuum modelling (NCM), only the carbon–carbon (C–C) bond

is replaced by a continuum element whose behaviour is described in the elasticity theory (see, [13-16]). The NCM approach is an adequate modelling technique for describing the mechanical behaviour of the CNTs, as it allows overcoming the disadvantages of the MD and CM modelling approaches, i.e. leads to accurate results without computational complexity and additional costs. Therefore, the NCM approach, employing the beam element for replacing the C–C bond, has been successfully used for simulation of the mechanical behaviour of CNTs [17–19], after Li and Chou [13] established a direct relationship between the structural mechanics parameters of the beam element and the molecular mechanics parameters.

Most of the numerical simulation studies towards the evaluation of the CNTs mechanical properties concern with the determination of their rigidity and Young's modulus by means of tensile and bending tests (see, for example [11, 20–23]). It has been recently concluded [24] that regardless of chirality, the evolution of the tensile rigidity as a function of the carbon nanotube diameter can be unified by a single equation; the same was concluded for the bending rigidity. Furthermore, given a certain value of the wall thickness, the Young's modulus is about the same, whatever the chirality of the nanotube. The works dealing with the CNTs shear modulus are scarcer and are not systematised so far. What can be concluded from these studies is that there are two methods commonly used to evaluate the CNTs shear modulus, G. One method consists on the direct determination of the shear modulus from the numerical results of the torsion tests [12, 14, 15, 17, 19, 25–27] or from analytical models for describing the torsional response [16, 28, 29]. The other method to assess the CNTs shear modulus, G, uses the results of the tensile test and resorts to the relationship between Young's modulus, E, and Poisson's ratio, v, for isotropic materials ($G = E/2\,(1+v)$) [25, 27, 30, 31]. Only a few works compare results of the shear modulus obtained by torsion and tensile tests [25, 27].

Although several studies regarding the Poisson's ratio have been carried out [10, 12, 18, 25, 28, 29, 31], there is no commonly accepted value of v. The most common values reported in the literature are in range of 0.1–0.3 (see, for example [16, 25, 28, 31]), but values of 0.64 [32], 0.66 [18] and close to zero [17, 33] are also reported.

In the current study, the equivalent beam approach is used in a comprehensive study to assess the torsional rigidity, shear modulus and Poisson ratio of various single-walled carbon nanotubes (SWCNT) structures, as non-chiral (zigzag, $\theta = 0^\circ$ and armchair, $\theta = 30^\circ$) and families of chiral ($\theta = 8.9^\circ$, 13.9° and 19.1° among others) SWCNTs for a wide range of nanotube lengths, chiral indices and diameters.

2 Materials and methods

2.1 Geometric definition of SWCNTs The atomic structure of SWCNTs is described in terms of the tube chirality, which is defined by the chiral vector $\boldsymbol{C}_h$ and the chiral angle, θ, between the chiral vector $\boldsymbol{C}_h$ and the direction $(n,0)$ [34]

$$\boldsymbol{C}_h = n\boldsymbol{a}_1 + m\boldsymbol{a}_2 \tag{1}$$

$$\theta = \sin^{-1}\left(\sqrt{3}m/2\sqrt{n^2+nm+m^2}\right), \tag{2}$$

where (n,m) is a pair of the lattice indices $\boldsymbol{a}_1$ and $\boldsymbol{a}_2$, the unit vectors of the graphene lattice; n and m are integers. The length of the unit vector $\boldsymbol{a}$ is defined as $a = \sqrt{3}a_{C-C}$ with the equilibrium carbon–carbon (C–C) covalent bond length a_{C-C} usually taken to be 0.1421 nm.

Basing on the chiral vector or the chiral angle, fundamental configurations of SWCNTs are defined: armchair nanotubes ($n = m$, $\theta = 30^\circ$), zigzag nanotubes ($m = 0$, $\theta = 0^\circ$) and chiral nanotubes ($n \neq m$, $0^\circ < \theta < 30^\circ$).

2.2 Finite element (FE) modelling of SWCNTs A three-dimensional (3D) finite element model (FEM) under nanoscale continuous modelling (NCM) approach, as proposed by Tserpes and Papanikos [14] was adopted. This approach is based on the concept of Li and Chou [13], who have modelled the deformation of CNTs using classical structural mechanics, i.e. the CNTs lattice can be simulated as a geometrical space-frame structure. In the approach by Tserpes and Papanikos [14], the C–C bonds are replaced by equivalent beam elements, i.e. the analogy between the bond length, a_{C-C}, and the element length is used. The beam element has a circular cross-section area, which diameter is sometimes considered equal to the SWCNT wall thickness, although other values are also considered for the wall thickness. In fact, most of the times, the SWCNT wall thickness value used is 0.34 nm (equal to the interlayer spacing of graphite).

The finite element meshes of the carbon nanotube structures used in the FE analyses were constructed using the academic software CoNTub 1.0 [35]. To convert the ASCII files generated by this code, which describe the atom positions, into the format usable by the commercial FE code ABAQUS®, the in-house application designated *InterfaceNanotubes* was developed. The FE model uses the coordinates of the carbon atoms for generating the nodes and then the connections of the nodes create the beam elements.

This model takes into account the chirality of the SWCNTs, and so is able to consider their anisotropic behaviour due to chirality. The geometrical characteristics of SWCNTs used for the FE analysis are shown in Table 1, where the number of nodes and elements of the finite element meshes of the SWCNTs is also indicated for a nanotube with a length of 20 nm.

2.3 FE analysis of SWCNTs

2.3.1 Structural mechanics of SWCNTs The elastic moduli of the beam elements are determined by establishing the link between inter-atomic potential energies of the molecular structure and strain energies of the equivalent continuum structure comprising of beams, undergoing axial, bending and torsional deformations [13].

Table 1 Geometrical characteristics of SWCNTs studied and number of nodes and elements of the finite element meshes used.

SWCNT type	(n,m)	D_n, nm	θ°	number of nodes[a]	number of elements[a]
non-chiral					
armchiar	(3, 3)	0.407	30	972	1448
	(5, 5)	0.678		1620	2414
	(6, 6)	0.814		1944	2897
	(9, 9)	1.221		2916	4346
	(10, 10)	1.356		3240	4829
	(12, 12)	1.628		3888	5795
	(15, 15)	2.034		4860	7244
	(20, 20)	2.713		6840	9659
zigzag	(5, 0)	0.392	0	930	1384
	(6, 0)	0.470		1115	1160
	(10, 0)	0.783		1860	2769
	(12, 0)	0.940		2232	3323
	(15, 0)	1.175		2790	4154
	(18, 0)	1.409		3348	4985
	(20, 0)	1.566		3720	5539
	(24, 0)	1.879		4464	6647
chiral					
family θ 8.9	(5, 1)	0.436	8.9	1044	1554
	(10, 2)	0.872		2088	3109
	(15, 3)	1.308		3132	4664
	(20, 4)	1.744		4176	6219
	(25, 5)	2.180		5220	7774
	(30, 6)	2.616		6264	9329
family θ 13.9	(6, 2)	0.565	13.9	1352	2013
	(9, 3)	0.847		2028	3020
	(12, 4)	1.129		2740	4027
	(15, 5)	1.412		3380	5034
	(18, 6)	1.694		4056	6041
	(21, 7)	1.976		4732	7048
	(24, 8)	2.259		5408	8055
	(27, 9)	2.541		6084	9062
family θ 19.1	(4, 2)	0.414	19.1	992	1477
	(6, 3)	0.622		1488	2216
	(8, 4)	0.829		1984	2955
	(10, 5)	1.036		2840	3694
	(12, 6)	1.243		2976	4433
	(14, 7)	1.450		3472	5172
	(16, 8)	1.657		3968	5911
	(18, 9)	1.865		4464	6650
	(20, 10)	2.072		4960	7389
	(22, 11)	2.279		5456	8128
	(24, 12)	2.486		5952	8867
$n+m$					
12	(7, 5)	0.818	24.5	1960	2920
	(11, 1)	0.903	4.3	2167	3222
18	(16, 2)	1.338	5.8	3208	4777
	(14, 4)	1.282	12.2	3072	4575
	(13, 5)	1.260	15.6	3020	4498
	(11, 7)	1.231	22.7	2950	4395
	(10, 8)	1.223	26.3	2932	4369
24	(22, 2)	1.806	4.3	4328	6445
	(19, 5)	1.717	11.4	4116	6130
	(17, 7)	1.674	16.5	4012	5976
	(15, 9)	1.644	21.8	3942	5873
	(14, 10)	1.635	24.5	3920	5841
	(13, 11)	1.629	27.2	3906	5821

[a]For nanotube length 20 nm.

Direct relationships between the structural mechanics parameters, i.e. tensile, E_bA_b, bending, E_bI_b, and torsional, G_bJ_b rigidities, and the bond force field constants, k_r, k_θ and k_τ, were stablished [13]

$$\frac{E_bA_b}{l} = k_r, \tag{3}$$

$$\frac{E_bI_b}{l} = k_\theta, \tag{4}$$

$$\frac{G_bJ_b}{l} = k_\tau, \tag{5}$$

where l is the beam length equal to 0.1421 nm; E_b and G_b are the beam Young's and shear moduli, respectively; A_b is the beam cross-sectional area, I_b and J_b are the beam moment of inertia and polar moment of inertia, respectively, and k_r, k_θ and k_τ, are the bond stretching, bond bending and torsional resistance force constants, respectively. Equations (3)–(5) provide the input for simulation of the CNTs as space-frame structures. The values of force constants [36, 37] and input data for the FE model are shown in Table 2.

2.3.2 Loading conditions Numerical simulation of conventional torsion tests was carried out in order to study the effect of nanotube diameter and chirality on its mechanical properties. For simulation torsion, a tangential force, F_φ, is applied at one extremity of the nanotube, leaving the other fixed. The nodes of the nanotube end under loading are restricted from moving in the radial direction. The torsional rigidity of the nanotube, GJ, is determined as

$$GJ = F_\varphi RL/\varphi, \tag{6}$$

where R is the nanotube radius and φ is the twist angle, taken from the FE analysis.

3 Results and discussion

3.1 Rigidities of SWCNTs: Effect of the length, chiral indices and chiral angles on the rigidities of SWCNTs Examples of the evolution of torsional rigidity, GJ, with nanotube length are shown in Fig. 1, for the cases of armchair (10, 10) and (20, 20), zigzag (10, 0) and (20, 0) and chiral (10, 2) and (24, 12) SWCNTs. In these examples, as in all cases of Table 1, the values of the rigidity are quite stable with the nanotube length. Papanikos et al. [17] also reported stable values for zigzag (20, 0) and armchair (20, 20) carbon nanotubes, with lengths greater than 50 nm.

Therefore, the length of 20 nm was chosen for the numerical simulation of the torsion test of CNTs. In order to analyse the influence of the chiral angle, θ, on the rigidity, GJ, SWCNTs with the same value of the sum of the chiral indices $(n+m)$ were considered, as shown in the examples of Fig. 2 for the families $(n+m) = 6$, 12, 18 and 24. Whatever the case, the torsional rigidity decreases from zigzag SWCNTs ($\theta = 0^\circ$) to armchair ($\theta = 30^\circ$), with a rate that becomes smaller as θ increases. The higher the value of $(n+m)$, the greater the rigidity and the respective decrease rate.

The evolutions of the torsional rigidity, GJ, as a function of the sum of chiral indices, $(n+m)$ are shown in Fig 3, for non-chiral and three families of chiral SWCNTs of Table 1. The GJ evolutions are relatively close, but not coincident. The GJ rigidities increase with the sum of the chiral indices according to a cubic power expression, which parameters depend on the case.

Figure 4 shows the evolutions of the GJ rigidities as a function of the SWCNT diameter, D_n, for the same cases as in Fig. 3. The evolutions in Fig. 4 can be described by a single cubic power function for all SWCNTs studied, i.e. regardless of the index and the angle of chirality.

Table 2 Input parameters for FE simulations of SWCNTs: Material and geometric properties of beam element.

parameter	value	formulation
force constant, k_r [36]	6.52×10^{-7} N nm^{-1}	–
force constant, k_θ [36]	8.76×10^{-10} N · nm · rad^{-2}	–
force constant, k_τ [36, 37]	2.78×10^{-10} N · nm · rad^{-2}	–
C–C bond/beam length, $l = a_{C-C}$	0.1421 nm	–
diameter, d	0.147 nm	$d = 4\sqrt{k_\theta/k_r}$
cross section area, A_b	0.01688 nm^2	$A_b = \pi d^2/4$
moment of inertia, I_b	2.269×10^{-5} nm^4	$I_b = \pi d^4/64$
polar moment of inertia, J_b	4.537×10^{-5} nm^4	$J_b = \pi d^4/32$
Young's modulus, E_b	5488 GPa	$E_b = k_r^2 l/4\pi k_\theta$
shear modulus, G_b	870.7 GPa	$G_b = k_r^2 k_\tau l/8\pi k_\theta^2$
rigidity, E_bA_b	92.65 nN	$E_bA_b = k_r l$
rigidity, E_bI_b	0.1245 nN · nm^2	$E_bI_b = k_\theta l$
rigidity, G_bJ_b	0.0395 nN · nm^2	$G_bJ_b = k_\tau l$

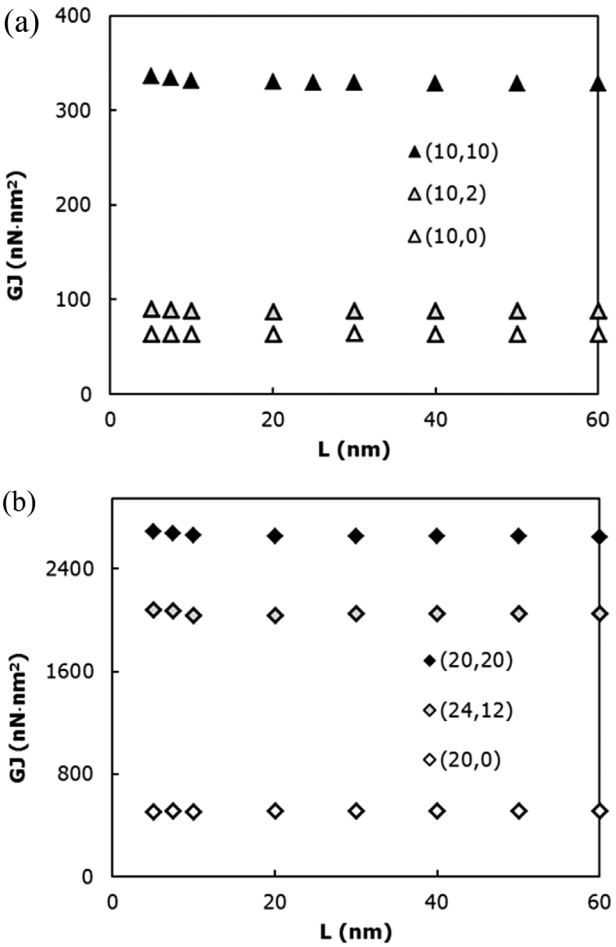

Figure 1 Evolution of the torsional rigidity, GJ, with nanotube length, L, for: (a) armchair (10, 10), zigzag (10, 0) and chiral (10, 2) SWCNTs; (b) armchair (20,20), zigzag (20,0) and chiral (24,12) SWCNTs.

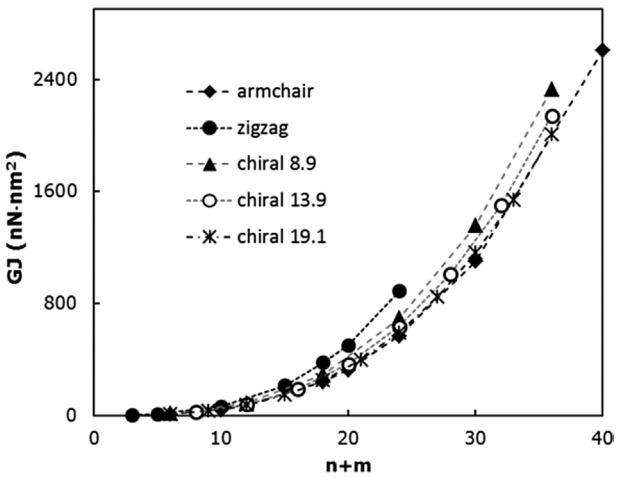

Figure 3 Evolution of the torsional rigidity, GJ, as a function of the sum of chiral indices, $(n+m)$, for non-chiral and chiral SWCNTs.

This makes such representation more suitable for further analyses than when the torsional rigidity is plotted as a function of $(n+m)$, identically to previously observed for the tensile and bending rigidities [24]. In Fig. 5, the values of GJ are plotted as a function of $(D_n - D_0)^3$. The fitting equation can be expressed as follows:

$$GJ = \gamma(D_n - D_0)^3. \tag{7}$$

The values of the fitting parameters are: $\gamma = 130.39$ nN/nm and $D_0 = 3.5 \times 10^{-3}$ nm. This equation is of the same type as those previously proposed for non-chiral SWCNTs [15], but replacing the chiral index, n, by the SWCNT diameter, D_n. Furthermore, a cubic equation relating the bending rigidity to the diameter of the nanotube has been successfully tested [24].

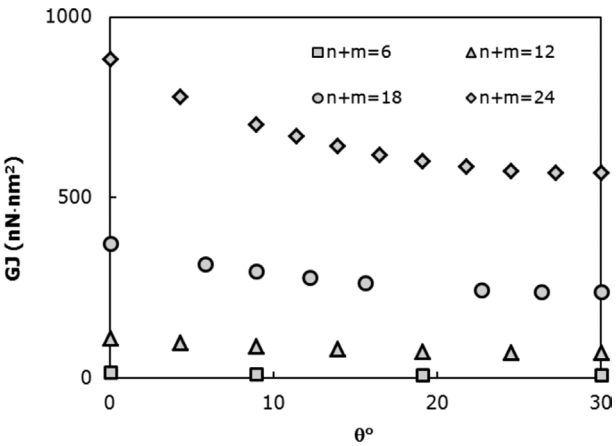

Figure 2 Evolution of the torsional rigidity, GJ, as a function of the chiral angle, θ for four families of SWCNTs with $(n+m) = 6$, 12, 18 and 24.

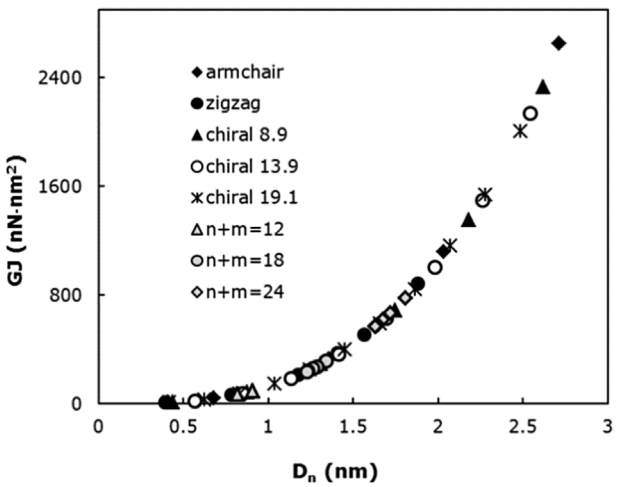

Figure 4 Evolution of the torsional rigidity, GJ, as a function of the nanotube diameter, D_n for armchair, zigzag and chiral SWCNT families $\theta = 8.9$, 13.9, 19.1° and $n+m = 12$, 18 and 24.

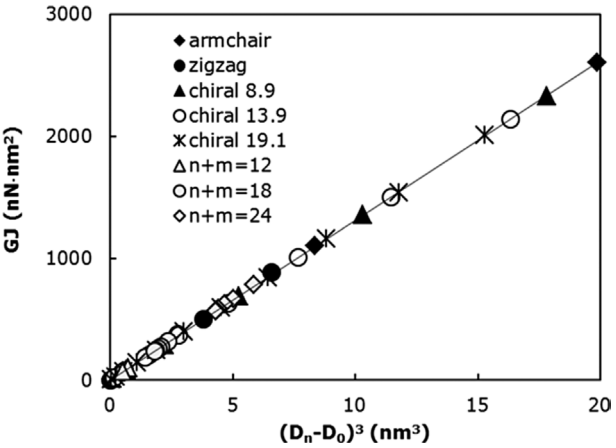

Figure 5 Evolution of the torsional rigidity, GJ as a function of $(D_n - D_0)^3$. The results are represented by symbols and fitting trends by lines.

It remains to note that the cubic function expressed by the above equation can be understood on the base of the quasi-cubic relationship between the polar moment of inertia and the nanotube diameter (see Eq. (9) in the following section).

A careful analysis of the results allows understanding that Eq. (7) does not accurately describe the evolution of torsional rigidity of all nanotubes, for low values of D_n. In fact, Fig. 6 shows that the ratio $GJ/(D_n - D_0)^3$ is stable in all range of nanotube diameters D_n, for the chiral family with $\theta = 13.9^\circ$, but slightly increases for zigzag ($\theta = 0^\circ$) and chiral family with $\theta = 8.9^\circ$ and clearly decreases for the chiral family with $\theta = 19.1^\circ$ and armchair ($\theta = 30^\circ$) nanotubes, when D_n becomes smaller than 1.0 nm. This means that, for small nanotube diameters, the ratio $GJ/(D_n - D_0)^3$ tends to decreases when the chiral angle, θ, increases from 0° (zigzag) to 30° (armchair).

3.2 Shear modulus of SWCNTs The shear modulus, G, of SWCNT, which considered as a hollow cylinder,

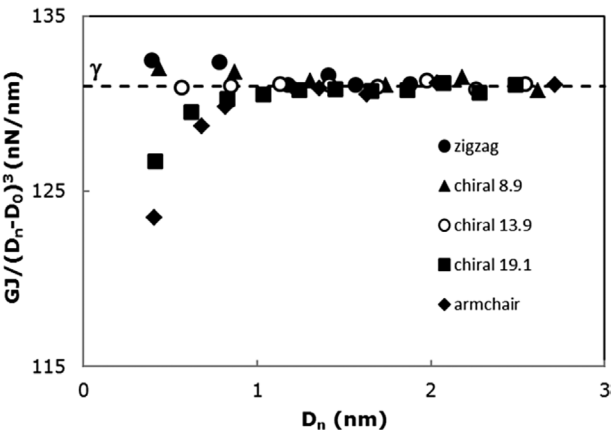

Figure 6 Evolution of the ratio $GJ/(D_n - D_0)^3$ with the nanotube diameter, D_n.

can be evaluated from the torsional rigidity value, GJ, by the following equation:

$$G = GJ/J, \tag{8}$$

where J is the polar moment of inertia, which can be written as

$$\begin{aligned} J &= \frac{\pi}{32}\left[(D+t)^4 - (D-t)^4\right] \\ &= \frac{\pi D^3 t}{4}\left[1 + \left(\frac{t}{D}\right)^2\right], \end{aligned} \tag{9}$$

where D is the mean diameter and t is the thickness of the hollow cylinder, respectively.

A robust methodology for determining the elastic moduli of SWCNT involves using of the rigidities under different mechanical tests [24]. This allows the appropriate assessment of the mean diameter of SWCNT, D. In fact, the knowledge of the tensile and bending nanotube rigidities, EA and EI, respectively, allows determining D, taking into account the cross-sectional area, A, and the moment of inertia, I, of the hollow cylinder:

$$A = \frac{\pi}{4}\left[(D+t)^2 - (D-t)^2\right] = \pi D t, \tag{10}$$

$$I = \frac{\pi}{64}\left[(D+t)^4 - (D-t)^4\right] = \frac{\pi D^3 t}{8}\left[1 + \left(\frac{t}{D}\right)^2\right], \tag{11}$$

and assuming $t = t_n$ (where t_n is the nanotube wall thickness), the SWCNT mean diameter D can be expressed as following [17]:

$$EI/EA = \frac{1}{8}\left(D^2 + t_n^2\right) \Rightarrow D = \sqrt{8(EI/EA) - t_n^2}. \tag{12}$$

Replacing D in the Eq. (9), the shear modulus can be calculated, at a given thickness, t_n, by the following expression, from the knowledge of the rigidities in tension, bending and torsion

$$G = \frac{GJ}{2\pi t_n \left(\frac{EI}{EA}\right)\sqrt{8\left(\frac{EI}{EA}\right) - t_n^2}}. \tag{13}$$

Moreover, based on the knowledge of the parameters γ and D_0, of Eq. (7) for torsional rigidity, as well as of the parameters, α and β of the same type of equations for tensile and bending rigidities [24]

$$EA = \alpha(D_n - D_0), \tag{14}$$

$$EI = \beta(D_n - D_0)^3. \tag{15}$$

Table 3 Fitting parameters α, β, γ and D_0.

parameter	value[a]
α [24]	$1131.66\,\mathrm{nN}\cdot\mathrm{nm}^{-1}$
β [24]	$143.48\,\mathrm{nN}\cdot\mathrm{nm}^{-1}$
γ (current study)	$130.39\,\mathrm{nN}\cdot\mathrm{nm}^{-1}$
D_0 (current study)	$3.5\times10^{-3}\,\mathrm{nm}$

[a]Includes armchair, zigzag and all types of chiral SWCNT studied.

Equation (13) for shear modulus can be written as follows:

$$G=\frac{\gamma(D_n-D_0)}{2\pi t_n\left(\frac{\beta}{\alpha}\right)\sqrt{8\frac{\beta(D_n-D_0)^2}{\alpha}-t_n^2}}. \tag{16}$$

The values of the fitting parameters α, β, γ and D_0 are shown in Table 3.

Equations (13) and (16) show that the value of the SWCNTs wall thickness influences the shear modulus. The wall thickness value reported in the literature is in the range from 0.066 to 0.69 nm, and therefore the study of its influence on the shear modulus value is essential in order to allow a correct comparison with results from other sources. Figure 7 shows the shear modulus calculated from Eq. (16) as a function of the inverse of the nanotube wall thickness (the range of t_n values is 0.06 to 0.69 nm), for armchair SWCNTs of Table 1. The evolution of the shear modulus as a function of the inverse wall thickness follows a quasi-linear trend in the whole range of thicknesses, for nanotubes with diameter $D_n \gtrsim 1.085$ nm. The deviation from the quasi-linear trend for small nanotube diameters, $D_n \lesssim 1.085$ nm is noticeable for high values of t_n: when t_n approaches the value of $D_n/2$.

In the following, the shear modulus was calculated with Eq. (13), using the values of the torsional rigidity, GJ, obtained from the current numerical simulation of the torsion tests, and values of the tensile, EA, and bending, EI, rigidities taken from a previous study [24]. Figure 8 compares the evolutions of the shear modulus with the nanotube diameter, D_n, for the non-chiral and the $\theta = 19.1^\circ$ chiral family, with results from the literature. For this purpose, shear modulus results obtained for the same value of wall thickness as used in the current study ($t_n = 0.34\,nm$) were considered [10, 12, 14–17, 25, 28]. Previous shear modulus results, obtained with t_n variable in the range 0.20–0.34 nm depending on the nanotube diameter [26] and deduced independently of the wall thickness [31], were also considered.

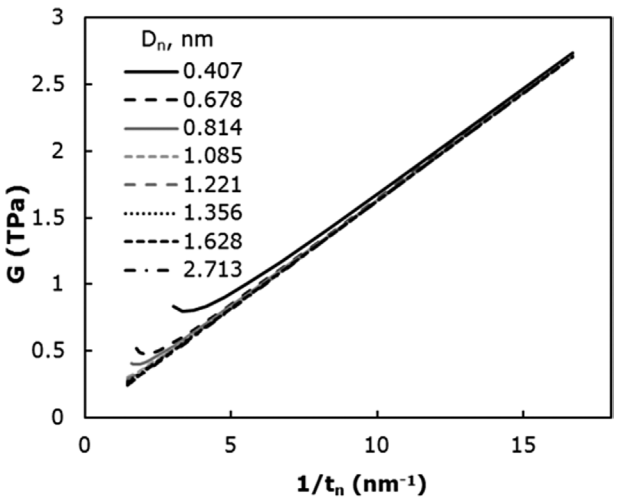

Figure 7 Evolution of the shear modulus with the inverse of the wall thickness for different nanotube diameters, according to Eq. (16).

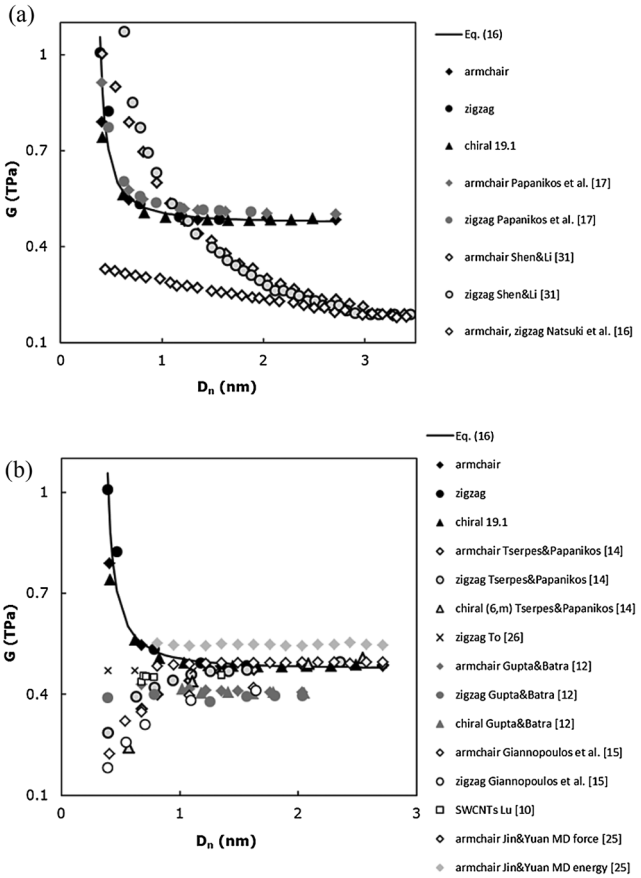

Figure 8 Comparison of the current shear modulus results (black symbols and those obtained by Eq. (16)) with those reported in the literature. Current values of G assumes $t_n = 0.34$ nm.

Figure 8(a) compares the current results of the shear modulus with others from the literature, for which the shear modulus initially also decreases with the diameter, and then its value becomes almost stable for high values of the nanotube diameter. In the current study, the shear modulus tends to a stable value equal to about 0.48 TPa, for nanotube diameters $D_n \geq 1$ nm. Good agreement is observed with the results of Papanikos et al. [17], where the modelling approach is similar to that of the current study. The shear modulus obtained with analytical models by Shen and Li [31] and Natsuki et al. [16] tends to 0.16 TPa for large nanotube diameters, $D_n \geq 3$ nm.

Figure 8(b) also shows the current shear modulus results versus the nanotube diameter, together with others from the literature. In this case, the literature results show a shear modulus evolution that is almost constant over the whole range of nanotube diameters [10, 12, 25, 26], or initially slightly increases with the diameter [14, 15, 28]. The current shear modulus results are particularly in good agreement with those obtained, for nanotube diameters $D_n \geq 1$ nm, with the molecular dynamic approach by Jin and Yuan [25], and also with the results of Tserpes and Papanikos [14], To [26] and Xiao et al. [28], who used NCM approach. Less agreement occurs between the current results and those by Gupta and Batra [12], using the CM approach, and by Giannopoulos et al. [15], who employed NCM approach involving linear spring elements.

Concerning the effect of chirality on the shear modulus results, some authors reported small differences between the shear modulus for armchair and zigzag SWCNTs [15]; these small differences includes also chiral nanotubes configurations, in case of the work by Tserpes and Papanikos [14]. In our study, and in agreement with other results from the literature [10, 12, 16, 17, 28, 29, 31], the difference between the shear modulus values of armchair, zigzag and chiral SWCNTs, is irrelevant (Fig. 8).

Finally, Table 4 shows the shear modulus results from the literature, including those shown in Fig. 8, and the current results. The value of the shear modulus evaluated with the present model is close to most of the values of the shear modulus published by other authors. The current shear modulus evaluated is in satisfactory agreement with the experimental results reported by Hall et al. [7]. In general, a good accordance was also observed concerning not only the NCM approach [13, 14, 17, 19, 26, 28, 29, 31] (as in current study) but also the MD modelling [10, 25]. Less good agreement is found with authors who use specific approaches as Giannopoulos et al. [15] and Natsuki et al. [16], who use linear spring elements within the NCM approach and analytical 2D modelling, respectively. Also, in case of Ghavamian et al. [27], significant discrepancy was found, probably due to the particular formulation for shear modulus determination in torsion. Finally, the insufficient agreement with the Gupta and Batra [12] is certainly related to the replacement of the whole CNT structure by a continuum element which is not a completely satisfactory method to evaluate CNT properties.

3.3 Poisson's ratio of SWCNTs Imposing the isotropic material condition, the Poisson's ratio can be calculated as follows:

$$\nu = \frac{E}{2G} - 1. \tag{17}$$

Taking in account that $J = 2I$, this equation can be rewritten as follows:

$$\nu = \frac{EI}{GJ} - 1, \tag{18}$$

Table 4 Comparative study of the shear modulus of SWCNTs.

reference	t_n, nm	method	test	G, TPa	comments
Jin and Yuan [25]	0.34	MD: force approach	torsion	0.492	average value for armchair
			tensile	0.491	
Jin and Yuan [25]	0.34	MD: energy approach	torsion	0.547	average value for armchair
			tensile	0.536	
Lu [10]	0.34	MD: empirical force constant model	tensile	0.455	average value for non-chiral and chiral
Gupta and Batra [12]	0.34	CM: equivalent continuum tube	torsional vibrations	0.403	average value for non-chiral and chiral
Natsuki et al. [16]	0.34	NCM: analytical 2D model	torsion	0.300	average value for armchair and zigzag
Xiao et al. [28]	0.34	NCM: analytical approach	torsion	0.470	converged value for armchair and zigzag
Wu et al. [29]	0.268		torsion	0.418	converged value for armchair and zigzag SWCNTs
Shen and Li [31]	–		torsion	0.439	average value for armchair and zigzag
Giannopoulos et al. [15]	0.34	NCM: 3D FEM, linear spring elements	torsion	0.325	average value for armchair and zigzag
Li and Chou [13]	0.34	NCM: 3D FEM, beam elements	torsion	0.480	armchair and zigzag
Tserpes and Papanikos [7]	0.34		torsion	0.485	armchair: $D_n = 2.443$ nm
Papanikos et al. [15]	0.34		torsion	0.509	converged average value for armchair and zigzag
Lu and Hu [19]	0.34	NCM: 3D FEM, elliptical cross-section beam elements	torsion	0.469	armchair: $D_n = 2.443$ nm
To [26]	0.34	NCM: 3D FEM	torsion	0.475	zigzag: $D_n = 1.331$ nm
Ghavamian et al. [27]	0.34	NCM: 3D FEM, beam elements	torsion	0.378	armchair
			tensile	0.500	
Hall et al. [7]	–	Experimental: SEM	electrostatic torsion	0.410	SWCNTs unidentified
current study	0.34	NCM: 3D FEM, beam elements	tensile + bending + torsion	0.484	converged average value for non-chiral and chiral

which formulation permits determining the Poisson's ratio for a given SWCNT, from the knowledge of its bending, *EI*, and torsion, *GJ*, rigidities, respectively.

Moreover, Eqs. (7) and (15) allow defining a unique equation for the Poisson's ratio, independent of the nanotube type and diameter

$$\nu = \frac{\beta}{\gamma} - 1. \tag{19}$$

Figure 9 shows the evolution of the Poisson's ratio, ν, with nanotube diameter, D_n, for non-chiral (armchair and zigzag) and the $\theta = 19.1^\circ$ family of chiral SWCNTs; the values of the Poisson's ratio were obtained by Eq. (18), using the torsional rigidity values, *GJ*, of the current study and the bending rigidity values, *EI*, obtained in our previous study [24]. This figure also shows the Poisson's ratio calculated with Eq. (19), which is independent of D_n. For three types of nanotubes, the Poisson's ratio tends towards approximately the value of about 0.10, for high D_n values, which was also obtained by Eq. (19). In case of zigzag nanotubes, the values of the Poisson's ratio are close to the value obtained by Eq. (19), in all range of D_n values. But, for the cases of the chiral with $\theta = 19.1^\circ$ and armchair families, the value of the Poisson's ratio increases when D_n decreases below 1.5 nm. This means that for values of the nanotube diameters such that $D_n < 1.5$ nm, the Poisson's ratio strongly depends on the chiral angle and increases from zigzag nanotubes ($\theta = 0^\circ$) to armchair nanotubes ($\theta = 30^\circ$). This is in agreement with the results of Fig. 6, which shows that the value of the torsion rigidity does not follow a linear correlation with $(D_n - D_0)^3$ (see also Fig. 5), for very low values of the nanotube diameter, D_n.

It is worth to notice that the evaluation of the Poisson's ratio from the results of bending and torsion rigidities (Eqs. (18) and (19)) constitutes a robust methodology, given the relatively high degree of accuracy of these quantities. In the contrast, most authors [10, 16, 18, 25, 28, 29, 31, 33] use the definition of Poisson's ratio in tension, for its evaluation. This requires the knowledge of the axial, $\varepsilon_{\parallel}$, and normal $\varepsilon_{\perp}$ strains, as follows:

$$\nu = -\frac{\varepsilon_{\perp}}{\varepsilon_{\parallel}}. \tag{20}$$

Figure 10 and Table 5 allow comparing the current Poisson's ratio results with those from the literature.

Table 5 contains the comprehensive information on the methodology and formulation for assessing the Poisson's ratio used in the previous works, selected for the comparative study. Table 5 also shows, whenever it is possible, whether or not they agree with the relationship $G = E/2(1+\nu)$, for isotropic material.

As shown in Fig. 10, the current results show trends of the Poisson's ratio evolution of the SWCNTs comparable to those of the works of Xiao et al. [28] and Shen and Li [31], i.e. its value initially decreases with the diameter, and then becomes almost constant for high values of the diameter. Values of the Poisson's ratio independent of the nanotube diameter were reported by Dominguez-Rodriguez et al. [33] and Papanikos et al. [17]. Finally, the values of Poisson's ratio continuously decreasing with increasing of the nanotube diameter were reported by Tserpes and Papanikos [14]. The dissimilarities of the Poisson's ratio values in Fig. 10 and Table 5 are due to different modelling approaches, employing analytical or numerical simulation methods, to the force fields constants selected and to different formulations for Poisson's ratio assessment. For example, Dominguez-Rodriguez et al. [33] attributed the difference between the values of the Poisson's ratio obtained

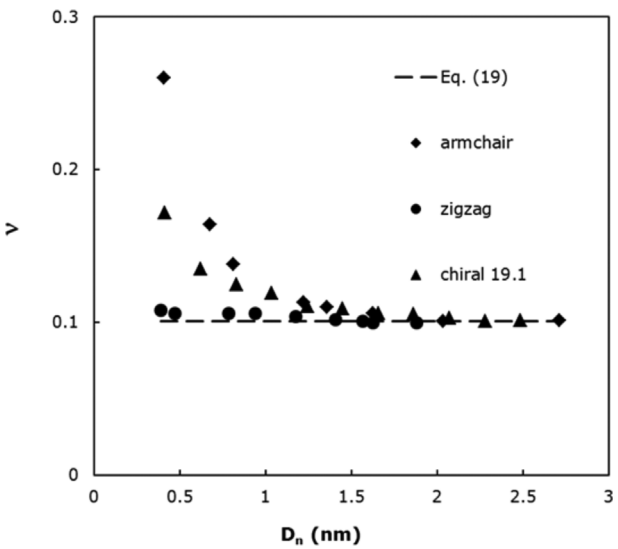

Figure 9 Evolution of the calculated Poisson's ratio of the SWCNTs with the nanotube diameter.

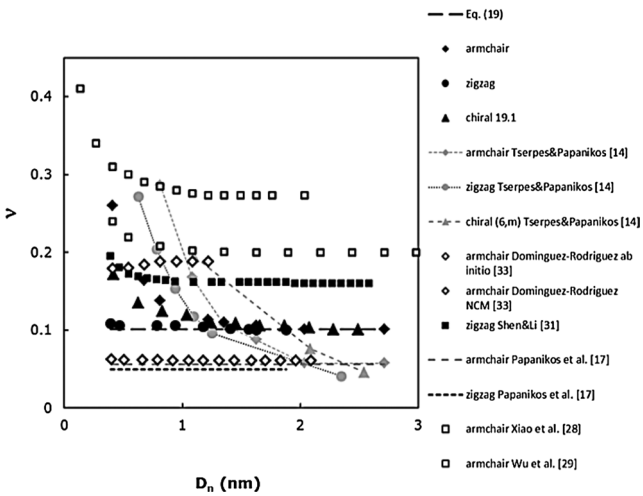

Figure 10 Comparison of the Poisson's ratio results with those reported in the literature. In case of the results by Tserpes and Papanikos [14], the Poisson's ratio was determined from their values of *E* and *G*, using Eq. (17).

Table 5 Comparative study of the Poisson's ratio of SWCNTs.

reference	method	test	formulation	ν	comments
Jin and Yuan [25]	MD	tensile	$\nu = -\frac{\varepsilon_\perp}{\varepsilon_\parallel}$	0.259[a]	average for armchair
Lu [10]	MD: empirical force constant model	tensile	$\nu = -\frac{\varepsilon_\perp}{\varepsilon_\parallel}$	0.278[b]	average for non-chiral and chiral
Domínguez-Rodríguez et al. [33]	*ab initio* (DFT)	tensile	$\nu = -\frac{\varepsilon_\perp}{\varepsilon_\parallel}$	0.185	average for armchair
	NCM: FEM, beam elements			0.061	
Gupta and Batra [12]	CM: equivalent continuum tube	axial + torsional vibrations	normal mode vibrations	0.140–0.249[a]	non-chiral and chiral: $D_n = 0.392-2.051$ nm
Natsuki et al. [16]	NCM: analytical approach	tensile	$\nu = -\frac{\varepsilon_\perp}{\varepsilon_\parallel}$	0.27[b]	armchair and zigzag
Xiao et al. [28]				0.2[a]	converged for armchair and zigzag
Wu et al. [29]				0.273[a]	converged for armchair and zigzag
Shen and Li [31]				0.16[b]	converged for armchair and zigzag
Papanikos et al. [17]	NCM: 3D FEM, beam elements	bending + torsion	$\nu = \frac{\beta^*}{\gamma^*} - 1$	0.056[b]	armchair
				0.049[b]	zigzag
Avila and Lacerda [18]		tensile	$\nu = -\frac{\varepsilon_\perp}{\varepsilon_\parallel}$	0.15–0.29	non-chiral and chiral: $D_n = 0.407-1.800$ nm
current results		bending + torsion	$\nu = \frac{EI}{GJ} - 1$ and $\nu = \frac{\beta}{\gamma} - 1$	0.10[a]	converged average for non-chiral and chiral

β^* and γ^* relates the bending and torsion rigidities, respectively, with the chiral index, n by cubic equations: $EI = \beta^*(n-n_0)^3$ and $GJ = \gamma^*(n-n_0)^3$.
[a]ν value satisfies the relationship $G = E/2(1+\nu)$; [b]ν value does not satisfy the relationship $G = E/2(1+\nu)$.

by the equivalent beam approach and density functional theory (DFT), to the input values of the force field constants (k_r, k_θ) in the numerical simulations. Nevertheless, the evaluation of the Poisson's ratio by imposing the isotropic material condition allows reliable values.

4 Conclusions An equivalent beam approach has been used in order to carry out a systematic evaluation of the torsional rigidity, shear modulus and Poisson's ratio of various SWCNT structures, namely non-chiral and chiral families of single-walled nanotubes over a wide range of chiral indices, nanotube lengths and diameters.

The main conclusions of this comprehensive study are as follows:

(i) A single equation valid for armchair, zigzag and chiral SWCNTs allows correlating the torsional rigidity with the nanotube diameter.
(ii) A robust methodology for calculation of the shear modulus is suggested. This makes use of values of the parameters that describe the evolutions of the tensile, bending and torsional rigidities with the nanotube diameter.
(iii) For a given value of the wall thickness, the shear modulus is about the same, whatever the SWCNT chirality. For the thickness value commonly used ($t_n = 0.34$ nm), the value of the shear modulus is $G = 0.484$ GPa. This value was compared with those previously reported in literature.
(iv) The average value of Poisson's ratio converges for ν close to 0.10 for large diameters, whatever the nanotube, chiral or non-chiral. This value was calculated assuming isotropy, and resorting to data from torsion and bending tests.
(v) The evaluation of the torsional rigidity as a function of the nanotube diameter and respective shear modulus, as suggested in the current work, as well as the evaluation of tension and bending rigidities and Young's modulus, earlier proposed by the authors [24], allow easily characterise the mechanical behaviour of SWCNTs, whatever the chirality and diameter. This can be useful, particularly for understanding and modelling the mechanical behaviour of CNT reinforced materials.

Acknowledgements This research work is sponsored by national funds from the Portuguese Foundation for Science and Technology (FCT) and by FEDER funds "Programa Operacional Factores de Competitividade" via the projects PTDC/EME–TME/122472/2010 and PEst-C/EME/UI0285/2013 as well as by FEDER funds "Programa Operacional da Região Centro" via the project CENTRO-07-0224-FEDER-002001 (MT4MOBI). All supports are gratefully acknowledged.

References

[1] J. Robertson, Mater. Today **7**, 46 (2004).
[2] E. Neubauer, M. Kitzmantel, M. Hulman, and P. Angerer, Compos. Sci. Technol. **70**, 2228 (2010).

[3] Y. Lan, Y. Wang, and Z. F. Ren, Adv. Phys. **60**, 553 (2011).
[4] L. Wang, Z. Zhang, and X. Han, NPG Asia Mater. **5**, e40 (2013).
[5] C. Kallesøe, M. B. Larsen, P. Bøggild, and K. Mølhave, Rev. Sci. Instrum. **83**, 023704 (2012).
[6] J. P. Salvetat, G. A. D. Briggs, J. M. Bonard, R. R. Bacsa, A. J. Kulik, T. Stockli, T. Burnham, and L. Forro, Phys. Rev. Lett. **82**, 944 (1999).
[7] A. R. Hall, L. An, J. Liu, L. Vicci, M. R. Falvo, R. Superfine, and S. Washburn, Phys. Rev. Lett. **96**, 256102 (2006).
[8] R. Rafiee and R. M. Moghadam, Composites B **56**, 435 (2014).
[9] K. N. Kudin, G. E. Scuseria, and B. I. Yakobson, Phys. Rev. B **64**, 235406 (2001).
[10] J. P. Lu, Phys. Rev. Lett. **79**, 1298 (1997).
[11] H. W. Zhang, J. B. Wang, and X. Guo, J. Mech. Phys. Solids **53**, 1929 (2005).
[12] S. S. Gupta and R. C. Batra, Comput. Mater. Sci. **43**, 715 (2008).
[13] C. Li and T. W. Chou, Int. J. Solids Struct. **40**, 2487 (2003).
[14] K. I. Tserpes and P. Papanikos, Compos. B **36**, 468 (2005).
[15] G. I. Giannopoulos, P. A. Kakavas, and N. K. Anifantis, Comput. Mater. Sci. **41**, 561 (2008).
[16] T. Natsuki, K. Tantrakarn, and M. Endo, Carbon **42**, 39 (2004).
[17] P. Papanikos, D. D. Nikolopoulos, and K. I. Tserpes, Comput. Mater. Sci. **43**, 345 (2008).
[18] A. F. Ávila and G. S. R. Lacerda, Mater. Res. **11**, 325 (2008).
[19] X. Lu and Z. Hu, Composites B **43**, 1902 (2012).
[20] M. Meo and M. Rossi, Compos. Sci. Technol. **66**, 1597 (2006).
[21] V. Parvaneh and M. Shariati, Acta Mech. **216**, 281 (2011).
[22] M. M. Shokrieh and R. Rafiee, Mater. Des. **31**, 790 (2010).
[23] E. Mohammadpour and M. Awang, Appl. Phys. A **104**, 609 (2011).
[24] N. A. Sakharova, A. F. G. Pereira, J. M. Antunes, C. M. A. Brett, and J. V. Fernandes, Composites B **75**, 73 (2015).
[25] Y. Jin and F. G. Yuan, Compos. Sci. Technol. **63**, 1507 (2003).
[26] C. W. S. To, Finite Elem. Anal. Des. **42**, 404 (2006).
[27] A. Ghavamian, M. Rahmandoust, and A. Öchsner, Composites. B **44**, 52 (2013).
[28] J. R. Xiao, B. A. Gama, and J. W. Gillespie, Jr, Int. J. Solids Struct. **42**, 3075 (2005).
[29] Y. Wu, X. Zhang, A. Y. T. Leung, and W. Zhong, Thin-Walled Struct. **44**, 667 (2006).
[30] M. Rahmandoust, and A. Öchsner, J. Nanosci. Nanotechnol. **12**, 8129 (2012).
[31] L. Shen and J. Li, Phys. Rev. B **69**, 045414 (2004).
[32] V. N. Popov and V. E. Van Doren, Phys. Rev. B **61**, 3078 (2000).
[33] G. Domínguez-Rodríguez, A. Tapia, and F. Avilés, Comput. Mater. Sci. **82**, 257 (2014).
[34] M. S. Dresselhaus, G. Dresselhaus, and R. Saito, Carbon **33**, 883 (1995).
[35] S. Melchor and J. A. Dobado, J. Chem. Inform. Comput. Sci. **44**, 1639 (2004).
[36] W. D. Cornell, P. Cieplak, C. I. Bayly, I. R. Gould, K. M. Merz, D. M. Ferguson, D. C. Spellmeyer, T. Fox, J. W. Caldwell, and P. A. Kollman, J. Am. Chem. Soc. **117**, 5179 (1995).
[37] W. L. Jorgensen and D. L. Severance, J. Am. Chem. Soc. **112**, 4768 (1990).

(Page intentionally left blank)

4.2. Elastic properties of the SWCNTs' structures containing vacancy defects

This subchapter contains the paper by Sakharova *et al*. (2016a), which deals with the evaluation of the tensile, bending and torsional rigidities, and subsequently, the Young's and shear moduli and the Poisson's ratio of SWCNTs containing vacancy defects. It analyses and discusses the results of a systematic study, regarding the influence of the type and percentage of vacancy defects on the mechanical response of the SWCNTs in a wide range of nanotube diameters, chiral angles and chiral indices.

(Page intentionally left blank)

Composites Part B 89 (2016) 155–168

Contents lists available at ScienceDirect

Composites Part B

journal homepage: www.elsevier.com/locate/compositesb

Numerical simulation study of the elastic properties of single-walled carbon nanotubes containing vacancy defects

N.A. Sakharova [a, *], A.F.G. Pereira [a], J.M. Antunes [a, b], J.V. Fernandes [a]

[a] CEMUC, Department of Mechanical Engineering, University of Coimbra, Rua Luís Reis Santos, Pinhal de Marrocos, 3030-788 Coimbra, Portugal
[b] Escola Superior de Tecnologia de Abrantes, Instituto Politécnico de Tomar, Rua 17 de Agosto de, 1808-2200 Abrantes, Portugal

ARTICLE INFO

Article history:
Received 17 July 2015
Received in revised form
21 October 2015
Accepted 4 November 2015
Available online 30 November 2015

Keywords:
A. Nano-structures
B. Defects
B. Mechanical properties
C. Finite element analysis (FEA)

ABSTRACT

The mechanical behaviour of non-chiral and chiral single-walled carbon nanotubes containing different percentage (up to 10%) and types of vacancy defects is studied under tensile, bending and torsional loading. A three-dimensional finite element model is used in order to evaluate the corresponding rigidities and, subsequently, Young's and shear moduli and Poisson's ratio. The three rigidities decrease with the increase of the percentage of vacancies. Also, the Young's and shear moduli and the Poisson's ratio of single-walled carbon nanotubes are sensitive to the presence of vacancy defects in nanotube: elastic moduli decrease and the Poisson's ratio increases with increasing of the percentage of vacancies. The moduli of single-walled carbon nanotubes with 10.0% of vacancy defects, when compared with the values obtained for perfect nanotubes, are of about 43% for the Young's modulus and of about 33% for the shear modulus. On the contrary, the Poisson's ratio increases of about 4 times, compared with that obtained for the perfect nanotube.

1. Introduction

Carbon nanotubes (CNTs) have attracted great research interest, because of their unparalleled mechanical, optical and thermal properties [1]. In spite of various experimental studies which have been carried out to evaluate the mechanical properties of CNTs, there is a scattering in the experimental results reported in the literature. Such inconsistency is due to complexity of the characterization of nanomaterials at the atomic scale. Another reason of the result's scattering can be associated with the existence of defects in the CNT structure: it is almost impossible to produce carbon nanotubes with a perfect structure because of the manufacturing constraints. It should be noted that the perfection of the lattice of the CNTs, used in experimental studies, has a significant influence on the results. Thus, the numerical simulation of the mechanical properties of carbon nanotubes with defects is an important task, providing data that can be compared with experimental results. The defects of CNT structure, such as single and multiple vacancies, show suitable effects for numerous applications of nanotubes, for example concerning the strength of nanocomposites when CNT vacancy defects act as interfacial bonding places, the storage of hydrogen and the transition of nanotubes from one diameter to another in carbon nanotube heterojunctions. The defects in the CNTs can appear mainly due to the chemical synthesis [2], the chemical treatment in the purification process [3], or when the CNTs are subjected to irradiation [4].

There are three main classes of theoretical approaches for the modelling of the CNTs mechanical behaviour: atomistic, continuum and nanoscale continuum approaches [5]. The atomistic approaches (for example, ab initio [6] and classical molecular dynamics (MD) [7,8]) have big computation costs. In consequence, they have been progressively replaced by the continuum mechanics-based approach (CM) where the real atomic CNT structure is replaced by a continuum medium (see, for example [9,10]). Such replacement of the whole CNT structure allows effective simulation, greatly reducing the computational effort, but does not provide sufficient accuracy in the evaluation of the CNT mechanical properties. Finally, the nanoscale continuum modelling (NCM) approach, where the carbon–carbon (C–C) bond is replaced by a continuum element (as truss, spring and beam) has led to accurate results, overcoming the disadvantages of the MD and CM approaches (see, for example [11–14]). Since Li and Chou [13] have

* Corresponding author. Tel.: +351 239790747.
E-mail address: nataliya.sakharova@dem.uc.pt (N.A. Sakharova).

http://dx.doi.org/10.1016/j.compositesb.2015.11.029
1359-8368/

linked the interatomic potential energies to the strain energies of an equivalent beam element and established a direct relationship between sectional stiffness parameters and the force field constants, the NCM approach using beam elements has been successfully used to simulate the mechanical behaviour of CNT [14–17].

In recent years, numerical studies regarding the effect of the defects on the CNT mechanical properties have been carried out. For example, concerning the elastic behaviour, Scarpa et al. [18], Parvaneh and Shariati [19], Parvaneh et al. [20], Rahmandoust and Ochsner [21], Ghavamian et al. [22], Ghavamian and Ochsner [23,24] and Poelma et al. [25] simulate the vacancy defects by removing the carbon atoms without reconstruction of the C–C bonds. The studies of Scarpa et al. [18], Parvaneh and Shariati [19] and Parvaneh et al. [20] relate to a few specific types of nanotubes and vacancies, and also relatively small percentages of defects (less than 2.5%). Reduction of the Young's modulus was observed in nanotubes with defects, although it is insignificant in some cases. The studies of Rahmandoust and Ochsner [21], Ghavamian et al. [22] and Ghavamian and Ochsner [23,24] showed that the presence of 0.5 and 1.0% of the vacancy defects in the armchair and zigzag single-walled and multi-walled CNTs leads to the significant decrease of the CNT Young's modulus [21,22], natural frequency [23] and critical buckling load [24] with an approximately linear trend. Poelma et al. [25] found that the position of the single vacancy defect significantly influences the critical buckling load of the single-walled carbon nanotubes at the low temperatures. For studying the fracture behaviour, some authors [26,27] have chosen to rebuild the C–C bonds around the removed atoms. Among their findings, it should be pointed a substantial reducing of the nanotube strength. In summary, with regard to parameters such as rigidity, elastic modulus and Poisson's ratio, only the influence of vacancy defects on the elastic modulus has received main analysis so far, although limited to a few types of single-walled carbon nanotubes.

This study aims to contribute towards the study of the mechanical behaviour of single-walled carbon nanotubes (SWCNTs) containing different percentage and type of vacancy defects, using the NCM approach implemented with beam elements. Three dimensional finite element method was used in order to evaluate the tensile, bending and torsional rigidities, and subsequently, Young's and shear moduli and Poisson's ratio of various SWCNTs, as non-chiral (zigzag, $\theta = 0°$, and armchair, $\theta = 30°$) and three families of chiral ($\theta = 8.9°$; $13.9°$; $19.1°$) SWCNTs, for a wide range of chiral indices and diameters. The current systematic study allows improving the information concerning the influence of the presence and density of the vacancy defects on the SWCNTs mechanical properties, in order to better understanding the scattering generally observed in experimental results.

2. Materials and methods

2.1. Atomic structure of SWCNTs

The symmetry of the atomic structure of SWCNTs is characterized by the chirality, which is defined by the chiral vector $\boldsymbol{C_h}$ [28]:

Table 1
Geometrical characteristics of SWCNTs studied and number of nodes and elements of the finite element meshes used (nanotube length 20 nm).

SWCNT type		(n, m)	D_n, nm	$\theta°$	Number of nodes	Number of elements
Non-chiral	Armchair	(5, 5)	0.678	30	1620	2414
		(10, 10)	1.356		3240	4829
		(15, 15)	2.034		4860	7244
		(20, 20)	2.713		7640	11,420
	Zigzag	(5, 0)	0.392	0	930	1384
		(10, 0)	0.783		1860	2769
		(15, 0)	1.175		2790	4154
		(20, 0)	1.566		3720	5539
		(35, 0)	2.740		7420	11,095
Chiral	Family $\theta = 8.9°$	(5, 1)	0.436	8.9	1044	1554
		(10, 2)	0.872		2088	3109
		(15, 3)	1.308		3132	4664
		(20, 4)	1.744		4176	6219
		(25, 5)	2.180		5220	7774
		(30, 6)	2.616		6264	9329
	Family $\theta = 13.9°$	(6, 2)	0.565	13.9	1352	2013
		(9, 3)	0.847		2028	3020
		(12, 4)	1.129		2740	4027
		(15, 5)	1.412		3380	5034
		(18, 6)	1.694		4056	6041
		(21, 7)	1.976		4732	7048
		(24, 8)	2.259		5408	8055
		(27, 9)	2.541		6084	9062
	Family $\theta = 19.1°$	(4, 2)	0.414	19.1	992	1477
		(6, 3)	0.622		1488	2216
		(8, 4)	0.829		1984	2955
		(10, 5)	1.036		2840	3694
		(12, 6)	1.243		2976	4433
		(14, 7)	1.450		3472	5172
		(16, 8)	1.657		3968	5911
		(18, 9)	1.865		4464	6650
		(20, 10)	2.072		4960	7389
		(22, 11)	2.279		5456	8128
		(24, 12)	2.486		6504	9720

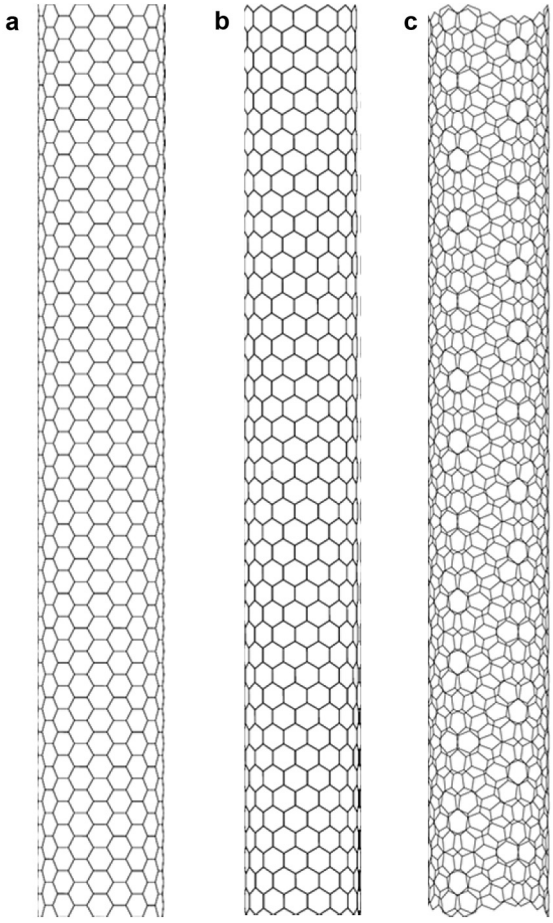

Fig. 1. FE meshes of SWCNTs: (a) armchair (10, 10), (b) zigzag (15, 0) and (c) chiral (15, 3).

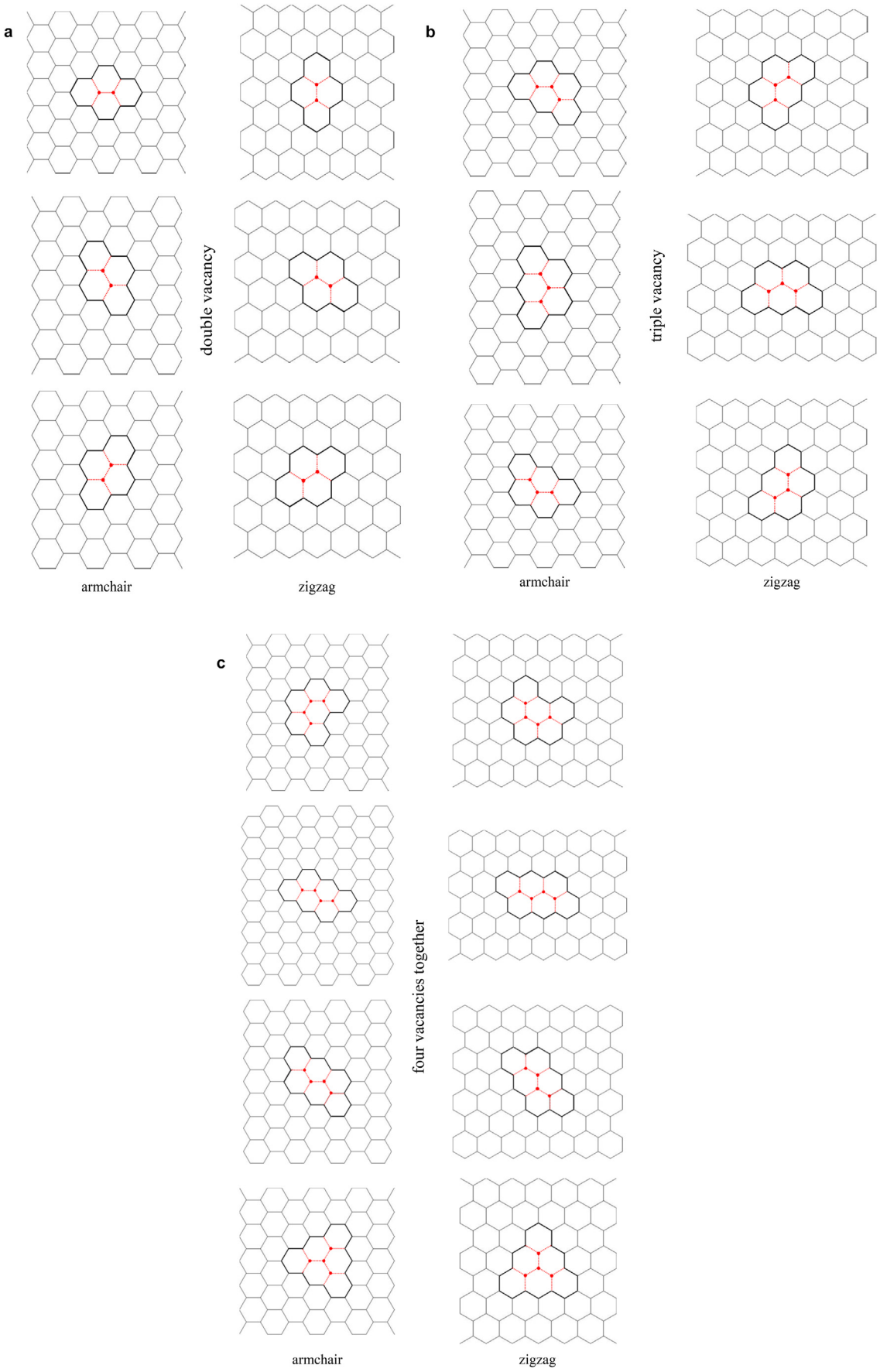

Fig. 2. Examples of configurations of double (a), triple (b) and four vacancies together (c) used in the analysis. The axis of the nanotube is horizontal.

Table 2
Input parameters for FE simulations of SWCNT: material and geometric properties of the beam element.

Parameter	Value	Formulation
Force constant, k_r [35]	6.52×10^{-7} N nm^{-1}	–
Force constant, k_θ [35]	8.76×10^{-10} N nm rad^{-2}	–
Force constant, k_τ [35,36]	2.78×10^{-10} N nm rad^{-2}	–
C–C bond/beam length ($l = a_{C-C}$)	0.1421 nm	–
Diameter (d)	0.147 nm	$d = 4\sqrt{k_\theta/k_r}$
Cross section area, A_b	0.01688 nm^2	$A_b = \pi d^2/4$
Moment of inertia, I_b	2.269×10^{-5} nm^4	$I_b = \pi d^4/64$
Polar moment of inertia, J_b	4.537×10^{-5} nm^4	$J_b = \pi d^4/32$
Young's modulus, E_b	5488 GPa	$E_b = k_r^2 l/4\pi k_\theta$
Shear modulus, G_b	870.7 GPa	$G_b = k_r^2 k_r l/8\pi k_\theta^2$
Rigidity, E_bA_b	92.65 nN	$E_bA_b = k_r l$
Rigidity, E_bI_b	0.1245 nN nm^2	$E_bI_b = k_\theta l$
Rigidity, G_bJ_b	0.0395 nN nm^2	$G_bJ_b = k_\tau l$

$$\boldsymbol{C_h} = n\boldsymbol{a_1} + m\boldsymbol{a_2} \quad (1)$$

where (n, m) is a pair of the lattice translation indices $\boldsymbol{a}_1$ and $\boldsymbol{a}_2$, the unit vectors of the hexagonal lattice, n and m are integers.

The values of n and m allow defining the chiral angle, θ, between the chiral vector, $\boldsymbol{C_h}$, and the direction $(n, 0)$ [28]:

$$\theta = \sin^{-1}\frac{\sqrt{3}m}{2\sqrt{n^2 + nm + m^2}} \quad (2)$$

The length of the unit vector $\boldsymbol{a}$ is defined as $a = \sqrt{3}a_{C-C}$ with the equilibrium carbon–carbon (C–C) covalent bond length a_{C-C} usually taken to be 0.1421 nm. The nanotube diameter, D_n, is defined as:

$$D_n = \frac{a\sqrt{n^2 + nm + m^2}}{\pi} \quad (3)$$

Three main configurations of SWCNTs are defined, basing on the chiral vector or the chiral angle: armchair nanotubes ($n = m$, $\theta = 30^\circ$), zigzag nanotubes ($m = 0$, $\theta = 0^\circ$) and chiral nanotubes ($n \neq m$, $0^\circ < \theta < 30^\circ$).

2.2. Configurations of SWCNTs and FE modelling

In this work a three-dimensional (3D) finite element (FE) model under NCM approach was adopted. The adopted 3D FE model is able to assess the mechanical properties of SWCNTs, by establishing equivalences between the bond length, a_{C-C}, and the equivalent beam length, l, and between the nanotube wall thickness, t_n, and the beam element diameter [13,15].

The FE meshes of the carbon nanotube structures were constructed using the academic software CoNTub 1.0 [29], which has been widely used for this purpose (see, for example Refs. [30–34]). This code generates ASCII files, describing atom positions and their connectivity, which can be entered as input data in available commercial and in-house FE codes. To convert the ASCII files, obtained from the CoNTub 1.0 program, into the format usable by the commercial FE code ABAQUS®, the in-house application designated by *InterfaceNanotubes* was developed [30]. The geometrical characteristics of the SWCNTs used for the present FE analyses are summarized in Table 1, where the number of nodes and elements of the SWCNTs FE meshes is also presented, for the length of nanotube considered, $L = 20$ nm. This length corresponds to the minimum recommended value from which the mechanical properties are independent of the SWCNT length [30].

Table 3
The number of nodes and elements of the meshes of the SWCNTs containing different vacancy configurations.

Vacancy type	0.5%		1.0%		2.0%		5.0%		10.0%[a]	
	Nodes	Elem.	Nodes	Elem.	Nodes	Elem.	Nodes	Elem.	Nodes	Elem.
Armchair (20, 20): $D_n = 2.713$ nm, L = 23.36 nm, 7640 nodes, 11,420 elements										
Single	7602	11,306	7562	11,189	7486	10,958	7259	10,277	7164	9555[b]
Double		11,325		11,225		11,035		10,460		9910
Triple		11,328		11,238		11,060		10,529		10,042
Four together		11,330		11,244		11,073		10,560		10,101
Mixed		11,326		11,234		11,029		10,460		9845
Zigzag (35,0): $D_n = 2.740$ nm, L = 22.38 nm, 7420 nodes, 11,095 elements										
Single	7383	10,984	7346	10,873	7272	10,651	7049	9979	6678	8882[b]
Double		11,000		10,910		10,725		10,165		9239
Triple		11,006		10,920		10,749		10,229		9364
Four together		11,009		10,928		10,762		10,252		9471
Mixed		10,998		10,905		10,721		10,167		9208
Chiral θ 19.1° (24, 12): $D_n = 2.486$ nm, L = 21.74 nm, 6504 nodes, 9720 elements										
Single	6471	9621	6439	9525	6374	9330	6179	8745	5854	7862
Double		9637		9557		9395		8907		8095
Triple		9643		9568		9416		8960		8203
Four together		9645		9573		9427		8989		8258
Mixed		9638		9557		9392		8894		8059

[a] The SWCNT mesh with 7690 nodes, 11,900 elements, L = 24.34 nm.
[b] The SWCNT meshes cannot contain solely single vacancies, due to their high percentage (10%); some quantity of double and triple vacancies is also present.

Examples of FE meshes for three types of SWCNTs are shown in Fig. 1. The vacancy defects considered in the current study have the following types of configuration, as shown in Fig. 2: single vacancies (one atom is missing), double vacancies (two neighbouring atoms are missing – Fig. 2(a)), triple vacancies (three neighbouring atoms are missing – Fig. 2(b)) and four vacancies together (four neighbouring atoms are missing – Fig. 2(c)). By removing the carbons atoms from the nanotube, the bond interactions (i.e. beams in the FE model) corresponding to the missing atoms are removed [18,19,21,22]. Atoms in the percentage of 0.0, 0.1, 0.5, 1.0, 2.0, 5.0 and 10.0% were removed from the SWCNTs shown in Table 1. The defects were regularly distributed around the centre and along the length of the nanotubes, with the exception of the ends of the nanotube.

2.3. FE analysis of SWCNTs

Li and Chou [13] proposed direct relationships between the structural mechanics parameters, i.e. tensile, E_bA_b, bending, E_bI_b, and torsional G_bJ_b, rigidities, and the force field constants, k_r, k_θ, and k_τ:

$$\frac{E_bA_b}{l} = k_r, \tag{4}$$

$$\frac{E_bI_b}{l} = k_\theta, \tag{5}$$

$$\frac{G_bJ_b}{l} = k_\tau, \tag{6}$$

where l is the beam length equal to 0.1421 nm; E_b and G_b are the beam Young's and shear moduli, respectively; A_b is the beam cross-sectional area, I_b and J_b are the beam moment of inertia and polar moment of inertia, respectively, and k_r, k_θ, and k_τ are the bond stretching, bond bending and torsional resistance force constants, respectively. Eqs. (4)–(6) establish the basis for the application of continuum mechanics to the analysis of the mechanical behaviour of CNTs, and provide the input data for numerical simulation. The input data and the values of force constants [35,36] for the FE model are given in Table 2.

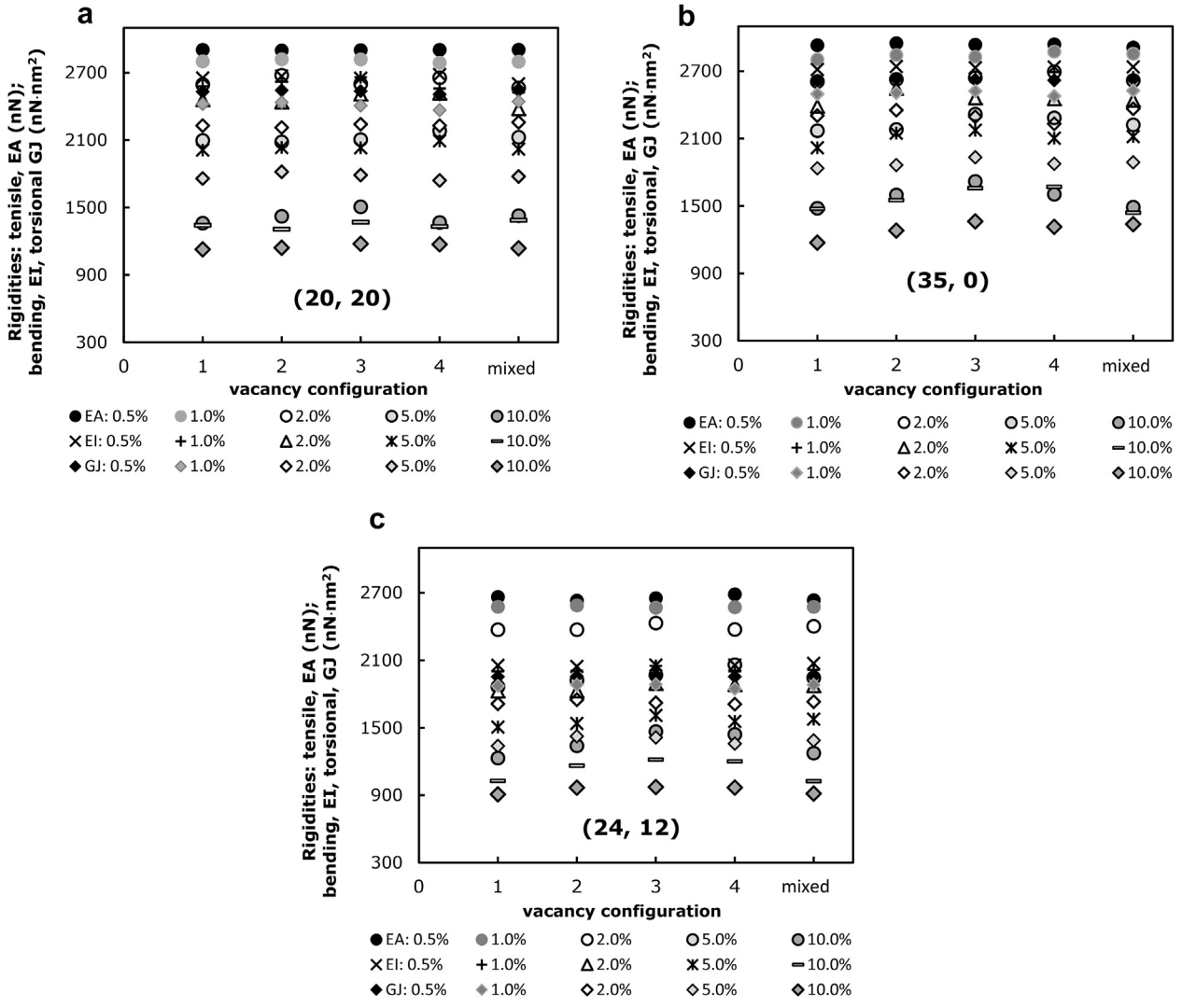

Fig. 3. Effect of the vacancy configuration on the tensile, bending and torsional rigidities of (a) armchair (20, 20), (b) zigzag (35, 0) and (c) chiral (24, 12) SWCNTs.

3. Results and discussion

3.1. Rigidities of SWCNTs with vacancy defects

The tensile, bending and torsional rigidities of SWCNTs were evaluated from conventional mechanical numerical tests as described in the following.

The tensile rigidity, *EA*, of SWCNT is determined as:

$$EA = \frac{F_x L}{u_x}, \tag{7}$$

where F_x, is the tensile axial force applied at one nanotube end, leaving the other end fixed, L is the nanotube length and u_x is the axial displacement taken from the FE analysis.

Similarly, the bending rigidity of the nanotube, *EI*, is represented as:

$$EI = \frac{F_y L^3}{3u_y}, \tag{8}$$

where F_y is the transverse force applied at one end of the nanotube, leaving the other fixed, u_y is the transverse displacement, taken from the FE analysis.

Finally, the torsional rigidity of the nanotube, *GJ*, is determined as:

$$GJ = \frac{F_\varphi R L}{\varphi}, \tag{9}$$

where F_φ is the tangential force applied at one end of the nanotube, leaving the other fixed, R is the nanotube radius and φ is the twist angle, taken from the FE analysis. In case of torsion, the nodes under loading, at the end of the nanotube, are prevented from moving in the radial direction.

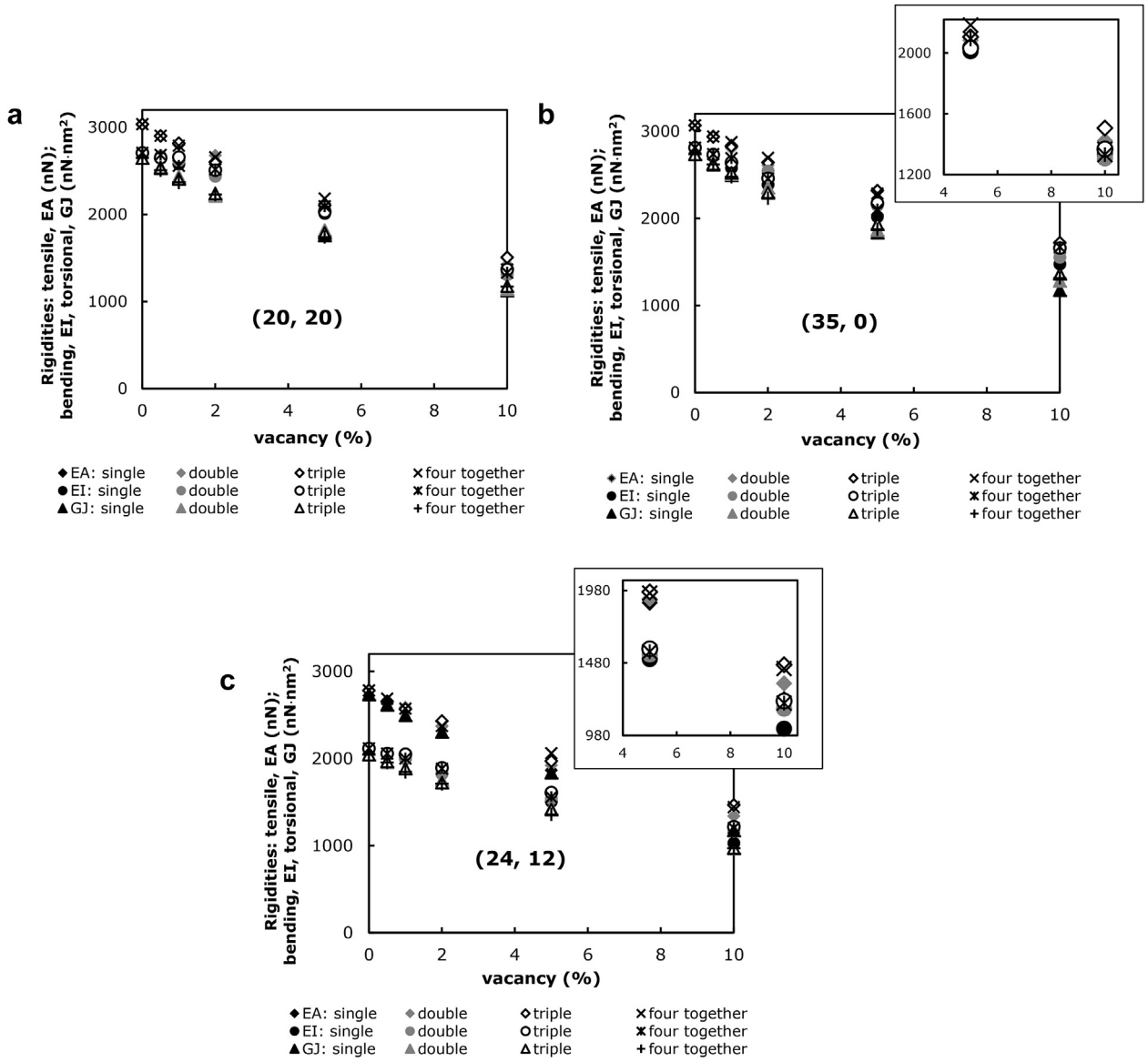

Fig. 4. Effect of the vacancy percentage on the tensile, bending and torsional rigidities of (a) armchair (20, 20), (b) zigzag (35, 0) and (c) chiral (24, 12) SWCNTs, containing different vacancy types.

Firstly, a study was carried out in order to understand the role of the configuration type of the vacancy defects on the tensile, bending and torsional rigidities of SWCNTs. In this regard, atoms in proportions equal to 0.5, 1.0, 2.0, 5.0, 10.0% were removed from the meshes of armchair (20, 20), zigzag (35, 0) and chiral (24, 12) SWCNTs, in such way that each mesh contains only one type of defects: (i) single vacancies; (ii) double vacancies; (iii) triple vacancies; (iv) four vacancies together. For comparison, the same meshes, containing assortment of all types of defects (mixed defects), were considered for each percentage of the defects studied. The number of nodes (atoms) and elements (beams) of the FE meshes of (20, 20), (35, 0) and (24, 12) nanotubes, with different defect configurations, are shown in Table 3. The vacancy configuration alters the number of beam elements, i.e. vacancy defects of the different type have dissimilar number of the elements, for the same number of the missing atoms (nodes). The number of elements increases with the size of the vacancy defect, for a given percentage of removed atoms.

The results concerning the effect of the type of vacancy configuration on the tensile, bending and torsional rigidities of armchair (20, 20), zigzag (35, 0) and chiral (24, 12) nanotubes are shown in Fig. 3. The type of vacancy configuration does not cause significant influence on the values of the three rigidities, with exception of the zigzag (35, 0), with 5.0 and 10.0% of vacancies, and the chiral (24, 12), with 10.0% of vacancies, for which the *EA* and *EI* rigidities are somewhat sensitive to vacancy configuration: these rigidities are higher for nanotubes structures with multiple vacancies (double, triple and four vacancies together) than for nanotubes with single vacancies and the mixed cases. This result is certainly related to the number of elements that are relatively high for the cases of multiple vacancies when compared with single or mixed vacancies cases, particularly when the percentage of vacancies is high (5.0 and 10.0%).

Fig. 4 shows examples of the evolutions of the tensile, *EA*, bending, *EI*, and torsional, *GJ*, rigidities as a function of the percentage of the vacancies, for the case of (20, 20), (35, 0) and (24, 12) nanotubes, with different vacancy configurations. The tensile rigidity, *EA*, decreases with increasing of the percentage of vacancies in SWCNT, similarly for all types of defects. The same is true for the *EI* and *GJ* rigidities.

Parvaneh and Shariati [19], using the NCM approach and implementing spring elements and non-linear connectors, studied the effect of the presence of the isolated single, double and triple vacancies in armchair (7, 7) and zigzag (12, 0) SWCNTs on their Young's modulus. For this purpose, one vacancy of each configuration was introduced in the nanotubes with different aspect ratio, i.e. the ratio between the SWCNT length and diameter. For nanotubes with low aspect ratio, the results showed that the Young's modulus values of the defective SWCNTs are slightly influenced by vacancy type. For the cases of nanotubes with high aspect ratio, similar to those in the current study, this influence is insignificant. In both cases, the percentage of defects is very low (less than 2.5%).

Taking into account the results from Figs. 3 and 4, i.e. in generally the type of vacancy configuration does not significantly affect the value of rigidities, a study was carried out for the SWCNTs with different percentage (0.0, 0.5, 1.0, 2.0, 5.0 and 10.0%) of the

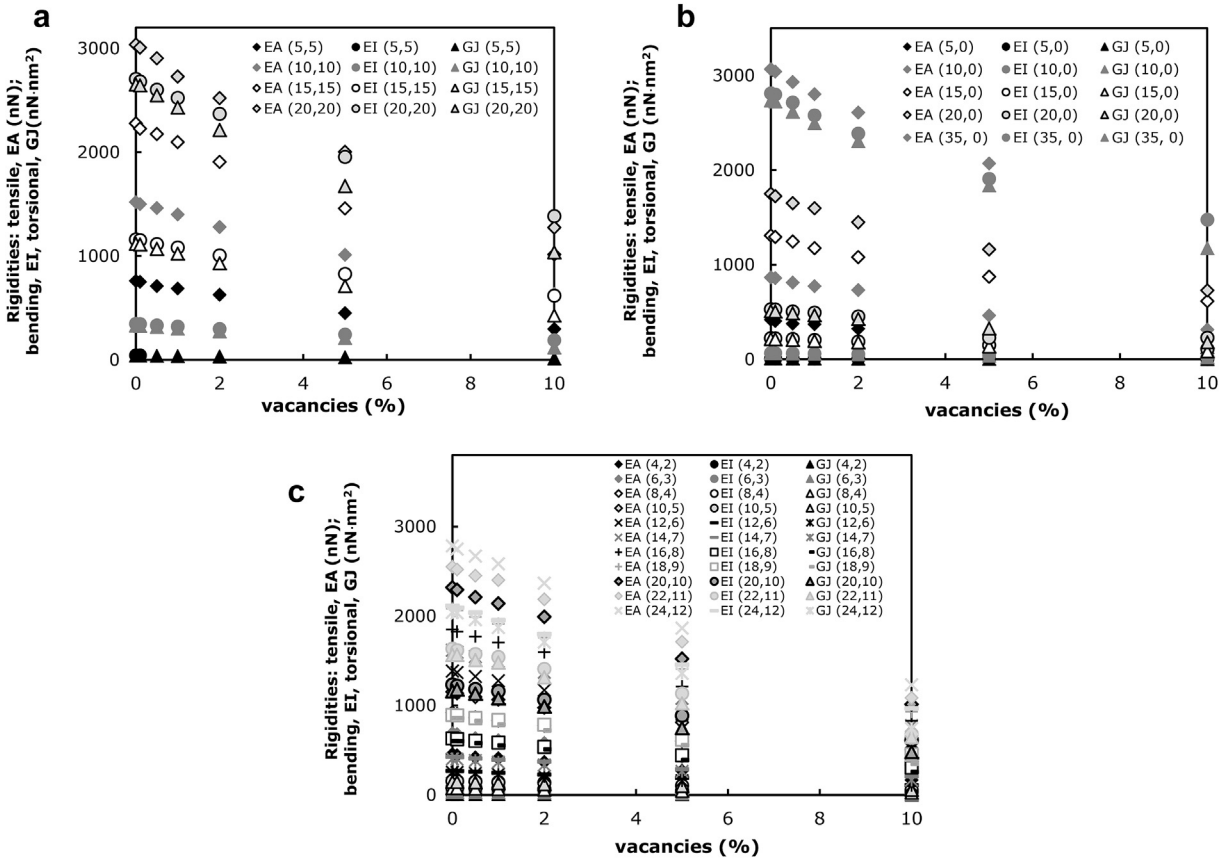

Fig. 5. Evolution of the tensile, *EA*, bending, *EI*, and torsional, *GJ*, rigidities with the percentage of vacancies in SWCNTs for armchair (a), zigzag (b) and chiral family $\theta = 19.1^{\circ}$ (c) SWCNTs.

vacancy defects, including simultaneously single vacancies, double vacancies, triple vacancies and four vacancies together. Fig. 5 shows the evolutions of the tensile, *EA*, bending, *EI* and torsional, *GJ* rigidities of non-chiral and chiral SWCNTs with the percentage of the vacancies. The three rigidities decrease with increasing amount of the vacancies in the SWCNT. The values of the tensile, *EA*, bending, *EI*, and torsional, *GJ*, rigidities as a function of the SWCNT diameter, D_n, are plotted in Fig. 6(a)–(c) for SWCNTs with different percentage of the vacancy defects. The values of the rigidities, *EA*, *EI* and *GJ* decrease with increasing of the percentage of vacancies in the SWCNT, for a given value of the nanotube diameter. The evolutions of the tensile rigidity, *EA*, can be unified for each content of the vacancy defects, whatever the chirality. This is also true for the evolutions of the bending rigidity, *EI*, and for the evolutions of the torsional rigidity, *GJ*. The results concerning the evolutions of the rigidities with nanotube diameter, D_n, can be fitted by a quasi-linear trend for the case of tensile rigidity, *EA*, and close to a cubic power trend for the cases of bending, *EI*, and torsional, *GJ*, rigidities, as shown in Fig. 7(a)–(c). These dependencies can be simply described, correspondingly:

$$EA = \alpha^p \left(D_n - D_{0EA}^p\right) \tag{10}$$

$$EI = \beta^p \left(D_n - D_{0EI}^p\right)^3 \tag{11}$$

$$GJ = \gamma^p \left(D_n - D_{0GJ}^p\right)^3 \tag{12}$$

where the fitting parameters α^p and D_{0EA}^p, β^p and D_{0EI}^p, and γ^p and D_{0GJ}^p concern the cases of tensile, bending and torsional rigidities, respectively, for a given percentage, p, of vacancy defects, whatever the chirality of the SWCNTs. The parameters of Eqs. (10)–(12) were previously obtained by the authors [30] for the case of perfect (without defects) SWCNTs. The full list of the fitting parameters is given in Table 4, where D_0^p is an average value of the parameters D_{0EA}^p, D_{0EI}^p, D_{0GJ}^p for three types of the mechanical test at each percentage of defects, p; the values of these parameters are close to zero whatever the type of test and the percentage of vacancy defects. Fig. 8 shows that the evolution of the parameters α, β and γ with the percentage of vacancy defects follows a nearly linear trend. The mean difference between the values of *EA*, *EI* and *GJ* rigidities calculated with Eqs. (10)–(12), and the values obtained directly from FE analysis is presented in Table 5.

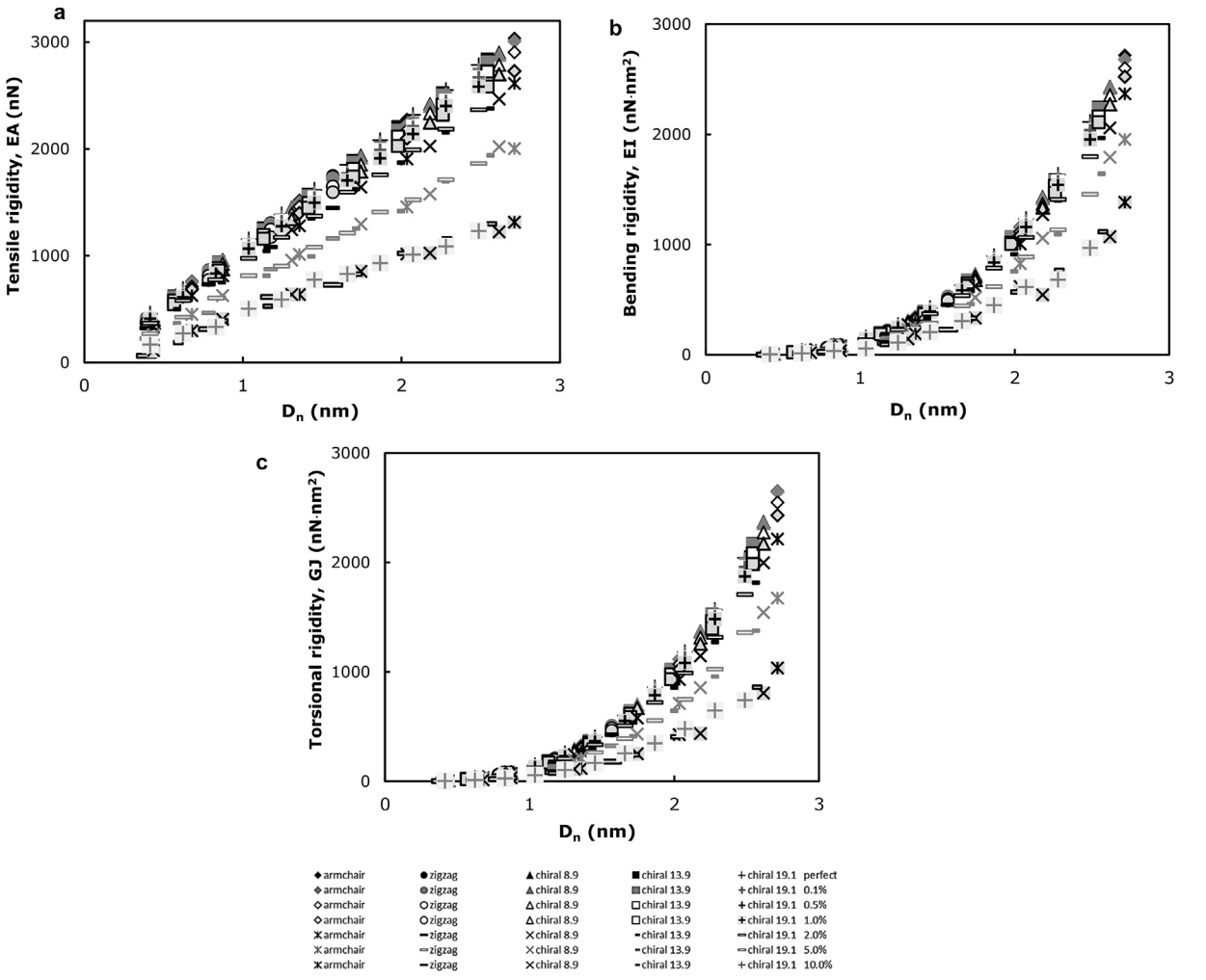

Fig. 6. Evolution of the nanotube rigidities as a function of the nanotube diameter, D_n, for perfect non-chiral and chiral SWCNTs and for SWCNTs containing different percentage of vacancies: (a) the tensile rigidity, *EA*; (b) bending rigidity, *EI*, and (c) torsional rigidity, *GJ*.

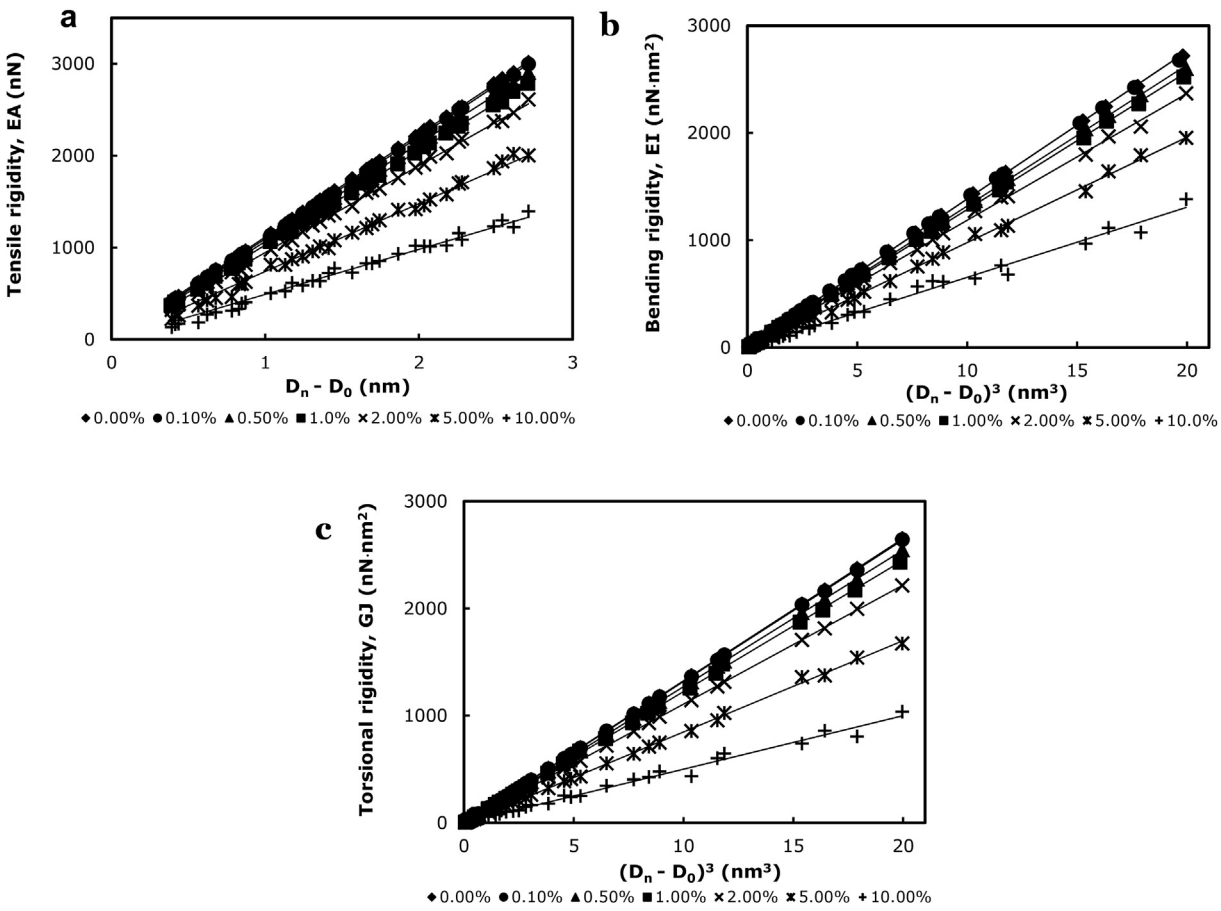

Fig. 7. Evolution of the rigidities for perfect and defect non-chiral and chiral SWCNTs: (a) tensile rigidity, *EA*, as a function of $(D_n - D_0)$; (b) bending rigidity, *EI*, and (c) torsional rigidity, *GJ*, as a function of $(D_n - D_0)^3$.

Table 4
Fitting parameters α, β, γ and D_0.

Parameter[a]	% Vacancies						
	0.0	0.1	0.5	1.0	2.0	5.0	10.0
α (nN nm^{-1})	1131.66	1116.94	1095.39	1051.67	961.12	784.04	522.34
β (nN nm^{-1})	143.48	141.01	139.75	137.32	126.02	105.11	71.36
γ (nN nm^{-1})	130.39	127.97	126.83	123.69	111.00	86.00	49.70
D_0 (nm)	$3.5\cdot10^{-3}$	$4.0\cdot10^{-4}$	0.010	0.025	0.010	0.016	$1.0\cdot10^{-3}$

[a] The values of parameters include armchair, zigzag and all types of chiral SWCNT studied.

3.2. Elastic moduli of SWCNTs with vacancy defects

Using the nanotube rigidities, *EA*, *EI*, and *GJ*, the nanotube Young's, *E*, and shear, *G*, moduli can be assessed. Considering a hollow cylindrical profile for the CNT, the cross-sectional area, *A*, of the equivalent hollow cylinder and the moments of inertia, I and J, can be written:

$$A = \frac{\pi}{4}\left[(D+t)^2 - (D-t)^2\right] = \pi D t \tag{13}$$

$$I = \frac{\pi}{64}\left[(D+t)^4 - (D-t)^4\right] \tag{14}$$

$$J = \frac{\pi}{32}\left[(D+t)^4 - (D-t)^4\right] \tag{15}$$

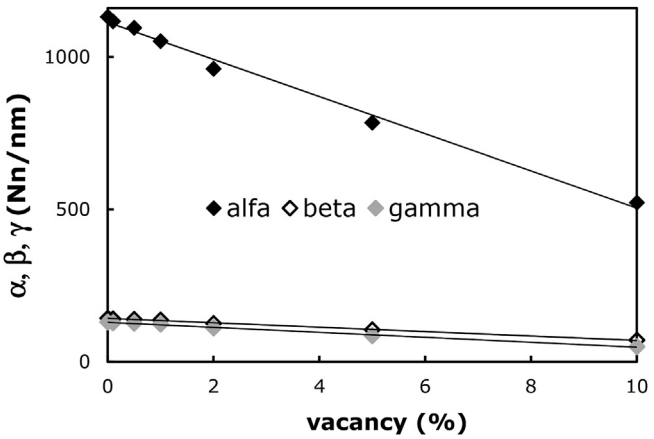

Fig. 8. Evolution of the fitting parameters, α, β and γ with the percentage of the vacancies.

Table 5
The mean difference between the rigidities values calculated with Eqs. (10)–(12), and the values obtained from FE analysis.

Vac. percent.	0.0%	0.1%	0.5%	1.0%	2.0%	5.0%	10.0%
Rigidities	Mean difference, %						
EA (nN)	0.39	0.87	0.95	1.48	2.03	2.53	3.66
EI (nN nm^2)	2.82	3.64	3.78	1.36	4.72	6.52	6.68
GJ (nN nm^2)	1.25	1.56	3.13	1.48	3.35	6.92	7.87

where D and t are the mean diameter and thickness of the equivalent hollow cylinder, respectively.

Assuming $t = t_n$ (where t_n is the nanotube wall thickness), the expression for D can be derived from Eqs. (13) and (14):

$$\frac{EI}{EA} = \frac{1}{8}\left(D^2 + t_n^2\right) \Rightarrow \quad D = \sqrt{8\left(\frac{EI}{EA}\right) - t_n^2} \tag{16}$$

Thus, using Eqs. (13)–(16), the elastic moduli of the nanotube can be calculated using the following expressions, taking into account the rigidities in tension, bending and torsion:

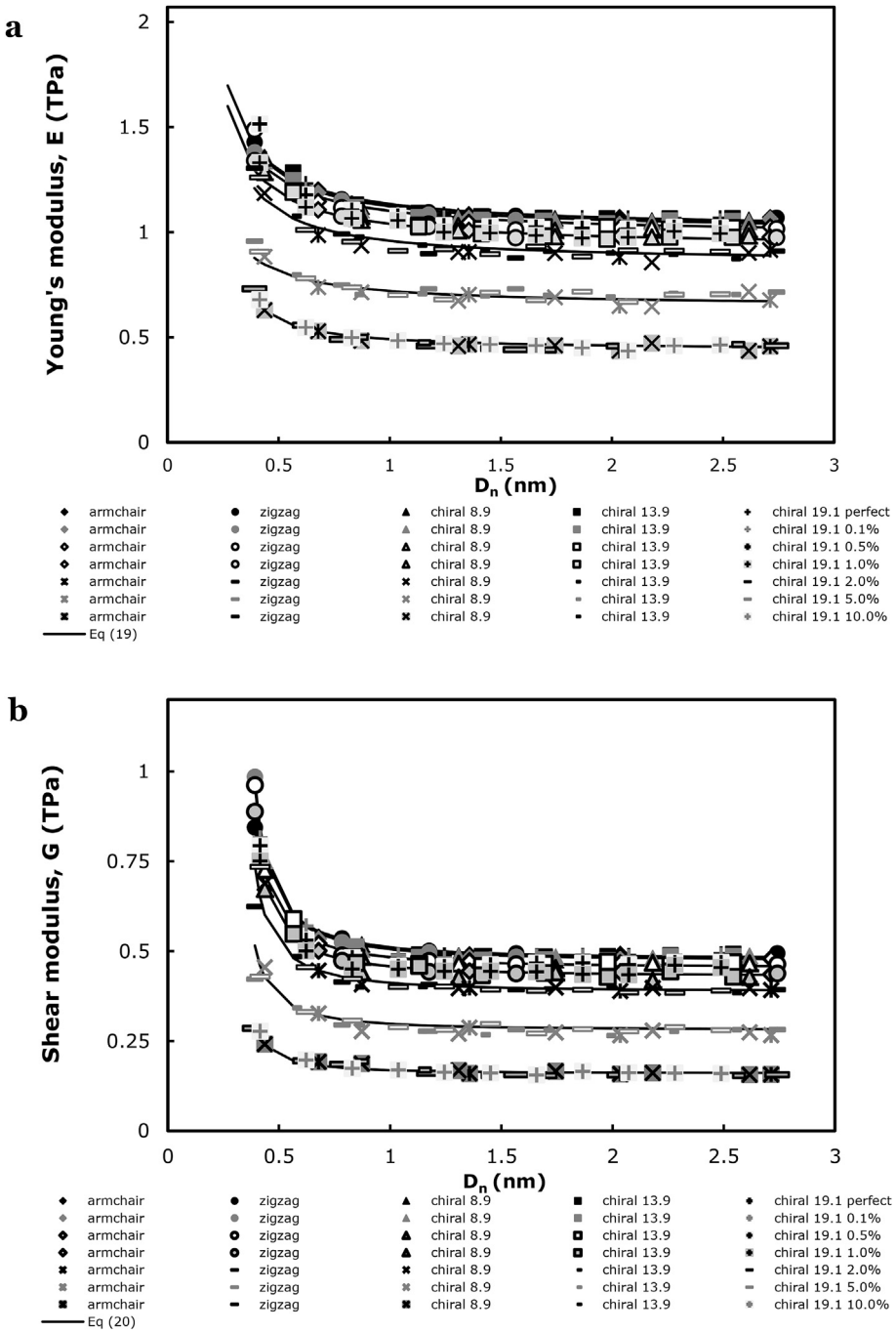

Fig. 9. Evolution of the Young's modulus (a) and shear modulus (b) as a function of the nanotube diameter, D_n for perfect and with defect SWCNTs.

Table 6
The stabilized values of Young's modulus and shear modulus of defective SWCNTs for different percentage of vacancies.

Vac. percent.	0.0%	0.1%	0.5%	1.0%	2.0%	5.0%	10.0%
E, TPa	1.083	1.079	1.054	1.000	0.902	0.719	0.470
G, TPa	0.492	0.490	0.478	0.446	0.386	0.286	0.164

$$E = \frac{EA}{A} = \frac{EA}{\pi t_n \sqrt{8\left(\frac{EI}{EA}\right) - t_n^2}} \tag{17}$$

$$G = \frac{GJ}{J} = \frac{GJ}{2\pi t_n \left(\frac{EI}{EA}\right)\sqrt{8\left(\frac{EI}{EA}\right) - t_n^2}} \tag{18}$$

Eqs. (10)–(12) for *EA*, *EI* and *GJ* rigidities enable writing Eqs. (17) and (18) for Young's and shear moduli as follows:

$$E = \frac{EA}{A} = \frac{\alpha(D_n - D_0)}{\pi t_n \sqrt{8\frac{\beta(D_n - D_0)^2}{\alpha} - t_n^2}} \tag{19}$$

$$G = \frac{GJ}{J} = \frac{\gamma(D_n - D_0)}{2\pi t_n \left(\frac{\beta}{\alpha}\right)\sqrt{8\frac{\beta(D_n - D_0)^2}{\alpha} - t_n^2}} \tag{20}$$

These equations allows determining Young's modulus and shear modulus of any percentage of vacancy defects in the SWCNTs, knowing the parameters of Table 3 and the wall thickness, t_n (the most widely used value is $t_n = 0.34$ nm, which is equal to the interlayer spacing of graphite).

Fig. 9 shows the results of the Young's and shear moduli as a function of the nanotube diameter, D_n, for the various percentages of defects in the SWCNTs. The elastic moduli results obtained for perfect SWCNTs are in good agreement with the results available in the literature, as previously discussed [30]. In the case of defective nanotubes, the Young's modulus value decreases with increasing the nanotube diameter, and tends to stabilize for high values of the nanotube diameter. The same trend is observed for the shear modulus. The stabilized values of Young's modulus (Fig. 9(a)) and shear modulus (Fig. 9(b)) are shown in Table 6. These values decrease with increasing of the content of the vacancies in the SWCNT, as can be easily seen in Fig. 10(a). The moduli of SWCNTs with 10.0% of vacancy defects are about 43% the Young's modulus and of about 33% the shear modulus of perfect single-walled carbon nanotubes.

Fig. 10(b) shows the reduction of the moduli as a function of the percentage of vacancies. A quasi-linear trend of the decrease of both Young's and shear moduli with the increase of the vacancy defects is observed up to 5.0% of defects, as shown in the figure. Similar equation ($E_{reduction} = -7.69 \cdot Vacancy$) was reported by Ghavamian et al. [22] for the reduction of the Young's modulus of armchair (10, 10) and zigzag (14, 0) SWCNTs making use of results from perfect nanotubes and with 0.5 and 1.0% of single vacancy defects, which is close to that in Fig. 10(b).

The results regarding to the Young's modulus of the defective nanotubes have been object of some analysis in the literature. Fig. 11 allows easy comparison of the present results with those from the works of Parvaneh and Shariati [19] and Ghavamian et al. [22], who studied the Young's modulus of the defective nanotubes up to about 1.5% and 1.0% of vacancy defects, respectively. The results in this figure, concerning armchair and zigzag nanotubes, are

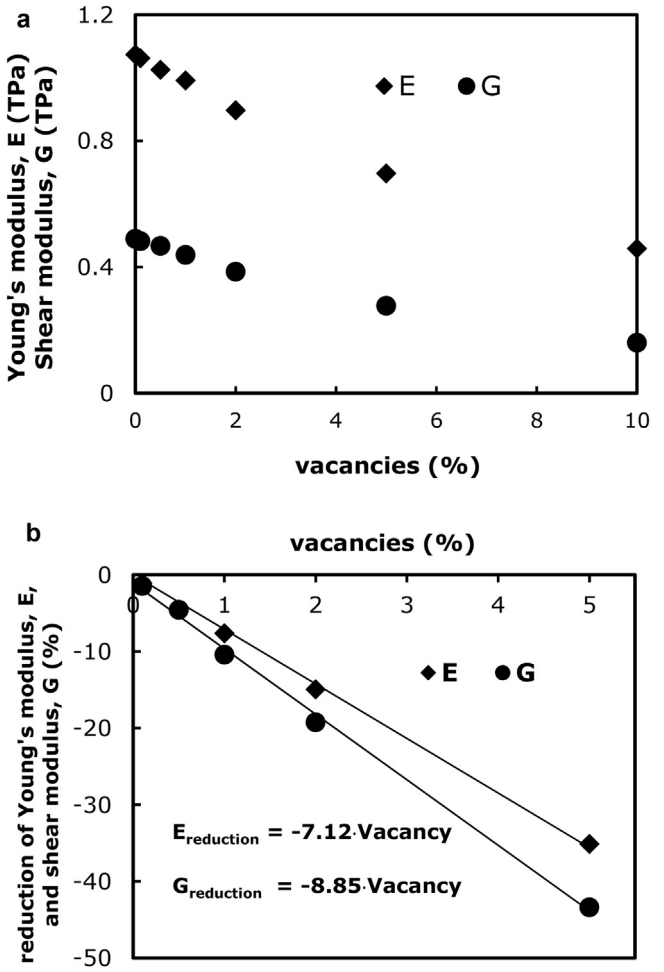

Fig. 10. Young's and shear moduli (a) and their reduction (b) as a function of the percentage of vacancy defects.

separated into two groups: (i) small nanotube diameters (less than 1 nm) showing higher Young's modulus and (ii) higher nanotube diameters, for which the Young's modulus value is almost stabilized (see Fig. 9(a)). Current results and those of Parvaneh and Shariati [19] and Ghavamian et al. [22] display consistency, showing similar values and trends in each group.

3.3. Poisson's ratio of SWCNTs with vacancy defects

The Poisson's ratio can be calculated, taking into account the isotropic material condition ($E = G/2(1 + \nu)$) and the fact that $J = 2I$, as follows:

$$\nu = \frac{E}{2G} - 1 = \frac{EI}{GJ} - 1 \tag{21}$$

Furthermore, Eqs. (19) and (20) allow defining a unique equation for the Poisson's ratio, independent of the nanotube type and diameter:

$$\nu = \frac{\beta}{\gamma} - 1 \tag{22}$$

Fig. 12 shows the evolution of the Poisson's ratio, ν, with nanotube diameter, D_n, for non-chiral (armchair – Fig. 12(a) and zigzag – Fig. 12(b)) and the $\theta = 19.1°$ family of chiral SWCNTs (Fig. 12(c)); the values of the Poisson's ratio were obtained by Eq.

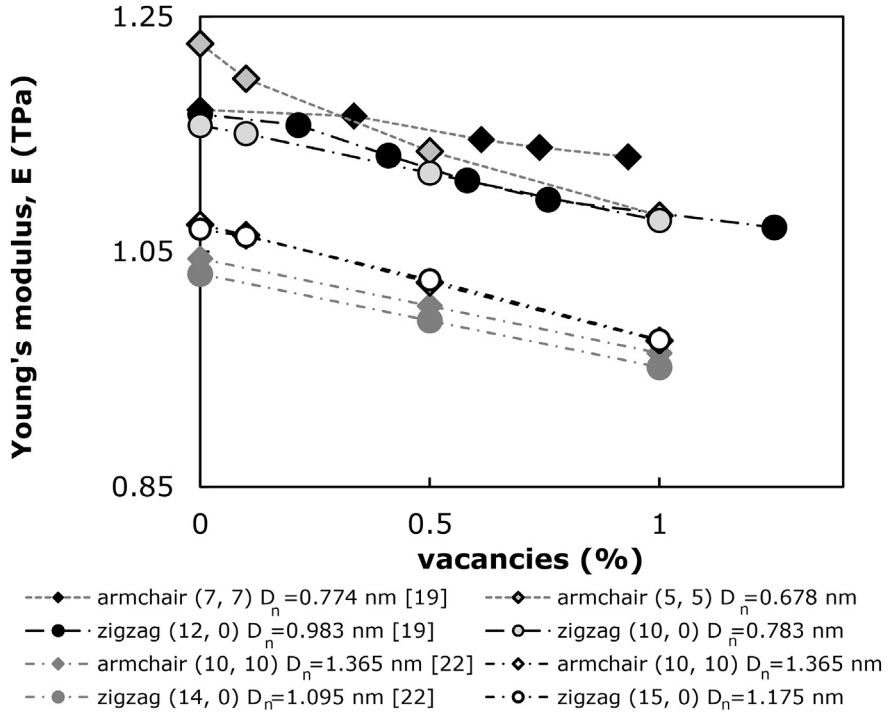

Fig. 11. Comparative study with literature results on the evolution of the Young's modulus with the percentage of vacancy defects.

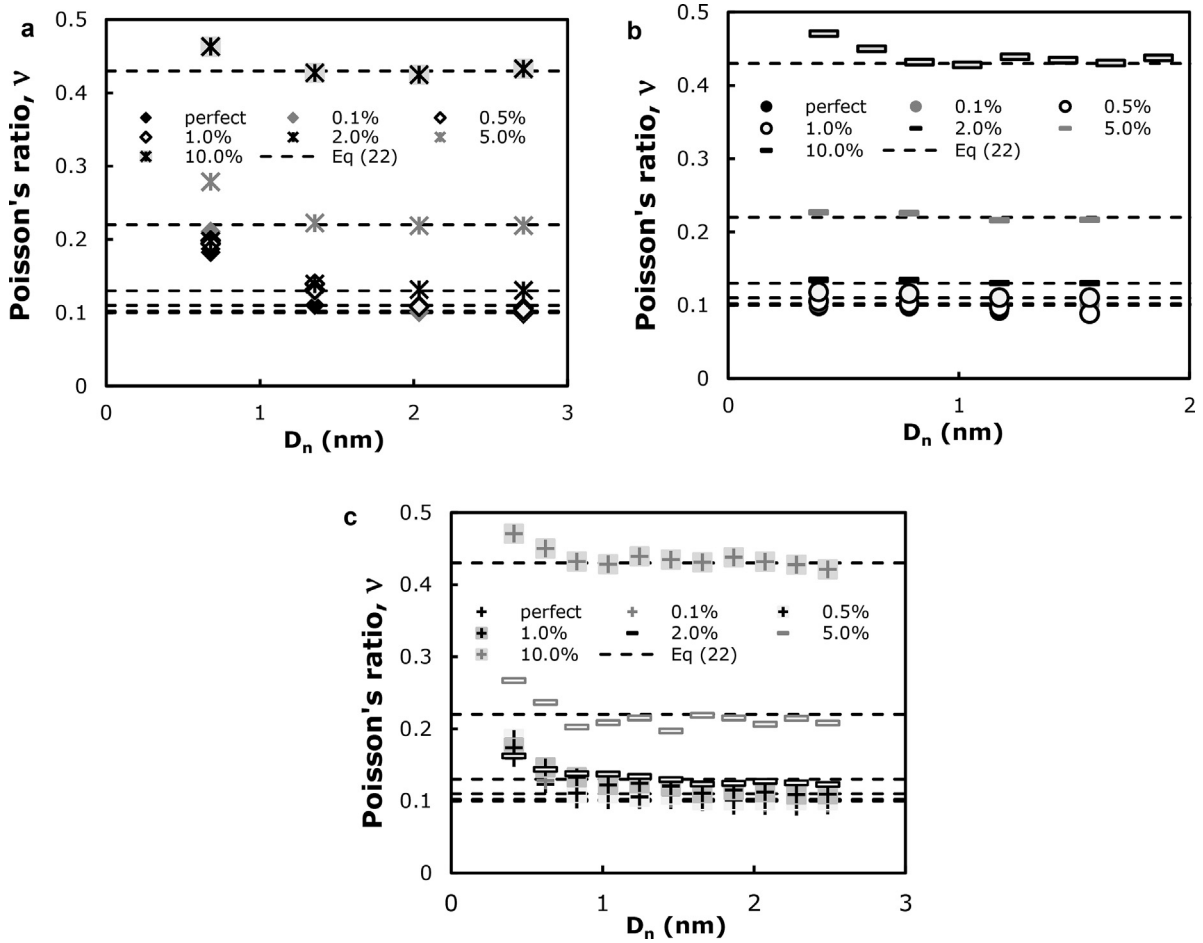

Fig. 12. Evolution of the calculated Poisson's ratio as a function of the nanotube diameter for armchair (a), zigzag (b) and $\theta = 19.1^\circ$ chiral (c) SWCNTs with different percentage of vacancies.

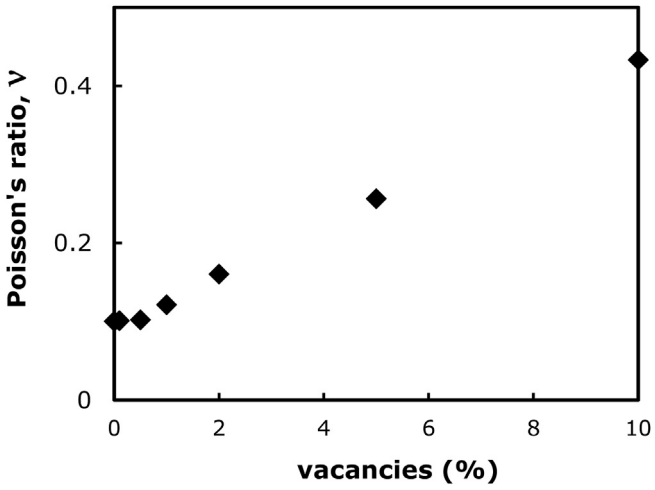

Fig. 13. The Poisson's ratio as a function of the percentage of vacancy defects.

(21). The Poisson's ratio values calculated with Eq. (22), which does not depend on D_n, are also shown in this figure (dashed lines). Regardless of the type of nanotube, the Poisson's ratio tends towards approximately the values of about 0.100, 0.101, 0.102, 0.118, 0.168, 0.256 and 0.430, for SWCNTs with 0.0, 0.1, 0.5, 1.0, 2.0, 5.0 and 10.0% of vacancies, respectively, as obtained by Eq. (22).

Fig. 13 shows the evolution of the stabilized values of the Poisson's ratio with the content of the vacancy defects. The Poisson's ratio increases with the increase of the percentage of vacancies, for all types of SWCNTs studied. Significant increase of ν, of about 4 times when compared with the value for perfect SWCNT, is observed for the case of the SWCNTs with 10.0% of vacancy defects.

4. Conclusions

The tensile, bending and torsional rigidities, as well as the Young's and shear moduli, and Poisson's ratio of non-chiral and chiral SWCNTs containing vacancy defects were predicted using finite element analysis within nanoscale continuum modelling approach. The main conclusions can be drawn as follows:

- The tensile, bending and torsional rigidities of non-chiral and chiral SWCNTs are not significantly influenced by the type of vacancy configuration (single, double, triple or four vacancies together);
- The tensile, bending and torsional rigidities of non-chiral and chiral SWCNTs are sensitive to the presence of vacancy: the three rigidities decrease with the increase of the percentage of vacancies;
- Equations describing the relationship between each of the three rigidities and the nanotube diameter have been obtained for SWCNTs with various percentages of vacancy defects; these relationships allow the easy evaluation of the Young's and shear moduli, and Poisson's ratio, of SWCNT with vacancy defects;
- The Young's and shear moduli of SWCNTs decrease with increasing percentage of vacancies in nanotubes; the Poisson's ratio of SWCNTs increases with increasing percentage of vacancies in the nanotubes.

Acknowledgements

This research work is sponsored by national funds from the Portuguese Foundation for Science and Technology (FCT) via the projects PTDC/EME–TME/122472/2010 and PEst-C/EME/UI0285/2013 as well as by FEDER funds “Programa Operacional da Região Centro” via the project CENTRO-07-0224-FEDER-002001 (MT4MOBI). All supports are gratefully acknowledged.

References

[1] Robertson J. Realistic applications of CNTs. Mater Today 2004;7(10):46–52.
[2] Gao RP, Wang ZL, Bai ZG, de Heer WA, Dai LM, Gao M. Nanomechanics of individual carbon nanotubes from pyrolytically grown arrays. Phys Rev Lett 2000;85(3):622–5.
[3] Andrews R, Jacques D, Qian D, Dickey EC. Purification and structural annealing of multiwalled carbon nanotubes at graphitization temperatures. Carbon 2001;39(11):1681–7.
[4] Terrones M, Banhart F, Grobert N, Charlier JC, Terrones H, Ajayan PM. Molecular junctions by joining single-walled carbon nanotubes. Phys Rev Lett 2002;89(7):075505.
[5] Rafiee R, Moghadam RM. On the modelling of carbon nanotubes: a critical review. Compos Part B 2014;56:435–49.
[6] Kudin KN, Scuseria GE, Yakobson BI. C2F, BN and C nanoshell elasticity from ab initio computations. Phys Rev B 2001;64(23):235406.
[7] Chen X, Cao GX. A structural mechanics study of single-walled carbon nanotubes generalized from atomistic simulation. Nanotechnology 2006;17(4):1004–15.
[8] Zhang HW, Wang JB, Guo X. Predicting the elastic properties of single-walled carbon nanotubes. J Mech Phys Solids 2005;53(9):1929–50.
[9] Pantano A, Parks DM, Boyce MC. Mechanics of deformation of single- and multi-wall carbon nanotubes. J Mech Phys Solids 2004;52(4):789–821.
[10] Kalamkarov AL, Georgiades AV, Rokkam SK, Veedu VP, Ghasemi-Nejhad NM. Analytical and numerical techniques to predict carbon nanotubes properties. Int J Solids Struct 2006;43(22–23):6832–54.
[11] Odegard GM, Gates TS, Nicholson LM, Wise KE. Equivalent continuum modelling of nano-structured materials. Compos Sci Technol 2002;62(14):1869–80.
[12] Giannopoulos GI, Kakavas PA, Anifantis NK. Evaluation of the effective mechanical properties of single-walled carbon nanotubes using a spring based finite element approach. Comput Mater Sci 2008;41(4):561–9.
[13] Li C, Chou TW. A structural mechanics approach for the analysis of carbon nanotubes. Int J Solids Struct 2003;40(10):2487–99.
[14] Hu N, Nunoya K, Pan D, Okabe T, Fukunaga H. Prediction of buckling characteristics of carbon nanotubes. Int J Solids Struct 2007;44(20):6535–50.
[15] Tserpes KI, Papanikos P. Finite element modeling of single-walled carbon nanotubes. Compos Part B 2005;36(5):468–77.
[16] Ghavamian A, Rahmandoust M, Öchsner A. On the determination of the shear modulus of carbon nanotubes. Compos Part B 2013;44(1):52–9.
[17] Mohammadpour E, Awang M. Predicting the nonlinear tensile behavior of carbon nanotubes using finite element simulation. Appl Phys A 2011;104(2):609–14.
[18] Scarpa F, Adhikari S, Wang CY. Mechanical properties of non-reconstructed defective single-wall carbon nanotubes. J Phys D Appl Phys 2009;42:142002.
[19] Parvaneh V, Shariati M. Effect of defects and loading on prediction of Young's modulus of SWCNTs. Acta Mech 2011;216(1–4):281–9.
[20] Parvaneh V, Shariati M, Torabi H. Bending buckling behavior of perfect and defective single-walled carbon nanotubes via a structural mechanics model. Acta Mech 2012;223(11):2369–78.
[21] Rahmandoust M, Ochsner A. Influence of structural imperfections and doping on the mechanical properties of single-walled carbon nanotubes. J Nano Res 2009;6:185–96.
[22] Ghavamian A, Rahmandoust M, Ochsner A. A numerical evaluation of the influence of defects on the elastic modulus of single and multi-walled carbon nanotubes. Comp Mater Sci 2012;62:110–6.
[23] Ghavamian A, Ochsner A. Numerical modeling of eigenmodes and eigenfrequencies of single- and multi-walled carbon nanotubes under the influence of atomic defects. Comp Mater Sci 2013;72:42–8.
[24] Ghavamian A, Ochsner A. Numerical investigation on the influence of defects on the buckling behavior of single-and multi-walled carbon nanotubes. Physica E 2012;2012(46):241–9.
[25] Poelma RH, Sadeghian H, Koh S, Zhang GQ. Effects of single vacancy defect position on the stability of carbon nanotubes. Microelectron Reliab 2012;52(7):1279–84.
[26] Xiao S, Hou W. Fracture of vacancy-defected carbon nanotubes and their embedded nanocomposites. Phys Rev B 2006;73(11):115406.
[27] Hou W, Xiao S. Mechanical behaviors of carbon nanotubes with randomly located vacancy defects. J Nanosci Nanotechnol 2007;7(12):4478–85.
[28] Dresselhaus MS, Dresselhaus G, Saito R. Physics of carbon nanotubes. Carbon 1995;33(7):883–91.
[29] Melchor S, Dobado JA. CoNTub: an algorithm for connecting two arbitrary carbon nanotubes. J Chem Inf Comput Sci 2004;44(5):1639–46.
[30] Sakharova NA, Pereira AFG, Antunes JM, Brett CMA, Fernandes JV. Mechanical characterization of single-walled carbon nanotubes: numerical simulation study. Compos Part B 2015;75:73–85.
[31] Arora G, Sandler SI. Molecular sieving using single wall carbon nanotubes. Nano Lett 2007;7(3):565–9.

[32] Yengejeh SI, Kazemi SA, Ochsner A. Influence of combined loading on the structural stability of carbon nanotubes. Mater Chem Phys 2015;158:96–106.
[33] Yengejeh SI, Oechsner A. On the stiffness of carbon nanotubes with spiral distortion. J Nano Res 2014;29:85–92.
[34] Contreras ML, Ávila D, Alvarez J, Rozas R. Computational algorithms for fast-building 3D carbon nanotube models with defects. J Mol Graph Model 2012;38:389–95.
[35] Cornell WD, Cieplak P, Bayly CI, Gould IR, Merz KM, Ferguson DM, et al. A second generation force-field for the simulation of proteins, nucleic acids and organic molecules. J Am Chem Soc 1995;117(19):5179–97.
[36] Jorgensen WL, Severance DL. Aromatic aromatic interactions – free energy profiles for the benzene dimer in water chloroform and liquid benzene. J Am Chem Soc 1990;112:4768–74.

4.3. Modelling and mechanical behaviour of SWCNT HJs

This subchapter consists of two complementary papers by Sakharova *et al*. (2016b, 2017b). The first paper, by Sakharova *et al*. (2016b), is focused on the analysis of the geometry of the connection region of armchair – armchair and zigzag – zigzag heterojunctions (HJs between nanotubes with different radii), and on the study of their tensile, bending and torsional rigidities. In the second paper, by Sakharova *et al*. (2017b), the study of the mechanical response of armchair – armchair and zigzag – zigzag SWCNT HJs is deepened and outcomes regarding the Young's and shear moduli are analysed.

In summary, this subchapter analyses and discusses results regarding the HJ geometry (diameters ratio and relative lengths of the constituent nanotubes) and the loading conditions on their tensile, bending and torsional rigidities, and Young's and shear moduli.

(Page intentionally left blank)

Journal of Nano Research *Online: 2016-01-06*
ISSN: 1661-9897, Vol. 38, pp 73-87
doi:10.4028/www.scientific.net/JNanoR.38.73

Numerical Simulation of the Mechanical Behaviour of Single-walled Carbon Nanotube Heterojunctions

Nataliya A. Sakharova[1,a *], André F.G. Pereira [1,b], Jorge M. Antunes[2,c] and José V. Fernandes [1,d]

[1]CEMUC – Department of Mechanical Engineering, University of Coimbra, Rua Luís Reis Santos, Pinhal de Marrocos, 3030-788 Coimbra, Portugal

[2]Escola Superior de Tecnologia de Abrantes, Instituto Politécnico de Tomar Rua 17 de Agosto de 1808-2200 Abrantes, Portugal

[a]nataliya.sakharova@dem.uc.pt (* Corresponing author), [b]andre.pereira@dem.uc.pt, [c]jorge.antunes@ipt.pt, [d]valdemar.fernandes@dem.uc.pt

Keywords: Carbon nanotubes heterojunctions, numerical simulation, elastic behaviour, rigidity

Abstract. The study of the mechanical behaviour of single-walled carbon nanotube heterojunctions has been carried out, implementing nanoscale continuum approach. A three-dimensional finite element model is used in order to evaluate the elastic behaviour of cone heterojunctions. It is shown that the bending rigidity of heterojunctions is sensitive to bending conditions. The torsional rigidity does not depend on torsion conditions. Both rigidities of the heterojunction are compared with those of the thinner and thicker constituent nanotubes.

Introduction

In recent years, the research interest focused on carbon nanotube junctions has increased significantly, because of their singular properties and numerous potential applications in nanodevices for health, electronics and biotechnology needs. From the point of view of the construction of nanodevices, the carbon nanotube (CNT) junctions are necessary constituents for circuits, amplifiers, switches, rectifiers, molecular storages, field-effect transistors and nanodiodes. The current state of research regarding the synthesis, properties and realistic application of CNT junctions is included in the comprehensive review of Wei and Liu [1]. CNT heterojunctions (CNT HJs), i.e. structures composed by two interconnecting carbon nanotubes, have attracted special research interest because of their singular electrical and optical properties, and attractive potential application as nanodiodes and filters [2, 3].

In spite of developments achieved in recent years in this research field, many challenges still remain. One of them is to understand the deformation behaviour of CNT heterojunctions, since the stability and efficiency of nanodevices is highly dependent on the mechanical properties of their components. Because of the challenge of measuring the mechanical properties of nano-dimensional objects, the studies aimed at describing the mechanical properties of CNT heterojunctions have been carried out mainly by mechanical modelling and numerical simulation (see for example [3, 5-7]), similarly to the case of isolated single-walled (SWCNT) and multi-walled (MWCNT) carbon nanotubes. There are three groups of modelling approaches for the simulation of the mechanical behaviour of isolated SWCNT and MWCNT: the atomistic approach (ab initio, molecular dynamics (MD)) [8], the continuum modelling (CM) approach [9] and the nanoscale continuum modelling approach (NCM) [10, 11]. Molecular dynamics and nanoscale continuum approaches combined with finite element modelling (FEM) have become the most prevalent methods to simulate the mechanical behaviour of CNT heterojunctions. A few studies to assess the mechanical properties of CNT HJs were also performed recurring to MD approach [6, 12, 13]. Lee et al. [6] investigated the temperature effect on the mechanical properties, yield stress and Young's modulus, of (6, 0)-(8, 0) SWCNT HJs under tension and compression, by using MD simulation approach, employing reactive empirical bond order (REBO) potential to describe the carbon-carbon (C-C) interaction. Also employing REBO potential, Li et al. [12] investigated the tensile strength and failure modes of

single-walled and double-walled CNT HJs at different temperatures and strain rates. Qin et al. [13] performed MD simulation study, using second-generation Tersoff–Brenner potential, in order to evaluate Young's modulus and failure stress of single-walled and double-walled CNT HJs. The studies using the NCM approach were mainly devoted to the characterization of the buckling [4], shear [7, 14] and tensile [14, 15] behaviours of HJs, and the evaluation of their Poisson ratio [3]. The aforementioned investigations must be understood as the beginning of broader necessary studies on the mechanical properties of the CNT HJs.

The present study aims to contribute towards the characterisation of the mechanical behaviour of armchair – armchair and zigzag – zigzag SWCNT heterojunctions, using the NCM approach. The three dimensional (3D) finite element (FE) method was used in order to evaluate the bending and torsional rigidities of SWCNT HJs.

Geometric definition of SWCNT HJs

As is well-known, the fundamental configurations of CNTs can be defined by the chiral vector, $\mathbf{C_h}$, or the chiral angle, θ, between the chiral vector $\mathbf{C_h}$ and the direction (n, 0) [16]:

$$\mathbf{C_h} = n\mathbf{a_1} + m\mathbf{a_2}, \tag{1}$$

$$\theta = \sin^{-1}\frac{\sqrt{3}m}{2\sqrt{n^2+nm+m^2}}, \tag{2}$$

where (n,m) is a pair of the lattice translation indices $\mathbf{a_1}$ and $\mathbf{a_2}$, the unit vectors of the graphene hexagonal lattice; n and m are integers. The length of the unit vector $\mathbf{a}$ is defined as $a = \sqrt{3}a_{C-C}$ with the equilibrium carbon-carbon (C-C) covalent bond length $a_{C\text{-}C} = 0.1421$ nm.

These fundamental configurations of CNTs are: zigzag (m = 0, θ = 0°), armchair (n = m, θ = 30°), and chiral (n≠m, 0° <θ < 30°) nanotubes.
The SWCNT diameter can be calculated as follows:

$$D_n = \frac{a\sqrt{n^2+nm+m^2}}{\pi}. \tag{3}$$

While the isolated SWCNTs can be viewed as a rolled graphene sheet with specified width $L_{gr} = \pi D_n$, the heterojunction of two SWCNTs can be represented as a rolled graphene sheet with specific geometry, where two CNTs are connected by the introducing of a Stone–Wales defect (pentagon and heptagon defect) as illustrated in Fig. 1 [17] Similarly to SWCNT structures, the geometrical parameters of HJs are the chirality length and diameter. There are two main heterojunction configurations: (i) cone-heterojunctions (HJs of nanotubes with a given chiral angle but different radii) and (ii) radius-preserving heterojunctions (HJs preserving the radii, but with different chiral angles of the constituent nanotubes) [17]. According to the study of Yao et al. [18], most HJs (<95%) are cone-heterojunctions type.

The geometry of armchair – armchair cone-heterojunctions is shown in the Fig. 2. The axes of the two constituent nanotubes of the HJ are nearly parallel, and the axis of the thicker SWCNT is defined as the axis of the heterojunction [7, 19]. The overall length of the heterojunction is defined as follows:

$$L_{HJ} = L_1 + L_2 + L_3, \tag{4}$$

where L_1, L_2 and L_3 are the lengths of the thinner and thicker SWCNTs and the junction region, respectively.

As the heterojunction consists of two SWCNTs with different diameters, the diameter of HJ can be characterised by the average of both diameters:

$$\overline{D}_{HJ} = \frac{1}{2}(D_{n1} + D_{n2}). \quad (5)$$

And the aspect ratio of the heterojunction is defined as [12]:

$$\eta = \frac{L_3}{\overline{D}_{HJ}}. \quad (6)$$

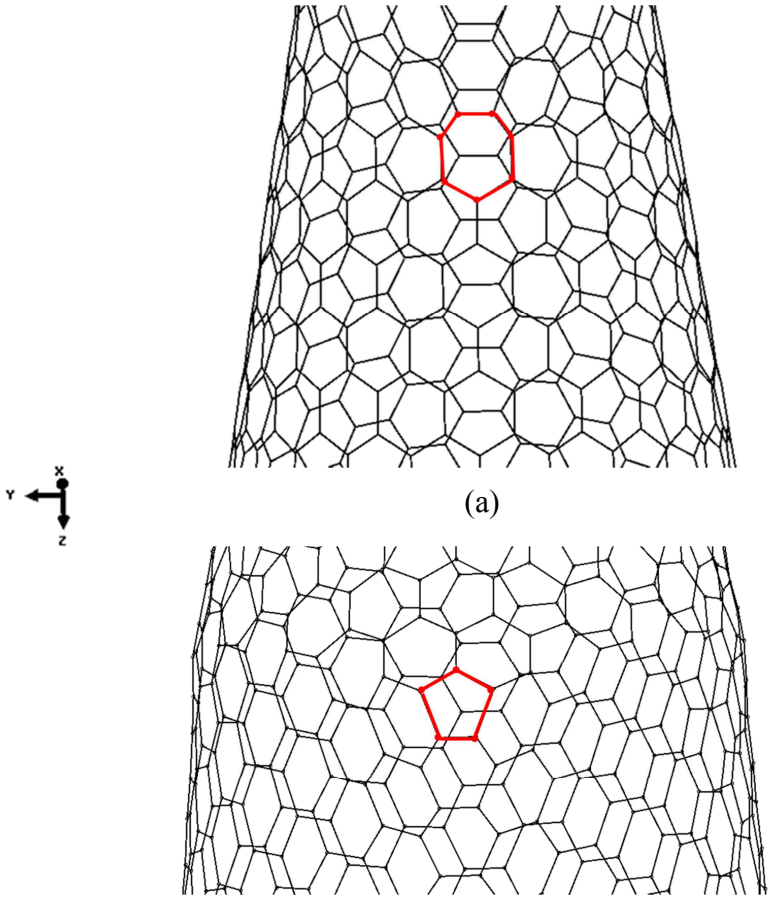

(a)

(b)

Figure 1 (a, b): Defects in the connecting region of armchair – armchair (10, 10) – (15, 15) heterojunction: (a) Heptagon defect; (b) Pentagon defect

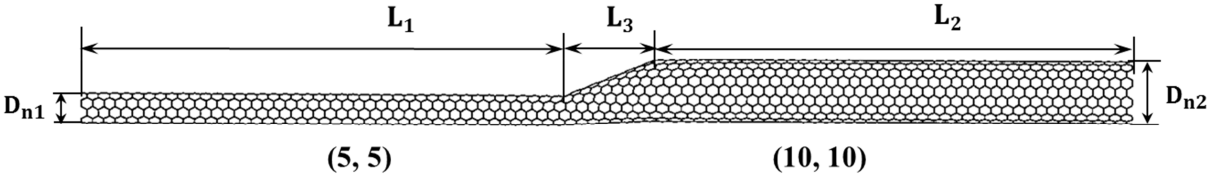

Figure 2: Geometry of armchair – armchair (5, 5) – (10, 10) HJ

Numerical simulation and analysis

Configurations and FE modelling of SWCNT HJs. The NCM approach, where the equivalent beam elements replace the carbon-carbon bonds of CNT, was used for the modelling of SWCNT HJs. The finite element model uses the coordinates of the carbon atoms to generate the nodes and then their suitable connection to create the beam elements. The links established between the inter-atomic potential energies of the molecular structure and strain energies of the equivalent continuum structure, consisting of beams undergoing axial, bending and torsional deformations, are the basis for the application of continuum mechanics to the analysis of the mechanical behaviour of CNT HJs [10]. The FE simulation uses the analogy between the bond length, $a_{C\text{-}C}$, and the element length L and between the nanotube wall thickness and the element thickness (see, Fig. 3). Assuming the beam element has a circular cross-section area, the wall thickness corresponds to the element diameter.

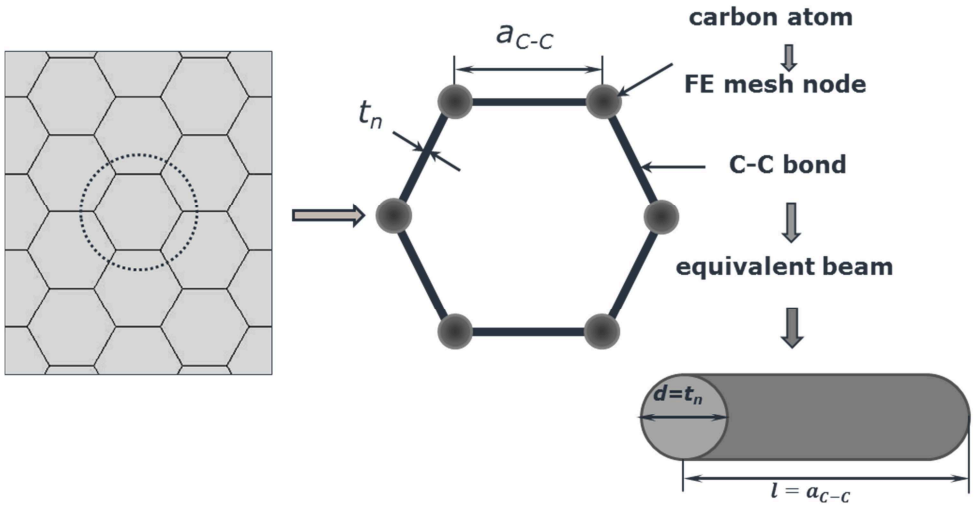

Figure 3: Modelling of HJ, replacing C-C bonds by beam elements

The meshes of the CNT HJs structures, to be used in the FE analyses, were constructed using the CoNTub 1.0 software [17]. This code generates ASCII files, describing atom positions, which can be entered as input in available commercial and in-house FE codes, in order to perform the simulation of mechanical tests. To convert the ASCII files, obtained from the CoNTub 1.0 program, into the format usable by the commercial FEA code ABAQUS®, previously developed in-house application designated *InterfaceNanotubes* [20] was used. Examples of finite element meshes for armchair – armchair and zigzag – zigzag SWCNT HJs are shown in Fig. 4.

The geometrical characteristics of SWCNT HJs used in the present FE analyses are summarized in Table 1. The HJs were constructed such that the length of the constituent nanotubes are equal to each other and their value is about one (case 1), two (case 2) and three (case 3) orders of magnitude of the length of the junction region.

Molecular interactions and equivalent properties of beam elements. According to molecular dynamics, the total inter-atomic potential energy of a molecular system is expressed as the sum of energy terms due to bonded and non-bonded interactions [19]:

$$U_{tot} = \sum U_r + \sum U_\theta + \sum U_\phi + \sum U_\omega + \sum U_{vdw}, \quad (7)$$

where U_r, U_θ, U_ϕ, U_ω are energies associated with bond stretching, bond bending, dihedral angle torsion, out-of plane torsion, respectively, and U_{vdw} is the energy associated with non-bonded van der Waals interactions. In covalent systems such as carbon nanotubes, non-bonded interactions are negligible in comparison with bonded ones [11] and the main contribution to the total potential energy is from the first four terms of Eq. 7 as outlined in Fig. 5.

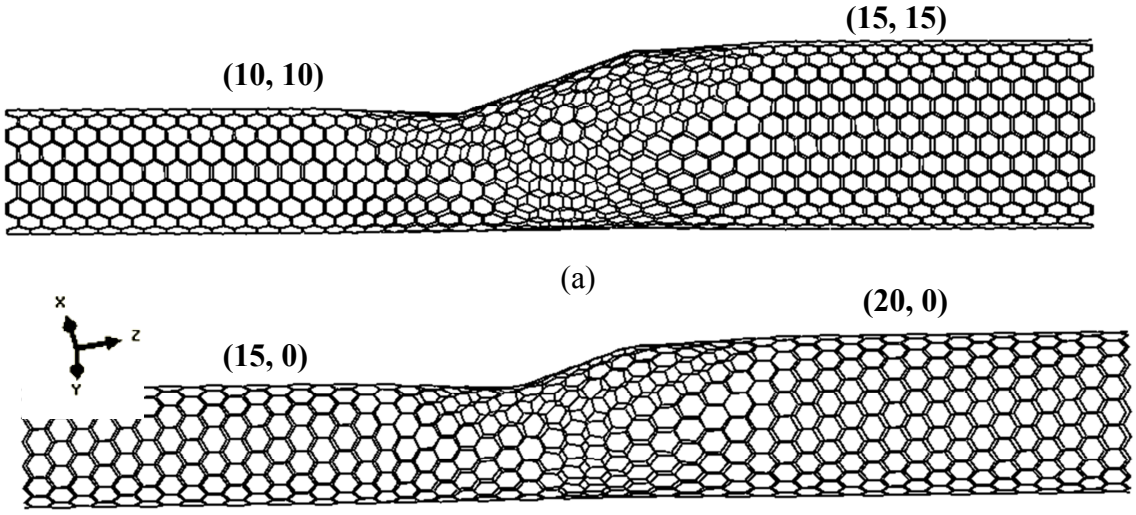

Figure 4: FE meshes HJs: (a) armchair – armchair (10, 10) – (15, 15) HJ; (b) zigzag – zigzag (15, 0) – (20, 0) HJ

Table 1: Geometrical characteristics of HJs under study

HJ	$(n_1, m_1) – (n_2, m_2)$	$\bar{D}_{HJ}$, nm	η	case	L_1, nm	L_2, nm	L_3, nm
armchair	(5, 5) – (10, 10)	1.018	1.940	1	9.97	10.01	1.97
				2	100.01	99.95	1.97
				3	1000.00	999.96	1.97
	(10, 10) – (15, 15)	1.696	1.166	1	10.04	9.94	1.98
				2	100.06	100.00	1.98
				3	1000.00	1000.02	1.98
	(15, 15) – (20, 20)	2.375	0.833	1	9.98	10.00	1.98
				2	100.00	100.01	1.98
				3	1000.06	1000.02	1.98
zigzag	(5, 0) – (10, 0)	0.588	1.950	1	10.00	10.06	1.15
				2	99.92	99.96	1.15
				3	1000.01	1000.06	1.15
	(10, 0) – (15, 0)	0.979	1.177	1	10.03	10.02	1.15
				2	100.14	100.12	1.15
				3	998.73	1000.26	1.15
	(15, 0) – (20, 0)	1.371	0.843	1	9.93	10.11	1.16
				2	100.03	100.00	1.16
				3	999.96	999.92	1.16

Consequently, under the assumption of small deformation, the energies associated with bond stretching, bending and torsion can be approximated by the functions [22]:

$$U_r = \frac{1}{2}k_r(\Delta r)^2,$$
$$U_\theta = \frac{1}{2}k_\theta(\Delta\theta)^2, \quad (8)$$
$$U_\tau = U_\phi + U_\omega = \frac{1}{2}k_\tau(\Delta\phi)^2,$$

where k_r, k_θ and k_τ are the bond stretching, bond bending and torsional resistance force constants, respectively, and Δr, $\Delta\theta$ and $\Delta\phi$ are the bond stretching increment, bond angle bending variation and angle variation of twist bond, respectively.

The elastic properties of the beam elements can be determined.by establishing the equivalence of the energies associated with the bond interactions, through Eq. 8, and the energies associated with elastic deformation of the beams.

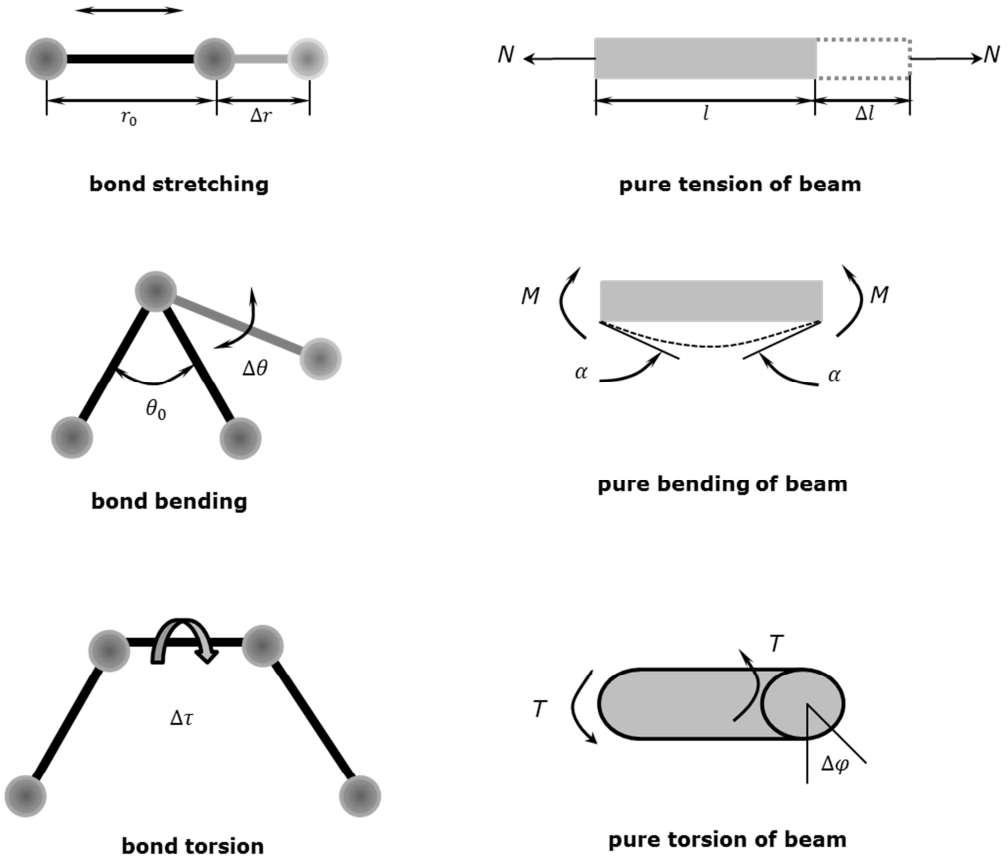

Figure 5: Equivalence between bond interactions in carbon nanotube and beam elements

Classical mechanics gives the following expression for the strain energy, U_A, of a beam with length, l, and cross-section area, A, under a pure axial force, N:

$$U_A = \frac{1}{2}\int_0^L \frac{N^2}{E_b A_b}\,dl = \frac{1}{2}\frac{N^2 l}{E_b A_b} = \frac{1}{2}\frac{E_b A_b}{l}(\Delta l)^2, \tag{9}$$

where Δl is the axial stretching displacement and E_b is the Young's modulus of the beam.

The strain energy, U_M, of a beam under a pure bending moment, M, according to classical mechanics, is expressed as:

$$U_M = \frac{1}{2}\int_0^L \frac{M^2}{E_b I_b}\,dl = \frac{1}{2}\frac{E_b I_b}{l}(2\alpha)^2, \tag{10}$$

where α is the rotational angle at the ends of the beam and I_b is the moment of inertia of the beam.

The strain energy, U_T, of a beam under a pure torsion moment, T, is expressed:

$$U_T = \frac{1}{2}\int_0^L \frac{T^2}{G_b J_b}\,dl = \frac{1}{2}\frac{G_b J_b}{l}(\Delta\beta)^2, \tag{11}$$

where $\Delta\beta$ is the relative rotation between the ends of the beam and J the polar moment of inertia.

The parameters U_r and U_A are stretching energies in molecular and structural systems, respectively, U_θ and U_M represent the bending energies, while U_τ and U_T are the torsional energies. Comparing Eqs. 8 with Eqs. 9-11, and assuming the equivalence of Δl to Δr, as well the equivalence of the rotational angle, 2α, to the total variation of the bond angle, $\Delta\theta$, and $\Delta\beta$ to $\Delta\phi$, direct

relationships can be established between the structural mechanics parameters, E_bA_b, E_bI_b, G_bJ_b and the force field constants, k_r, k_θ, k_τ [10]:

$$\frac{E_bA_b}{l} = k_r$$

$$\frac{E_bI_b}{l} = k_\theta \quad (12)$$

$$\frac{G_bJ_b}{l} = k_\tau.$$

Eqs. 12 are the basis for the application of continuum mechanics to the analysis of the mechanical behaviour of CNT HJs, and provide the input for simulation. The values of force constants [23, 24] and input data for the FE model are given in Table 2.

Table 2: Input parameters for FE simulations of SWCNT HJs: mechanical and geometric properties of beam element

Parameter	Value	Formulation
Force constant, k_r [23]	6.52×10^{-7} N nm^{-1}	–
Force constant, k_θ [23]	8.76×10^{-10} N·nm·rad^{-2}	–
Force constant, k_τ [23, 24]	2.78×10^{-10} N·nm·rad^{-2}	–
Beam length ($l = a_{C\text{-}C}$)	0.1421 nm	–
Diameter (d)	0.147 nm	$d = 4\sqrt{k_\theta/k_r}$
Cross section area, A_b	0.01688 nm^2	$A_b = \pi d^2/4$
Moment of inertia, I_b	2.269×10^{-5} nm^4	$I_b = \pi d^4/64$
Polar moment of inertia, J_b	4.537×10^{-5}·nm^4	$J_b = \pi d^4/32$
Young's modulus, E_b	5488 GPa	$E_b = k_r^2 l/4\pi k_\theta$
Shear modulus, G_b	870.7 GPa	$G_b = k_r^2 k_\tau l/8\pi k_\theta^2$
Tensile rigidity, E_bA_b	92.65 nN	$E_bA_b = k_r l$
Bending rigidity, E_bI_b	0.1245 nN·nm^2	$E_bI_b = k_\theta l$
Torsional rigidity, G_bJ_b	0.0395 nN·nm^2	$G_bJ_b = k_\tau l$

Loading conditions. Numerical simulations of conventional tensile, bending and torsion tests were carried out in order to study the effect of the average HJ diameter and the chirality of the constituent nanotubes on the heterojunction mechanical properties. The boundary and loading conditions are shown in Fig. 6.

In tension, the axial displacement is determined as:

$$u_z = \frac{F_z L_{HJ}}{EA}, \quad (13)$$

where F_z is an axial force applied at one nanotube's end, leaving the other end fixed, EA is the tensile rigidity of HJ and L_{HJ} is the heterojunction length.

Similarly, in bending, the transverse displacement is determined as:

$$u_y = \frac{F_y L_{HJ}^3}{3EI}, \tag{14}$$

where F_y is the transverse force applied at one end of the nanotube, leaving the other fixed, EI is the bending rigidity of the HJ.

Finally, the twist angle of the loaded end in torsion is determined as:

$$\varphi = \frac{TL_{HJ}}{GJ}, \tag{15}$$

where T is torsional moment applied at one end of the nanotube, leaving the other fixed, GJ is the torsional rigidity. The nodes under loading, at the end of the nanotube, are prevented from moving in the radial direction.

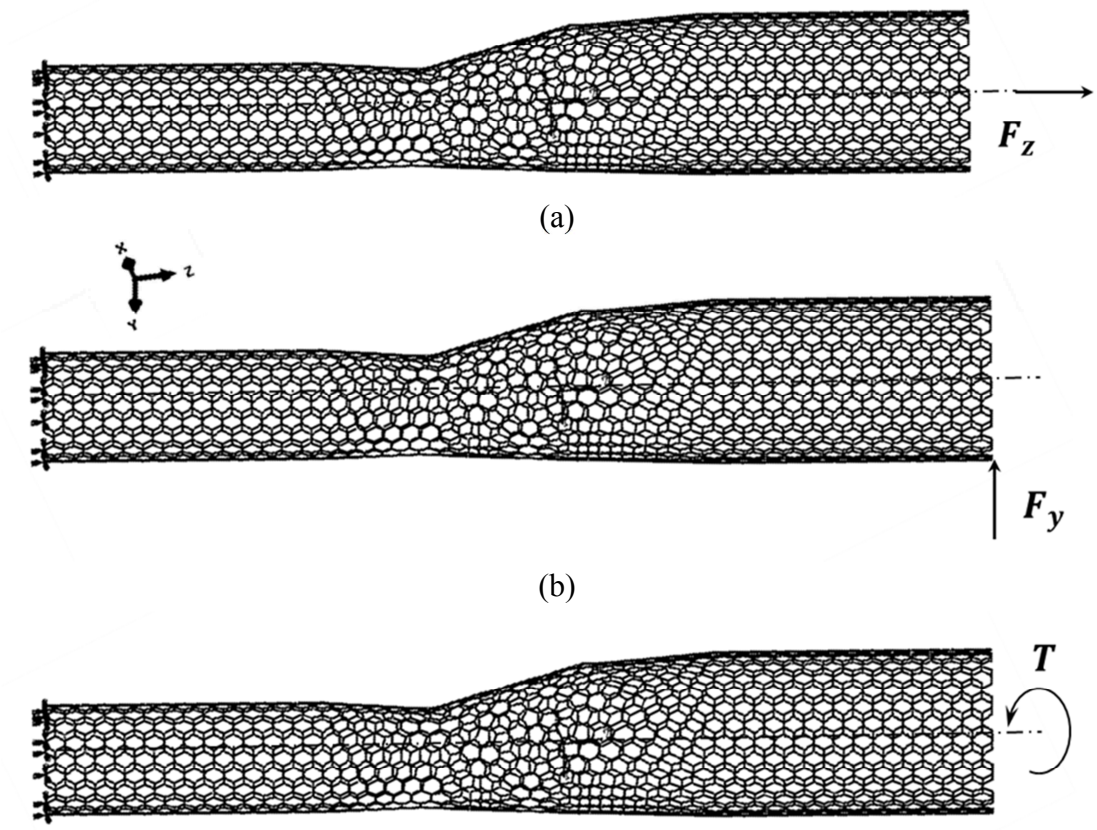

Figure 6 (a, b, c): Loading and boundary conditions for armchair – armchair (10, 10) – (15, 15) HJ: (a) tension; (b) bending; (c) torsion

Two loading conditions were considered in tension, bending and torsion, which consist of fixing the thinner and the thicker side of the nanotube of HJ structure.

Results and discussion

Geometry of the connecting region of HJs. Firstly, a study was carried out in order to describe the geometry of the connecting region of heterojunctions. The geometrical analysis showed that the angle α, between the axis of the nanotubes, which constitute the HJs, and the centre line of the junction as shown in Fig. 7, is equal to 12.7°, whatever the diameters of nanotubes that constitute the armchair-armchair and zigzag-zigzag cone heterojunctions.

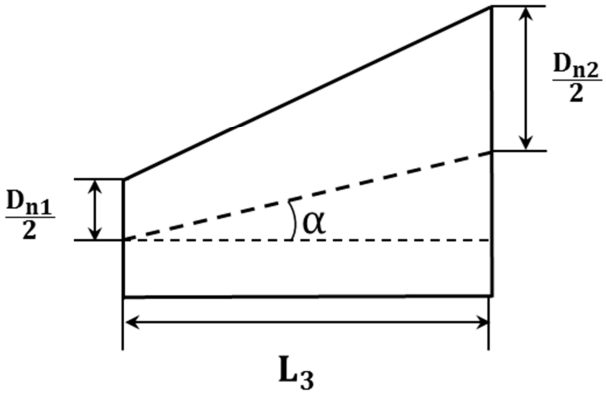

Figure 7: Geometry of the connecting region of SWCNT HJ

The length of the connecting region, L_3, can be represented by a linear function of $(D_{n2} - D_{n1})$ for armchair – armchair and zigzag – zigzag SWCNT HJs in the range of the HJ average diameters studied, as it is shown in Fig. 8. The fitted straight line equation allows determining L_3 as follows:

$$L_3 = 2.9157(D_{n2} - D_{n1}), \tag{16}$$

where D_{n1} and D_{n2} are diameters of the thinner and thicker nanotube, respectively. In the literature, a similar relationship for the connecting HJ region was proposed, basing on the geometrical analysis [13]:

$$L_3 = \frac{\sqrt{3}}{2}\pi(D_{n2} - D_{n1}) = 2.7207(D_{n2} - D_{n1}). \tag{17}$$

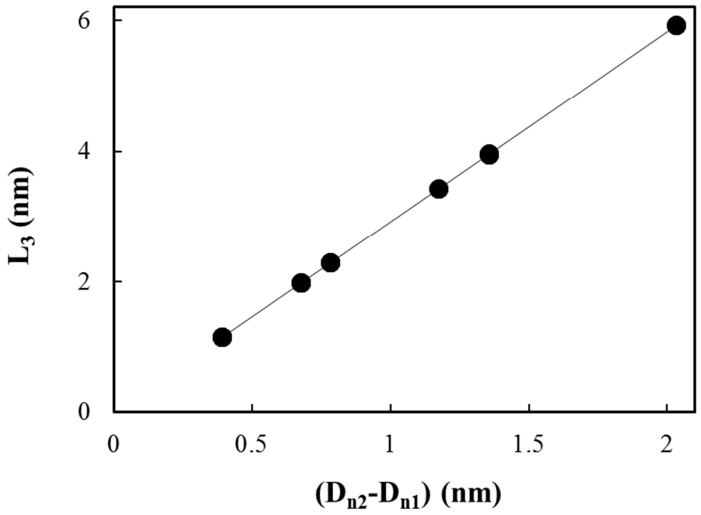

Figure 8: Length of the HJ connecting region, L_3, as a function of $(D_{n2} - D_{n1})$

Rigidities of SWCNT HJs. The heterojunction rigidities were assessed through numerical tests of tension, bending and torsion. The analysis of the mechanical behaviour of the HJs in tension showed that significant lateral displacements occur, introducing bending in HJs, as shown in the example of Fig. 9.Therefore, this test condition deviates from the pure tension and is not suitable for determining the rigidity of the heterojunction in tension.

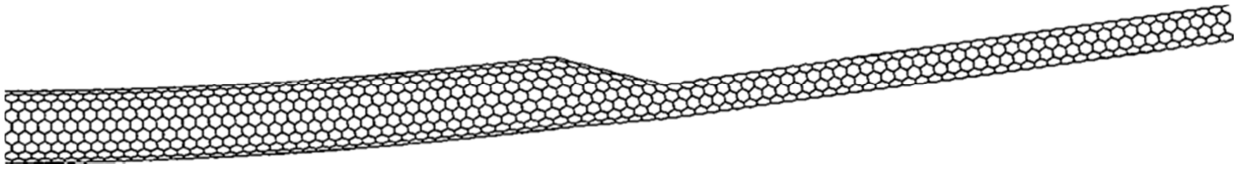

Figure 9: SWCNT HJ under tensile loading

Bending, EI, and torsional, GJ, rigidities of the SWCNT HJs can be obtained from Eqs. 14 and 15, respectively, as follows:

$$EI = \frac{F_y {L_{HJ}}^3}{3u_y}, \tag{18}$$

$$GJ = \frac{TL_{HJ}}{\varphi}. \tag{19}$$

As is known from previous studies, the mechanical behaviour of single-walled nanotubes is length-independent for nanotube lengths much smaller than 20 nm, the value used in a previous study [20]. It is now appropriate to investigate the influence of the overall length of heterojunctions on their rigidities. Fig. 10 shows the bending (Fig. 10a) and torsional (Fig. 10b) rigidities as a function of the overall HJ length for armchair – armchair HJs. EI and GJ are nearly insensitive to overall HJ length; just for (15, 15) – (20, 20) HJ the EI value is slightly lower for the length of about 20 nm (case 1) than for lengths of about 200 and 2000 nm (cases 2 and 3). Hereinafter, the results concerning the mechanical behaviour of SWCNT HJs are presented for the length of 200 nm (cases 2 – see Table 1).

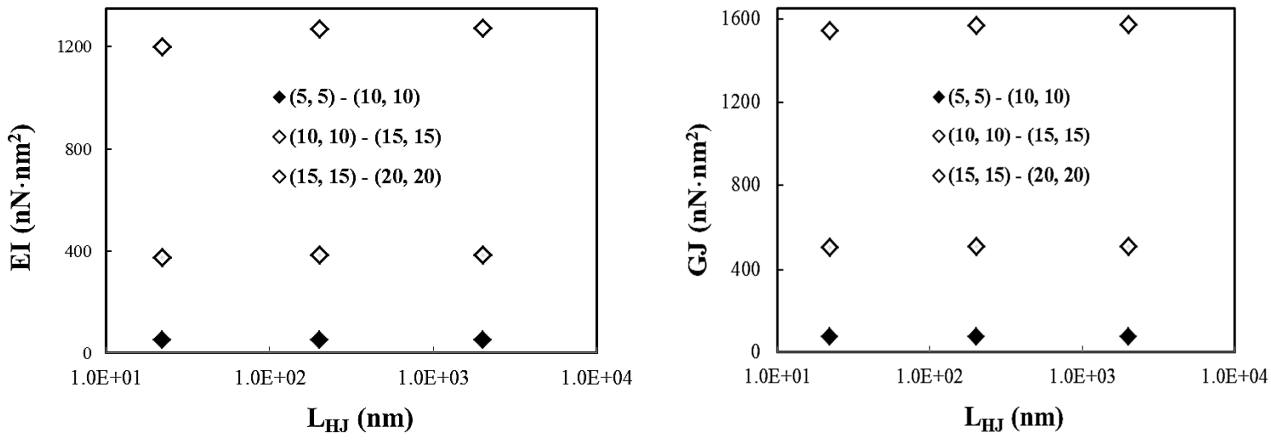

Figure 10 (a, b): Evolution of the rigidities of armchair – armchair SWCNT HJs as a function of the total length of the heterojunction: (a) bending rigidity; (b) torsional rigidity

The influence of the loading conditions on EI and GJ rigidities of HJs was investigated. Fig. 11 shows the bending (Fig. 11a) and torsional (Fig. 11b) rigidities results for armchair – armchair HJs for two loading cases: when the transversal force or torsion moment is applied on the thicker nanotube and the thinner one. EI rigidity is sensitive to the loading condition, i.e. if the transversal force is applied on the thinner or thicker SWCNT. When the force is applied on the thinner nanotube, the EI value is higher, when compared with the case of the application of the force on the thicker nanotube. GJ rigidity does not depend on which thinner or thicker nanotube torsional moment is applied.

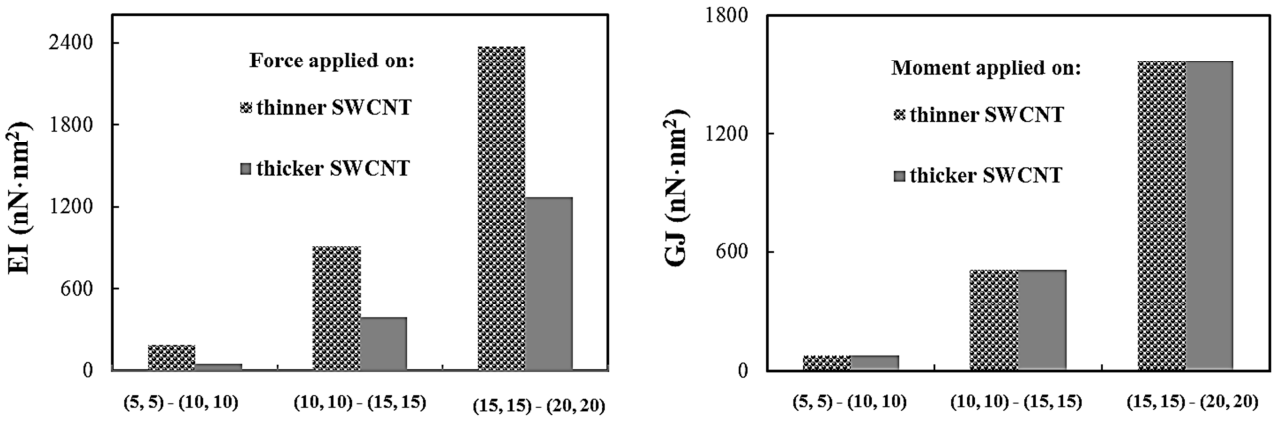

(a) (b)

Figure 11 (a, b): Rigidities of armchair – armchair SWCNT HJs for the two loading conditions: (a) bending rigidity; (b) torsional rigidity

Fig 12 compares the rigidities (EI – Fig. 12a; GJ – Fig. 12b) of the armchair-armchair and zigzag-zigzag SWCNT HJs. The bending and torsional rigidities for armchair-armchair HJs are higher than those for zigzag-zigzag HJs. Both, EI and GJ rigidities increase with increasing the heterojunction diameter. This result is in agreement with those, previously obtained for single-walled nanotubes [20], i.e. EI and GJ rigidities of isolated SWCNTs increase when nanotube diameter increases. In order to clarify the results shown in Fig. 12, the rigidities for armchair-armchair and zigzag-zigzag HJs were plotted in Fig. 13 as a function of the heterojunction aspect ratio, η.

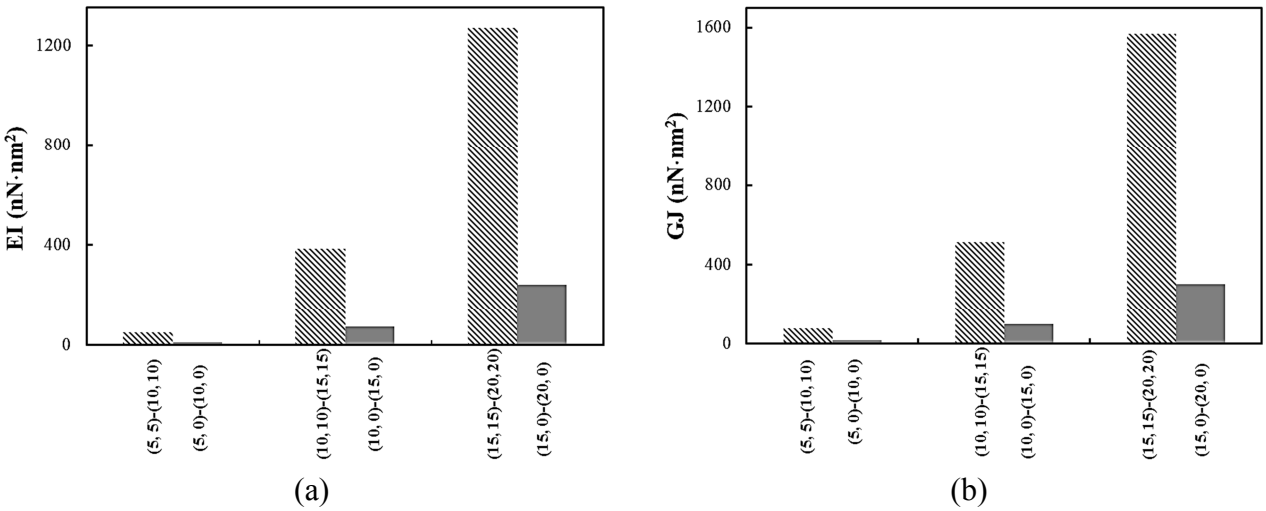

(a) (b)

Figure 12 (a, b): Rigidities of armchair – armchair HJs and zigzag – zigzag HJs: (a) bending rigidity; (b) torsional rigidity

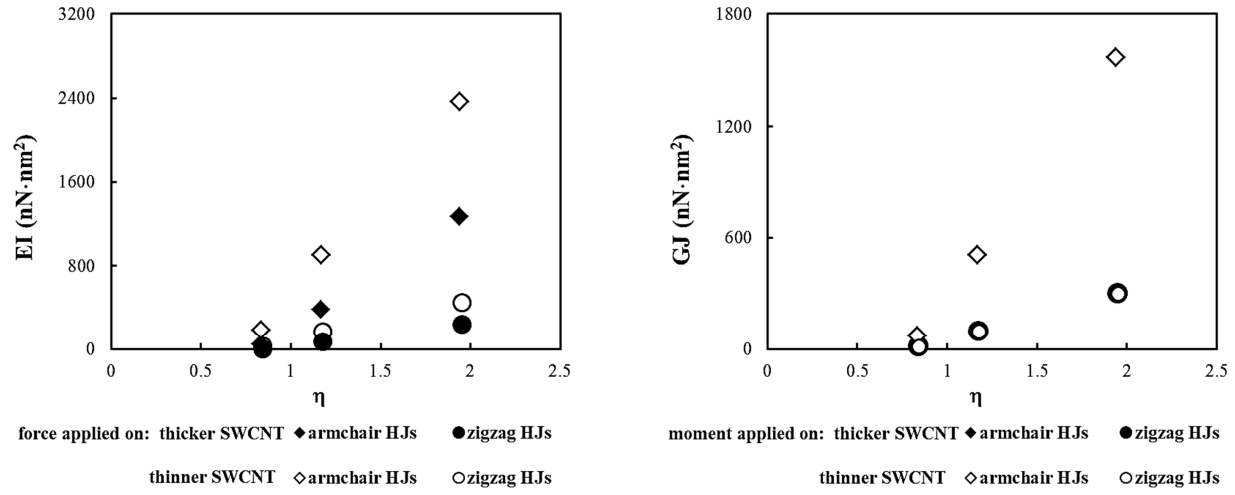

(a) (b)

Figure 13 (a, b): Evolution of the rigidities with the heterojunction aspect ratio for armchair – armchair and zigzag – zigzag HJs: (a) bending rigidity; (b) and torsional rigidity

Both rigidities for armchair-armchair and zigzag-zigzag HJs increase with the increasing of the HJ aspect ratio. The difference between the EI values for armchair – armchair HJs and zigzag – zigzag HJs is more significant when the force is applied on the thinner nanotube. On the contrary, the evolution of the torsional rigidity with the aspect ratio, η is not sensitive to the loading condition: the GJ evolutions do not change when the torsional moment is applied on the thicker or thinner nanotube.

Finally, the comparison of the bending rigidity, EI, and torsional rigidity, GJ, of the SWCNT HJs with those of the constituent nanotubes is shown in Figs. 14 and 15. The rigidity results for SWCNTs, obtained in the previous study [20], were used. The values of EI rigidity, for both cases of armchair – armchair and zigzag – zigzag HJs, are close to those obtained for the thinner constituent nanotubes, and are lower when compared with the rigidity values of the thicker constituent nanotubes. The values of GJ rigidity are higher than those obtained for the thinner constituent nanotubes and lower than for the case of thicker constituent nanotubes.

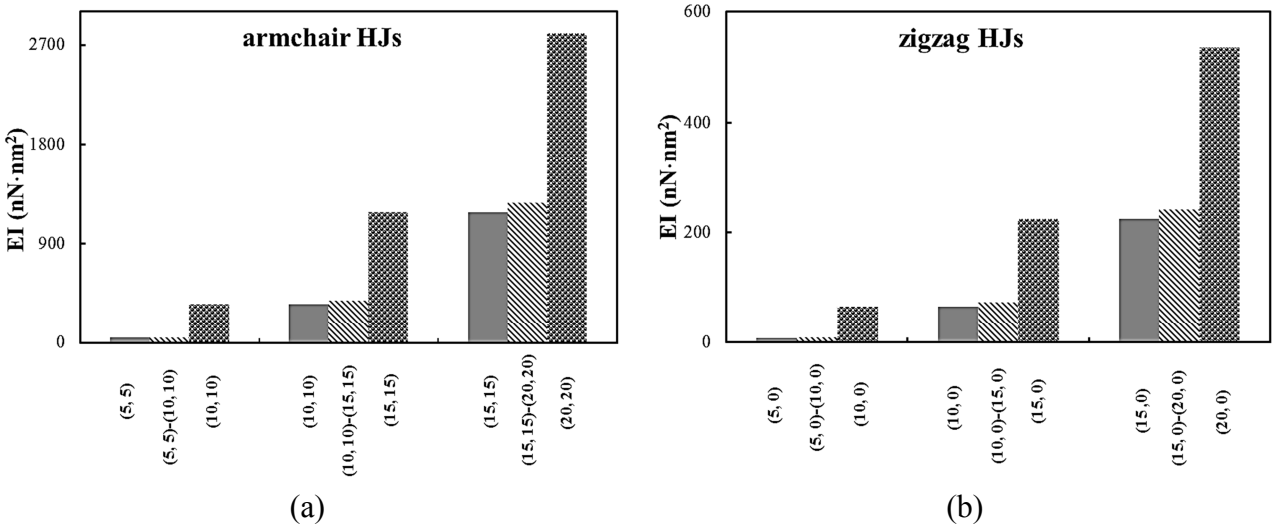

(a) (b)

Figure 14 (a, b): Comparison of the bending rigidity of HJs with those of the constituent nanotubes: (a) armchair – armchair HJs; (b) zigzag – zigzag HJs

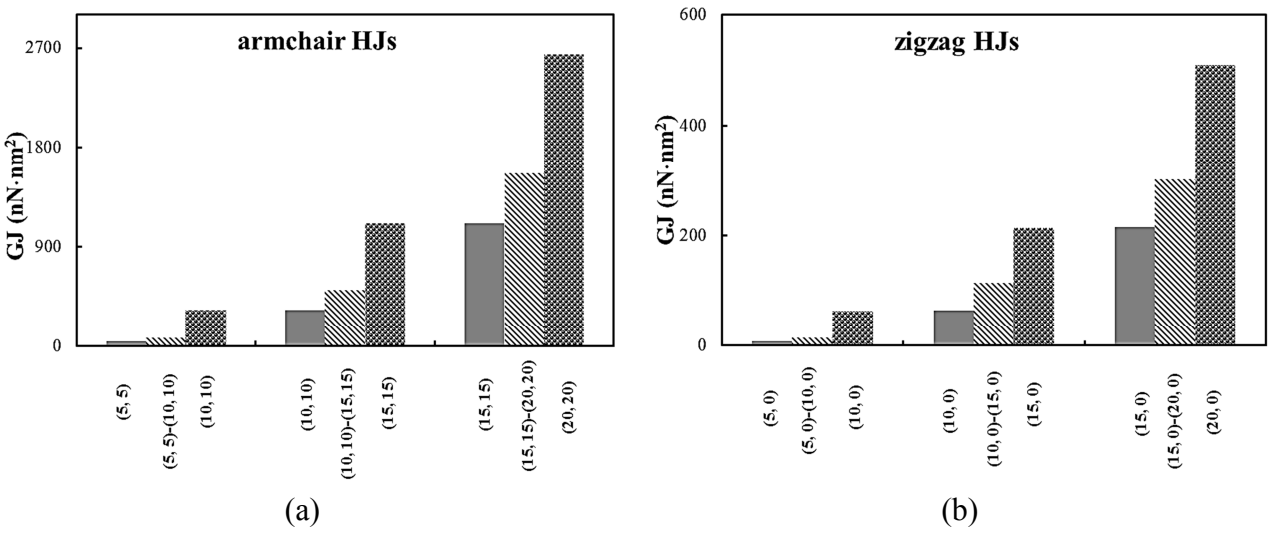

Figure 15 (a, b): Comparison of the torsional rigidity of HJs with those of the constituent nanotubes: (a) armchair – armchair HJs; (b) zigzag – zigzag HJs

Conclusions

The elastic behaviour of cone SWCNT heterojunctions, focusing on their bending and torsional rigidities, was studied using three-dimensional finite element method within the framework of nanoscale continuum modelling. The main conclusions that can be drawn are as follows:

An expression that allows assessing the length of the junction region of HJs as a function of the diameters of the constituent nanotubes was obtained. It was deduced for armchair and zigzag cone HJs in the range of the HJ diameters studied;

For the cases studied, with identical length of the constituent nanotubes, bending, EI, and torsional, GJ, rigidities of HJs are not sensitive to overall HJ length except in the case of HJs with high diameters and length values of about one order of magnitude of the junction region length. EI rigidity depends on the load application condition: on the thicker or thinner end of the nanotube. GJ rigidity does not depend on the torsional moment application condition;

Both bending and torsional rigidities of HJs, increase with increasing heterojunction diameter. EI rigidities of heterojunctions are comparable with those obtained for thinner constituent SWCNTs. GJ rigidities of heterojunctions are higher than those obtained for thinner constituent SWCNTs, and lower than those obtained for thicker constituent SWCNTs.

Acknowledgements

This research work is sponsored by national funds from the Portuguese Foundation for Science and Technology (FCT) and by FEDER funds “Programa Operacional Factores de Competitividade” via the projects PTDC/EME–TME/122472/2010 and PEst-C/EME/UI0285/2013 as well as by FEDER funds “Programa Operacional da Região Centro” via the project CENTRO-07-0224-FEDER-002001 (MT4MOBI). All supports are gratefully acknowledged.

References

[1] D.C. Wei, Y.Q. Liu, The intramolecular junctions of carbon nanotubes, Advanced Mater. 20 (2008) 2815–2841.

[2] Q. Liu, W. Liu, Z.M. Cui, W.G. Song, L.J. Wan, Synthesis and characterization of 3D double branched K junction carbon nanotubes and nanorods. Carbon 45 (2007) 268–273.

[3] F. Scarpa, J.W. Narojczyk, K.W. Wojciechowski, Unusual deformation mechanisms in carbon nanotube heterojunctions (5,5) – (10,10) under tensile loading, Phys. Stat. Solidi B 248 (2011) 82–87.

[4] S.I. Yengejeh, M.A. Zadeh, A. Öchsner, On the buckling behavior of connected carbon nanotubes with parallel longitudinal axes, Appl. Phys. A 115 (2014) 1335–1344.

[5] Z. Kang, M. Li, Q. Tang, Buckling behavior of carbon nanotube-based intramolecular junctions under compression: Molecular dynamics simulation and finite element analysis, Comput. Mater. Sci. 50 (2010) 253–259.

[6] W.-J. Lee, W.-S. Su, Investigation into the mechanical properties of single-walled carbon nanotube heterojunctions, Phys.Chem. Chem. Phys. 15 (2013) 11579–11585.

[7] S.I. Yengejeh, M.A. Zadeh, A. Öchsner, Numerical Charaterization of the shear behavior of hetero-junction carbon nanotubes, J. Nano Res. 26 (2014) 143–151.

[8] Q. Lu, B.Bhattacharya ,The role of atomistic simulations in probing the small scale aspects of fracture - a case study on a single-walled carbon nanotube, Eng. Fracture Mech. 72 (2005) 2037–2071.

[9] A. Pantano, D.M. Parks, M.C. Boyce, Mechanics of deformation of single-and multi-wall carbon nanotubes, J. Mech. Phys. Solids 52 (2004) 789– 821.

[10] C. Li, T.W. Chou, A structural mechanics approach for the analysis of carbon nanotubes, Int. J. Solids Struct. 40 (2003) 2487–2499.

[11] K.I. Tserpes, P. Papanikos, Finite Element modeling of single-walled carbon nanotubes, Compos. Part B–Eng. 36 (2005) 468–477.

[12] M. Li, Z. Kang, R. Li, X. Meng, Y. Lu, A molecular dynamics study on tensile strength and failure modes of carbon nanotube junctions, J. Phys. D: Appl. Phys. 46 (2013) 495301.

[13] Z. Qin, Q.-H. Qin, X.-Q. Feng, Mechanical property of carbon nanotubes with intramolecular junctions: Molecular dynamics simulations, Phys. Lett. A 372 (2008) 6661–6666.

[14] A. Ghavamian, A. Andriyana, A.B. Chin, A. Öchsner, Numerical investigation on the influence of atomic defects on the tensile and torsional behavior of hetero-junction carbon nanotubes, Mater. Chem. Phys. 164 (2015) 122–137.

[15] S.I. Yengejeh, M.A.Zadeh, A. Öchsner, On the tensile behavior of hetero-junction carbon nanotubes, Compos. Part B–Eng. 75 (2015) 274–280.

[16] M.S. Dresselhaus, G. Dresselhaus, R. Saito, Physics of carbon nanotubes, Carbon 33 (1995) 883–891.

[17] S. Melchor, J.A. Dobado, CoNTub: an algorithm for connecting two arbitrary carbon nanotubes, J. Chem. Inf. Comp. Sci. 44 (2004) 1639–1646.

[18] Y.G. Yao, Q.W. Li, J. Zhang, R. Liu, L.Y. Jiao, Y.T. Zhu, Z.F. Liu, Temperature-mediated growth of single-walled carbon-nanotube intramolecular junctions, Nat. Mater. 6 (2007) 283–286.

[19] Z. Kang, M. Li, Q. Tang, Buckling behavior of carbon nanotube-based intramolecular junctions under compression: Molecular dynamics simulation and finite element analysis, Comput. Mater. Sci. 50 (2010) 253–259.

[20] N.A. Sakharova, A.F.G. Pereira, J.M. Antunes, C.M.A. Brett, J.V. Fernandes, Mechanical characterization of single-walled carbon nanotubes: Numerical simulation study, Compos. Part B–Eng. 75 (2015) 73–85.

[21] A.K. Rappe, C.J. Casemit, K.S. Colwell, W.A. Goddard, W.M. Skiff, UFF, a full periodic-table force-field for molecular mechanics and molecular dynamics simulations, J. Am. Chem. Soc. 114 (1992) 10024–10035.

[22] B.R. Gelin, Molecular modelling of polymer structures and properties, Hanser/Gardner Publishers, Cincinnati (OH), 1994.

[23] W.D. Cornell, P. Cieplak, C.I. Bayly, I.R. Gould, K.M. Merz, D.M. Ferguson, et al., A second generation force-field for the simulation of proteins, nucleic acids and organic molecules, J. Am. Chem. Soc. 117 (1995) 5179–5197.

[24] W.L. Jorgensen, D.L. Severance, Aromatic aromatic interactions—free energy profiles for the benzene dimer in water chloroform and liquid benzene, J. Am. Chem. Soc. 112 (1990) 4768–4764.

(Page intentionally left blank)

XIV International Conference on Computational Plasticity. Fundamentals and Applications
COMPLAS 2017
E. Oñate, D.R.J. Owen, D. Peric and M. Chiumenti (Eds)

ELASTIC PROPERTIES OF CARBON NANOTUBES AND THEIR HETEROJUNCTIONS

N.A. SAKHAROVA[*], J.M. ANTUNES[*†], A.F.G. PEREIRA[*], B.M. CHAPARRO[†] AND J.V. FERNANDES[*]

[*] CEMMPRE – Department of Mechanical Engineering, University of Coimbra,
Rua Luís Reis Santos, Pinhal de Marrocos
3030-788 Coimbra, Portugal
e-mail: {nataliya.sakharova, andre.pereira, valdemar.fernandes}@dem.uc.pt,
www.uc.pt/en/iii/research_centers/CEMUC

[†] Escola Superior de Tecnologia de Abrantes, Instituto Politécnico de Tomar
Rua 17 de Agosto de 1808-2200 Abrantes, Portugal
email: jorge.antunes@ipt.pt, bruno.chaparro@sapo.pt, http://www.esta.ipt.pt

Key words: Carbon Nanotubes, Carbon Nanotubes Heterojunctions, Elastic Properties, Numerical simulation.

Abstract. Comprehensive studies on the modelling and numerical simulation of the mechanical behaviour under tension, bending and torsion of single-walled carbon nanotubes and their heterojunctions are performed. It is proposed to deduce the mechanical properties of the carbon nanotubes heterojunctions from the knowledge of the mechanical properties of the single-walled carbon nanotubes, which are their constituent key units.

1 INTRODUCTION

Systematic research has been conducted for studying nano-materials such as carbon nanotubes (CNTs) that are efficient components for designing new materials with required electronic and mechanical properties [1] and building blocks for optical and electronic nanodevices [2]. The CNT heterojunctions (two connected CNTs) are necessary constituents for such nanodevices as circuits, amplifiers, switches and nanodiodes [3]. The understanding of the CNTs' mechanical properties is indispensable in order to design composites reinforced with CNTs and CNT-based devices, since their stability and efficiency are dependent on the mechanical properties of the constituents, i.e. CNTs and CNT heterojuctions.

The elastic properties of CNTs can be assessed using experimental techniques (atomic force microscopy (AFM) and transmission electron microscopy (TEM) [4]) and computational approach. There are three main groups of methodologies for the modelling of CNTs mechanical behaviour: the atomistic approach, the continuum mechanics approach and the nanoscale continuum mechanics approach. In case of the nanoscale continuum modelling approach (NCM) each carbon-carbon (C-C) bond is replaced by a solid element, e.g. a beam element, whose behaviour is described by elasticity theory (see, [5, 6]).

A considerable part of the theoretical investigations has been devoted to the predicting of

the Young's modulus of single-walled carbon nanotubes (SWCNTs) [5, 6]. Less attention has been paid to understanding the mechanical behaviour of nanotube heterojunctions.

The present work is focused on the characterisation of mechanical properties of SWCNTs in a wide range of chiral indices, diameters as well as SWCNT cone-heterojunctions by modelling their structure and mechanical behaviour, using nanoscale continuum approach [5].

2 ATOMIC STRUCTURE OF CNTS AND THEIR HETEROJUNCTIONS

An ideal single-walled nanotube can be seen as a rolled-up graphene sheet, whose surface is composed by the repeated periodically hexagonal [2]. The symmetry of the atomic structure of a nanotube is characterized by the chirality, which is defined by the chiral vector $\boldsymbol{C_h}$:

$$\boldsymbol{C_h} = n\boldsymbol{a_1} + m\boldsymbol{a_2} \tag{1}$$

where *n* and *m* are integers, and $\boldsymbol{a_1}$ and $\boldsymbol{a_2}$ are the unit vectors of the hexagonal lattice.

The length of the unit vectors is defined as $a = \sqrt{3}a_{C-C}$ with the equilibrium carbon-carbon (C-C) covalent bond length a_{C-C} usually taken to be 0.1421 nm [2]. The nanotube circumference, L_c, and diameter, D_n are:

$$L_c = |\boldsymbol{C_h}| = a\sqrt{n^2 + nm + m^2} \tag{2}$$

$$D_n = \frac{L_c}{\pi} \tag{3}$$

The chiral angle, θ, is defined by the angle between the chiral vector $\boldsymbol{C_h}$ and the direction (*n*, *0*) [2] and it is given by:

$$\theta = \sin^{-1}\frac{\sqrt{3}m}{2\sqrt{n^2 + nm + m^2}} \tag{4}$$

Three major categories of carbon nanotubes can be defined based on the chiral angle θ: zigzag ($\theta = 0°$), armchair ($\theta = 30°$) and chiral ($0° < \theta < 30°$) SWCNTs. Three main symmetry groups can be also defined based on the chiral indices. In this case for armchair structure $n = m$, for zigzag structure $m = 0$, and for chiral structure $n \neq m$.

The CNT heterojunction can be represented as two CNTs that are connected by introducing an intermediate region with Stone–Wales defects [7]. Similarly to SWCNT structures, the geometrical parameters of heterojunctions (HJs) are the chirality, and diameter. There are two main heterojunction configurations [7]: (i) cone-heterojunctions (HJs of nanotubes with a given chiral angle but different radii) as armchair – armchair and zigzag – zigzag HJs, and (ii) radius-preserving heterojunctions (HJs preserving the radii, but with different chiral angles of the constituent nanotubes) as armchair – zigzag or chiral – armchair (or zigzag) HJs. According to the study of Yao *et al.* [8] most HJs (>95%) are cone-heterojunctions type.

The overall length of the heterojunction is defined as follows:

$$L_{HJ} = L_1 + L_2 + L_3 \tag{5}$$

where L_1, L_2 are the lengths of the narrower and wider SWCNTs regions, respectively, and L_3 is the length of the connecting region (see, Fig. 1).

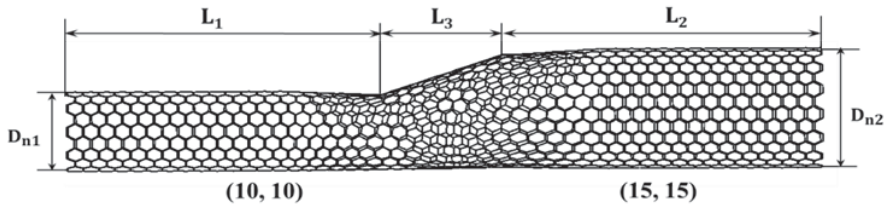

Figure 1: Geometry of cone armchair – armchair (10, 10) – (15, 15) HJ, obtained by using academic software CoNTub 1.0 © [7]

When the heterojunction consists of two SWCNTs with different diameters (i.e. cone-heterojunction), the diameter of HJ can be characterised by the average of the narrower and wider diameters (see for example: [7]):

$$\overline{D}_{HJ} = \frac{1}{2}(D_{n1} + D_{n2}) \tag{6}$$

And the aspect ratio of the cone-heterojunction is defined as [9]:

$$\eta = \frac{L_3}{\overline{D}_{HJ}} \tag{7}$$

The length of the connecting region, L_3, can be deduced basing on geometrical analysis [9]:

$$L_3 = \frac{\sqrt{3}}{2}\pi(D_{n2} - D_{n1}) = 2.7207(D_{n2} - D_{n1}) \tag{8}$$

where D_{n1} and D_{n2} are diameters of the narrow and wider nanotubes, respectively.

Other relationship for the connecting region, which follows a linear function with $(D_{n2} - D_{n1})$, for armchair – armchair and zigzag – zigzag cone-heterojunctions was previously proposed [10]:

$$L_3 = 2.9157(D_{n2} - D_{n1}) \tag{9}$$

3 NUMERICAL SIMULATION AND ANALYSIS

3.1 Finite element modelling of CNTs' structures

The NCM approach that replaces the carbon-carbon bonds of CNT by equivalent beam elements is used for modelling SWCNTs and SWCNT HJs. The finite element (FE) method uses the coordinates of the carbon atoms for generating the nodes and their suitable connection creates the beam elements. The relationships between the inter-atomic potential energies of the molecular CNT structure and strain energies of the equivalent continuum structure, consisting of beam elements undergoing axial, bending and torsional deformations, are the basis for the application of continuum mechanics to the analysis of the mechanical behaviour of SWCNTs and SWCNT HJs [5].

The meshes of the SWCNTs and SWCNT HJs structures to be used in the FE analyses, were built using the CoNTub 1.0 software [7]. This code generates ASCII files, describing atom positions and their connectivity that enter as input data in available commercial and in-

house FE codes. A previously developed in-house application, designated *InterfaceNanotubes* [6], was used to convert the ASCII files, acquired from the CoNTub 1.0 software, into the format compatible with the ABAQUS® commercial FE code. The geometrical characteristics of the SWCNTs used in the current FE analyses are summarized in Table 1. The nanotube length used in the numerical simulations was 30 times bigger than the outer diameter, so that the mechanical behaviour can be independent of the length [11].

Table 1: Geometrical characteristics of SWCNTs under study.

SWCNT type	(n,m)	D_n, nm	$\theta°$	SWCNT type	(n,m)	D_n, nm	$\theta°$
armchair	(5, 5)	0.678	30	zigzag	(14, 0)	1.096	0
	(10, 10)	1.356			(23,0)	1.802	
	(15, 15)	2.034			(32,0)	2.507	
	(20, 20)	2.713			(41,0)	3.212	
	(25, 25)	3.390			(50,0)	3.916	
	(30, 30)	4.068			(59,0)	4.618	
	(35, 35)	4.746			(77,0)	5.323	
	(40, 40)	5.424			(68,0)	6.027	
	(45, 45)	6.101			(86,0)	6.732	
	(50, 50)	6.780			(95,0)	7.436	
	(55, 55)	7.457					

The geometrical characteristics of SWCNT HJs used in the present FE analyses are summarized in Table 2. The HJs were constructed such that the lengths of the constituent nanotubes are almost equal to each other and their value is about two orders of magnitude of the length of the junction region.

Numerical simulations of conventional tensile, bending and torsion tests were carried out in order to study the mechanical properties of the SWCNTs and SWCNT HJ. In the latter case, two loading conditions, which consist of fixing the narrower and the wider side of the HJ structure, were considered.

3.2 Molecular interactions and equivalent properties of beam elements

The NCM approach uses the direct relationships between the structural mechanics parameters, i.e. tensile, E_bA_b, bending, E_bI_b, and G_bJ_b, torsional rigidities, and the bond force field constants, k_r, k_θ, and k_τ as follows [5]:

$$\frac{E_bA_b}{l} = k_r \tag{10}$$

$$\frac{E_bI_b}{l} = k_\theta \tag{11}$$

$$\frac{G_bJ_b}{l} = k_\tau \tag{12}$$

where l is the beam length equal to 0.1421 nm; E_b and G_b are the beam Young's and shear

moduli, respectively; A_b is the beam cross-sectional area; I_b and J_b are the beam moment of inertia and polar moment of inertia, respectively; and k_r, k_θ, and k_τ, are the bond stretching, bond bending and torsional resistance force constants, respectively.

Table 2: Geometrical characteristics of SWCNT HJs under study.

HJ	$(n_1, m_1) – (n_2, m_2)$	$\bar{D}_{HJ}$, nm	η	L_1, nm	L_2, nm	L_3, nm
armchair	(5, 5) – (10, 10)	1.018	1.940	100.01	99.95	1.97
	(10, 10) – (15, 15)	1.696	1.166	100.06	100.00	1.98
	(15, 15) – (20, 20)	2.375	0.833	100.00	100.01	1.98
zigzag	(5, 0) – (10, 0)	0.588	1.950	99.92	99.96	1.15
	(10, 0) – (15, 0)	0.979	1.177	100.14	100.12	1.15
	(15, 0) – (20, 0)	1.371	0.843	100.03	100.00	1.16

Equations 10 – 12 are the base for the application of continuum mechanics to the analysis of the mechanical behaviour of SWCNTs and SWCNT HJs. The input material and geometrical parameters of the beam element (see refs. [36, 37] from [12]) for the numerical simulations was previously summarised by the authors (see, for example [6, 10 – 12]).

4 ELASTIC PROPERTIES OF THE SINGLE-WALLED CARBON NANOTUBES

4.1 Rigidities of SWCNTs

The values of the tensile, EA, bending, EI, and torsional, GJ, rigidities were obtained from the respective numerical simulation tests results as described in the following. The tensile rigidity, EA, of SWCNT is determined as:

$$EA = \frac{F_x L}{u_x} \tag{13}$$

where F_x, is the tensile axial force applied at one nanotube end, leaving the other end fixed, L is the nanotube length and u_x is the axial displacement taken from the FE analysis.

Similarly, the bending rigidity of the nanotube, EI, is represented as:

$$EI = \frac{F_y L^3}{3u_y} \tag{14}$$

where F_y is the transverse force applied at one end of the nanotube, leaving the other fixed, u_y is the transverse displacement, taken from the FE analysis. Finally, the torsional rigidity of the nanotube, GJ, is determined as:

$$GJ = \frac{TL}{\varphi} \tag{15}$$

where T is torsional moment applied at one end of the nanotube, leaving the other fixed and φ is the twist angle, taken from the FE analysis. In case of torsion, the nodes under loading, at the end of the nanotube, are prevented from moving in the radial direction.

The evolutions of the tensile, EA, bending, EI, and torsional, GJ, rigidities with the nanotube diameter, D_n, were studied for the SWCNTs presented in Table 1. These evolutions are shown in Fig. 2. In previous studies [6, 12], the evolutions of the rigidities with nanotube diameter, D_n, were represented by a linear function for the case of the tensile rigidity, EA, and by a cubic power function for the cases of bending, EI, and torsional, GJ, rigidities, for armchair, zigzag and chiral SWCNTs, with diameters up to 2.713 nm. The fitting equations were expressed as follows, regardless of the nanotube chirality:

$$EA = \alpha(D_n - D_0) \tag{16}$$

$$EI = \beta(D_n - D_0)^3 \tag{17}$$

$$GJ = \gamma(D_n - D_0)^3 \tag{18}$$

The values of the fitting parameters [6, 12] were: $\alpha = 1131.66\ nN/nm$, $\beta = 143.48\ nN/nm$, $\gamma = 130.39\ nN/nm$ and $D_0 = 3.5 \cdot 10^{-3}\ nm$.

Figure 3 shows that the current results, up to nanotube diameters equal to 7.457 nm, also follows the trends described by Eqs. 16 – 18. The values of the fitting parameters calculated based on the results of the Fig. 3 are: $\alpha = 1121.20\ nN/nm$, $\beta = 140.25\ nN/nm$ and $\gamma = 130.39\ nN/nm$, which are close to those above mentioned. Given that the value of D_0 is negligible when compared with D_n, it was discarded in the fitting of the equations (i.e. D_0 was considered equal to zero).

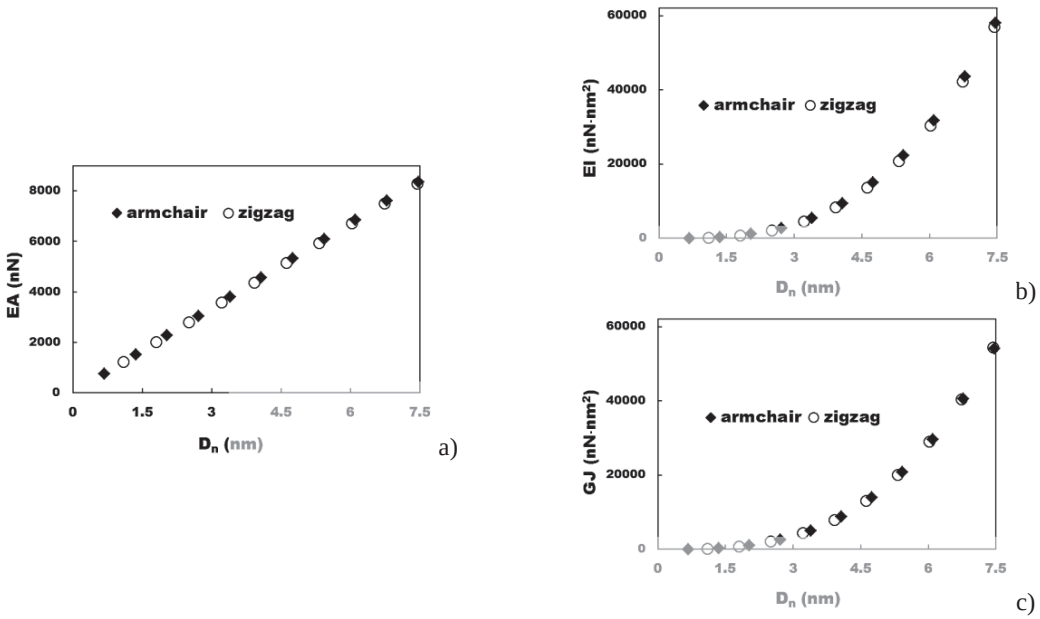

Figure 2: Evolution of: (a) the tensile, EA, (b) bending, EI, and (c) torsional, GJ, rigidities as a function of the nanotube diameter, D_n, for armchair and zigzag SWCNTs.

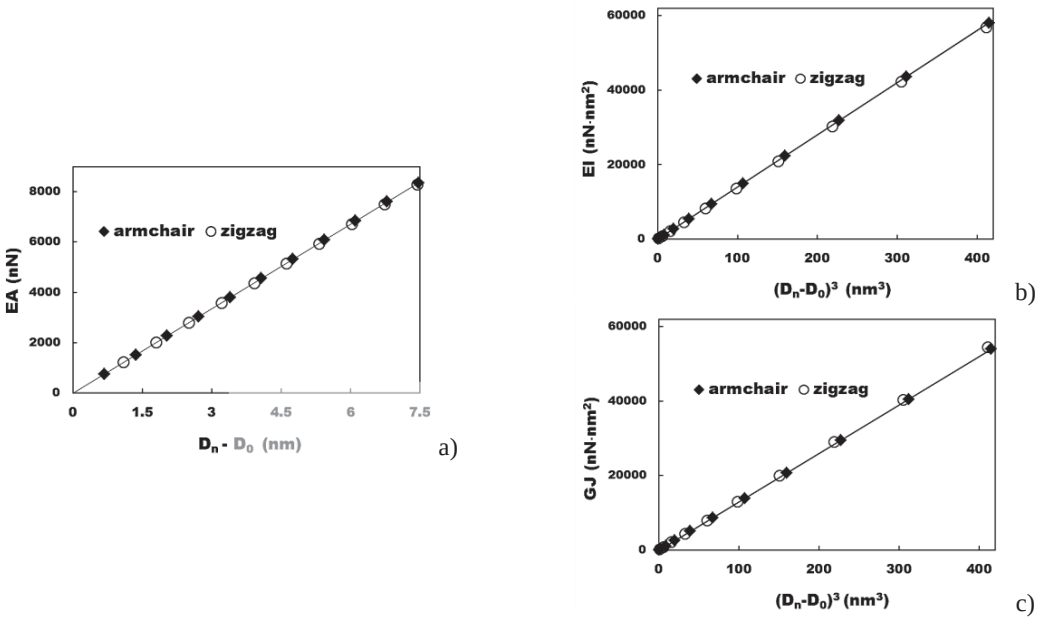

Figure 3: Evolution of: (a) the tensile, EA, rigidity as a function of $D_n - D_0$ and (b) bending, EI, and (c) torsional, GJ, rigidities, as a function of $(D_n - D_0)^3$ for armchair and zigzag SWCNTs.

The linear dependence of Eq. 16 can be understood on the base of the linear relationship between cross-sectional area and the nanotube diameter:

$$A = \frac{\pi}{4}[(D_n + t_n)^2 - (D_n - t_n)^2] = \pi D_n t_n \tag{19}$$

where t_n is the value wall thickness, which in the current study is $0.34\,nm$, equal to the interlayer spacing of graphite. In a similar way, the cubic dependences of Eqs. 17 – 18 can be understood based on the quasi-cubic relationships between the moment of inertia or the polar moment of inertia and the nanotube diameter (neglecting the value of $(t_n/D_n)^2$ in the following equations):

$$I = \frac{\pi}{64}[(D_n + t_n)^4 - (D_n - t_n)^4] = \frac{\pi D_n^3 t_n}{8}\left[1 + \left(\frac{t_n}{D_n}\right)^2\right] \tag{20}$$

$$J = \frac{\pi}{32}[(D_n + t_n)^4 - (D_n - t_n)^4] = \frac{\pi D_n^3 t_n}{4}\left[1 + \left(\frac{t_n}{D_n}\right)^2\right] \tag{21}$$

4.2 Young's and shear moduli of SWCNTs

The Young's modulus of the SWCNT is calculated, taking into account the tensile, EA, and bending, EI, rigidities, using the following expression [6]:

$$E = \frac{EA}{A} = \frac{EA}{\pi t_n \sqrt{8\left(\frac{EI}{EA}\right) - t_n^2}} \tag{22}$$

The shear modulus of the SWCNT is calculated, taking into account the tensile, EA, bending, EI, and torsional, GJ, rigidities by following equation [12]:

$$G = \frac{GJ}{J} = \frac{GJ}{2\pi t_n \left(\frac{EI}{EA}\right)\sqrt{8\left(\frac{EI}{EA}\right) - t_n^2}} \tag{23}$$

The relationships 16 – 18 and the knowledge of the values of the parameters α, β, γ allow the easy evaluation of the Young's and the shear moduli as a function of the nanotube diameter, without resorting to the numerical tests (D_0 was neglected in these equations):

$$E = \frac{\alpha D_n}{\pi t_n \sqrt{8\frac{\beta}{\alpha} D_n^2 - t_n^2}} \tag{24}$$

$$G = \frac{\gamma D_n}{2\pi t_n \left(\frac{\beta}{\alpha}\right)\sqrt{8\frac{\beta}{\alpha} D_n^2 - t_n^2}} \tag{25}$$

In the Fig. 4 (a, b) the values of the Young's modulus and shear modulus calculated by Eqs. 22 and 23, are plotted as a function of the nanotube diameter, D_n. The evolutions of the Young's modulus and shear modulus, obtained by Eqs. 24 and 25, are also shown in Fig. 4. The Young's modulus of SWCNTs decreases with increase of the nanotube diameter, and with further increase of the nanotube diameter, the Young's modulus tends to an approximately constant value as it is shown in the Fig. 4a. The same trend is observed for the evolution of the shear modulus with D_n (see, Fig. 4b). These trends in the evolution of the Young's and shear moduli with nanotube diameter extend up to diameters of about 7.5 nm, the trends already described for SWCNTs with diameters up to about 2.7 nm [6, 12]. Eqs. 24 and 25 allow obtaining acurate evolutions of the Young's and shear moduli, respectively, without resorting to the numerical simulation.

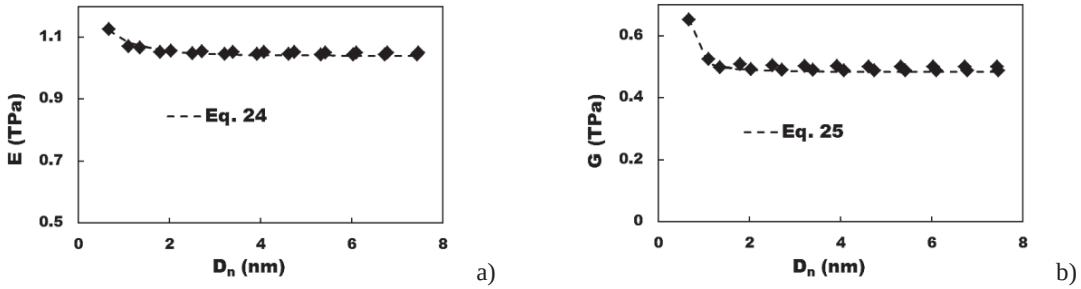

Figure 4: Evolution of: (a) Young's modulus, E, and (b) shear modulus, G, of SWCNTs as a function of the nanotube diameter, D_n.

5 ELASTIC PROPERTIES OF THE SINGLE-WALLED CARBON NANOTUBES HETEROJUNCTIONS

5.1 Rigidities of SWCNT HJs

The analysis of the mechanical behaviour of the armchair – armchair and zigzag – zigzag HJs, pointed out the occurrence of redundant bending deformation during the tensile test, making it difficult to analyse this test [10]. Therefore, we analyse the mechanical behaviour under bending and torsion.

The bending rigidity, $(EI)_{HJ}$, is obtained from the respective numerical simulation tests results as follows:

$$(EI)_{HJ} = \frac{F_y {L_{HJ}}^3}{3u_y} \tag{26}$$

where L_{HJ} is the heterojunction length, F_y is the transverse force applied at one end of the nanotube, leaving the other fixed, u_y is the transverse displacement, taken from the FE analysis. The torsional rigidity, $(GJ)_{HJ}$, is determined by:

$$(GJ)_{HJ} = \frac{TL_{HJ}}{\varphi} \tag{27}$$

where T is torsional moment applied at one end of the nanotube, leaving the other fixed and φ is the twist angle, taken from the FE analysis. The nodes under loading, at the end of the nanotube, are prevented from moving in the radial direction.

The $(EI)_{HJ}$ and $(GJ)_{HJ}$ rigidities for armchair-armchair and zigzag-zigzag HJs were plotted in Fig. 5 as a function of the heterojunction aspect ratio, $\eta = L_3/\bar{D}_{HJ}$ (see Fig. 1). Both rigidities, $(EI)_{HJ}$ and $(GJ)_{HJ}$ for armchair-armchair and zigzag-zigzag HJs increase with the increasing of the η. The bending and torsional rigidities for armchair-armchair HJs are higher than those for zigzag-zigzag HJs. The difference between the $(EI)_{HJ}$ values for armchair – armchair HJs and zigzag – zigzag HJs is more significant when the force is applied to the narrower nanotube. On the contrary, the evolution of the torsional rigidity with the aspect ratio, η is not sensitive to the loading condition: the $(GJ)_{HJ}$ values are at about the same whether the torsional moment is applied to the wider or narrower nanotube.

The bending, $(EI)_{HJ}$, and torsional, $(GJ)_{HJ}$, rigidities of the HJ structures can be calculated knowing the rigidities of the constituent SWCNTs. In fact, using Eq. 26 (or more suitably the equation of beam deflection) and Eq. 27, it is possible to obtain both rigidities for the HJs structures, considering that the respective transverse displacement (bending test) or the twist angle (torsion test) are equal to the sums of the corresponding transverse displacements or twist angles of each SWCNT constituent of the HJs:

$$(EI)_{HJ} = \frac{L_{HJ}^3}{\left(\frac{L_a^3}{(EI)_a} + \frac{3L_a^2 L_f + 3L_a L_f^2 + L_f^3}{(EI)_f}\right)} \tag{28}$$

$$(GJ)_{HJ} = \frac{L_{HJ}}{\left(\frac{L_a}{(GJ)_a} + \frac{L_f}{(GJ)_f}\right)} \tag{29}$$

where L_{HJ} is the overall length of HJ; $(EI)_a$ and $(EI)_f$ are the bending rigidities of the constituent SWCNTs and $(GJ)_a$ and $(GJ)_f$ are their torsional rigidities; L_a and L_f are the lengths of the constituent SWCNTs; the letters a and f refer to the nanotubes to which the force is applied and is fixed, respectively.

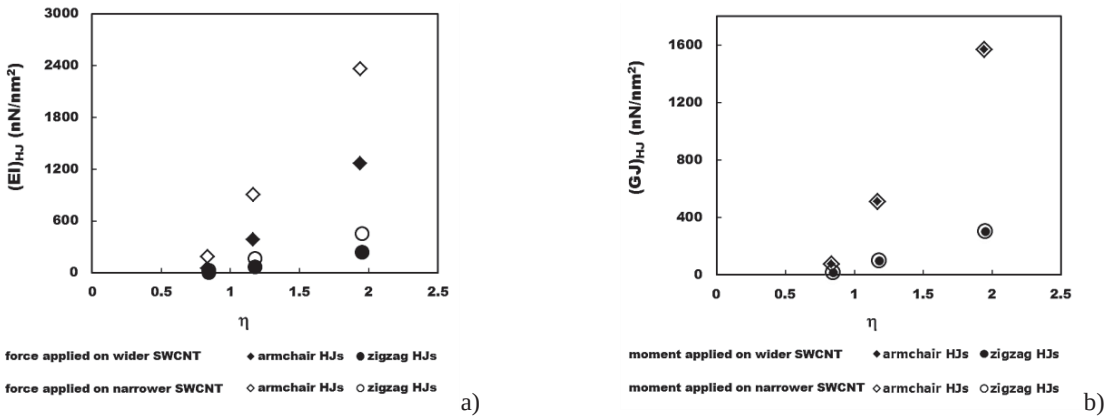

a) b)

Figure 5: Evolution of: (a) $(EI)_{HJ}$ rigidity and (b) $(GJ)_{HJ}$ rigidity with the heterojunction aspect ratio, η, for armchair – armchair and zigzag – zigzag HJs.

Figure 6 compares the values of the rigidities ($(EI)_{HJ}$ – Fig. 6a; $(GJ)_{HJ}$ – Fig. 6b) obtained from FE analysis (Eqs. 26 and 27) and those calculated with help of Eqs. 28 and 29. The results of the Fig. 6 evidence the accuracy of the proposed analytical solutions for evaluation of the bending and torsional rigidities of armchair – armchair and zigzag – zigzag heterojunctions. The mean difference between the values of rigidities, evaluated by Eqs. 28 and 29 and those obtained from FE analysis, is 1.22% for the $(EI)_{HJ}$ rigidity and 1.74% for the $(GJ)_{HJ}$ rigidity.

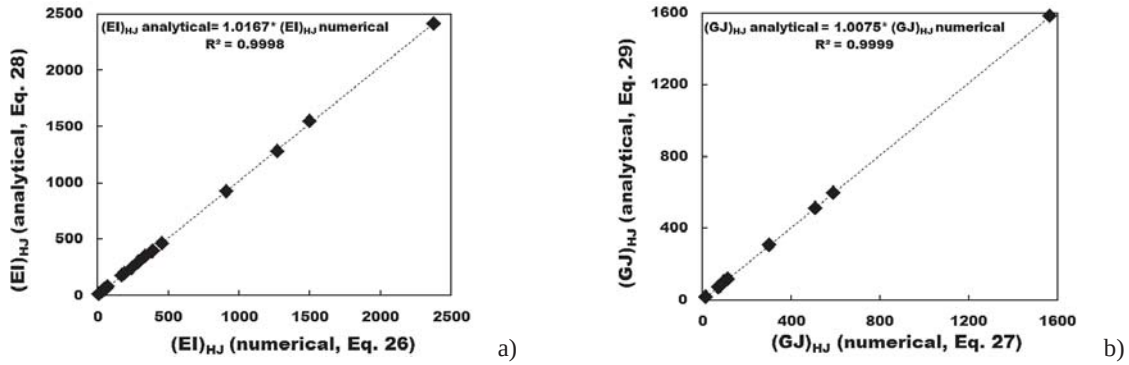

a) b)

Figure 6: Comparison of: (a) bending, $(EI)_{HJ}$ and (b) torsional, $(GJ)_{HJ}$ rigidities obtained from FE analysis and evaluated by Eqs. 28 and 29, for armchair – armchair and zigzag – zigzag HJs.

5.2 Young's and shear moduli of SWCNT HJs

The bending and torsional rigidities obtained from FE analysis were used for the evaluation of the heterojunction Young's, E_{HJ}, and shear, G_{HJ}, moduli equivalent to a SWCNT with diameter given by $\bar{D}_{HJ} = \frac{1}{2}(D_{n1} + D_{n2})$, respectively:

$$E_{HJ} = \frac{(EI)_{HJ}}{I_{HJ}} = \frac{(EI)_{HJ}}{\frac{\pi}{64}\left[\left(\bar{D}_{HJ} + t_n\right)^4 - \left(\bar{D}_{HJ} - t_n\right)^4\right]} \tag{30}$$

$$G_{HJ} = \frac{(GJ)_{HJ}}{J_{HJ}} = \frac{(GJ)_{HJ}}{\frac{\pi}{32}\left[\left(\bar{D}_{HJ} + t_n\right)^4 - \left(\bar{D}_{HJ} - t_n\right)^4\right]} \tag{31}$$

where $t_n = 0.34\ nm$ is the value of the nanotube wall thickness.

The Young's modulus and shear modulus of armchair-armchair and zigzag-zigzag SWCNT HJs were plotted as a function of the heterojunction aspect ratio, η (Fig. 7). Both, Young's modulus and shear modulus decrease with increasing of the HJ aspect ratio. Also, the Young's modulus of HJs is sensitive to the loading condition: the value of E_{HJ} is higher when the force is applied on the narrower nanotube. The difference between the E_{HJ} values of armchair – armchair HJs and zigzag – zigzag HJs is less significant when the force is applied on the narrower nanotube. On the contrary, shear modulus of HJs is insensitive to the loading condition: the value of G_{HJ} does not change when the torsional moment is applied on the wider or narrower nanotube. The difference observed between shear modulus of armchair HJs and zigzag HJ is relatively small.

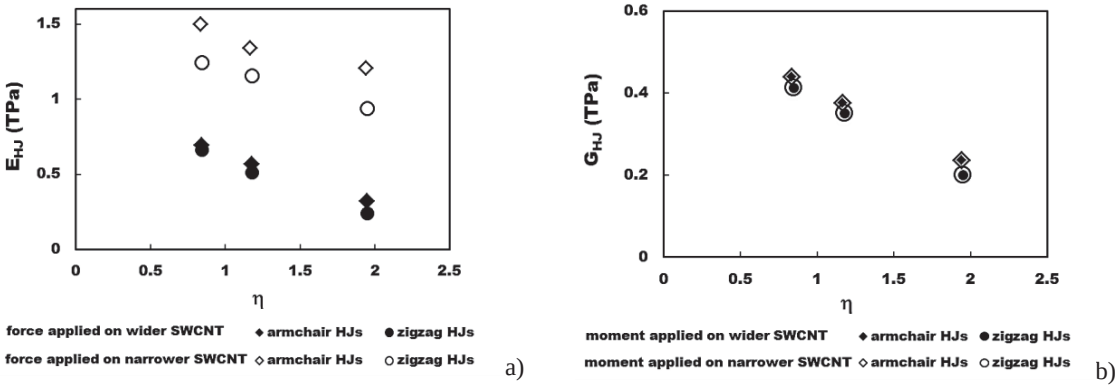

Figure 7: Evolution of the Young's modulus (a) and shear modulus (b) with the heterojunction aspect ratio for armchair – armchair and zigzag – zigzag HJs.

6 CONCLUSIONS

- Equations 16 – 18 establishing relationships between each of three rigidities and the nanotube diameter allowing the easy evaluation of the Young's modulus and shear modulus of SWCNTs by using Equations 24 and 25, without resorting to numerical simulation;
- Equations 28 and 29 allow the easy evaluation of the bending and torsion rigidities of

HJs structures, from the respective rigidities of the constituents SWCNT. These allows the accurate evaluation of the Young's and shear moduli of the SWCNTs, equivalent to the HJs structures.

ACKNOLEDGEMENTS

The authors gratefully acknowledge the financial support of the Portuguese Foundation for Science and Technology (FCT), Portugal, via Projects PTDC/EMS-TEC/0702/2014 (POCI-01-0145-FEDER-016779), PTDC/EMS-TEC/6400/ 2014 (POCI-01-0145-FEDER-016876), and UID/EMS/00285/ 2013, by UE/FEDER through Program COMPETE2020. N. A. Sakharova and A. F. G. Pereira were supported by a grant for scientific research from the Portuguese Foundation for Science and Technology (refs. SFRH/BPD/107888/ 2015, and SFRH/BD/102519/2014, resp.). All supports are gratefully acknowledged.

REFERENCES

[1] Robertson, J. Realistic applications of CNTs. *Mater Today* (2004) **7**: 46-52.

[2] Dresselhaus, M.S., Dresselhaus, G., Avouris, Ph. *Carbon Nanotubes: Synthesis, Structure, Properties, and Applications*, Springer Book Series: Topics in Applied Physics, Springer-Verlag Berlin Heidelberg, Germany, 80, (2001).

[3] Wei, D.C. and Liu, Y.Q. The intramolecular junctions of carbon nanotubes. *Adv Mater* (2008) **20**: 2815-2841.

[4] Wang, L., Zhang, Z., Han, X. In situ experimental mechanics of nanomaterials at the atomic scale. *NPG Asia Mater* (2013) **5**: e40-11.

[5] Li, C. and Chou, T.W. A structural mechanics approach for the analysis of carbon nanotubes. *Int J Solids Struct* (2003) **40**: 2487-2499.

[6] Sakharova, N.A., Pereira, A.F.G., Antunes, J.M., Brett, C.M.A., Fernandes, J.V. Mechanical characterization of single-walled carbon nanotubes: Numerical simulation study. *Compos Part B-Eng*. (2015) **75**: 73-85.

[7] Melchor, S. and Dobado, J.A. CoNTub: An algorithm for connecting two arbitrary carbon nanotubes. *J Chem Inf Comp Sci* (2004) **44**: 1639-1646.

[8] Yao, Y.G., Li, Q.W., Zhang, J., Liu, R., Jiao, L.Y., Zhu, Y.T., Liu, Z.F. Temperature-mediated growth of single-walled carbon-nanotube intramolecular junctions. *Nat Mater* (2007) **6**: 283-286.

[9] Qin, Z., Qin, Q.-H., Feng, X.-Q. Mechanical property of carbon nanotubes with intramolecular junctions: Molecular dynamics simulations. *Phys Lett A* (2008) **372**: 6661-6666.

[10] Sakharova, N.A., Pereira, A.F.G., Antunes, J.M., Fernandes, J.V. Numerical simulation of the mechanical behaviour of single-walled carbon nanotubes heterojunctions. *J Nano Res* (2016) **38**: 73- 87.

[11] Sakharova, N.A., Pereira, A.F.G., Antunes, J.M., Fernandes, J.V. Numerical simulation on the mechanical behaviour of the multi-walled carbon nanotubes. *J Nano Res* (2017) **47**: 106-119.

[12] Pereira, A.F.G., Antunes, J.M., Fernandes, J.V., Sakharova, N.A. Shear modulus and Poisson's ratio of single-walled carbon nanotubes: numerical evaluation. *Phys Status Solidi B* (2016) **253**: 366-376.

Chapter 5

Conclusions and future perspectives

This chapter contains the main conclusions of this thesis and the perspectives concerning further numerical simulation studies on carbon nanotubes as well as non-carbon nanotubes and complex carbon nanotubes structures.

(Page intentionally left blank)

5.1. Introduction

The previous analytical and numerical studies on the evaluation of the mechanical properties of the carbon nanotubes show variability of results due to the different modelling approaches and formulations used. Furthermore, there is a scarcity of parametric studies concerning the effect of the carbon nanotube length, diameter, chirality and wall thickness values on their elastic properties. Systematic studies can be particularly useful to understand and model the mechanical behaviour of the CNT-based complex structures, such as CNTs reinforced materials and CNTs 2D and 3D networks, and to provide a benchmark for ascertaining the mechanical properties of carbon nanotubes. The understanding of the mechanical response of carbon nanotube heterojunctions is also an important issue with respect to their applications, which demands deeper research efforts.

In this context, a nanoscale continuum modelling approach was used to carry out a systematic evaluation of the tensile, bending and torsional rigidities and, subsequently, Young's and shear moduli and Poisson's ratio of various single-walled carbon nanotube structures. Namely, non-chiral and several families of chiral nanotubes were studied, over a wide range of chiral indices, nanotube lengths and diameters. Three-dimensional finite element modelling was used for this purpose. Also, a comprehensive study was conducted on the modelling and numerical simulation of the mechanical behaviour of single-walled carbon nanotube heterojunctions. The conclusions of this thesis are next described.

5.2. Elastic properties of perfect and with defects SWCNTs' structures

The results of the systematic study on the tensile, bending and torsional rigidities of SWCNTs can be summarised as follows.

The tensile, EA, rigidity increases quasi-linearly with the sum of the chiral indices, $(n + m)$, and the bending, EI, and torsional, GJ, rigidities increase with the sum of the chiral indices according to a cubic power expression, which parameters depend on the case. The EA evolutions for armchair, zigzag and chiral SWCNTs are not entirely coincident. The same is true for EI and GJ evolutions.

In order to better clarify these trends, the tensile, EA, bending, EI, and torsional, GJ, rigidities were analysed as a function of nanotube diameter, D_n. The evolutions of the rigidities with nanotube diameter, D_n, can be described by a single linear

function for the case of the tensile rigidity, EA, and by a single cubic power function for the cases of bending, EI, and torsional, GJ, rigidities for all SWCNTs studied, i.e. regardless of the index and the angle of chirality. This allows unifying the evolutions of each of three rigidities with D_n and makes their representation more suitable for further analyses than when rigidities are analysed as a function of $(n + m)$.

The representation of the EA, EI and GJ rigidities as a function of nanotube diameter was used to analyse the mechanical response of the SWCNTs with vacancy defects. As a result, relationships between the elastic rigidities and the diameter are proposed for the perfect SWCNTs and containing vacancy defects, as follows:

$$EA = \alpha^p\left(D_n - D_{0EA}^p\right) \tag{5.1}$$

$$EI = \beta^p\left(D_n - D_{0EI}^p\right)^3 \tag{5.2}$$

$$GJ = \gamma^p\left(D_n - D_{0GJ}^p\right)^3 \tag{5.3}$$

where the fitting parameters α^p and D_{0EA}^p, β^p and D_{0EI}^p, and γ^p and D_{0GJ}^p refer to cases of tensile, bending and torsion rigidities, respectively, for a given percentage, p, of vacancy defects, whatever the chirality of the SWCNTs. The full list of the fitting parameters is given in **Table 5.1**, where D_0^p is an average value of the parameters D_{0EA}^p, D_{0EI}^p, D_{0GJ}^p for three types of the mechanical test at each percentage of defects, p. The value of p equal to zero corresponds to the case of the perfect (without defects) SWCNTs, where $\alpha^p = \alpha$, $\beta^p = \beta$, $\gamma^p = \gamma$ and $D_0^p = D_0$.

Table 5.1. Fitting parameters α^p, β^p, γ^p and D_0^p.

Parameter*	p [% vacancies]						
	0.0	0.1	0.5	1.0	2.0	5.0	10.0
α^p [nN·nm^{-1}]	1131.66	1116.94	1095.39	1051.67	961.12	784.04	522.34
β^p [nN·nm^{-1}]	143.48	141.01	139.75	137.32	126.02	105.11	71.36
γ^p [nN·nm^{-1}]	130.39	127.97	126.83	123.69	111.00	86.00	49.70
D_0^p**[nm]	$3.5\cdot10^{-3}$	$4.0\cdot10^{-4}$	0.010	0.025	0.010	0.016	$1.0\cdot10^{-3}$

*The values of the parameters include armchair, zigzag and all types of chiral SWCNTs studied.
**The values of D_0^p are so small that they can be considered zero, at first approximation.

The mean difference between the values of EA, EI and GJ rigidities calculated with Eqs. (5.1) to (5.3), and the values obtained directly from FE analysis is 0.39%, 2.82% and 1.25%, respectively, for the case of the perfect SWCNTs and 3.66%, 6.68% and 7.87%, respectively, for the case of the SWCNTs with 10% of vacancy defects. The evolution of the parameters α^p, $\beta^p$and γ^p with the percentage of vacancy defects follows a nearly linear trend that causes the decrease of the three rigidities with the increase of the percentage of vacancies.

The values of the rigidities obtained by FE analysis allowed evaluating the Young's, E, and shear, G, moduli, and the Poisson's ratio, ν, of the SWCNTs without and with vacancy defects, as follows:

$$E = \frac{EA}{A} = \frac{EA}{\pi t_n \sqrt{8\left(\frac{EI}{EA}\right) - t_n^2}} \tag{5.4}$$

$$G = \frac{GJ}{J} = \frac{GJ}{2\pi t_n \left(\frac{EI}{EA}\right)\sqrt{8\left(\frac{EI}{EA}\right) - t_n^2}} \tag{5.5}$$

$$\nu = \frac{E}{2G} - 1 = \frac{EI}{GJ} - 1 \tag{5.6}$$

The value of the nanotube wall thickness used in current calculations is t_n = 0.34 nm, equal to the interlayer spacing of graphite, the most widely accepted in literature.

Parametric studies on the influence of chiral indices, nanotube diameter and wall thickness on the elastic constants of SWCNTs were carried out. The Young's modulus, E, of perfect SWCNTs, calculated using Eq. (5.4), decreases with increasing the sum of the chiral indices, for the SWCNTs with small chiral indices $n + m \leq 10$ (which corresponds to the nanotube diameter up to about $D_n = 1\ nm$); afterwards the Young's modulus tends to stabilize at the value of about 1.078 TPa. In the case of representation of the Young's modulus as a function of the nanotube diameter, D_n, its evolution can be unified, regardless of the SWCNT configurations.

The comparison between the experimental results reported in the literature and those of the present study shows that the current Young's modulus is in

satisfactory agreement with the experimental values of the Young's modulus reported by Krishnan et al. (1998), who used thermal vibrations to estimate the SWCNT Young's modulus, and the results of Yu et al. (2000), who used the tensile test.

The evolution of the shear modulus, G, with the nanotube diameter is similar to that observed for the Young's modulus, i.e. the shear modulus value calculated by Eq. (5.5) also decreases initially with the diameter, and then tends to a stable value of about 0.48 TPa, for nanotube diameters $D_n \geq 1\,nm$, regardless of the type of nanotube. This value is in satisfactory agreement with those previously reported in literature from theoretical approaches, and with the experimental value obtained by electrostatic torsion in the work of Hall et al. (2006).

The average value of Poisson's ratio, ν, calculated with Eq. (5.6) assuming isotropy, and resorting to data from torsion and bending tests, converges for a value close to 0.10 for large nanotube diameters, whatever the nanotube chirality. For values of the nanotube diameters such that $D_n < 1.5\,nm$, the Poisson's ratio strongly depends on the chiral angle and increases from zigzag nanotubes ($\theta = 0°$) to armchair nanotubes ($\theta = 30°$). This is in agreement with the results for the torsion rigidity that does not follow a linear correlation with $(D_n - D_0)^3$, for very low values of the nanotube diameter, D_n.

For the nanotubes containing vacancy defects, the Young's modulus value decreases with increasing the nanotube diameter, and tends to stabilize for high values of the nanotube diameter, as in SWCNTs without defects. The same trend is observed for the shear modulus. The stabilized values of Young's modulus and shear modulus are shown in **Table 5.2**. These values decrease with increasing content of vacancies in the SWCNTs. The stabilized values of the Poisson's ratio for each percentage of vacancy defects studied are also shown in the **Table 5.2**. The Poisson's ratio increases with the increase of the percentage of vacancies, for all types of SWCNTs studied. For SWCNTs with 10.0% of vacancy defects, the Young's modulus is about 43% of that of the perfect nanotubes, and the shear modulus is about 33%. Contrariwise, the Poisson's ratio increases about 4 times, compared to that obtained for the perfect nanotube.

Table 5.2. The stabilized values of Young's and shear moduli, and Poisson's ratio of defective SWCNTs for different percentage of the vacancies.

Vac. percent.	0.0%	0.1%	0.5%	1.0%	2.0%	5.0%	10.0%
E [TPa]	1.078	1.062	1.025	0.992	0.897	0.697	0.458
G [TPa]	0.480	0.482	0.467	0.438	0.385	0.277	0.160
ν	0.100	0.101	0.102	0.118	0.168	0.256	0.430

The reduction of the Young's and shear moduli as a function of the percentage of vacancies follows quasi-linear trends for SWCNTs containing up to 5.0% of vacancy defects:

$$E_{reduction}(\%) = -7.12 \cdot Vacancy\ (\%) \tag{5.7}$$

$$G_{reduction}(\%) = -8.85 \cdot Vacancy\ (\%) \tag{5.8}$$

When using Eqs (5.4) and (5.5), the choice of the value of the nanotube wall thickness, t_n, influences the calculation of the SWCNT elastic moduli. In this context, a study on effect of the wall thickness on the values of the elastic moduli of perfect SWCNTs was carried out. The Young's modulus determined by Eq. (5.4) as a function of the inverse of the wall thickness $1/t_n$ (for the range of t_n values 0.066 – 0.69 nm) follows a quasi-linear trend, for nanotubes with diameter $D_n \gtrsim 1.085\ nm$. This linear dependence can be understood based on Eq. (5.4), neglecting the value of t_n^2. The current quasi-linear trend of the Young's modulus as a function of the inverse of the wall thickness is in good agreement with the results of Young's modulus published by other authors for a considerable number of modelling approaches. For small nanotube diameters, $D_n \lesssim 1.085\ nm$, there is deviation from the quasi-linear trend when the nanotube wall thickness is approaching half of its diameter, $t_n \approx D_n/2$. The evolution of the shear modulus calculated by Eq. (5.5) as a function of the inverse of the wall thickness also follows a quasi-linear trend for nanotubes with diameter $D_n \gtrsim 1.085\ nm$, which is no longer observed for small nanotube diameters, $D_n \lesssim 1.085\ nm$ when t_n approaches the value of $D_n/2$.

From Eqs. (5.4) – (5.6), the Young's, E, and shear, G, moduli, and Poisson's ratio, ν, of the SWCNTs without and with vacancy can be calculated taking into account the relationships Eqs. (5.1) – (5.3) between each of the three rigidities and the nanotube diameter, using the following expressions:

$$E = \frac{EA}{A} = \frac{\alpha^p (D_n - D_0)}{\pi t_n \sqrt{8 \frac{\beta^p}{\alpha^p} (D_n - D_0)^2 - t_n^2}} \tag{5.9}$$

$$G = \frac{GJ}{J} = \frac{\gamma^p (D_n - D_0)}{2\pi t_n \left(\frac{\beta^p}{\alpha^p}\right) \sqrt{8 \frac{\beta^p (D_n - D_0)^2}{\alpha^p} - t_n^2}} \tag{5.10}$$

$$\nu = \frac{E}{2G} - 1 = \frac{\beta^p}{\gamma^p} - 1 \tag{5.11}$$

Equations (5.9) – (5.11) allows easy and rapid evaluation of the Young's, E, and shear, G, moduli, and Poisson's ratio, ν, of the single-walled carbon nanotubes, without resorting to numerical simulation. They establish three robust methodologies for calculation of the nanotube elastic constants. One, for evaluation the Young's modulus, makes use of values of the parameters that describe the evolutions of the tensile and bending rigidities with the nanotube diameter. The second permits the evaluation of the shear modulus from results of tensile, bending and torsion tests. And the third is to assess the Poisson's ratio from torsion and bending tests data. These methodologies are valid for perfect and defective carbon nanotubes, over a wide range of diameters and chirality. The evaluation of the Young's and shear moduli by Eqs. (5.9) and (5.10), respectively, gives accurate results when compared with those obtained by Eqs. (5.4) and (5.5), from the rigidities results of the numerical simulations. Eq. (5.11) leads to a value of the Poisson's ratio of about 0.10. This value is independent of the nanotube diameter and corresponds to that obtained by Eq. (5.6) for large nanotube diameters.

5.3. Elastic properties of the SWCNT heterojunctions

A study was carried out in order to describe the geometry of the connecting region of heterojunctions. It was shown that the angle between the direction of the axes of the nanotubes constituting the HJs, and the centre line of the junction is equal to 12.7°, whatever the diameters of nanotubes. Besides, the length of the connecting region, L_3, follows a quasi linear function with the difference between the diameters of the nanotubes, $(D_{n2} - D_{n1})$, for armchair – armchair and zigzag – zigzag HJs, as follows:

$$L_3 = 2.9157(D_{n2} - D_{n1}) \tag{5.12}$$

Since the analysis of the mechanical behaviour of the armchair – armchair and zigzag – zigzag HJs, pointed out the occurrence of redundant bending deformation during the tensile test, the mechanical behaviour was only analysed under bending and torsion. It was found that both the bending and the torsional rigidities of HJs increase with increasing heterojunction diameter. The values of the bending rigidity of heterojunctions are comparable with those obtained for the narrower constituent nanotube, and lower than those obtained for wider constituent nanotube. In a different way, the values of the torsional rigidity of heterojunctions are between of those obtained for the narrower and wider constituent nanotubes.

Among the findings of this study, it is worth to highlight that the bending, $(EI)_{HJ}$, and torsional, $(GJ)_{HJ}$, rigidities of the HJ structures can be calculated from the rigidities of the constituent SWCNTs. The bending rigidity of HJs structures, with overall length, L_{HJ}, can be obtained from the equation of beam deflection, and considering that the HJ transverse displacement is equal to the sum of the corresponding transverse displacements of each SWCNT constituent of the HJs, as follows:

$$(EI)_{HJ} = \frac{L_{HJ}^3}{\left(\frac{L_a^3}{(EI)_a} + \frac{3L_a^2 L_f + 3L_a L_f^2 + L_f^3}{(EI)_f}\right)} \tag{5.13}$$

The torsional rigidity of the HJs can be calculated assuming that the respective twist angle is equal to the sum of the corresponding twist angles of each SWCNT constituent of the HJs, as follows:

$$(GJ)_{HJ} = \frac{L_{HJ}}{\left(\frac{L_a}{(GJ)_a} + \frac{L_f}{(GJ)_f}\right)} \tag{5.14}$$

The letters a and f refer to the nanotubes at whose ends the force (moment) is applied and is fixed, respectively.

The accuracy of the proposed analytical solutions, Eqs. (5.13) and (5.14), was evidenced. These expressions, which make easy the evaluation of the bending and torsion rigidities of SWCNT HJs from the respective rigidities of the constituents

SWCNTs, enable, in turn, the evaluations of Young's, E_{HJ}, and shear, G_{HJ}, moduli of the heterojunction, assuming its diameter equal to the mean value of the diameters of the nanotubes that make up the heterojunction, $\overline{D}_{HJ} = \frac{1}{2}(D_{n1} + D_{n2})$:

$$E_{HJ} = \frac{(EI)_{HJ}}{I_{HJ}} = \frac{(EI)_{HJ}}{\frac{\pi}{64}\left[\left(\overline{D}_{HJ} + t_n\right)^4 - \left(\overline{D}_{HJ} - t_n\right)^4\right]} \tag{5.15}$$

$$G_{HJ} = \frac{(GJ)_{HJ}}{J_{HJ}} = \frac{(GJ)_{HJ}}{\frac{\pi}{32}\left[\left(\overline{D}_{HJ} + t_n\right)^4 - \left(\overline{D}_{HJ} - t_n\right)^4\right]} \tag{5.16}$$

It was found that both, the Young's and shear moduli decrease with increasing HJ aspect ratio ($\eta = L_3/\overline{D}_{HJ}$). The value of the Young's modulus obtained for the heterojunctions is sensitive to how the load is imposed, that is if the force is applied at the narrower or the wider nanotube, whereas the shear modulus of HJs is insensitive to the loading condition. The elastic moduli results from the literature are summarised in the work of Sakharova *et al*. (2017a). The discrepancies reported are due to different modelling approaches and formulations for Young's and shear moduli determination. Also, when using tensile tests, the existence of redundant bending deformation is usually not taken into account by most authors, which can influence their results of Young's modulus of HJs.

5.4. Future perspectives

This work contributed to the systematic characterization of the elastic properties of single-walled carbon nanotubes and their heterojunctions, by numerical simulation. The results obtained can be useful for understanding and modelling the mechanical behaviour of CNT-based structures, especially CNT reinforced materials. The outcomes achieved have provided a benchmark in relation to ascertaining the elastic properties of chiral and non-chiral SWCNTs by numerical models. Some issues that merit further research efforts are now suggested.

First of all, considering the ambiguity of the evolution of the SWCNT elastic constants with the nanotube diameter in the case of small nanotube diameters, reported in the literature, the development of a special model for SWCNTs with the diameter value less than $1nm$ will be helpful.

The achieved contribution for the systematic characterization of the mechanical properties of SWCNTs, which are fundamental building blocks for complex structures, can be the basis to understand the mechanical behaviour of multi-walled carbon nanotubes (MWCNTs), in which the building of an adequate numerical model has received fewer analyses to date, in spite of their high level of commercialization. A simplified FE model to evaluate the elastic properties of armchair and zigzag MWCNTs, which does not take into account the van der Waals forces acting between layers, was already developed by the applicant (Sakharova *et al*., 2017c, see Appendix A). In this context, it will be of interest to develop a modelling approach that allows simulating the van der Waals interactions between adjacent layers, in order to compare the results and to proceed with the correct selection of the numerical simulation method to be used for MWCNTs.

The results concerning the mechanical behaviour of the isolated SWCNTs obtained in this work should allow the modelling of the mechanical response of complex carbon nanotube based structures. In this context, the mechanical characterization by numerical simulation of CNT-reinforced composites, as well 2D and 3D CNTs networks are suggested.

The modelling approach successfully used in this work to numerically simulate the mechanical response of the SWCNTs has a prospective application in the study of the mechanical behaviour of non-carbon nanotubes (such as, for example, boron nitride, aluminium nitride, gallium nitride, chalcogenides nanotubes with a hexagonal honeycomb-like structure). Also, the modelling and numerical simulation of the mechanical behaviour of heterostructures with carbon and non-carbon nanotubes are investigations of potential interest.

References

Hall AR, An L, Liu J, Vicci L, Falvo MR, Superfine R, Washburn S (2006) Experimental measurement of single-wall carbon nanotube torsional properties. Physical Review Letters, 96, 256102.

Krishnan A, Dujardin ., Ebbesen TW, Yianilos PN, Treacy MMJ (1998) Young's modulus of single-walled nanotubes. Physical Review B, 58, 14013 – 14018.

Sakharova NA, Antunes JM, Pereira AFG, Fernandes JV (2017a) Developments in the evaluation of elastic properties of carbon nanotubes and their heterojunctions by numerical simulation. AIMS Materials Science, 4, 706 – 737.

Sakharova NA, Pereira AFG, Antunes JM, Fernandes JV (2017c) Numerical simulation on the mechanical behaviour of the multi-walled carbon nanotubes. Journal of Nano Research, 47, 106 – 119

Yu MF, Files BS, Arepalli S, Ruoff RS (2000) Tensile loading of ropes of single wall carbon nanotubes and their mechanical properties. Physical Review Letters, 84, 5552 – 5554.

Appendix A

This appendix contains the paper by Sakharova *et al*. (2017c), which deals with a simplified finite element model to evaluate the elastic properties of armchair and zigzag multi-walled carbon nanotubes. This simplified model does not take into account the van der Waals forces acting between layers in the MWCNTs.

(Page intentionally left blank)

Journal of Nano Research *Online: 2017-05-10*
ISSN: 1661-9897, Vol. 47, pp 106-119
doi:10.4028/www.scientific.net/JNanoR.47.106

Numerical Simulation of the Mechanical Behaviour of the Multi-Walled Carbon Nanotubes

Nataliya A. Sakharova[1,a *], André F.G. Pereira [1,b], Jorge M. Antunes[2,c] and José V. Fernandes [1,d]

[1]CEMUC – Department of Mechanical Engineering, University of Coimbra, Rua Luís Reis Santos, Pinhal de Marrocos, 3030-788 Coimbra, Portugal

[2]Escola Superior de Tecnologia de Abrantes, Instituto Politécnico de Tomar Rua 17 de Agosto de 1808-2200 Abrantes, Portugal

[a] nataliya.sakharova@dem.uc.pt (* Corresponing author), [b]andre.pereira@dem.uc.pt, [c]jorge.antunes@ipt.pt, [d]valdemar.fernandes@dem.uc.pt

Keywords: Multi–walled carbon nanotubes; Numerical simulation; Rigidity; Young's modulus.

Abstract. The mechanical behaviour of non-chiral multi-walled carbon nanotubes under tensile and bending loading conditions was investigated. For this purpose, a simplified finite element model of armchair and zigzag multi-walled carbon nanotubes, which does not take into account the van der Waals forces acting between layers, was tested in order to evaluate their tensile and bending rigidities, as well as the Young's modulus. The current numerical simulation results are compared with data reported in the literature. The robustness of the simplified model for evaluation of the Young's modulus of multi-walled carbon nanotubes is discussed.

Introduction

The unique mechanical, optical, thermal and electrical properties of carbon nanotubes (CNTs) empower a wide range of further requests and enhancements in the performance of existing applications. In recent years, the research interest has been focused on multi-walled carbon nanotubes (MWCNTs), i.e. structures formed by two or more concentric single-walled carbon nanotubes (SWCNTs), because of their outstanding mechanical properties which can be advantageous for the improvement of structural composites and their consequent high level of commercialization [1]. Multi-walled carbon nanotube are comprised of 2 to 50 coaxial single-walled carbon nanotubes with an interlayer spacing of approximately 0.34 nm, which interact with each other by non-covalent interactions, adequately described by a weak van der Waals force using the Lennard-Jones potential. The diameter of MWCNTs can attain 30 nm in contrast to 0.7–2.0 nm for typical SWCNTs.

There are two approaches for evaluation of the elastic properties of CNTs (for both structure types, SWCNTs and MWCNTs): experimental [2, 3] and computational (see, for example, [4-10]). Due to the fact that the experimental results reported in the literature are limited, owing to the complexity of the nanomaterials characterization at the atomic scale, modelling and computer simulation methods for predicting the mechanical properties of CNTs have been progressed [4]. There are three main groups of methodologies for the modelling of CNTs mechanical behaviour: the atomistic approach, the continuum mechanics approach and the nanoscale continuum mechanics approach. The atomistic modelling approach (see, for example [5]) due to its large computational cost, has been progressively replaced by the continuum mechanics modelling approach (CM). In this case, the existent discrete CNT structure is replaced by a continuum medium (see, for example [6]), but this technique does not seem to be sufficiently adequate to model nanotube mechanical behaviour [7]. In case of the nanoscale continuum modelling approach (NCM) each carbon-carbon (C-C) bond is replaced by a continuum element, e.g. a beam element, whose behaviour is described by elasticity theory (see, [8 – 10]). The NCM approach overcomes the disadvantages of the MD and CM modelling approaches, leading to accurate results without computational complexity and additional costs. Consequently, the NCM approach has been successfully used for simulation of the

mechanical behaviour of SWCNTs [10 – 12], after Li and Chou [8] established a direct relationship between the structural mechanics parameters of the beam element and the molecular mechanics parameters. One of the remaining challenges in this research area is building an adequate numerical model of MWCNTs in order to accomplish accurate evaluation of their mechanical properties.

In spite of numerous numerical simulation studies performed towards the evaluation of the mechanical properties of carbon nanotubes, the modelling and numerical characterization of multi-walled carbon nanotubes have received less research attention than SWCNTs. The essential difference between the simulation of SWCNTs and MWCNTs is to consider, in the simulation of these latter, the non-covalent weak van der Waals force, which leads to significant modelling and computing efforts. The first simulations taking into account the van der Waals force were performed by Li and Chou [13], by introducing a nonlinear truss rod model in their study on the elastic behaviour of multi-walled carbon nanotubes with up to 4 layers under tension and torsion. This model comprises the complex mesh of the truss rods in addition to the beam element mesh for the simulation of each SWCNT composing the MWCNT. The following studies in this research area were mostly focused on the search for a modelling technique, which permits simplifying the simulation procedure of MWCNTs. Since Kalmakarov et al. [14] proposed a spring with no mass as the best element to simulate the van der Waals force, several models of MWCNTs with up to 5 layers, employing spring elements for describing the van der Waals interactions, were successfully developed by Rahmandoust and Öchsner [15] and Ghavamian et al. [16]. Rahmandoust and Öchsner [15] concluded that the modelling of the van der Waals interactions between non-covalent neighbour atoms is not necessary in the case of uniaxial tensile test, because the MWCNT models with and without considering the van der Waals force showed similar Young's modulus results. In case of torsion testing, a difference in the shear modulus of about 9.0% is observed between results obtained with and without consideration of the van der Waals interactions in the MWCNT models. In their finite element model of double-walled carbon nanotubes, Fan et al. [17] proposed to consider an interlayer pressure to model the van der Waals interaction. The mentioned models help to save the computing efforts and show reasonable agreement with the results in the literature. Besides the springs, other elements were tested to model the van der Waals force, as for example, beam elements were used by Nahas and Abd-Rabou [18] to simulate not only the covalent C-C bonds but also the van der Waals force between layers, in double- and triple-walled CNTs.

This work aims to contribute towards the study of the mechanical behaviour of non-chiral (armchair and zigzag) MWCNTs, with different number (up to 10) of walls, under tension, bending and torsion loading conditions, focusing on the respective rigidities and Young's moduli. The NCM approach, employing beam elements, was used to simulate individual layers, i.e. each SWCNT composing the MWCNTs. A simplified finite element model of MWCNTs, without taking into account the van der Waals forces, was considered.

Geometric definition

The fundamental configurations of CNTs are defined by the chiral vector $\mathbf{C_h}$ or the chiral angle, θ, between the chiral vector $\mathbf{C_h}$ and the direction (*n*, 0) [19]:

$$\mathbf{C_h} = n\mathbf{a_1} + m\mathbf{a_2}, \tag{1}$$

$$\theta = \sin^{-1}\frac{\sqrt{3}m}{2\sqrt{n^2+nm+m^2}}, \tag{2}$$

where (n,m) is a pair of the lattice translation indices $\mathbf{a_1}$ and $\mathbf{a_2}$, the unit vectors of the graphene hexagonal lattice; n and m are integers. The length of the unit vector $\mathbf{a}$ is defined as $a = \sqrt{3}a_{C-C}$ with the equilibrium carbon-carbon (C-C) covalent bond length $a_{C\text{-}C} = 0.1421$ nm.

In this way, zigzag ($m = 0$, $\theta = 0°$), armchair ($n = m$, $\theta = 30°$), and chiral ($n \neq m$, $0° < \theta < 30°$) nanotubes are the fundamental configurations of CNTs.

The single-walled CNT diameter is calculated as follows:

$$D_n = \frac{a\sqrt{n^2+nm+m^2}}{\pi}. \quad (3)$$

MWCNTs comprise two or more coaxial SWCNTs (layers). The distance between layers in MWCNTs is generally considered similar to the interlayer spacing of graphene, 034 nm. The most common values experimentally determined for the interlayer distance are close to this value. For example, Kharissova and Kharisov [20] and Kiang et al. [21] reported values in the ranges of 0.32 – 0.35 nm and 0.342 – 0.375 nm, respectively.

Numerical simulation and analysis

Configurations and finite element modelling of MWCNTs. The NCM approach that replaces the carbon-carbon bonds of CNT by equivalent beam elements was used for modelling each layer of MWCNTs. The finite element (FE) model uses the coordinates of the carbon atoms for generating the nodes and their suitable connection creates the beam elements. The relationships found out between the inter-atomic potential energies of the molecular CNT structure and strain energies of the equivalent continuum CNT structure, consisting of beams undergoing axial, bending and torsional deformations, are the basis for the application of continuum mechanics to the analysis of the mechanical behaviour of MWCNTs [13]. The FE simulation uses the analogy between the bond length, a_{C-C}, and the element length l, assuming this element with a circular cross-section area (see Fig. 1).

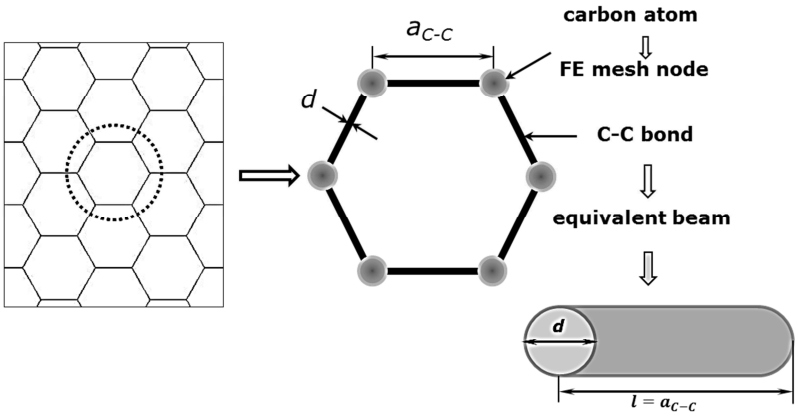

Figure 1: Modelling of CNT, replacing the C-C bonds by beam elements.

The meshes of the MWCNTs structures to be used in the FE analyses, were built using the CoNTub 1.0 software [22]. This code generates ASCII files, describing atom positions and their connectivity that enter as input data in available commercial and in-house FE codes. A previously developed in-house application, designated *InterfaceNanotubes* [10], was used in order to convert the ASCII files, acquired from the CoNTub 1.0 software, into the format compatible with the commercial FE code ABAQUS®. An example of finite element mesh for armchair MWCNT is shown in Fig. 2. The geometrical characteristics of MWCNTs used in the present FE analyses are summarized in Table 1. The interlayer spacing, d_{int}, in the numerical models of MWCNT structures was chosen to be as close as possible to the interlayer spacing of graphene, 0.34 nm, i.e. 0.339 nm and 0.352 nm for armchair and zigzag MWCNTs, respectively. The nanotube length used in the numerical simulations was 30 times bigger than the outer diameter, such that the mechanical behaviour can be independent of the length.

In the current study, a simplified model of the MWCNTs that does not take into account the non-covalent van der Waals interactions between the carbon atoms in the adjacent layers will be used to

simulate their mechanical behaviour under simple tension and bending. The current results are compared with those from the numerical simulation studies, where the van der Waals interactions are considered in the MWCNTs models.

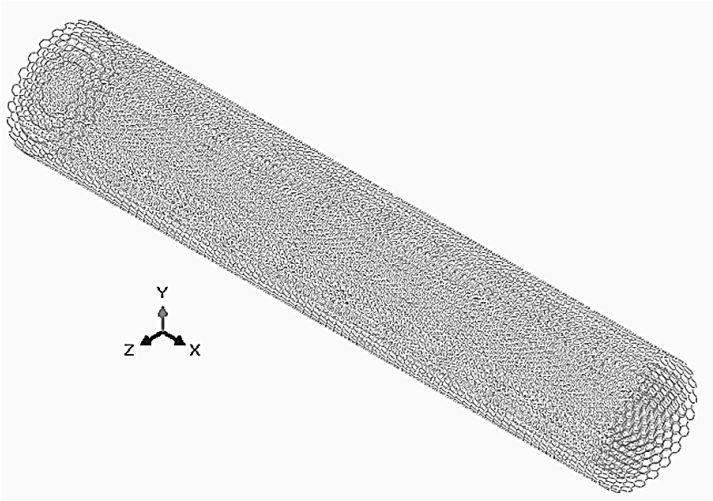

Figure 2: Example of FE mesh, for armchair MWCNT with 4 layers: (10,10)(15,15)(20,20)(25,25).

Table 1: Geometrical characteristics of MWCNTs under study.

Interlay. spacing, d_{int} [nm]	CNT type	N, number of layers	(n, m)	Outer layer diameter, D_{out} [nm]
0.339	armchair	1	(10,10)	1.356
		2	(10,10) (15,15)	2.034
		3	(10,10) (15,15) (20,20)	2.713
		4	(10,10) (15,15) (20,20) (25,25)	3.390
		5	(10,10) (15,15) (20,20) (25,25) (30.30)	4.068
		6	(10,10) (15,15) (20,20) (25,25) (30.30) (35,35)	4.746
		7	(10,10) (15,15) (20,20) (25,25) (30.30) (35,35) (40.40)	5.424
		8	(10,10) (15,15) (20,20) (25,25) (30.30) (35,35) (40.40) (45,45)	6.101
		9	(10,10) (15,15) (20,20) (25,25) (30.30) (35,35) (40.40) (45,45) (50,50)	6.780
		10	(10,10) (15,15) (20,20) (25,25) (30.30) (35,35) (40.40) (45,45) (50,50) (55,55)	7.457
0.352	zigzag	1	(14,0)	1.096
		2	(14,0) (23,0)	1.802
		3	(14,0) (23,0) (32,0)	2.507
		4	(14,0) (23,0) (32,0) (41,0)	3.212
		5	(14,0) (23,0) (32,0) (41,0) (50,0)	3.916
		6	(14,0) (23,0) (32,0) (41,0) (50,0) (59,0)	4.618
		7	(14,0) (23,0) (32,0) (41,0) (50,0) (59,0) (68,0)	5.323
		8	(14,0) (23,0) (32,0) (41,0) (50,0) (59,0) (68,0) (77,0)	6.027
		9	(14,0) (23,0) (32,0) (41,0) (50,0) (59,0) (68,0) (77,0) (86,0)	6.732
		10	(14,0) (23,0) (32,0) (41,0) (50,0) (59,0) (68,0) (77,0) (86,0) (95,0)	7.436

Molecular interactions and equivalent properties of beam elements. The elastic properties of the beam elements can be determined by establishing the equivalence between the energies associated with the bond interactions, as bond stretching, U_r, and bond bending, U_θ [23] and the energies related to elastic deformations of the beams, in stretching, U_A, and bending, U_M, as follows:

$$U_r = U_A \Rightarrow \frac{1}{2}k_r(\Delta r)^2 = \frac{1}{2}\frac{E_b A_b}{l}(\Delta l)^2 \quad (4)$$

$$U_\theta = U_M \Rightarrow \frac{1}{2}k_\theta(\Delta\theta)^2 = \frac{1}{2}\frac{E_b I_b}{l}(2\alpha)^2 \quad (5)$$

where k_r and k_θ are the bond stretching and bond bending constants, and Δr and $\Delta\theta$ are the bond stretching increment and bond angle bending variation; Δl is the axial stretching displacement of the beam with length, l, α is the rotational angle at the ends of the beam, A_b and I_b are the cross-sectional area and moment of inertia of the beam, respectively; and E_b is the Young's modulus of the beam.

Direct relationships can be established between the structural mechanics parameters, E_bA_b, E_bI_b and the force field constants, k_r, k_θ [8] through the Eqs. 4 and 5:

$$\frac{E_b A_b}{l} = k_r \quad (6)$$

$$\frac{E_b I_b}{l} = k_\theta \quad (7)$$

Equations 6 and 7 are the base for the application of continuum mechanics to the analysis of the mechanical behaviour of MWCNTs, and provide the input for simulation. The values of force constants and input data for the FE model are given in Table 2.

Table 2: Mechanical and geometric properties of beam elements, giving input parameters for FE simulations.

Parameter	Value	Formulation
Force constant, k_r [24]	6.52×10^{-7} [N nm^{-1}]	–
Force constant, k_θ [24]	8.76×10^{-10} [N·nm·rad^{-2}]	–
Beam length, $l = a_{C-C}$	0.1421 [nm]	–
Beam diameter, d	0.147 [nm]	$d = 4\sqrt{k_\theta/k_r}$
Cross section area, A_b	0.01688 [nm^2]	$A_b = \pi d^2/4$
Moment of inertia, I_b	2.269×10^{-5} [nm^4]	$I_b = \pi d^4/64$
Young's modulus, E_b	5488 [GPa]	$E_b = k_r^2 l/4\pi k_\theta$
Tensile rigidity, E_bA_b	92.65 [nN]	$E_bA_b = k_r l$
Bending rigidity, E_bI_b	0.1245 [nN·nm^2]	$E_bI_b = k_\theta l$

Loading conditions. Numerical simulations of conventional tensile and bending tests were carried out in order to study the effect of chirality, outer layer diameter and number of layers on the MWCNTs mechanical properties. The boundary and loading conditions are shown in Fig. 3. The FE analysis was performed using the commercial FE code ABAQUS®.

In order to simulate the mechanical behaviour of MWCNT in tension, an axial displacement u_x is applied to all nodes of one nanotube end, leaving the other end immobile. The tensile rigidity of the nanotube, EA, is determined as:

$$EA = \frac{F_x L}{u_x} \quad (8)$$

where L is the nanotube length and F_x is an axial force, taken from the FE analysis.

In bending, a transverse displacement, u_y, is applied at one nanotube end, leaving the other end immobile. The bending rigidity of the nanotube, EI, is determined as:

$$EI = \frac{F_y L^3}{3u_y} \tag{9}$$

where F_y is the transverse force taken from the FE analysis.

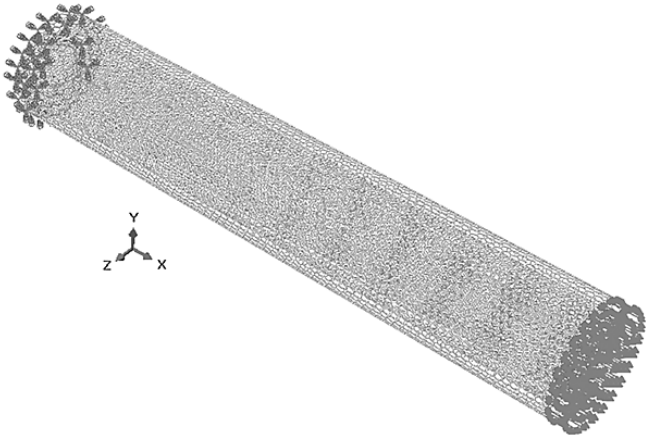

(a)

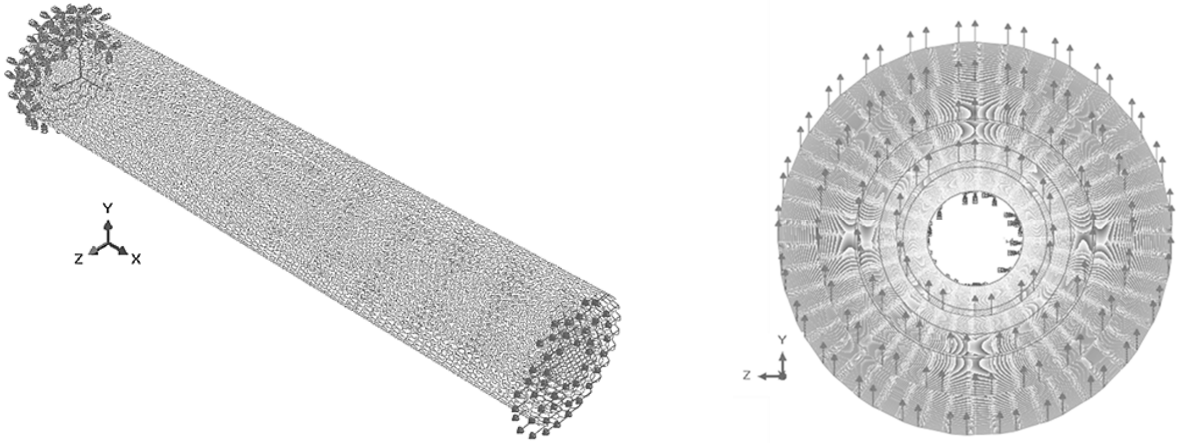

(b)

Figure 3(a, b): Example of loading and boundary conditions for armchair MWCNT with 4 layers: (10,10)(15,15)(20,20)(25,25).

Young's modulus of SWCNTs and MWCNTs. The Young's modulus of SWCNTs (inner and outer layers of the MWCNTs) and MWCNTs were calculated using the following expression taking into account the rigidity in tension, EA, calculated from the FE analysis:

$$E = \frac{EA}{A} \tag{10}$$

A hollow cylindrical profile, i.e. a geometry similar to the SWCNT, as shown in the Fig. 4a (with mean diameter D_n and thickness t_n), has the cross-sectional area and the moment of inertia given by, respectively:

$$A = \frac{\pi}{4}[(D_n + t_n)^2 - (D_n - t_n)^2] = \pi D_n t_n \tag{11}$$

$$I = \frac{\pi}{64}[(D_n + t_n)^4 - (D_n - t_n)^4] = \frac{\pi D_n^3 t_n}{4}\left[1 + \left(\frac{t_n}{D_n}\right)^2\right] \tag{12}$$

For the case of the MWCNT, the cross-sectional area and the moment of inertia of the equivalent hollow cylinder with the inner layer diameter, D_{in}, the outer layer diameter, D_{out}, and the thickness of layers, t_n (see, Fig. 4b), given by, respectively:

$$A = \frac{\pi}{4}[(D_{out} + t_n)^2 - (D_{in} - t_n)^2] \quad (13)$$

$$I = \frac{\pi}{64}[(D_{out} + t_n)^4 - (D_{in} - t_n)^4] \quad (14)$$

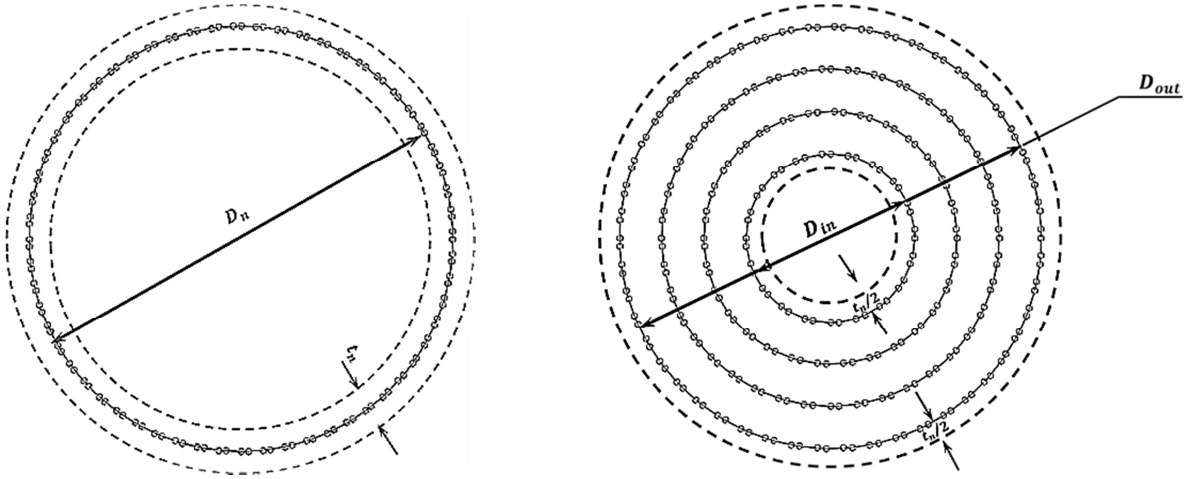

(a) (b)

Figure 4 (a, b): Schematic representations of the profiles of: (a) SWCNT and (b) MWCNT.

Assigning $\overline{D} = (D_{in} + D_{out})/2$ as the average diameter of the MWCNT, Eqs. 13 and 14 can be modified as follows:

$$A = \frac{\pi}{2}\overline{D}(D_{out} - D_{in} + 2t_n) \quad (15)$$

$$I = \frac{\pi}{16}\overline{D}(D_{out} - D_{in} + 2t_n) \cdot [2\overline{D}^2 - D_{out}D_{in} + t_n(D_{out} - D_{in}) + t_n^2] \quad (16)$$

Similarly to what was carried out for the SWCNTs in the previous studies [10], from Eqs. 15 and 16, it is now possible to write:

$$\frac{EI}{EA} = \frac{1}{8}[2\overline{D}^2 - D_{out}D_{in} + t_n(D_{out} - D_{in}) + t_n^2] \Rightarrow$$

$$\overline{D} = \frac{1}{\sqrt{2}}\sqrt{8\left(\frac{EI}{EA}\right) - t_n^2 + D_{out}D_{in} - t_n(D_{out} - D_{in})} \quad (17)$$

Consequently, the Young's modulus of MWCNTs can be calculated from Eqs. 15 and 17, taking into account the cross-section area and the moment of inertia:

$$E = \frac{EA}{A} = \frac{EA}{\pi(D_{out} - D_{in} + 2t_n)\sqrt{\left(\frac{EI}{EA}\right) + [D_{out}D_{in} - (D_{out} - D_{in})t_n - t_n^2]/8}} \quad (18)$$

The nanotube wall thickness considered is t_n = 0.34 nm, as very commonly used [8, 10, 13, 15, 16].

Results and discussion

Rigidities of SWCNTs and MWCNTs. The evolutions of the tensile, EA, and bending, EI, rigidities with the nanotube diameter were studied for individual SWCNTs, corresponding to the inner and outer layers of the MWCNTs in Table 1. Fig. 5 shows the evolutions of the EA and EI rigidities as a function of the SWCNT diameter, D_n. The results of Fig. 5 comprise not only previously studied cases of the SWCNTs with D_n up to 2.713 nm [10], but also those with higher D_n

up to 7.457 nm. The evolutions of the rigidities with nanotube diameter, D_n, can be represented by a quasi-linear function for the case of tensile rigidity, EA, and close to a cubic power function for the case of bending, EI, rigidity, for armchair and zigzag SWCNTs studied, as shown in Fig. 6. The linear dependence can be understood on the base of the linear relationship between cross-sectional area and the nanotube diameter (Eq. 11). In a similar way, the cubic dependence can be understood

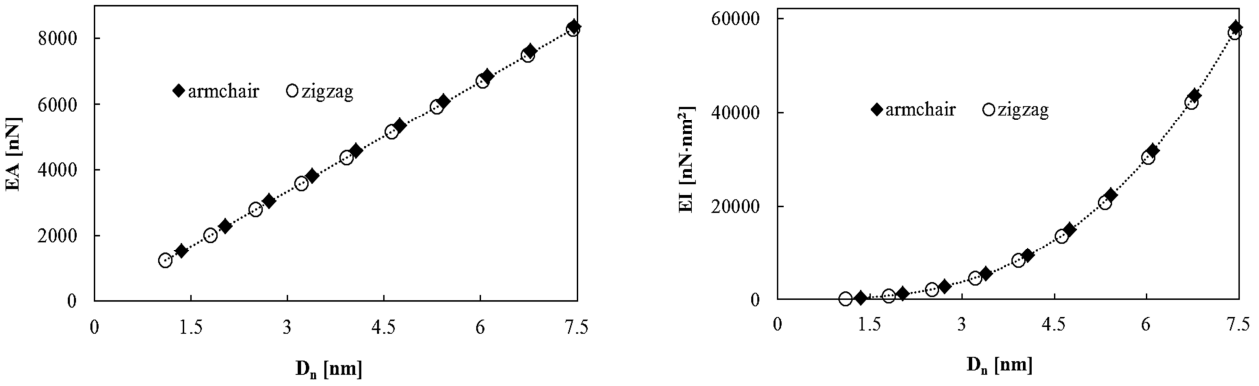

(a) (b)

Figure 5 (a, b): Evolution of: (a) the tensile, EA, and (b) bending, EI, rigidities, as a function of the nanotube diameter, D_n, for individual structures of armchair and zigzag (SWCNTs).

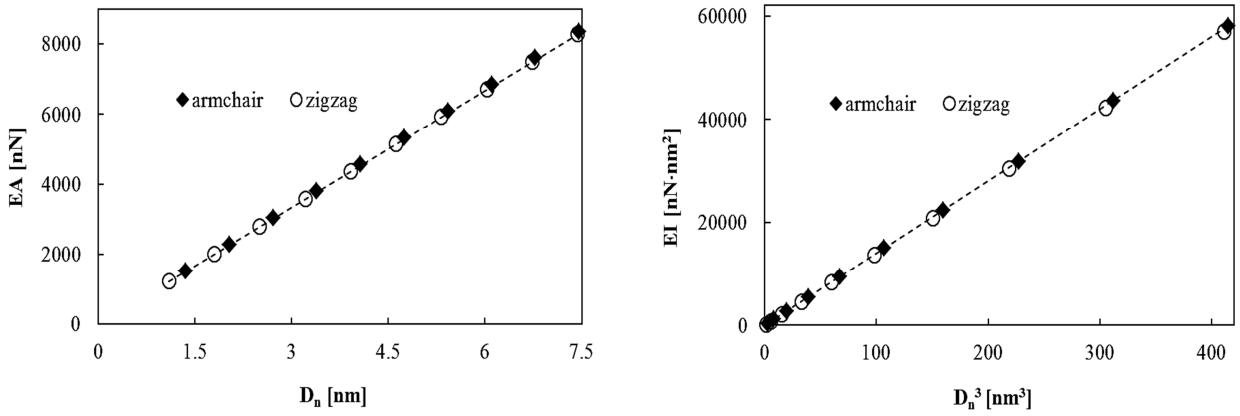

(a) (b)

Figure 6 (a, b): Evolution of: (a) the tensile, EA, rigidity as a function of the nanotube diameter, D_n, and (b) bending, EI , rigidity as a function of D_n^3, for individual structures of armchair and zigzag (SWCNTs).

based on the quasi-cubic relationship between the moment of inertia and the nanotube diameter (Eq. 12, neglecting the value of $(t_n/D_n)^2$). These linear relationships extend up to diameters of about 7.5 nm, those already found for SWCNTs up to about 2.7 nm [10].

The values of the tensile, EA_{MW}, and bending, EI_{MW}, rigidities of the MWCNTs, obtained from Eqs. 8 and 9, are represented as a function of the outer layer diameter, D_{out}, in the Figs. 7a and 7b, respectively. The evolution of the tensile rigidity, EA_{MW}, with the outer layer diameter, D_{out}, can be described by a square power trend, and for the bending rigidity, EI_{MW}, a fourth power trend can be used as shown in the Figs. 8a and 8b, respectively. These trends are related with the square power relationship between the cross-sectional area and the outer layer diameter, D_{out} (see, Eq. 13), and the fourth power relationship between the moment of inertia and the outer layer diameter, D_{out} (see, Eq. 14), being the inner layer diameter, D_{in}, constant for each MWCNT structure (armchair and zigzag) studied. The evolutions of tensile, EA_{MW}, rigidity with D_{out}^2 can be separated for the cases of armchair and zigzag MWCNTs. The same is true for the evolutions of bending, EI_{MW}, rigidity as a function of D_{out}^4. This dissimilarity between the values of both rigidities for armchair and zigzag MWCNTs can be attributed to the different interlayer spacing for armchair (d_{int} = 0.339 nm) and zigzag (d_{int} = 0.352 nm) structures.

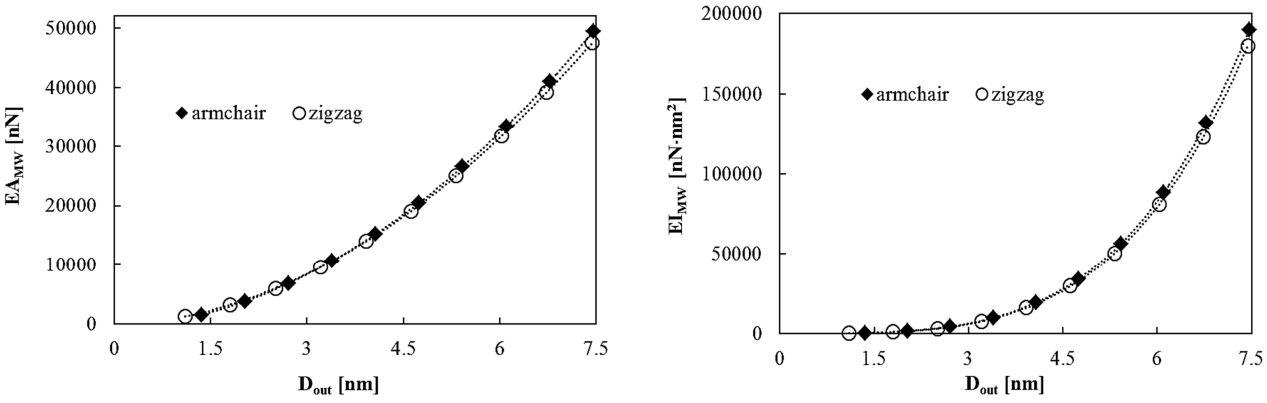

(a) (b)

Figure 7 (a, b): Evolution of: (a) the tensile, EA_{MW}, and (b) bending, EI_{MW}, rigidities, as a function of the outer layer diameter, D_{out}, for armchair and zigzag MWCNTs.

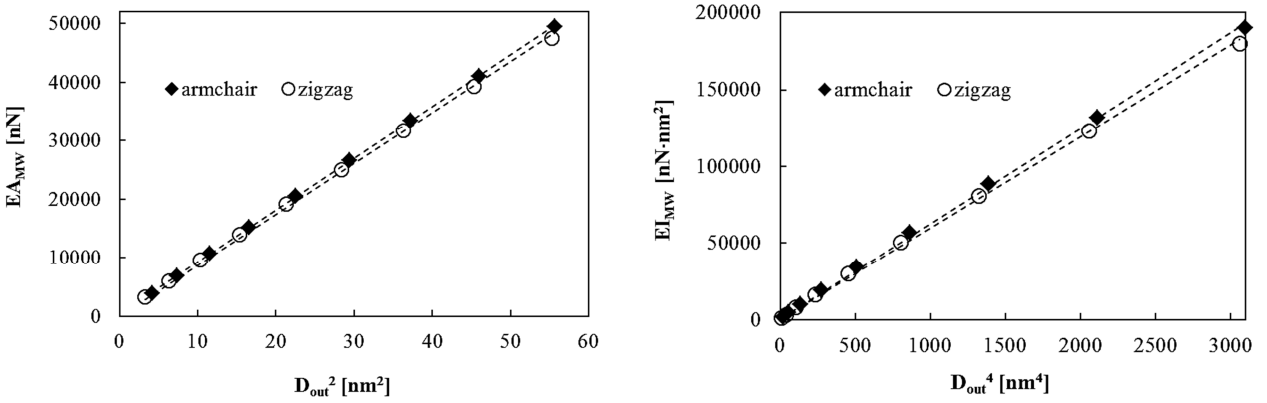

(a) (b)

Figure 8 (a, b): Evolution of: (a) the tensile, EA_{MW}, rigidity as a function of D_{out}^2 and (b) bending, EI_{MW}, rigidity, as a function of D_{out}^4, for armchair and zigzag MWCNTs.

Young's modulus of MWCNTs. The MWCNTs Young's modulus values were calculated by Eq. 10, just using the tensile test results, and Eq. 18, which uses the results of tensile and bending tests. Figure 9 compares the Young's modulus results as a function of the outer layer diameter (Fig. 9a) and the number of layers (Fig. 9b) constituting the MWCNT structure, for armchair and zigzag MWCNTs. The Young's modulus values obtained by both equations are shown. The Young's modulus of the armchair structure are slightly higher than the zigzag structure, and for each structure the evolution is similar, regardless of the calculation approach used (Eq. 10 or Eq. 18). Hereinafter, the Young's modulus values obtained by Eq. 18 are used.

The Young's modulus value of the armchair MWCNTs is about the same regardless of the outer layer diameter (Fig. 9a) or the number of layers (Fig. 9b) constituting the MWCNT. In the case of zigzag structures a slight decrease of the Young's modulus value is observed when the outer layer diameter (Fig. 9a) or the number of layers (Fig. 9b) increase. The Young's modulus values of zigzag MWCNTs are in average 3.9% lower than for armchair MWCNTs.

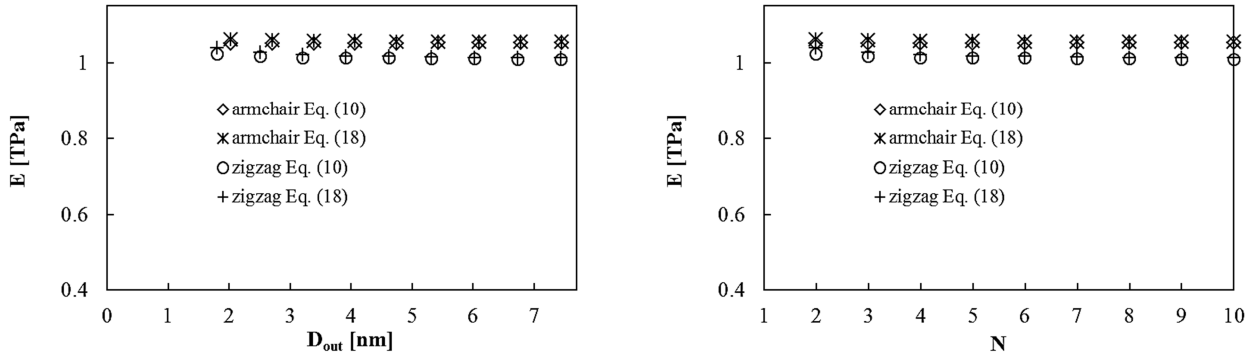

(a) (b)

Figure 9 (a, b): Evolutions of the Young's modulus of MWCNTs with: (a) the outer layer diameter and (b) the number of layers constituting the MWCNT. The Young's moduli of MWCNTs were evaluated by Eqs. 10 and 18.

Figure 10 compares the Young's modulus of the MWCNTs with the Young's moduli of SWCNTs corresponding to the inner and outer layers, for armchair (Fig. 10a) and zigzag (Fig. 10b) structures. The Young's modulus values for the armchair MWCNTs are very close to the valuesobtained for the inner and outer layers. The Young's modulus values for zigzag MWCNTs are lower than the Young's moduli of the inner and outer layers. As mentioned above concerning rigidities, the dissimilarity between the Young's modulus of the armchair and zigzag MWCNTs are also certainly related with the different interlayer spacing between these structures.

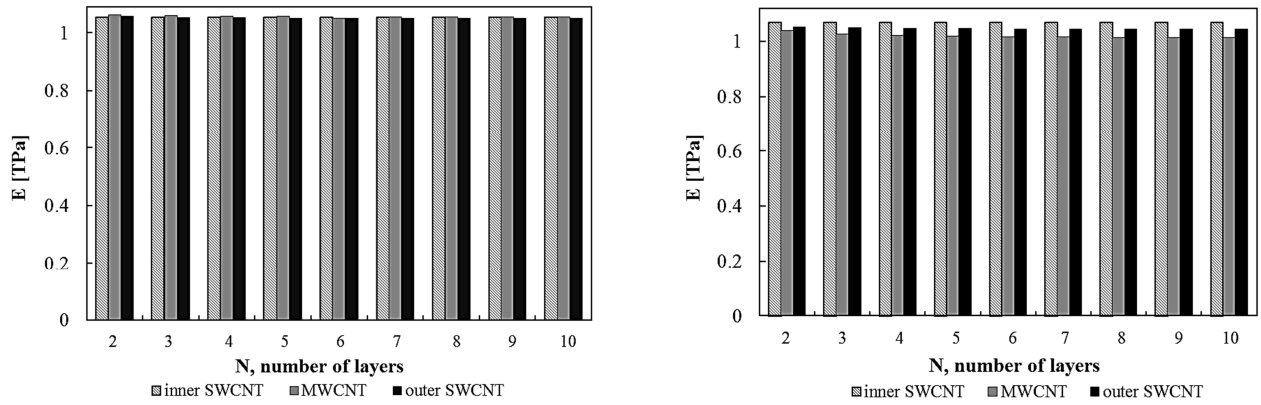

(a) (b)

Figure 10 (a, b): Young's moduli of MWCNTs compared with the Young's moduli of inner and outer constituent SWCNTs for nanotubes structures: (a) armchair and (b) zigzag.

Comparison with literature results. Table 3 summarize the current Young's modulus results of MWCNTs and those from literature that were obtained taking into account the van der Waals interactions. Figure 11 compares the evolutions of these Young's modulus with the number of layers, N, constituting the MWCNTs. For this purpose, MWCNT structures with 3 (Fig. 11a) and 4 or 5 (Fig. 11b) layers were considered [13, 14, 16 – 18]. As in the current work, an interlayer spacing, d_{int}, is equal to 0.339 nm and 0.352 nm for armchair and zigzag MWCNTs, respectively, was used in the selected studies [13, 14, 16 – 18].

Table 3: Comparison of the current Young's modulus results with those reported in the literature, using the NCM approach and taking into account the van der Walls interaction between layers.

Reference	t_n, [nm]	Interlayer spacing, d_{int} [nm]	Approach for the van der Waals interactions between layers	MWCNT type*	N, max. numb layers	Young's modulus, E [TPa]
Li and Chou [13]	0.34	0.339	truss rods	armchair (3,3)(8,8)(13,13)(18,18)	4	1.05 – 1.10
		0.352		zigzag (5,0)(14,0)(23,0)(32,0)		1.05 – 1.12
Kalamkarov et al. [14]	0.68	0.339	spring elements	armchair (5, 5)(10, 10)(15, 15)(20, 20)	4	1.00 - 1.45
		0.352		zigzag (5, 0)(14, 0)(23, 0)(32, 0)		0.96 – 1.50
Ghavamian et al. [16]	0.34	0.339	spring elements	armchair (10,10)(15,15)(20,20)(25,25)(30,30)	5	1.040 – 1.044
		0.352		zigzag (14,0)(23,0)(32,0)(41,0)(50,0)		1.030 – 1.035
Fan et al. [17]	0.34	0.352	spring elements: linear part of the interlayer pressure	zigzag (5,0)(14,0)(23,0)	3	1.006 – 1.011
				zigzag (18,0)(27,0)(36,0)		1.040 – 1.019
Nahas and Abd-Rabou [18]	0.346	–	beam elements	armchair	3	0.98 – 1.02
				zigzag		0.87 – 0.94
Current study	0.34	0.339	–	armchair (Table 1)	10	1.061 – 1.054
		0.352		zigzag (Table 1)		1.069 – 1.012

*The MWCNTs were produced starting from the smallest diameter layer (indicated in the table in the initial position) by adding subsequent layers until maximum number of layers.

All selected studies share the same modelling approach for the simulation each layer of the MWCNT structure: a NCM approach employing 3D beam elements. Regarding the simulation of the non-covalent van der Waals interactions between layers, truss rod elements [13], spring elements [14, 16, 17] and beam elements [18] were used. Particularly good agreement is observed when comparing the current Young's modulus results with those of Fan et al. [17] (Fig. 11a), for zigzag MWCNTs, Ghavamian et al. [16] (Fig. 11b), for armchair and zigzag MWCNTs, where the spring elements for simulation of the van der Waals interactions were considered, and Li and Chou [13] (Fig. 11b), for armchair MWCNTs, who used the truss rod elements for simulation of the van der Waals forces. When compared with the current results, the smallest difference of 0.75% occurs for the Young's modulus calculation performed by Fan et al. [17] for (18,0) (27,0) (36,0) zigzag MWCNTs. Differences of 1.15% and 1.68% occur for the results of Ghavamian et al. [16] for armchair and zigzag MWCNTs, respectively. The comparison with the results reported by Li and Chou [13] shows differences of 1.65% and 8.84% for armchair and zigzag MWCNTs respectively. The Young's modulus values obtained by Nahas and Abd-Rabou [18] (Fig. 11a) show differences of 3.4% and 9.5% for armchair and zigzag MWCNTs, respectively, when compared with the current results. The Young's modulus calculated by Nahas and Abd-Rabou [18] is also lower than those obtained in the other studies [13, 14, 16, 17]. The biggest differences (27.0% for armchair and 32.0% for zigzag MWCNTs) are found with the Young's modulus results predicted by Kalamkarov et al. [14] (Fig. 11b). It can be concluded from the current results that, even without taking into account the van der Waals interactions between carbon atoms in the adjacent layers, reliable Young's modulus values are obtained when compared with some of the literature results. This simplified MWCNT model helps to save modelling and computing efforts and facilitates the numerical simulation of the MWCNTs, particularly for long nanotubes.

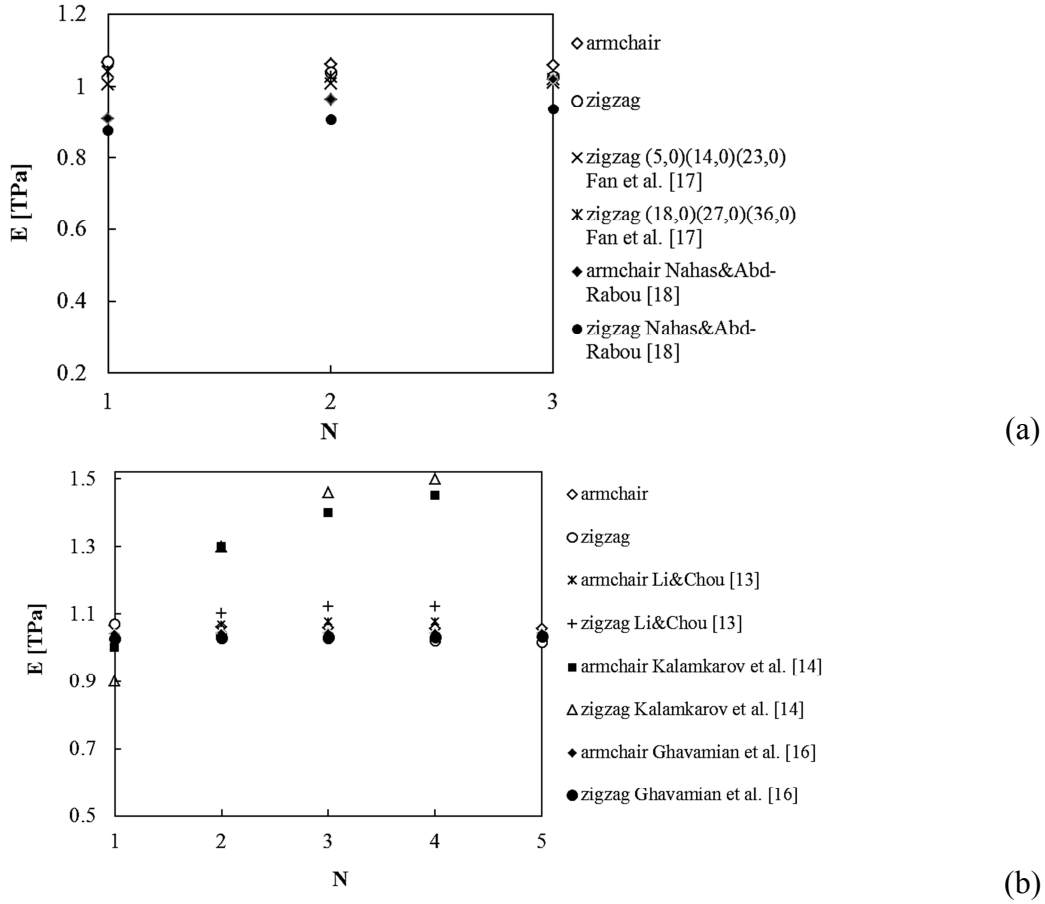

Figure 11 (a, b): Comparison of the current Young's modulus results with those reported in the literature, using the NCM approach and taking into account the van der Walls interaction between layers, for: (a) MWCNTs with 3 layers and (b) MWCNTs with 4 or 5 layers.

Conclusions

A simplified finite element model of multi-walled carbon nanotubes, which does not take into account the van der Waals forces acting between layers, has been used in order to carry out a systematic evaluation of the tensile and bending rigidities, and consequently the Young's modulus of non-chiral MWCNT structures.

A square power law relates the tensile rigidity of MWCNTs to the outer diameter. A fourth power law relates the bending and torsional rigidities to the outer diameter of the MWCNT.

The Young's modulus of armchair and zigzag MWCNTs is approximately constant with increasing the number of layers and consequently the outer layer diameter. The Young's modulus values determined for the zigzag structures are lower than for the armchair structures.

The current Young's modulus values are in good agreement with the results available in the literature, taking into account the van der Waals interactions.

Acknowledgements

The authors gratefully acknowledge the financial support of the Portuguese Foundation for Science and Technology (FCT), Portugal via the project UID/EMS/00285/2013, by UE/FEDER through the program COMPETE2020. Two of the authors, N.A. Sakharova and A.F.G. Pereira, were supported by scientific research grants from the Portuguese Foundation for Science and Technology (SFRH/BPD/107888/2015 and SFRH/BD/102519/2014, respectively). All supports are gratefully acknowledged.

References

[1] H. Kurita, M. Estili, H. Kwon, T. Miyazaki, W. Zhou, J.-F. Silvain, A.Kawasaki, Load-bearing contribution of multi-walled carbon nanotubes on tensile response of aluminium, Compos. Part A-Appl. S. 68 (2015) 133–139.

[2] L. Wang, Z. Zhang, X. Han, In situ experimental mechanics of nanomaterials at the atomic scale, NPG Asia Materials 5 (2013) e40.

[3] C. Kallesøe, M.B. Larsen, P. Bøggild, K.Mølhave, 3D mechanical measurements with an atomic force microscope on 1D structures, Rev Sci Instrum 82 (2012) 023704.

[4] S.I. Yengejeh, S.A. Kazemi, A. Öchsner, Advances in mechanical analysis of structurally and atomically modified carbon nanotubes and degenerated nanostructures: A review, Compos. Part B-Eng. 86 (2016) 95–107.

[5] H.W. Zhang, J.B. Wang, X. Guo, Predicting the elastic properties of single-walled carbon nanotubes, J. Mech. Phys. Solids 53 (2005) 1929–1950.

[6] S.S. Gupta, R.C. Batra, Continuum structures equivalent in normal mode vibrations to single-walled carbon nanotubes, Comput. Mater. Sci. 43 (2008) 715–723.

[7] R. Rafiee, R.M. Moghadam, On the modelling of carbon nanotubes: A critical review, Compos.: Part B-Eng. 56 (2014) 435–449.

[8] C. Li, T.W. Chou, A structural mechanics approach for the analysis of carbon nanotubes, Int. J. Solids Struct. 40 (2003) 2487–2499.

[9] K.I. Tserpes, P. Papanikos, Finite Element modeling of single-walled carbon nanotubes, Compos. Part B–Eng. 36 (2005) 468–477.

[10] N.A. Sakharova, A.F.G. Pereira, J.M. Antunes, C.M.A. Brett, J.V. Fernandes, Mechanical characterization of single-walled carbon nanotubes: Numerical simulation study, Compos. Part B–Eng. 75 (2015) 73–85.

[11] P. Papanikos, D.D. Nikolopoulos, K.I. Tserpes, Equivalent beams for carbon nanotubes, Comput. Mater. Sci. 43 (2008) 345–352.

[12] X. Lu, Z. Hu, Mechanical property evaluation of single-walled carbon nanotubes by finite element modelling, Compos.: Part B-Eng. 43 (2012) 1902–1913.

[13] C. Li, T.W. Chou, Elastic moduli of multi-walled carbon nanotubes and the effect of van der Waals forces. Compos. Sci. Technol. 63 (2003) 1517–1524.

[14] A.L. Kalamkarov, A.V. Georgiades, S.K. Rokkam, V.P. Veedu, N.M. Ghasemi-Nejhad, Analytical and numerical techniques to predict carbon nanotubes properties, Int. J. Solids Struct. 43 (2006) 6832–6854.

[15] M. Rahmandoust, A. Öchsner, On finite element modeling of single- and multi-walled carbon nanotubes, J. Nanosci. Nanotech. 12 (2012) 8129–8136.

[16] A. Ghavamian, M. Rahmandoust, A. Öchsner, A numerical evaluation of the influence of defects on the elastic modulus of single and multi-walled carbon nanotubes, Comput. Mater. Sci. 62 (2012) 110–116.

[17] C.W. Fan, Y.Y. Liu, Chyanbin Hwu, Finite element simulation for estimating the mechanical properties of multi-walled carbon nanotubes, Appl. Phys. A-Mater. 95 (2009) 819–831.

[18] M.N.Nahas, M. Abd-Rabou, Finite element modeling of multi-walled carbon nanotubes, Int. J. Eng. Sci. 10 (2010) 63–71.

[19] M.S. Dresselhaus, G. Dresselhaus, R. Saito, Physics of carbon nanotubes, Carbon 33 (1995) 883–891.

[20] O.V. Kharissova, B.I. Kharisov, Variations of interlayer spacing in carbon nanotubes, RSC Adv. 58 (2014) 30807–30815.

[21] C.-H.Kiang, M. Endo, P.M. Ajayan, G. Dresselhaus, M.S. Dresselhaus, Size effects in carbon nanotubes, Phys. Rev. Lett. 81 (1998) 1869–1872.

[22] S. Melchor, J.A. Dobado, CoNTub: an algorithm for connecting two arbitrary carbon nanotubes, J. Chem. Inf. Comp. Sci. 44 (2004) 1639–1646.

[23] B.R. Gelin, Molecular modelling of polymer structures and properties, Hanser/Gardner Publishers, Cincinnati (OH), 1994.

[24] W.D. Cornell, P. Cieplak, C.I. Bayly, I.R. Gould, K.M. Merz, D.M. Ferguson, et al., A second generation force-field for the simulation of proteins, nucleic acids and organic molecules, J. Am. Chem. Soc. 117 (1995) 5179–5197.

(Page intentionally left blank)